Hydrogen Sulfide Capture and Removal Technologies: A Comprehensive Review of Recent Developments and Emerging Trends

Pudi, Abhimanyu; Rezaei, Mohsen; Signorini, Virginia; Andersson, Martin Peter; Baschetti, Marco Giacinti; Mansouri, Seyed Soheil

Published in:
Separation and Purification Technology

Link to article, DOI:
10.1016/j.seppur.2022.121448

Publication date:
2022

Document Version
Publisher's PDF, also known as Version of record

Separation and Purification Technology 298 (2022) 121448

Contents lists available at ScienceDirect

Separation and Purification Technology

journal homepage: www.elsevier.com/locate/seppur

Review

Hydrogen sulfide capture and removal technologies: A comprehensive review of recent developments and emerging trends

Abhimanyu Pudi [a,c], Mohsen Rezaei [a], Virginia Signorini [b], Martin Peter Andersson [a], Marco Giacinti Baschetti [b], Seyed Soheil Mansouri [a,*]

[a] Department of Chemical and Biochemical Engineering, Technical University of Denmark, Søltofts Plads 228A, 2800 Kongens Lyngby, Denmark
[b] Department of Civil, Chemical, Environmental and Material Engineering, University of Bologna, via Terracini 28, 40131 Bologna, Italy
[c] Sino-Danish College, University of Chinese Academy of Sciences, 19A Yuquan Road, Shijingshan District, Beijing 100049, China

ARTICLE INFO

Keywords:
Sour gas sweetening
Solvents
Porous materials
Electrochemical removal
Composite materials
Biofilter

ABSTRACT

Hydrogen sulfide is a highly flammable, acutely toxic, and extremely hazardous gas that must be captured and removed from a number of important gaseous and liquid streams. This long-standing challenge of capturing H_2S has seen the rise of different materials used in different types of technologies over the years. Some of the well-known examples are alkanolamines used as absorbents and metal oxides used as adsorbents. This work presents an exhaustive review of the latest developments and emerging materials in this field, including ionic liquids, deep eutectic solvents, zeolites, carbon-based materials, metal organic frameworks, polymeric membranes, biological methods, advanced oxidation processes, etc. In addition to a detailed discussion of the state of the art, this review also provides a general technology map and identifies opportunities and challenges to guide future work.

1. Introduction

Capture and conversion of hydrogen sulfide (H_2S) has been one of the longstanding economic and environmental challenges of the past century. H_2S is a highly irritating, odorous, and toxic chemical found as an impurity in many important fuel gases, such as natural gas, biogas, syngas, coke oven gas, landfill gas, refinery gas, etc., and wastewater streams. Removal of this compound from these streams is imperative in terms of both economics and safety. The inherent tendency of H_2S to form an acidic solution in the presence of water leads to corrosion in equipment and pipelines. Its presence also reduces the heating value of the fuel gases and leads to poisoning of catalysts. Most importantly, its combustion leads to the emission of sulfur dioxide and other harmful sulfur oxides that cause acid rain. Moreover, as shown in Table 1, H_2S is a poisonous gas that is hazardous even at low concentrations. It irritates the eyes and airways after prolonged exposure at about 5 ppm and causes instant death at 1000–2000 ppm [1,2]. Therefore, H_2S emission must be controlled and limited for the improvement of global atmospheric chemistry and the quality of life [3].

As a result, the utility of many fuel gases towards energy generation or chemical production requires purification to remove and/or convert H_2S (and other acid gases such as CO_2). The permissible level of H_2S in a gas stream depends on the specific end use and the relevant local regulations. For example, pipeline gas in the US and Denmark requires H_2S content to be <4 ppm [4], while reformer and fuel cell applications generally require it to be below 1 ppm [5,6]. The methods for hydrogen sulfide capture can be broadly classified into two categories: physicochemical techniques and biological techniques. They may also be classified as wet desulfurization and dry desulfurization methods. They can be further categorized into microbiological methods, absorption, adsorption, membrane separation, cryogenic distillation, advanced oxidation processes, etc. This comprehensive review focuses on the recent trends (covering the past 5 or 10 years) in each of these technologies. Each of them has advantages and disadvantages depending on many factors, which will be covered here. However, cryogenic distillation is not discussed in this work due to its high costs and other practical issues that prevented any noticeable technological progress in H_2S removal over the past decade [7]. On the other hand, it must be noted that cryogenic separation, either as a standalone solution or followed by absorption, is likely the most economical option when the end goal is to obtain liquified natural gas (or biomethane, etc.) or to re-inject the liquified acid gases into a geological reservoir [8,9].

* Corresponding author.
E-mail address: seso@kt.dtu.dk (S.S. Mansouri).

https://doi.org/10.1016/j.seppur.2022.121448
Received 15 April 2022; Received in revised form 2 June 2022; Accepted 5 June 2022
Available online 9 June 2022

Table 1
Effect of H_2S concentration and contact time on human health [1,2].

Effects and period of exposure	Concentration of H_2S in air (ppm)
Maximum permissible concentration for prolonged (~8h) exposure	10
Relatively mild symptoms after exposure for several hours	70–150
Maximum concentration that can be inhaled for 1 h without serious consequences	170–300
Dangerous after exposure of 30 min to one hour	400–500
Fatal in exposure of 30 min or less	600–800

2. Technologies for H_2S capture/removal

2.1. Biological technologies

The heart of the biological techniques is the use of an oxidizing group of bacteria that grows at every corner of the environment where there are inorganic reduced sulfur compounds like H_2S. These gram-negative bacteria can use sulfide or sulfur as an electron donor and have been categorized into two domains, photoautotrophs and chemolithotrophs. The following sulfur oxidation reactions are common to both the domains [10]:

$$2S + 3O_2 + 2H_2O \rightarrow 2H_2SO_4 + 2H^+ + SO_4 \quad (1)$$

$$CO_2 + 2H_2S \rightarrow CH_2O + H_2O + 2S \quad (2)$$

Photoautotrophs absorb photons to obtain energy to sustain cell metabolism and growth. CO_2 acts as a terminal electron acceptor and carbon source for the photosynthetic reaction, whereas H_2S acts as the electron donor that consequently converts to sulfur and possibly further oxidizes to sulfate. *Thiobacillus aquaesulis* (moderate thermophiles), *Thiomicrospira thvasirae, Thiobacillus novellus, Paracoccus denitrificans, and Thiobacillus acidophilus* (acidophilic) are some examples of this domain. Sulfur oxidizing photoautotrophic bacteria are present in an anaerobic zone where the oxidizing process is naturally occurring by green sulfur bacteria and the purple sulfur bacteria like *Cholrobium* and *Allochromatium species*, respectively [11].

Green sulfur bacteria can carry out an extracellular sulfide oxidizing process [10]. For instance, *Cholorobium limicola* is the most suitable species capable of oxidizing sulfide out of the cell, which allows to easily separate sulfur from the sulfide-rich environment [12]. There are also some genera of purple bacteria, which can oxidize H_2S, including *Chromatium, Thioalkalicoccus, Thiorhodococcus, Thiocapsa, Thiocyctis, Thiococuus, Thiospirillum, Thiodictyon*, *Thiopedia*, *Ectothiorhodospira, Halorhodospira,* and *Thiorhodospira*. Among them, the last three genera can also produce sulfur outside the cell. The reactions involved in anaerobic light-dependent sulfide oxidation are [13,14]:

$$2nH_2S + nCO_2 \xrightarrow{light} 2nS^0 + n(CH_2O) + nH_2O \quad (3)$$

$$2H_2S + 2nCO_2 + 2nH_2O \xrightarrow{light} nSO_4^{2-} + 2nH^+ + 2n(CH_2O) \quad (4)$$

H_2S oxidizing chemolithotrophs are either aerobic, which use O_2 as an electron acceptor, or anaerobic bacteria, which use nitrite or nitrate as electron acceptor [15]. These bacteria grow on H_2S as an energy source and use CO_2 as a carbon source. *Thiobacilllus ferrooxidans,* for instance, is an aerobic one that oxidizes H_2S, elemental sulfur, and ferrous ion to sulfate and ferric ion [12]. *Thiobacilllus denitrifcans* is able to use both O_2 and NO_3^- to convert H_2S to sulfate. It has been found that some species of chemotrophs are capable of growing heterotrophically on organic sulfur compounds along with H_2S to obtain energy: polithionates by *Thiobacillus thiooxidans* [16]; methyl mercaptan, dimethyl sulfide, and dimethyl disulfide by *Thiobacillus novellus* [17]; and thiosulfate and tetrathionate by *Thermothrix azorensis* [18]. Some species, like those mentioned above, biodegrade H_2S inside the cell. However, similar to green sulfur bacteria, there is also the extracellular oxidation of H_2S, e.g. by *Thiomicrospra frisia* [19] and *Thiobacillus thioparus* [20]. Among chemotrophs, *Thiobacillus* spp. are widely used for the biodegradation of H_2S [21–23] since they have been found to grow in wide environmental conditions. *Thiobacillus* thiooxidans and *Thiobacillus* ferrooxidans, for example, can grow at low pH (<6) [24]. *Thermothrix azorensis* is a thermophile species and can live at up to 86 °C [18]. *Thioalkalispira microaerophila* is an alkaliphile and has optimum growth at pH 10 [25]. The aerobic reactions for a colorless sulfur-oxidizing system are shown below. In this system, production of elemental sulfur and sulfate ion varies with the oxygen level [26].

$$H_2S + H_2O \rightarrow HS^- + H_3O^+ \quad (5)$$

$$H_2S + 2O_2 \rightarrow SO_4^{2-} + 2H^+ \quad (6)$$

$$HS^- + 0.5O_2 \rightarrow S^0 + H_2O \quad (7)$$

$$S^0 + H_2O + 0.5O_2 \rightarrow SO_4^{2-} + 2H^+ \quad (8)$$

Although sulfur-oxidizing bacteria are generally autotrophic, there are some genera such as *Alcaligens*, *Paracoccus*, *Pseudomonas*, *Xanthobacter*, and *Bacillus* that grow heterotrophically but have shown the use of reduced inorganic sulfur compounds in their metabolism [27]. These bacteria (so-called mixotrophic microorganisms), in the presence of reduced organic carbon sources (e.g. glucose and amino acids), can use an organic carbon source but an inorganic energy source [15]. Furthermore, some mixotrophs such as *Pseudomonas acidovorans* and *Pseudomonas putida* [23,28] are capable of biodegrading H_2S and organic sulfur compounds, and some others such as *Beggiatoa* sp. and *Thiothrix* sp. [15,29] can use H_2S and other organic compounds (e.g. acetate) as an energy source. Besides direct sulfide oxidation, there is an indirect method wherein ferric iron regenerated by iron-oxidizing bacteria acts as an agent to oxidize reduced sulfur [30].

Oxidation of H_2S by using oxygen as an electron acceptor is a well-known process utilizing colorless sulfur-oxidizing bacteria. As these bacteria can maintain high growth rates without light, they are preferred over green or purple sulfur-oxidizing bacteria [31]. To employ a colorless sulfur-oxidizing approach to fulfill gas-phase H_2S abatement for most industrial emissions, the most common techniques are based on different types of equipment, such as a biofilter (BF), a biotrickling filter (BTF), and a bioscrubber (BS). Some of the recent studies in this area are summarized in Table 2.

Table 2
Recent studies in the removal of H_2S using biological technologies.

Packing Bed/Medium	Pollutant	H_2S Amount	EBRT (s)	Removal Efficiency (%)	EC_{max} (g $m^{-3}h^{-1}$)	Reference
Biofilter (BF)						
Compost or compost/hog fuel	H_2S	10–450 ppm	38	90–100%	na	[491]
Cell-laden Caalginate	H_2S, NH_3	60–120 ppm	72	>90%	na	[28]
Pig manure + sawdust	H_2S	10–45 g $m^{-3}h^{-1}$	13.5–27	>90%	na	[492]
Wood chips, granular activated carbon (GAC)	H_2S, NH_3	30–450	20–60	75–99%	45–75	[493]
Wood-based medium	H_2S, methanethiol, ethylamine, dimethyl sulfide	1.07 mg H_2S/m3	30	>96% (all Compound but methanethiol, 70%)	na	[494]
Granulated sludge	H_2S, NH_3	170–680 g m^{-3} d^{-1}	na	100%	na	[495]
Peat	H_2S	1400 ppm	na	65–100%	55	[23]
Pine bark	H_2S, dimethyl sulfide, EtSH	2500 ppm	53.3	60%	8	[35]
Mixture of bark, peat, wood-four, block, and shell	H_2S	1.35–24.88 ppm	13.-16	99.2%	na	[496]
Expanded schist	H_2S	7–35 g $m^{-3}h^{-1}$	30	97%	30	[497]
Plastic bio-ball	H_2S, CO_2, CH_4	2000–3000 ppm	na	80%	na	[498]
Wood chips	H_2S, CO_2, CH_4	13.96–10,000 ppm	289	97%	169	[39]
Expanded schist	H_2S	100 ppm	13–63	47–100%	7.9	[499]
Salak fruit seeds	H_2S, CO_2, CH_4	8550 g $m^{-3}h^{-1}$	240	97%	na	[34]
Cellular concrete waste	H_2S	100 ppm	63	70%	5.6	[48]
CM-5	H_2S	49–80 g $m^{-3}h^{-1}$	20–121	100%	60	[43]
Biochar	H_2S	39 g $m^{-3}h^{-1}$	80	70%	28	[42]
Biotrickling filter (BTF)						
Polypropylene pall rings	H_2S, Toluene	170 ppm	36	100%	19	[500]
Structured plastic	H_2S	60–155 ppm	4–10	85–99%	na	[501]
Polyurethane foam	Odorous air (H_2S)	5–35 ppm	1.6–2.3	>97%	>100	[66]
Volcanic stones	H_2S	7–25 g $m^{-3}h^{-1}$	60	100%	na	[64]
na	Biogas (H_2S)	3200–3500 ppm	na	95%	228.6	[65]
PVC, PET, OPUF, Teflon	H_2S	8–108 g $m^{-3}h^{-1}$	1.6–4.8 min	95.72%	98	[59]
Ceramic	H_2S	176.21 (BTF) and 478.88 (BF)	137	86–95% (BTF) and 83–97% (BF)	251.93	[502]
Polypropylene rings	Biogas (H_2S)	101.7–422 g $m^{-3}h^{-1}$	1–4 min	91.4% (for 1 min), 100% (for 4 min)	386 ± 10.5	[57]
Bioscrubber (BS)						
Alkaline solution		2000 ppm	na	> 99.8%	na	[76]
Plastic	H_2S	90 g $m^{-3}h^{-1}$	5	99%	90	[503]
Fixed film	H_2S	10–100 ppm	12.71	98%	19.24	[78]
Biochar	H_2S	105–1020 ppm	80	98%	8	[79]
Liquid	H_2S	37–100 g $m^{-3}h^{-1}$	2.4–6-6 min	80%	na	[77]
Liquid	H_2S, CO_2, CH_4	na	5–20 min	98%	na	[504]

2.1.1. Biofilter

A typical biofiltration reactor (see Fig. 1a) is a column packed with mostly organic media, like compost and wood chip, that has bacterial supplementing nutrients and a diverse microbial community developing a biofilm [32]. As pollutant-laden airflow is driving through the media, a transfer action occurs between the flow and the fixed growth biofilm that results finally in the biodegradation and conversion of the pollutant into a benign substance, water, and carbon dioxide. Packing media and biofilm are the brain of a BF as they are responsible for all processes of absorption and adsorption, phase transfer, and finally biodegradation [33]. BF represents a very promising approach for abatement of H_2S since it has a high loading rate acceptance, is easy to operate, and is cost-effective and eco-friendly. For these reasons, many research studies have been dedicated to improving its performance and kinetics and to minimizing drawbacks by testing different packing media and microbial population in the form of either consortium or single species growth. The performance indices for a BF includes inlet loading rate (ILR) or inlet concentration, maximum elimination capacity (EC), and empty bed residence time (EBRT) – the greater the ILR and EC and the lower the EBRT, the higher the reliability and efficiency.

Lestari et al. [34] and Ben Jaber et al. [35] provided great demonstrations of biofiltration as a potent technology for H_2S abatement. Lestari et al. achieved an elimination capacity of 169 g $m^{-3}h^{-1}$ for 10,000 ppm H_2S in an empty bed residence time (EBRT) of 289 s for co-treatment of H_2S, CO_2, and CH_4 in a BF packed with wood chips. Ben Jaber et al. achieved the removal of 85% of 2500 ppm H_2S for co-treatment of H_2S, dimethyl disulfide (DMDS), and ethanethiol (EtSH) on Pine bark. The flexibility of biofiltration is then shown in a study by

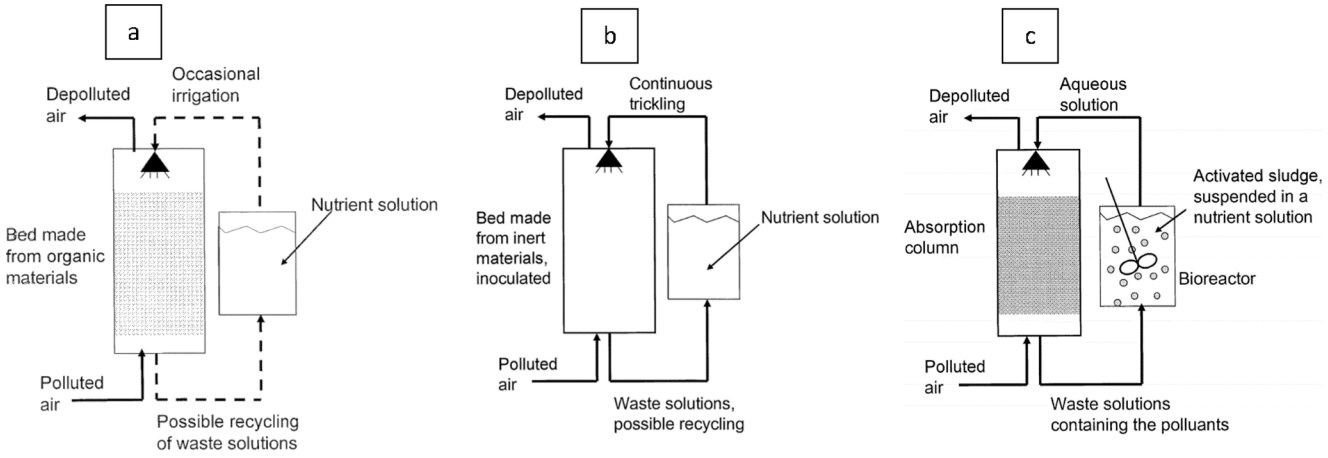

Fig. 1. Schematic view of biofiltration reactors for air purification: a) biofilter, b) biotrickling filter, c) bioscrubber. Reprinted with permission from [485]. © 2005 Taylor & Francis.

Courtois et al. [36] which demonstrated that it is possible to obtain good removal, in the order of 36 g $m^{-3}h^{-1}$ H_2S, by using a BF reactor with EBRT as low as 19 s.

Packing material due to its supportive function for microbial growth and being the bioprocess's deck is the most important part of a biofilter. An ideal packing media is expected to have many features such as a high mechanical resistance, the ability to host diverse microbial population and to provide essential nutrients, a large buffer capacity, a suitable moisture-holding capacity, high specific area, high porosity, etc. Startup period of a BF also is affected by microbial growth supplied by packing media [37]. Organic media, such as compost, wood chip, pine bark, peat, etc., have been shown to be interesting packing materials in the biofiltration of H_2S due to supplying indigenous nutrients and microbes [34,38,39]. However, their use comes with a few adverse issues, such as compaction and lack of uniformity. Compaction may cause a channelizing phenomenon, disrupting the water and gas flow pattern, thus reducing filter's performance. Non-uniform function affects microbial propagation and distribution of the flows [40,41]. To avoid these phenomena and meet the above-mentioned features, some studies successfully tested different modifications of pristine materials, especially compost, which is usually chosen as a suitable media able to satisfy most of the requirements. Das et al. [42] have surveyed the effect of adding biochar to compost on the removal of H_2S using a biofilter. They have shown, after 52 days of operation, that the maximum elimination capacity (EC_{max}) increased from 19 g m^{-3} h^{-1} with compost alone to 33 g m^{-3} h^{-1} with compost + biochar at an EBRT of 119 s. In addition, Zhu et al. [43] have evaluated the use of packing media CM-5 (Composite media-5) which is a mixture of cement, matured compost, calcium carbonate, inorganic binding media, porous perlite, and plant fiber) with and without sterilization. They indicated a successful microbial population and adaptation without sterilization during startup operation but not with sterilized CM-5, possibly due to lower nutrient bioavailability and microbial propagation following sterilization.

Sulfur-oxidizing bacteria convert H_2S to sulfur (Eq. (7)) as an intermediate and sulfate (Eqs. (6) and (8)) as a final product which are both solid compounds. However, the oxidation process would end up in sulfur if the system undergoes oxygen-limited conditions [44,45] due to the higher energy barrier of Eq. (5). In an industrial biofiltration reactor, a consortium of oxidizing bacteria is usually employed so that different sulfur-oxidizing bacteria will go through different metabolisms. Therefore, the produced sulfur can be deposited both inside and outside the cells. Deposition of a large amount of sulfur (yellow deposits) and sulfate in high inlet sulfide loading rates or inlet concentration (e.g. critical concentration of 380 ppm/min reported by [46]) may result in the accumulation of deposits on the bed, reducing H_2S mass transfer and, as a result, deteriorating the removal efficiency [47,48].

Production of sulfate and reduction of H_2S, considering Eq. (6), which shows 1 mol of H_2S can produce 2 mol of H^+, end up in sulfuric acid generation as a reaction product of H_2S biodegradation. This is the phenomena causing structural failure of sewers where H_2S dissolves in water droplets from which sulfuric acid is produced by *Thiobacillus* bacteria under aerobic conditions [49,50]. In a biofilter, sulfuric acid generation has been reported to reduce the pH down to <1. The increased acidity by forming sulfuric acid can limit the bacterial function and propagation and, subsequently, reduce the H_2S mass transfer into the biofilm, adversely affecting the removal efficiency. Here, acidophilic species like *Thiobacillus* genus have been recommended as they can efficiently function also in these conditions, i.e., at pH values as low as 0.2 [46,51,52]. Ben Jaber et al., [53] reported a removal efficiency higher than 96% at pH of 1.2 for an inlet H_2S concentration of 250 ppm. However, it dropped to 78% when pH decreased to 0.5 by increasing the H_2S concentration to 360 ppm. They concluded that the increased inlet H_2S caused a microbial inhibition as a result of sulfate accumulation and decrease of H_2S mass transfer under strong acidic pH [48]. Also, the literature on the pH variation in biofilters shows that a decline in pH usually occurs at the lower section of the reactor [39,54]. Higher pH usually observed at the top of biofilters may be due to the fact that this section is usually more accessible to nutrient/water solution, thus suggesting that the use of a high nutrient solution recirculation rate could help in limiting the pH drop. In this concern, Ben Jaber et al. [35] have investigated the effect of nutrient solution spraying to assess its effect on pH variation in different heights of the reactors. Tests were conducted on three biofilters, but the results were somewhat inconclusive as the different spraying rates did not significantly affect the pH.

2.1.2. *Biotrickling filter*

The working principle of a biotrickling filter (see Fig. 1b) is the same as for a BF, but the major differences are that the nutrient solution in a BTF is continuously trickling over the media and that the packing material for BTFs are often inert porous inorganic structures like polyurethane foam (PUF). This media, thus, does not supply indigenous microorganisms that, therefore, must be provided by engineered augmentation methods [55]. The process generally is such that the sulfur-oxidizing bacteria, immobilized on the already packed media, develop a biofilm which is covered by a water layer formed by trickling solution. The H_2S laden airstream flows through the filter allowing the acid gas to transfer from the gas phase to the water layer and then into the biofilm where it is biodegraded into simple, odorless and harmless compounds [56]. Biogasclean QSR, SulfurexBF, and Biosulfex are a few examples of commercial BTF technologies.

BTF studies that have been published for removal of H_2S are listed in Table 2. The performance of an H_2S-biodegrading BTF depends on a large number of parameters including solution pH, nutrient material, gas flow rate, EBRT, inlet loading rate, temperature, dissolved oxygen, packing media, biomass society, and mass transfer rate. Controlling these parameters leads to an improved biomass activity and mass transfer rate to fulfill a successful H_2S abatement using BTF.

In an H_2S-degrading BTF, mass transfer is a limiting parameter that depends on solution trickling rate and contaminant solubility in the water layer on the biofilm. A very low trickling rate might reduce the H_2S transfer due to an insufficient wetting of the bed. When the bed is not sufficiently wet, the biofilm cannot be uniformly developed, thus deteriorating the H_2S biodegradation. Although a high trickling rate increased the development of the liquid phase and subsequently improved the H_2S solubility and diffusion into the biofilm, it also led to establishing a tick liquid phase, limiting oxygen diffusion into the biofilm and decreasing the H_2S removal efficiency [57]. Turpin et al. [58] reported that adding sodium hypochlorite or sodium hydroxide with chlorine to the trickling solution can improve the H_2S mass transfer.

Organic media such as wood and compost, which were suitable materials for traditional biofiltration, may not be suitable options for a BTF as they have a low mechanical strength as well as high moisture-holding capacity, making the bed drown and compact as a result of the continuously trickling liquid. These materials have been used together with bulking agents such as woodchips to increase mechanical properties, but inorganic or synthetic materials are currently the first choice for BTFs. Indeed they have shown very interesting results for the removal of H_2S in BTFs because of a high and uniform porosity (e.g. PUF has a porosity of 98%) as well as a high mechanical strength [55]. In the study by Tayar et al. [59] on the removal of H_2S from real sewage biogas, the effect of different packing media on the BTF performance was evaluated. The authors showed that the highest removal efficiency of up to 95.72% and elimination capacity of 98 g S $m^{-3}h^{-1}$ was obtained with PUF. In another study, Soreanu et al. [60] have reported successful results using both Lava rock and plastic fiber. They obtained a removal efficiency of 95% for daily H_2S loading rates up to 212 g H_2S m^{-3} with plastic fiber and 232 g H_2S m^{-3} day with lava rocks. In general, very high H_2S removal efficiencies are reported for BTFs with inorganic packing media such as 99% with PUF (specific surface area, SSA: 600 m^2m^{-3}) [61], 99% with Pall Rings (SSA: 320 m^2m^{-3}) [62], 90% with Pall Rings (SSA: 515 m^2m^{-3}), >95% using polyethylene HDPE (SSA: 859 m^2m^{-3}) [63], and close to 100% with volcanic stones (SSA is not reported) [64].

As is the case in BFs, the production of sulfate in a BTF indicates a decline in pH, which decreases the solubility of H_2S and adversely affects the BTF performance. It has been shown [65], therefore, that maintaining pH near natural or alkaline region ($7 < pH < 12$) helps improve mass transfer rate of H_2S. Gabriel and Deshusses [66] have reported that microbial propagation is higher under neutral pH also in a full-scale BTF. Kim and Deshusses [67] have also obtained a high removal efficiency for an H_2S-removing BTF under pH 5–6.3 due to increased microbial growth. They suggested that pH should be adjusted constantly between 7 and 8 during startup operation to enhance H_2S solubility and mass transfer. The effect of pH, however, does not seem to be completely clear. Fortuny et al. [61] have found that pH tends to fall in a high H_2S elimination period and is difficult to control. However, during steady-state operation, a decrease in pH, even to the value of 3.5, did not cause a significant effect on the removal efficiency. In addition, other studies have shown that the removal efficiency of H_2S can be high even under strongly acidic pH. For example, Rodriguez et al. [68] have reported a higher removal efficiency at a pH of 1.8. Literature shows that the effect of pH on the BTF performance is crucial since it largely affects the biomass activity and H_2S transfer rate, which impact the removal efficiency of H_2S. In general, a pH near to the neutral region seems to enhance the BTF efficiency, but pH control depends on the H_2S inlet loading rate and the current mass transfer rate of the system.

As mentioned above, the oxygen level in H_2S biodegradation is important to determine the degradation products: sulfur (under low oxygen pressure) or sulfate (under high oxygen pressure). Montebello et al. [69] have reported that the main product is sulfate when the O_2/H_2S ratio is >2 and sulfur when the ratio is <0.5. A few industrial-scale projects are planned to produce sulfur for agriculture recovery goals. However, the yellow sulfur deposit can clog the filter bed, thus lowering mass transfer and deteriorating the BTF performance because of the increased gas pressure drop [70]. In this condition, the use of intracellular sulfur-oxidizing bacteria can be a solution to operate under lower oxygen levels without losing performance. The removal efficiency of H_2S is based on the combined activity of different bacterial species with different oxygen-mediated growths to synergize the conversion of H_2S. Therefore, limiting oxygen level in a BTF may reduce the removal efficiency of some species. Qiu and Deshusses [71] have recorded a removal efficiency of 95% H_2S at the O_2/H_2S ratio of 2:1 and 50% at the ratio of 1:2. This indicates the need to find and choose a special species of bacteria that can enhance the removal efficiency of a BTF operated at low oxygen levels.

EBRT is one of the important operational parameters as it affects both the inlet loading rate and the mass transfer rate of in a BTF. A higher EBRT allows a higher mass transfer rate and a lower amount of H_2S loaded per unit time that both result in an increase in the H_2S removal efficiency; however, the reduced loading rate usually causes an overall reduction in elimination capacity. When a BTF is operated at a lower EBRT, the inlet loading rate increases making it possible to obtain a high value for elimination capacity. Nonetheless, due to the occupancy of the active sites on the biofilm by the increased inlet mass, the excess mass cannot be degraded by the system, potentially leading to a decline in the removal efficiency. Other studies also reported a declined H_2S removal efficiency with an increase in EBRT [72–74]. For instance, Fortuny et al. [74] have shown that the H_2S removal efficiency decreased from 88% to 40% when EBRT decreased from 90 s to 30 s.

2.1.3. Bioscrubber

Bioscrubbing is a common biological technique for the removal of H_2S from the gas stream. It comprises two main parts, an absorption/separator chamber and a fluidized-bed or suspended growth bioreactor column (see Fig. 1c). The first is a physical process and the second is a biological process. The gas stream containing the pollutant passes first through the absorption chamber, which contains an absorbent solution, so the contaminate is transferred from the gas phase to the aqueous phase which is then directed into the bioreactor where it can be treated by the suspended heterotrophic or autotrophic sulfur-oxidizing bacteria [75]. Examples of successfully used commercial bioscrubbers are Sulfothane, SulfurexBR, THIOPAQ (a reference technology for low-pressure biogas treatment), and THIOPAQ O&G (developed for high-pressure sour gas streams typically associated with oil and gas and petrochemical industries) [76]. Table 2 shows the performance of bioscrubbers that have been recently studied for the removal of H_2S.

As mentioned in the preceding subsections, one drawback of employing BFs or BTFs is the frequent clogging of the bed due to the accumulation of the produced elemental sulfur on the bed. This requires periodical cleaning, which interrupts the process. Although BFs and BTFs can be operated by supplying an excessive amount of oxygen to complete the oxidation process toward sulfate production, not all parts of the biofilm usually receive a sufficient amount of oxygen, resulting in sulfur production in these areas. In this regard, bioscrubbing offers as an alternative method as it can uniformly supply sufficient oxygen demand [75]. San-Valero et al. [77] evaluated a bioscrubber comprising an absorption column and an aerated bubble column bioreactor for the desulfurization of H_2S-rich biogas. They operated the bioreactor under near-alkaline pH (8 ± 0.5) to improve H_2S oxidation instead of H_2S stripping. They converted 80% of the H_2S loading rate of 37, 59, and 100 g S $m^{-3}h^{-1}$ at a gas residence time of 6.6, 4.1, and 2.4 min, respectively, with a production of up to 24,000 g SO_4^{2-} m^{-3}.

Potivichayanon et al. [78] developed a fixed-film bioscrubber for H_2S removal. They reported an increasing sulfate production trend with a maximum H_2S removal efficiency of 98%. Kanjanarong et al. [79] have reported the highest sulfate production of 4630 mg L^{-1} with a maximum H_2S removal efficiency of 98% and EC_{max} 8 g m^{-3}h by inoculating sulfur bacteria from palm oil wastewater plant. A bioscrubber has other advantages too, such as easy control of nutrients and pH, no addition of oxygen or nitrogen to the sweet gas, possibility to work at high inlet loading rates and with water-soluble compounds like H_2S, etc. On the other hand, it also comes with a few limitations. The most important perhaps is the disposal of the excess sludge, which needs to be further managed in a wastewater post-treatment process and, as a result, lower the cost-effectiveness of the process [75].

Biological processes are continually advancing and are adaptable technologies for environmental pollution control. The main advantage of these methods is the production of various intra- and extra-cellular enzymes that degrade compounds in natural biocatalytic activity. This means that the chemical additives with their expensive material flow as well as harmful byproducts can be completely removed by biological techniques. Since bioscrubbing processes separate the steps of absorption and oxidation of H2S, the sweet gas outlet from the scrubber stays free from the addition of air. This makes bioscrubbers preferable for biogas upgrading to biomethane. Even if biological techniques do not show enough potential to overcome the limitations of physicochemical technologies in high-volume applications, looking for a cost-effective solution to purify highly sour streams in bio-based industries, such as wastewater treatment, livestock farming, municipal solid waste landfills, and food industry, may bring engineers toward using biological techniques. A biological solution could be attractive to treat these bioprocess-originated wastes (e.g. biogas) since the waste has a large number of indigenous degrading bacteria. Although a large number of studies in H_2S removal using biological methods have been published, a few knowledge gaps exist that must be explored further, such as the effect of recirculating rate of nutrient solution, the use of special species of sulfur-oxidizing bacteria, surveying of possible microbial inhibitors like sulfate concentration, and development of a comprehensive model to improve performance prediction for full-scale studies.

2.2. Absorption

Acid gas removal by absorption into a liquid solvent has been the dominant technique applied for purifying fuel gases since the 20th century. Based on the strength of the interactions between the solvent and H_2S, the absorption mechanism can be classified as either chemical or physical. Although chemical absorption is characterized by strong interactions, it is limited by stoichiometry. On the other hand, physical absorption has virtually no solubility limits. Chemical absorption is typically observed at low pressures while physical absorption is observed at high pressures. Therefore, physical solvents are preferred over chemical solvents at high partial pressures or concentrations of H_2S in the feed gas (e.g. syngas cleaning). While the regeneration of chemical solvents is achieved by the application of heat in a desorption column, the regeneration of physical solvents can be achieved by a simple pressure/temperature swing operation over one or more flash tanks, by air stripping or by the application of heat in a column, depending on the gas quality requirements. In general, a sharp distinction between physical and chemical absorbents is not always possible since all solvents exhibit physical interactions with a solute. Therefore, absorption technologies are instead reviewed by classifying them into five main types: common physical solvents, alkanolamines, ionic liquids, deep eutectic solvents, and hybrid blends.

2.2.1. Common physical solvents

Physical solvents for acid gas removal are typically polar molecules that have positive and negatively charged portions that weakly interact with the polar H_2S and CO_2 molecules with no chemical reaction. These absorption processes typically operate at low temperatures (may require refrigeration), high pressures (>50 bar), and high partial pressures of H_2S (>3 bar). Physical solvents also tend to absorb carbonyl sulfide (COS), organic sulfides (RSH), and heavy hydrocarbons (particularly 5+ carbons and aromatics). Therefore, if the concentration of heavy hydrocarbons is not negligible, this process may not be suitable. As a result, physical solvents have seen a significant adoption in syngas purification and a relatively limited application in natural gas sweetening. The most commonly used physical solvents are methanol (Rectisol), dialkyl ethers of polyethylene glycol (Selexol, Coastal AGR II, and Genosorb), sulfolane, N-methyl-2-pyrrolidone (NMP) (Purisol), propylene carbonate (Fluor Solvent), and morpholine derivatives (Morphysorb) [80].

Rectisol and Selexol are the most common physical solvent processes due, in part, to their ability to provide deep removal: sweet gas concentration of about 0.1 ppm of H_2S and COS with Rectisol and about 1 ppm with Selexol. This capability for deep contaminant removal makes them, especially Rectisol, ideal for applications in chemical synthesis, which typically requires <1 ppm of sulfur compounds. Rectisol requires a high refrigeration duty and water washing to recover methanol from effluent streams. These additional steps add cost and complexity compared to other physical solvents. It exhibits high volatility and low H_2S selectivity over CO_2. Selexol offers low vapor pressure, high thermal and chemical stability, HCN removal, dehydration, and selective H_2S removal. However, it has high viscosity which reduces mass transfer rates and tray efficiencies, especially at reduced temperatures. Purisol has a relatively higher vapor pressure compared to Selexol and Fluor Solvent and requires water washing to recover lost solvent. However, it has the highest selectivity among the conventional physical solvents for H_2S over CO_2. This makes it highly suitable for the purification of syngas with high CO_2 content. Fluor Solvent is suitable for bulk CO_2 removal with little to no H_2S present in the feed. It provides high hydrocarbon and hydrogen recoveries and has low solvent losses. Morphysorb has high volatility and high H_2S selectivity [81].

2.2.2. Alkanolamines

For nearly a century, alkanolamines largely symbolized chemical or reactive absorption of acid gases [82]. Due to the extensive research that uncovered their absorption–desorption characteristics and the subsequent widespread industrial adoption for natural gas sweetening, absorption of CO_2 and H_2S using alkanolamines stands out as the most mature technology available for this purpose [83–85]. The mechanism follows the formation of bisulfide and sulfide ions at a pH range of 8–10.

$$H_2S + H_2O \rightarrow HS^- + H_3O^+ \quad (9)$$

$$HS^- + H_2O \rightarrow S^{2-} + H_3O^+ \quad (10)$$

$$R_1R_2R_3NH^+ + H_2O \rightarrow R_1R_2R_3NH + H_3O^+ \quad (11)$$

Monoethanolamine (MEA), diethanolamine (DEA), diglycolamine (DGA), diisopropylamine (DIPA), triethanolamine (TEA), 2-amino-2-methyl-1-propanol (AMP) and *N*-methyldiethanolamine (MDEA) are few of the most commonly used absorbents. In addition to the non-commercial solvents, countless commercial formulations are available, such as FLEXSORB series, OASE series, ADEG, ADIP, UCARSOL series, GAS/SPEC series, etc. However, the choice of an amine or an amine blend depends on several different factors, such as lean amine loading, rich amine loading, cyclic loading capacity, rates of absorption and desorption, desired selectivity for H_2S over CO_2, etc. In general, primary (e.g. MEA) and secondary (e.g. DEA) amines are much more reactive towards both H_2S and CO_2, while sterically hindered (e.g. AMP) and tertiary (e.g. MDEA) amines are less reactive but more selective towards H_2S.

MEA is the most used and studied alkanolamine for acid gas removal due to its high reactivity, low cost, ease of reclamation, and low solubility of hydrocarbons. These advantages resulted in MEA being the first-choice solvent for several decades. The disadvantage of MEA is the large

enthalpy of reaction with carbon dioxide, high degradation, high corrosivity, high volatility, no H_2S selectivity, and the formation of a stable carbamate that limits its absorption capability [86,87]. DEA has largely the same advantages as MEA with lower corrosivity and higher vapor pressure [88]. Abdulrahman and Sebastine [89] studied the effect of MEA, DEA, and MDEA on natural gas sweetening and recommended 35 wt% DEA as the best solvent for cost-effective and simultaneous removal of CO_2 and H_2S. However, MDEA has gained a significant share of the market in the past two decades due to its several advantageous properties relative to MEA and DEA: high selectivity for H_2S over CO_2, high loading capacity, low solvent vapor pressure, low corrosivity, high degradation resistance, and efficient energy utilization [90–93]. In addition, MEA and DEA form highly stable carbamates in reaction with CO_2, resulting in a low rate of hydrolysis to bicarbonate. This phenomenon reduces the H_2S uptake of the amines and limits the loading of CO_2 to about 0.5 mol of CO_2 per mole of amine [94]. On the other hand, sterically hindered amines form unstable carbamates while tertiary amines do not form any carbamates, making them advantageous over primary and secondary amines.

In the quest to improve the absorption performance of H_2S over that achieved with MDEA, various amines (especially, sterically hindered amines) and amine blends have received increased attention over the years. Mandal et al. [95] demonstrated that the H_2S absorption performance of AMP is only slightly worse than that of MDEA. Lu et al. [96] reported that an aqueous blend of 1.5 kmol/m^3 MDEA + 1.0 kmol/m^3 2-(*tert*-butylamino)-2-ethoxyethanol (TBEE) provides a superior performance compared to aqueous MDEA (2.5 kmol/m^3) towards selective H_2S absorption regardless of the operational conditions considered. They concluded that primary and secondary sterically hindered amines, such as TBEE and AMP, possess properties similar to those of tertiary amines. More recently, Du et al. [97] and Li et al. [98] tested aqueous solutions of 2-(*tert*-butylamino) ethanol (TBE) and AMP towards selective absorption of H_2S from a feed gas containing 85% CO_2 and 15% H_2S. TBE is more sterically hindered and has lower molecular weight than AMP, and this structural difference presents itself in the results. At low amine concentrations, AMP performs better in terms of selectivity of H_2S and absorption rates of H_2S and CO_2. As the amine concentration increased, TBE takes over as the better solvent with better selectivity at the same H_2S removal efficiency. The authors observed that the selectivity of both solvents initially increases and then decreases with an increase in the gas–liquid contact time. Selectivity also decreases with increasing absorption temperature. These patterns are consistent with the data reported in the literature and with known kinetic and thermodynamic insights. Shoukat et al. [99] studied various aqueous and non-aqueous solutions of twelve different amines for hydrogen sulfide removal from natural gas at temperatures relevant to subsea operation. The non-aqueous amines are based on monoethylene glycol (MEG) and triethylene glycol (TEG). They reported several tertiary amines that can provide better H_2S loading than MDEA in aqueous solutions: 2-dimethylaminoethanol, 3-dimethylamino-1-propanol, 3-(diethylamino)-1,2-propanediol, 2-[2-(diethylamino)ethoxy]ethanol (DEAE-EO), 6-dimethylamino-1-hexanol, and 3-diethylamino-1-propanol. In addition, a few general observations from their results are:

- A decrease in the number of hydroxyl groups and the addition of an ethoxy group in amines increase the H_2S absorption in aqueous amine solutions.
- The H_2S absorption generally increases with increasing pKa. However, this is not always the case, questioning the longstanding assumption that higher basicity implies higher acid gas loading.
- An increase in the chain length of the alkyl group reduces the H_2S loading in aqueous ethanolamines but enhances the H_2S loading in aqueous propanolamines.
- Even though replacing water with TEG or MEG significantly decreased the H_2S loading in all tested solvents, the non-aqueous solution of (DEAE-EO) in MEG showed higher loading than aqueous MDEA at same weight concentration.

When an aqueous amine blend is formed by adding a small quantity of a compound to the base amine, the former is referred to as an activator or a promoter. These promoters are likely not practical or advantageous to deploy on their own and, therefore, used as additives to improve the performance of the base amine. A well-known example of such an activator is piperazine (PZ) which has a high resistance for thermal and oxidative degradation [100]. Lin et al. [101] and Sheng et al. [102] reported that PZ has a higher rate of reaction with CO_2 than the commonly used absorbents such as MEA, DEA, AMP, and MDEA. However, PZ has a low aqueous solubility and is relatively expensive [103]. Therefore, it is usually employed as an additive. In addition, the blends of PZ and most amines exhibit lower volatility than single amines due to the non-ideality of the mixed amine solution [104,105].

Yunhai et al. [106] compared aqueous solutions of MEA, MDEA, MEA + MDEA, and MEA + MDEA + PZ for H_2S absorption from pipeline natural gas that was supplemented with H_2S during experiments. The ability of H_2S absorption for the four systems is MEA > (MEA-MDEA-PZ) > (MEA-MDEA) > MDEA, demonstrating that addition of PZ increases the loading of H_2S. However, this is not the case when both CO_2 and H_2S are present in the feed gas. Zhan et al. [107] studied the effect of different operating conditions on the simultaneous absorption of H_2S and CO_2 into an aqueous solution of MDEA and PZ in a rotating packed bed. Due to the higher reaction rate between PZ and CO_2 relative to that between MDEA and CO_2, the removal efficiency of CO_2 increased with an increase in the concentration of PZ. On the other hand, this led to a decrease in the removal efficiency of H_2S. Haghtalab and Izadi [108] also observed this phenomenon in aqueous MDEA + PZ and DIPA + PZ solutions in terms of reduced H_2S loading with addition of PZ.

Lee et al. [109] carried out absorption–desorption of CO_2 and H_2S from a feed gas containing 35% CH_4, 15% CO_2, 50 ppmv H_2S, and N_2 using 11 different aqueous blends of 4.5 wt% MDEA and 5 wt% additive. The additives considered are PZ, AMP, tetraethylenepentamine, diethylenetriamine, 1-dimethylamino-2-propanol, bis(3-aminopropyl)amine (APA), 2-amino-1-butanol, 5-amino-1-pentanol, *N*-propylethylenediamine, dibutylamine, and 1,4-diaminobutane. They are screened based on lean loading, rich loading, cyclic capacity, absorption rate, and regeneration rate. The results showed that PZ is an excellent activator for CO_2 absorption but is poor in the case of H_2S. Overall, APA provides the best performance for H_2S absorption, although it does not exhibit selectivity for H_2S over CO_2 at high enough gas–liquid contact times. When compared to aqueous MDEA, the aqueous blend of MDEA and APA exhibit higher absorption–desorption rates for H_2S, lower absorption–desorption rates for CO_2, and higher H_2S loading capacity. On the other hand, it also exhibits slightly higher capacity for CO_2.

Zhan et al. [107] also found that increasing MDEA concentration over 1.68 mol·L^{-1} in an aqueous MDEA + PZ solution drastically reduces the removal efficiency of CO_2 while also reducing the removal efficiency of H_2S to a lesser extent. Foo et al. [110] and Fu et al. [111] reported that increasing the MDEA concentration increased the solution viscosity. The increasing viscosity inevitably hinders the diffusion of amine molecules in the liquid phase, lowering the absorption rate and capacity of the solvent. Tian et al. [112] reported a similar deteriorating performance of an aqueous MDEA + MEA solution with increasing MDEA concentrations at low H_2S partial pressures. Therefore, there exists an optimal MDEA concentration that provides the best absorption capacity for H_2S for a given MDEA-based solvent. However, the impact of solvent viscosity is much higher on the absorption of CO_2 than that of H_2S; while H_2S absorption is limited by the gas-side mass transfer, CO_2 absorption is limited by the liquid-side mass transfer and reaction kinetics [95,96,113].

Table 3 provides many representative examples of the recent trends in the published works on H_2S absorption using alkanolamines. Unless otherwise noted, the reported experimental results are obtained using

Table 3
Recent developments in hydrogen sulfide absorption.

Solvent	Feed	Amount or Partial Pressure of H_2S	Loading or Solubility (mol/mol)	Removal Efficiency (%)	Reference
Alkanolamines					
30–50 wt% MDEA + 0.0–7.5 wt% MEA	Simulated coke oven gas at 1 atm and 303.2–323.2 K	0.3–0.5 kPa	0.022–0.096	313.2 K, 0.5 kPa H_2S: 93.61–95.88 (6 sieve trays)	[112]
3.5–11.6 wt% MEA	Pipeline natural gas with added H_2S at 298.15–333.15 K	0–45 kPa	~0.1–1.0	na	[106]
19.0–46.3 wt% MDEA		1–50 kPa	~0.05–0.85	na	
3.5–8.5 wt% MEA + 19.0–36.3 wt% MDEA		1–50 kPa	~0.01–0.90	na	
5.6 wt% MEA + 26.3 wt% MDEA + 3.0–7–0 wt% PZ		4–55 kPa	~0.09–0.95	na	
20 wt% MDEA	N_2 and H_2S at 278.15–313.15 K	0.03–1 kPa	0.015–0.254	278.15 K: 100	[99]
20 wt% MDEA in MEG	N_2 and H_2S at 278.15 K	0.03 kPa	0.010	278.15 K: 77	
		1 kPa	0.089		
20 wt% MDEA in TEG	N_2 and H_2S at 278.15 K	0.03 kPa	0.006	278.15 K: 17	
		1 kPa	0.040		
20 wt% t-BDEA	N_2 and H_2S at 278.15 K	0.03 kPa	0.009	na	
		1 kPa	0.407		
20 wt% DIPA	N_2 and H_2S at 278.15 K	0.03 kPa	0.012	na	
		1 kPa	0.185		
20 wt% TEA	N_2 and H_2S at 278.15 K	0.03 kPa	0.013	na	
		1 kPa	0.165		
20–50 wt% DEAE-EO	N_2 and H_2S at 278.15–313.15 K	0.5–1 kPa	0.094–0.416	278.15 K, 20 wt% amine: 100	
20 wt% DEAE-EO in MEG	N_2 and H_2S at 278.15 K	1 kPa	0.280	278.15 K: 76	
20 wt% DEAE-EO in TEG	N_2 and H_2S at 278.15 K	1 kPa	0.073	278.15 K: 21	
20–50 wt% 3DEA-1P	N_2 and H_2S at 278.15–313.15 K	0.5–1 kPa	0.061–0.355	278.15 K, 20 wt% amine: 100	
20 wt% 3DEA-1P in MEG	N_2 and H_2S at 278.15 K	1 kPa	0.193	278.15 K: 57	
20 wt% 3DEA-1P in TEG	N_2 and H_2S at 278.15 K	1 kPa	0.080	278.15 K: 24	
0.84–2.94 mol/L MDEA + 0.12–0.58 mol/L PZ	CO_2 and H_2S at 1 atm and 302.95–318.15 K	10,000 ppmv	na	100 (rotating packed bed)	[107]
10–30 wt% TBE	CO_2 and H_2S at 298.15–318.15 K	15 vol%	na	50–94	[97,98]
10–30 wt% AMP				65–95	
Ionic Liquids					
$[N_{2224}]_2$[maleate]	H_2S at 313.2 K	1.1 bar	1.43	na	[176]
$[N_{2224}]_2$[maleate] + maleic acid (1:1)		1.18 bar	1.3	na	
[BDMAEEH][Tf_2N] + MAA (1:1)		1.18 bar	0.8	na	
[BDMAEEH][MAA]		1.18 bar	1.0	na	
[BDMAEEH][Tf_2N]		1.1 bar	0.4	na	
[DBNH][1,2,4-triaz]	H_2S at 298.2 K	1 bar	1.4	na	[175]
	H_2S at 313.2 K	0.012–1.019 bar	0.253–1.198	na	
	H_2S at 333.2 K	1 bar	1.0	na	
[DBNH][1,2,3-triaz]	H_2S at 313.2 K	0.016–1.089 bar	0.287–1.081	na	
[DBUH][1,2,4-triaz]		0.022–1.025 bar	0.447–1.174	na	
[DBUH][1,2,3-triaz]		0.022–1.028 bar	0.412–1.046	na	
[DBNH][Im]	H_2S at 298.2 K	0.1 bar	1.18	na	[177]
		0.01–1 bar	0.63–1.36		
	H_2S at 313.2 K	0.1 bar	0.95		
		0.01–1 bar	0.40–1.26		
	H_2S at 333.2 K	0.01–1 bar	0.27–1.08		
[DBUH][Im]	H_2S at 313.2 K	0.1 bar	0.98	na	
		1 bar	1.26		
[DBNH][Pyr]		0.1 bar	0.99	na	
		1 bar	1.31		
[DBUH][Pyr]		0.1 bar	0.95	na	
		1 bar	1.17		
[TMGH][PhO]	H_2S at 298.2 K	0.1 bar	0.69	na	[172]
		0.01–1 bar	0.38–0.97		
	H_2S at 313.2 K	0.1 bar	0.56		
		0.01–1 bar	0.20–0.85		
	H_2S at 333.2 K	0.1 bar	0.47		
		0.01–1 bar	0.08–0.78		
[DBUH][PhO]	H_2S at 313.2 K	0.1 bar	0.6	na	
		1 bar	0.8		
[hmim][PhO]		0.1 bar	0.59	na	
		1 bar	0.84		
[P_{4444}][PhO]		0.1 bar	0.62	na	
		1 bar	0.88		
40–70 wt% [BDMAEE][Ac]	H_2S at 298.2 K	1 bar	0.950–1.044	na	[170]
[NEMH][Bu]	H_2S at 298.2 K	0.035–1.056 bar	0.012–0.156	na	[168]
	H_2S at 308.2 K	0.056–1.070 bar	0.008–0.114		
	H_2S at 318.2 K	0.030–1.050 bar	0.007–0.098		
[NEMH][Ac]	H_2S at 298.2 K	0.042–1.060 bar	0.009–0.127	na	
[NEMH][Pro]		0.037–1.057 bar	0.011–0.151	na	
[NEMH][MOAc]		0.043–1.059 bar	0.010–0.142	na	

(*continued on next page*)

Table 3 (*continued*)

Solvent	Feed	Amount or Partial Pressure of H_2S	Loading or Solubility (mol/mol)	Removal Efficiency (%)	Reference
[TEAH][Bu]		0.040–1.096 bar	0.009–0.135	na	
[TEAH][MOAc]		0.056–1.015 bar	0.010–0.138	na	
[C_4Py][BF_4]	H_2S at 313.15 K	1 bar	0.07	na	[154]
[C_4Py][SCN]			0.1	na	
[emim][BF_4]	H_2S at 298.15 K	0.3 kPa – 1.4 Mpa	0–1.46	na	[155]
	H_2S at 313.15 K	0.3 kPa – 1.84 Mpa	0–1.26	na	
	H_2S at 333.15 K	0.3 kPa – 1.82 Mpa	0–0.674	na	
	H_2S at 353.15 K	0.3 kPa – 1.76 Mpa	0–0.425	na	
Deep Eutectic Solvents					
ChCl/urea (1:1.5)	H_2S at 313.2 K	0.114–2.021 bar	0.0037–0.055	na	[212]
	H_2S at 323.2 K	0.106–2.011 bar	0.0025–0.046		
	H_2S at 333.2 K	0.098–2.015 bar	0.0021–0.037		
	H_2S at 353.2 K	0.10–1.98 bar	0.0014–0.023		
ChCl/urea (1:2.0)	H_2S at 313.2–353.2 K	0.101–2.021 bar	0.0015–0.046	na	
ChCl/urea (1:2.5)	H_2S at 313.2–353.2 K	0.099–2.013 bar	0.0011–0.035	na	
TBAB/ProH (1:1)	H_2S at 298 K	245 kPa	0.40	na	[213]
		496 kPa	0.60		
TBAB/AcH (1:1)		225 kPa	0.32	na	
		511 kPa	0.59		
TBAB/ForH (1:1)		178 kPa	0.21	na	
		506 kPa	0.55		
ChCl/ProH (1:2)		184 kPa	0.13	na	
		540 kPa	0.44		
ChCl/AcH (1:2)		249 kPa	0.16	na	
		522 kPa	0.33		
ChCl/ForH (1:2)		262 kPa	0.12	na	
		510 kPa	0.25		
[C_4-TMHDA][Cl]/Im (1:2)	H_2S at 303.2 K	1 bar	0.996	na	[214]
[C4-TMPDA][Cl]/Im (1:2)			0.482	na	
[C_4-TMEDA][Cl]/Im (1:2)			0.364	na	
[C_4-TMEDA][Cl]/1,2,4-triaz (1:2)			0.273	na	
[C_4-TMEDA][Cl]/1,2,3-triaz (1:2)			0.239	na	
[C_4-TMHDA][Cl]/Im (1:2)	H_2S at 313.2 K	1 bar	0.71	na	
[C_1-TMHDA]Ac/MDEA (1:2)	H_2S at 313.2 K	1 bar	1.44	na	[215]
[C_1-TMHDA]Ac/Pyrol (1:2)			1.17	na	
[C_1-TMHDA]Ac/AA (1:2)			1.09	na	
[C_1-TMHDA]Ac/Im (1:2)			1.02	na	
Hybrid Blends					
30–50 wt% MDEA + 2.5–7.5 wt% [N_{1111}][Arg]	Simulated coke oven gas at 1 atm and 303.2–323.2 K	0.3–0.5 kPa	0.039–0.143	313.2 K, 0.5 kPa H_2S: 100 (4 sieve trays)	[231]
30–50 wt% MDEA + 2.5–7.5 wt% [N_{1111}][Gly]	Simulated coke oven gas at 1 atm and 303.2–323.2 K	0.3–0.5 kPa	0.035–0.98	313.2 K, 0.5 kPa H_2S: 100 (6 sieve trays)	[230]
30–50 wt% DIPA + 5–50 wt% [bmim][Ac]	CO_2 and H_2S at 0.2–2.5 Mpa and 323.15–348.15 K	0.046–0.668 Mpa	0.010–0.153	na	[232]
Benchmarks					
Sulfolane	H_2S at 298.2 K	1 bar	0.072	na	[505]
	H_2S at 313.2 K	1 bar	0.043		
Dimethylsulfoxide	H_2S at 298.2 K	1 bar	0.123		[506]
1-methyl-2-pyrrolidine (NMP)	H_2S at 298.2 K	1 bar	0.0133		[507]
50 wt% MDEA	H_2S at 298.2 K	1 bar	0.944		[508]
	H_2S at 313.2 K	0.1 bar	0.3		
		1 bar	0.85		
	CH_4 and H_2S at 480–604 kPa and 323 K	2.6–177.59 kPa	0.084–0.775		[509]
[bmim][PF_6]	H_2S at 298.15–403.15 K	69–9630 kPa	0.016–0.875		[149]
Methanol	H_2S at 298.15 K	1400 kPa	0.8		[150]
		1 bar	0.027		[510]
TEGDME	H_2S at 313.2 K	1 bar	0.162		[511]

absorption bottles, equilibrium cells or reaction vessels. However, the industrial absorption–desorption operations are carried out in tray or packed columns. The design and operational modes of the employed equipment can have a significant impact on the process performance. For example, gas–liquid contact time and area are important parameters that affect the absorption and selectivity of H_2S over CO_2. In this regard, HiGee technology carried out in a rotating packed bed (RPB) is one of the cutting-edge process intensification technologies that can provide a more precise control over the fundamental transfer phenomena in gas–liquid operations [114]. The efficiency of mass transfer and micromixing can be up to 1–3 orders of magnitude larger than that in a conventional packed bed [114,115].

Zhan et al. [107] used stainless wire mess packing in an RPB to test the absorption performance of an aqueous MDEA + PZ solution for a feed gas containing CO_2 and H_2S. Increasing the high gravity factor (β), which is the ratio of the centrifugal force to the acceleration due to gravity, increases the gas–liquid interfacial area and enhances the mass transfer of both H_2S and CO_2 by breaking the liquid into very fine elements [116]. However, when β is increased beyond a value (122.5 in this experiment), the enhancement in the interfacial area is gradually overshadowed by the decrease in the liquid residence time in the RPB. This led to a further increase in the removal efficiency of H_2S with a simultaneous decrease in the same for CO_2, resulting in an increase of H_2S selectivity. This is consistent with previously reported studies by Qian et al. [113], Guo et al. [117], and Jiao et al. [118]. Increasing the liquid-to-gas flowrate to an optimal value also enhances H_2S absorption

and selectivity by increasing the interfacial refresh rate without increasing the size of the liquid elements. Unlike the regular onshore operation of these gas–liquid contactors, offshore installations face additional technical and operational challenges due to the unstable sea environments. Iliuta and Larachi [119] studied two-phase countercurrent flow dynamics during simultaneous absorption of H_2S and CO_2 into an aqueous MEA solution in a packed bed column with Raschig Super-Rings exposed to static inclination and heaving motion. Although the inclination and the heaving motion decrease the removal efficiencies of both the compounds, the effect is significantly more pronounced for CO_2 and is only marginal for H_2S.

Although experiments offer valuable information on the performance of different absorbents and equipment, they are expensive and time-consuming. Modeling and simulation studies present a cheaper and more systematic alternative to understand and improve existing operations while also guiding lab- and pilot-scale experiments towards fewer and more efficient runs. Many such published works provide suggestions for improvement and optimization of H_2S removal processes based on economic and sustainability parameters [89,120–128]. Zahid et al. [127] used Aspen HYSYS to evaluate the removal of acid gases from the associated and non-associated sour gas feeds using a blend of DGA and MDEA solvents at a total strength of 50 wt%. Their results show that an aqueous blend of 45 wt% DGA and 5 wt% MDEA at a flowrate of around 2800 USGPM can effectively replace 50 wt% DGA for processing of associated gas by reducing the energy consumption by 5.3 GJ/h and the overall gas processing cost by US$3.42/MMSCF of sweet gas. Park et al. [128] performed sensitivity analysis in Aspen Plus to find the optimal operating conditions for a pilot-scale H_2S absorption–desorption column sequence when using a 45 wt% MDEA solution to treat 500 m^3hr^{-1} of coke oven gas containing 0.3% H_2S. They found an optimal solvent-to-feed ratio of 1.3 kg/kg that can achieve 99% H_2S removal while reducing the solvent usage and heat duty of the absorption column by 35% and 23%, respectively.

Accurate thermodynamic modeling forms the backbone of aforementioned simulation studies. Due to extensive amount of experimental data available, many classical thermodynamic models have been fitted to these data and used in different commercially available process simulators [129–132]. Although these models have provided good accuracy in the modeling and optimization of absorption processes, they are restricted to a limited domain of compounds and thermodynamic conditions covered by the data used for model fitting. However, achieving an optimal and novel solvent formulation requires a detailed understanding of the complex molecular and structural interactions that drive the chemistry of H_2S (and CO_2) absorption in alkanolamine-based solvents [83,133,134]. For example, Puxty et al. [83] reported that the distance of the hydroxyl functionality from the amine and the structural features around it appear crucial for the screening of CO_2 absorbents, but they could only speculate the possible reasons behind it. As such, the predictive capabilities of thermodynamic models for the calculation of quantities of engineering interest can be improved with a molecular-based knowledge of these mixtures. Although there has been some work in this area over the past decade for CO_2 absorption [135–138], there are no known works published for selective H_2S absorption or simultaneous H_2S and CO_2 absorption.

Despite the advantages that led to their extensive use in the natural gas industry, there are also difficulties in the commercial use of these alkanolamine-based solvents. These processes suffer from the high amount of energy required for the desorption column, loss of alkanolamine due to its high volatility, transfer of water into the gas outlet during desorption, and degradation of alkanolamine to form corrosive compounds [139]. These drawbacks make this treatment unattractive in terms of economics and sustainability, impeding their widespread implementation outside the oil and gas industry.

2.2.3. Ionic liquids

Ionic liquids (ILs) are defined as fused salts with melting points below 100 °C [140]. However, some recommend dropping the melting point constraint and defining ionic liquids simply as liquids composed only of ions (see Fig. 2) [141]. These liquids present several excellent properties that make them advantageous over organic solvents, such as a high and tunable solvent capacity, low corrosivity, negligible volatility, low flammability, wide liquid range, and relatively high thermal and chemical stability [142,143]. Although ILs have been around for a long time, their use in acid gas removal is less than two decades old [141]. In the past few years, a number of reviews [144–147] were published for CO_2 capture using ILs. However, there has only been one such review [148] for H_2S removal discussed in the context of simultaneous acid gas removal from natural gas. This section specifically focuses on the direct use of ILs as absorbents for H_2S.

Jou and Mather [149] first investigated H_2S absorption in 1-butyl-3-methylimidazolium hexafluorophosphate ([bmim][PF_6]) and reported that it functions as a physical absorbent. They further opined that ILs are unlikely to replace alkanolamines for acid gas removal but would be useful for bulk removal at high partial pressures. Around the same time, Pomelli et al. [150] conducted an experimental and theoretical study on H_2S solubility in different [bmim]-based ILs and in a series of bis(trifluoromethyl)sulfonylimide ([Tf_2N]) based ILs. They reported a poor correlation between Kamlett-Taft parameters and the solubility of H_2S in these ILs. More importantly, they found that the interactions between the anion and H_2S are as strong as traditional hydrogen bonds while the cation selection has little impact on H_2S solubility in ILs. This finding was later confirmed by multiple studies [151–153]. These studies demonstrated that the capacity and regeneration energy of ILs could be adjusted by actively tuning their reaction enthalpy through the design of the anion. Recently, Wang et al. [154] reported that pyridinium-based ILs showed excellent performance in selective separation of H_2S over CO_2 owing to the active proton in H_2S molecule. Their results also indicated that the solubilities of H_2S and CO_2 in ILs slightly increased

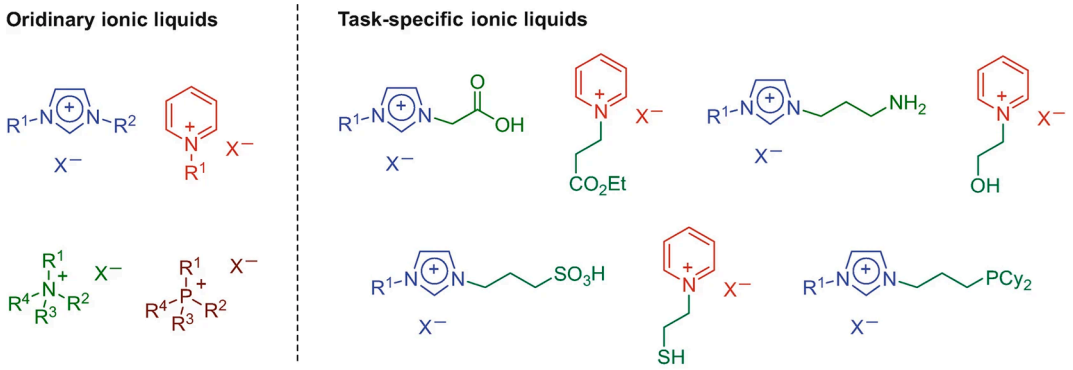

Fig. 2. Examples of ordinary ionic liquids and task-specific ionic liquids. Reprinted with permission from [486]. © 2019 Springer Nature.

with the growing length of the alkyl chains on the cations. The molar solubility of H_2S in these ILs is in the following order: $[C_8Py][SCN] > [C_6Py][SCN] > [C_4Py][SCN] > [C_4Py][NTf_2] > [C_4Py][NO_3] > [C_4Py][BF_4]$. Among the ILs with the same cation, the [SCN] anion exhibited the highest ideal H_2S/CO_2 selectivity up to 8.99 at 303.15 K, which was about 1.5–4 times larger than that of the conventional imidazolium-based ILs. Jalili et al. [155] demonstrated that $[emim][BF_4]$ (also called $[C_2mim][BF_4]$) has H_2S absorption capacity similar to that of other $[BF_4]$-based ILs and can remove H_2S with the same or better selectivity than that of $[C_2mim][eFAP]$ [156], $[C_8mim][Tf_2N]$ [157], $[C_4mim][PF_6]$ [158], and $[C_8mim][PF_6]$ [159]. However, ordinary ILs are physical absorbents and, therefore, have much lower absorption capacities for H_2S (and CO_2) at low–medium partial pressures.

To overcome this challenge and develop viable alternatives to alkanolamines, researchers turned towards task-specific ionic liquids (TSILs), which are formed from the covalent tethering of a functional group to the cation or to the anion or to both ions of an otherwise ordinary IL [160,161]. The addition of one or more tethered functional groups provides TSILs with increased structural tunability over their physicochemical properties. One such property is the chemical interaction with H_2S, allowing them to have a much higher absorption capacity than ordinary ILs. Huang et al. [162] reported the first class of carboxylate-functionalized, task-specific imidazolium-based ILs with a high capacity for H_2S. The H_2S solubility can reach up to about 0.6 mol/mol at 298 K and 1.0 bar, an order of magnitude higher than those of ordinary ILs. However, these functionalized ILs also have high chemical affinity to CO_2 through the formation of a carbene-CO_2 adduct, resulting in an unsatisfactory H_2S/CO_2 selectivity of only 1–2 at 298.2–333.2 K. Huang et al. [163] then designed a series of dual Lewis base (DLB) functionalized ILs tethered with both carboxyl and tertiary amine groups on their anions to enhance the ideal selectivity of H_2S over CO_2. These DLB-ILs exhibit similar or higher H_2S absorption capacities than 35 wt% aqueous MDEA. For example, triethylbutylammonium imidazole-1-yl-acetate ($[N_{2224}][IMA]$) has a H_2S solubility of 0.85 mol/mol and a H_2S/CO_2 selectivity of 10 at 298 K and 1 bar. Due to the very weak acid-base interaction between the DLB-ILs and CO_2, the ideal selectivity of H_2S over CO_2 is significantly higher with values at 60 °C ranging from 29 to 70 at 0.1 bar and from 13 to 26 at 1 bar. However, they suffer from high viscosity (>2500 cP at 298 K) and complex synthesis. As noted in the previous section, viscosity has a significant impact on hydrodynamics and mass transfer. A key limitation of ILs is their high viscosity, which primarily hinders the liquid-side mass transfer and indirectly leads to slow diffusion of gas molecules across the interface. The process then requires longer contact times and an increase in the size of the absorption column. Moreover, higher viscosity results in a higher cost of initial solvent inventory and a higher pumping load. Therefore, it is imperative to find ways to make ILs with viscosities suitable for absorption.

Subsequently, Huang et al. [164] combined alkanolamines (MDEA and DMEA) with formic acid and acetic acid to synthesize cost-effective protic ionic liquids (PILs) [165–167] with high ideal selectivity (8.9–19.5 at 303.2 K) for H_2S over CO_2. Although these PILs have viscosities lower than the DLB-ILs, they proved to be physical absorbents with higher H_2S absorption capacities (0.04–0.16 at 1 bar of H_2S and 303.2–333.2 K) than ordinary ILs. Similarly, Zhao et al. [168] investigated ten carboxylate-functionalized PILs with cations based on amines and morpholine derivatives. These PILs have very low viscosities (as low as 4.3 cP at 298.2 K) and high H_2S physical absorption capacities. However, trimethylamine butyrate is the only one with a thermal decomposition temperature above 50 °C, making the rest likely impractical for recycling within the process. Huang et al. [169] studied a novel class of hydrophobic PILs with a free tertiary amine group tethered to a tertiary ammonium cation paired with Tf_2N as anion for highly selective chemical absorption of H_2S from CO_2. The authors suggested that the higher the alkalinity of the free tertiary amine group, the higher the solubility of H_2S due to the strong acid-base interactions or proton transfer reaction. In these ILs, as the free tertiary amine gets closer to the positively charged center of the cation, the increasing electron-withdrawing effect reduces the alkalinity of the functional group. The interaction between the free tertiary amine group and CO_2 in these PILs follows the same behavior as in the DLB-ILs due to the absence of active protons. Their results demonstrate that the absorption of CO_2 is both chemically and physically unfavorable in comparison with the absorption of H_2S. On the other hand, these hydrophobic PILs are cost-intensive and have large molecular weights (low absorption capacity in units of mol/kg), making them economically unfavorable. Similar PILs with a free tertiary amine group but with a carboxylate ion were then formed to make the PILs hydrophilic and use aqueous PILs as the absorbents [170]. The solubilities of H_2S and CO_2 in the studied PILs follow the sequence of [BDMAEE][Ac] > [TMPDA][Ac] ≫ [TMEDA][Ac] > [BMEE][Ac]. The solubilities of both gases decrease with increasing PIL concentration or temperature, but the dependence of CO_2 solubilities on the PIL concentration or the temperature is more significant than H_2S solubilities. Mixing with water reduces the viscosity of PILs largely. For example, the viscosities of 40–70 wt% aqueous [BDMAEE][Ac] fall in the range of 8.02–48.0 cP at 293.2 K and are comparable to those of aqueous MDEA [171]. Although these aqueous PILs exhibit high H_2S absorption capacities (up to 1.044 mol/mol at 1 bar and 298.2 K), the equilibrium selectivities are only 1–2 which is on par with ordinary ILs, carboxylate-based ILs, and aqueous MDEA but much inferior to the PILs mentioned above. On the other hand, the kinetic selectivity of H_2S is still quite high.

Huang et al. [172] then moved towards a theoretical and experimental study of phenolic ILs due to the strong basicity of the anion. These ILs enhance the solubility of polar gases (H_2S and CO_2) and reduce the solubility of non-polar gases (CH_4), causing an enhanced selectivity for CO_2/CH_4 and H_2S/CH_4 [173]. As such, these ILs show comparably high absorption capacities for H_2S with the solubilities of H_2S approaching 0.60 mol/mol at 0.1 bar and 0.85 mol/mol at 1 bar. The absorption isotherms indicate that there must be a strong interaction between [PhO] and H_2S. On the other hand, it is surprisingly found that these phenolic ILs show varied absorption capacities for CO_2: $[P_{4444}][PhO] > [hmim][PhO] > [DBUH][PhO] > [TMGH][PhO]$. For example, $[P_{4444}][PhO]$ can absorb as high as 0.77 mol/mol of CO_2 at 1 bar, while [hmim][PhO], [DBUH][PhO] and [TMGH][PhO] can absorb only 0.62, 0.21 and 0.090 mol/mol of CO_2 at the same pressure. This wide variation in CO_2 solubilities indicates that the cations affect CO_2 absorption chemistry. Based on the experimental results, the authors deduced that the strong interaction of phenolic ILs with H_2S is independent of the hydrogen-bond donating ability of cations, while the interaction of phenolic ILs with CO_2 is highly dependent on the hydrogen-bond donating ability of cations. Calculations based on density functional theory confirmed that the hydrogen-bond donating ability of cations differentiates the interaction of phenolic ILs with H_2S and CO_2. Since the active protons of H_2S can form relatively stable coplanar structures with the strongly basic [PhO] anion, the IL-H_2S is dominated by this proton transfer mechanism with the hydrogen-bond donating ability of cations having a negligible impact. This finding is consistent with several other studies [150,153,174]. However, CO_2 is non-ionizable and the angular CO_2 forms relatively unstable non-coplanar structures with [PhO], making the interaction of phenolic ILs with CO_2 rather sensitive to the hydrogen-bond donating ability of cations. Phenolic ILs with weak hydrogen bond donors in the cation can interact with CO_2 strongly by restructuring the hydrogen bond network between the ions of the IL. However, if the cation has strong hydrogen bond donation centers, they can only interact with CO_2 very weakly since they form strong hydrogen bonds with [PhO]. Thus, phenolic ILs allow for highly efficient and selective absorption of H_2S from CO_2 with appropriate combination of the strong anionic basicity and cationic hydrogen bond donation. For example, [TMGH][PhO] stands out as a promising candidate for the selective capture of H_2S. The high solubilities of H_2S in [TMGH][PhO] are due to the strong basicity of [PhO], while the high selectivities (9.4 at 1 bar and 313.2 K) of H_2S/CO_2 in [TMGH][PhO] are due to the strong

hydrogen bond donors of [TMGH]. However, the downsides of these ILs are their high viscosities (125.7–435.1 cP at 303.2 K) and the poisonous nature of phenolic compounds.

Zhang et al. [175] investigated the use of four azole-derived PILs that are easily synthesized in a one-step neutralization reaction. The mechanism of absorption of both H_2S and CO_2 in these PILs is observed to be the similar to that observed in phenolic ILs. The H_2S absorptions capacities in mol/mol units (mol/kg in parenthesis) of [DBNH][1,2,4-triaz], [DBNH][1,2,3-triaz], [DBUH][1,2,4-triaz], and [DBUH][1,2,3-triaz] can reach up to 1.20 (6.21), 1.09 (5.64), 1.15 (5.20), and 1.05 (4.74), respectively, at 313.2 K and 1.0 bar. In comparison, H_2S loading of 50% aqueous MDEA at the same conditions is 0.85 mol/mol and 3.56 mol/kg. These PILs also exhibit high H_2S solubilities at low pressures. In addition, they exhibit remarkably high kinetic and thermodynamic selectivities for H_2S/CH_4 and CO_2/CH_4. However, [DBNH][1,2,3-triaz] and [DBUH][1,2,4-triaz] have high viscosities, while [DBUH][1,2,3-triaz] has a melting point of 313.2 K, making them impractical for industrial use. Due to its lower viscosity (42.6 cP at 313.2 K), [DBNH][1,2,4-triaz] proves another promising absorbent for H_2S removal. Zhang et al. [176] later synthesized different PILs for capture and conversion of H_2S into value-added mercaptan acids. The conversion step replaces both the conventional desorption step and the subsequent Claus process, pitching a potentially new and advantageous process for H_2S removal. Although more work is necessary to probe this process pathway, their work also presented a few new TSILs with either a free tertiary amine group tethered to the tertiary ammonium cation or a free carboxylic acid group tethered to the carboxylate anion, which exhibited the highest relative (mol/mol) H_2S absorption capacities reported in the literature so far. However, since viscosities and selectivities are not reported, further analysis is not possible at this time. Xiong et al. [177] developed four low viscosity superbase-derived PILs (SPILs) [178] for the simultaneous removal of H_2S and CO_2 from natural gas. These SPILs offer the highest absolute (mol/kg) H_2S absorption capacities reported so far in the literature at even low H_2S concentrations (5.31–6.81 mol/kg at 1 bar and 4.31–5.15 mol/kg at 0.1 bar and 313.2 K) and excellent ideal selectivity for CO_2/CH_4 (92.6–240) and H_2S/CH_4 (367–653). [DBNH][Im], [DBNH][Pyr], [DBUH][Im], and [DBUH][Pyr] show dynamic viscosity values as low as 8.3 cP, 5.1 cP, 18.3 cP, and 9.7 cP at 313.2 K, respectively, significantly lower than those reported for most ILs. These numbers are better than those of 50% aqueous MDEA. Owing to their low viscosities and high absorption capacities, these SPILs may be great alternatives to aqueous alkanolamines currently reported. However, due to their low first decomposition temperature of around 353 K and strong interaction with H_2S, they require a low regeneration pressure (0.005 bar) and lose a portion of their H_2S capacity (25% loss for [DBNH][Im]) after four regeneration cycles.

In summary, TSILs made of strongly basic anions could result in chemisorption of H_2S while those made of weakly basic anions may or may not offer the same effect. However, addition of one or more Lewis basic sites (such as a tertiary N-group or a carboxyl group) is much more likely to result in strong H-bonding with H_2S. A free tertiary amine group on the cation could also lead to an increase in the chemisorption capacity of the IL. However, this tertiary amine group should be ideally placed further away from the positively charged center of the cation to avoid an electron-withdrawing effect that reduces the basicity of the N-group. Selectivity of H_2S over CO_2 is heavily dependent on two factors: cationic H-bond donation (stronger the better) and anionic basicity (stronger the better). Moreover, absorption capacities in both relative (mol/mol) and absolute (mol/kg) units must be considered during material selection. Although relative capacity is a good measure of stoichiometric efficiency, absolute capacity has a crucial impact on process economics.

As showcased so far, there are a wide variety of ILs that can be designed for the capture of H_2S from gaseous streams at different conditions. Most of these studies still focus on the experimental measurement of single gas solubility in ILs [179], covering only a limited proportion of the design space characterized by all the possible cation–anion combinations. Casting the net over a much wider search space with the experimental approach is not only unrealistic but also expensive in terms of time and cost. In this context, predictive thermodynamic models based on computational chemistry or group contribution methods or a combination of both have been developed and applied for theoretical IL screening or design [180–183].

Mortazavi-Manesh et al. [180] extended the experimental solubility of acid gases by comparing 425 ILs using the conductor-like screening model for realistic solvation (COSMO-RS) [184,185] and the Peng-Robinson equation of state [186]. They demonstrated that the variance in the molecular weight or area of the anion is twice that of the same properties of the cation, concluding that solubilities within these ILs are more sensitive to the anion. They also deduced the various factors that could improve the solubility and selectivity of H_2S and CO_2 in ILs. Their results suggest that ILs with higher molecular surface areas have higher absorption capacities of H_2S and C_2H_6, but ILs with higher molecular weights also dissolve more CH_4. They suggested that the most promising IL candidates contain N_{4111}, PMG, and TMG as cations and BF_4, NO_3, and CH_3SO_4 as anions. Zhao et al. [182] also used COSMO-RS and demonstrated a systematic screening method to choose from over ten thousand ILs, but it was not applied for H_2S absorption.

While a preliminary screening based on thermodynamic and physical properties is helpful to narrow down the list of possible choices from a large number of ILs, the optimal IL absorbent should be identified based on its performance in a continuous process. Process simulators are widely used for such purposes. Santiago et al. [187] employed COSMO-RS for a preliminary screening of over 700 ILs and then used Aspen Plus for the simulation of the physical absorption process with selected ILs. They found that the process is strongly controlled by kinetics even though all the selected ILs have no thermodynamic restrictions (>99% equilibrium-based H_2S recoveries). The IL that shows the best thermodynamic behavior ([emim][$MePO_3$]) faces severely limited transport phenomena, resulting in very low H_2S recovery at near room temperatures. On the other hand, the IL that provides the best process performance ([emim][DCN]) has much lower viscosity (16.83 cP vs. 149.12 cP at 25 °C), highlighting the importance of absorption rates which are usually not reported in most experimental studies. Lemus et al. [188] extended this methodology to IL blends (one with a high H2S solubility and one with low viscosity) and found that solvent viscosity remains the key property even in IL blends. As a result, they did not succeed in formulating IL–IL blends with enhanced thermodynamic/kinetic properties for H_2S physical absorption, obtaining the best behavior with the pure ILs with the lowest viscosity. The authors then separately created an IL blend of a chemical absorbent with a high H_2S absorption capacity ([bmim][Ac]) and a physical absorbent with the lowest viscosity ([emim][DCN]) and found that this IL blend results in an enhanced absorption behavior forming a favorable compromise between thermodynamic and kinetics. A blend of 25% [bmim][Ac] + 75% [emim][DCN] at 10 bar of pressure offers the maximum H_2S recovery of >98%. Wang et al. [189] developed a more systematic, four-step screening method to find the optimal IL absorbents for simultaneous removal of H_2S and CO_2 from natural gas. The prospective candidates are sequentially screened based on an integrated mass-based Absorption-Selectivity-Desorption index (ASDI) derived from the Henry constants in the first step, ASDI derived from vapor-liquid equilibrium data in the second step, physical properties (melting point and viscosity) in the third step, and rate-based Aspen Plus simulation in the fourth step. Based on this method, 1-butyl-

1-methyl-pyrrolidinium dihydrogen phosphate ([BeMPYO][H_2PO_4]) and 1-ethyl-3-methylimidazolium dihydrogen phosphate ([emim][H_2PO_4]) are identified as the two best absorbents for this task.

In addition to IL screening methods, technical and economic comparisons between IL-based processes and the industrially established processes provides a vital perspective on the commercialization ability of IL-based absorption. Kazmi et al. [190] compared an aqueous MDEA solvent with imidazolium-based ILs for the simultaneous capture of H_2S and CO_2 from natural gas at 30 °C and 68 bar. The energies for the amine and IL-based acid gas removal process were estimated to be 18,619 kW and 3981 kW, respectively. They found that replacing amine-based solvents with ILs reduced the thermal energy consumption and total annualized cost by up to 78.6% and 59.8% respectively. 99.77% of the IL could be recovered after being passed through three flash drums, while the absorbed acid gases were completely removed. However, mass transfer limitations of the IL were not considered, making it difficult to assess the realistic performance. Wang et al. [191] simulated and compared [bmim][Tf_2N] with the Rectisol (methanol) process [192] for simultaneous capture of H_2S and CO_2 from syngas in the coal industry. The IL-based process performs better with a higher CO_2 capture ratio, higher solvent recovery ratio, and lower cold energy consumption. Haider et al. [193] reviewed a few other simulation-based studies analyzing the technical, economic, and sustainability aspects of IL-based processes used for acid gas removal. These studies demonstrate the high potential of ILs to remove H_2S and CO_2 from fuel gases at lower or comparable cost compared to the existing technologies.

There is no question that the use of ILs as H_2S (and CO_2) absorbents holds very high promise. However, the scale-up and commercialization of IL-based processes remain difficult due to their high production cost, complicated synthesis, toxicity, high viscosity, etc. Although ILs were believed to have negligible vapor pressure [194], this has since been proven untrue for many ILs [195,196]. Similarly, emerging evidence that many ILs are toxic and poorly biodegradable questioned the status of ILs as green and sustainable solvents [197–200]. Although several PILs exhibit high absorption capacities and low viscosities at lower costs, maintaining high thermal and electrochemical stabilities alongside low viscosities has been a challenge [201,202]. An optimal trade-off between ease of preparation, viscosity, and thermochemical stability should be an immediate focus area for research. Overcoming these drawbacks is likely to require the development of new candidate ions or new candidate solvents beyond ionic liquids.

2.2.4. Deep eutectic solvents

Deep eutectic solvents (DESs), discovered only about two decades ago [203,204], have quickly emerged as alternatives to ILs in many applications [205]. DESs are multicomponent mixtures of hydrogen bond acceptors (HBAs) and donors (HBDs) (see Fig. 3) characterized by significant depressions in melting points compared to those of the neat constituent components [204,206]. DESs and ILs share many general characteristics, such as low volatility, high thermal stability, high tunability, wide liquid range, etc. However, DESs are typically non-toxic, biodegradable, inexpensive, and easier to make than ILs [207,208]. Over the years, DESs have been applied for capture of CO_2, sulfur dioxide, and ammonia [146,205,209–211]. However, H_2S capture with DESs has hardly been explored.

Liu et al. [212] studied DES systems composed of choline chloride (ChCl) and urea at three different ratios (1.5, 2.0, and 2.5) of ChCl/urea for the absorption of H_2S, CO_2, and CH_4. The behavior of the absorption isotherms suggest that the mechanism of absorption is physical for all the studied gases. They also studied the absorption mechanism based on quantum chemistry calculations and Monte Carlo (MC) simulations. While the strong hydrogen bond between Cl of ChCl and H of H_2S governs the absorption of H_2S in ChCl–urea eutectic mixtures, the free volume of solvents governs that of CO_2 and CH_4. A decrease in ChCl/urea ratios does not change the major site for binding with H_2S in ChCl–urea mixtures but decreases the number of interaction sites, resulting in a decrease in H_2S solubilities. On the other hand, the solubilities of CO_2 and CH_4 in ChCl/urea (1:2.0) are higher than those in ChCl/urea (1:1.5) and ChCl/urea (1:2.5) since ChCl/urea (1:2.0) has the lowest melting point and, therefore, the highest proportion of free volume. Based on the different solubility trends of the three gases, the H_2S/CO_2, H_2S/CH_4, and CO_2/CH_4 selectivities can be tuned by adjusting the ratio of ChCl/urea in mixtures. Even though the ideal selectivities in these DESs are higher than those reported for many physical solvents, the absorption capacities of H_2S and CO_2 in ChCl–urea mixtures are similar to those in propylene carbonate but inferior to most other physical solvents. In addition, the thermal decomposition temperatures of these ChCl/urea DESs are found to be about 450 K, which is sufficiently higher than the temperatures used for solvent regeneration.

Wu et al. [213] explored the H_2S absorption capabilities of two series of DESs, tetrabutylammonium bromide (TBAB)/carboxylic acid (1:1 to 1:4) and ChCl/carboxylic acid (1:2 to 1:4). Both DESs acts as physical absorbents and exhibit the same trends. Solubility of H_2S increases with decreasing carboxylic acid concentration and increasing alkyl chain on the acid. As in the case of ChCl/urea, H_2S absorption is dominated by the strong interaction between the HBA (here, TBAB or ChCl) and H_2S. Therefore, decreasing the ratio of HBA/carboxylic acid decreases the number of absorption sites available. In addition, the authors speculate that the H_2S solubility goes down with increasing acidity of the carboxylic acid. When comparing the two HBAs, TBAB-based DESs performed better than ChCl-based DESs. This could be due to the stronger and more complex hydrogen bond network within the ChCl-based DESs, resulting in a lower free volume available for absorption. Comparing these DESs with ChCl/urea DESs shows that both the new series of DESs perform remarkably better than the ChCl/urea DESs studied by Liu et al. [212]. These carboxylic acid based DESs also perform comparably to or better than many ordinary ILs. It was also found that CO_2 has as high a solubility as H_2S in these solvents while the solubility of CH_4, CO and H_2 was negligible, making these DESs good candidates for simultaneous physical absorption of H_2S and CO_2.

As is the case with TSILs, functionalization of DESs could open more possibilities due to the resulting chemisorption allowing for higher absorption capacities and selectivities. Shi et al. [214] designed a series of five task-specific DESs (TSDESs) using semi-quaternized diamines with free tertiary amine groups as HBAs and azoles as HBDs in a 1:2 ratio. Previously, tethering tertiary amine groups to the cations and using azole-based anions have shown success in designing TSILs for H_2S absorption (see Section 2.2.3). Out of the five TSDESs, only [C_4-TMEDA][Cl]/1,2,3-triaz has a viscosity value (66.2 cP) below 100 cP at 313.2 K, making the rest possibly impractical for industrial applications. On the other hand, all the prepared candidates have high enough decomposition temperatures (>400 K) to be conveniently regenerated. When it comes to H_2S absorption, [C_4-TMHDA][Cl]/Im exhibited the highest capacity of 0.996 mol/mol at 303.2 K and 1.0 bar. This was the highest value reported for any DES at the time and is on par with some of the top-performing ILs. As expected, the strong H-bond between H_2S and the tertiary amine group on the HBA governs the solubility of H_2S. In agreement with observations made for TSILs, TSDESs with higher alkalinities and larger free volumes exhibit higher H_2S absorption capacities. The authors also found that these TSDESs have very low affinity to CO_2, resulting in low physisorption capacities for CO_2 and high ideal selectivities for H_2S (5.2–12.1). Moreover, when subjected to regeneration at 342.2 K and 0.1 bar, [C_4-TMHDA][Cl]/Im showed excellent reversibility with 92% of the capacity retained after 5 cycles.

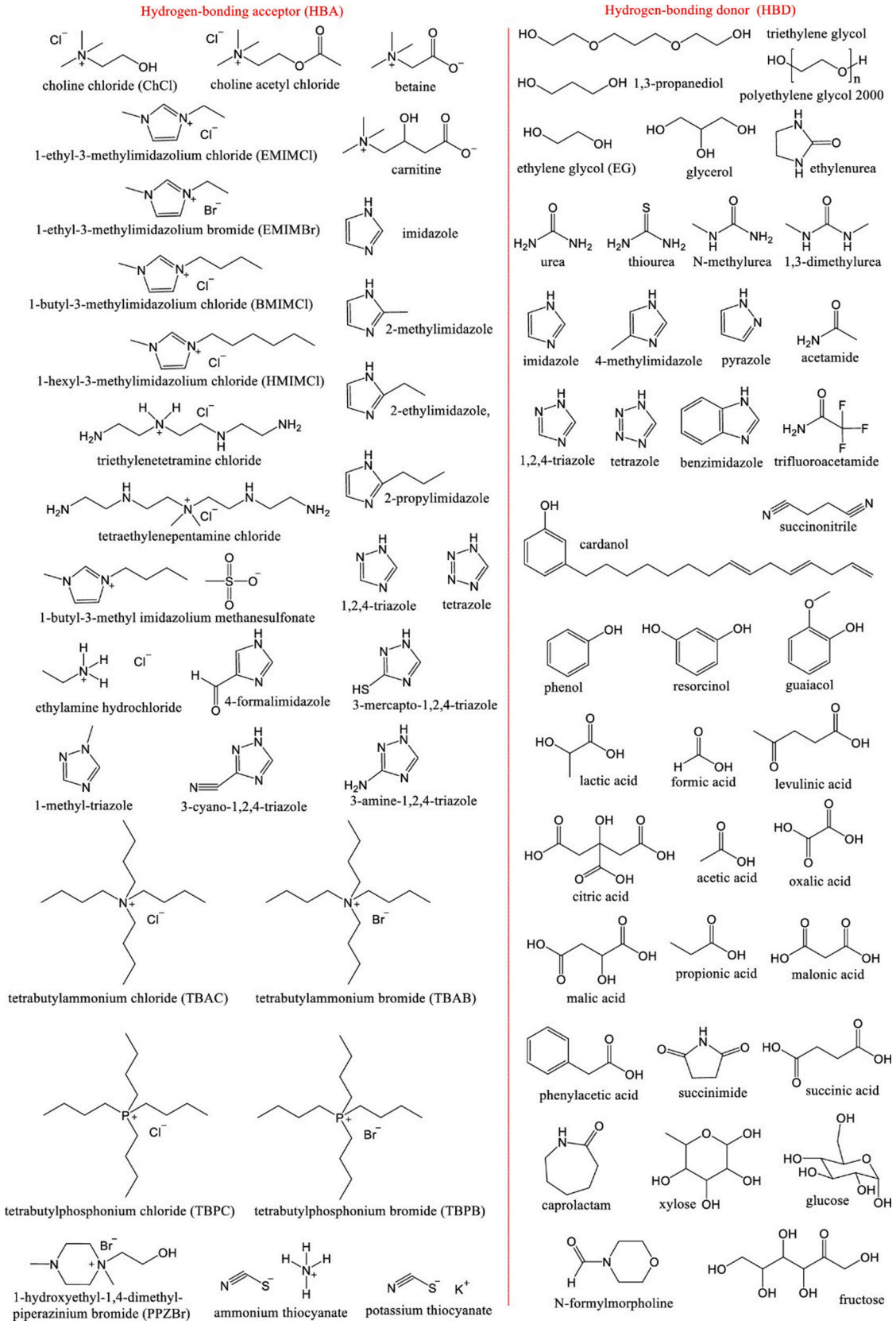

Fig. 3. Examples of commonly used components to form DESs. Reprinted with permission from [211]. © 2020 American Chemical Society.

Most recently, Shi et al. [215] designed another set of TSDESs but with chemical dual sites. By replacing the chloride ion in the earlier HBAs with the acetate ion, they hypothesized that the tertiary amine and the acetate anion form dual chemical interactions with H_2S, which could lead to higher absorption capacities. Their results show the H_2S absorption capacity at 313.2 K and 1 bar is 1.44 mol/mol in [C_1-TMHDA]Ac/MDEA, 1.17 mol/mol in [C_1-TMHDA]Ac/Pyrol, 1.09 mol/mol in [C_1-TMHDA]Ac/AA, and 1.02 mol/mol in [C_1-TMHDA]Ac/Im, following the order of alkalinity of the HBDs. All these values are the highest reported among DESs so far, while the relative absorption capacity of [C_1-TMHDA]Ac/MDEA is the highest reported for any absorbent discussed in this work or elsewhere. Considering their high capacities and ideal H_2S/CO_2 selectivities (6.9–9.3), these TSDESs are among the very few that rank high in both the indices. Spectroscopic analysis and computational studies revealed that the acetate ion and the tertiary amine groups in both MDEA and the cation of the HBA strongly interact with H_2S; the tertiary amine in the HBA has the strongest impact among them. This DES also retained 92% of its absorption capacity after 6 cycles with regeneration performed at 342.2 K and 0.1 bar. However, [C_1-TMHDA]Ac/MDEA has a higher than practical viscosity of about 160 cP and 100 cP at 303.2 K and 313.2 K, respectively. On the other hand, [C_1-TMHDA]Ac/Pyrol and [C_1-TMHDA]Ac/Im have viscosities below 75 cP at 313.2 K, making them potentially better candidates for large-scale studies.

Computational studies on structural interactions within DESs and between DESs and gas solutes are the key to unlocking the full potential of these solvents. This knowledge is especially important in the case of H_2S absorption where there have only been a few experimental studies so far. Karibayev et al. [216] explored these interactions using molecular dynamics (MD) simulations and ab initio computations for H_2S and CH_4 absorption in four DESs: TBAB/caprolactum (CPL) (1:1), tetrabutylammonium chloride (TBAC)/CPL (1:1), ChCl/urea (1:2), and methyltriphenylphosphonium bromide (MTPPB)/MEA (1:6). MD simulations of TBAB/CPL DES showed a 15% decrease in the interaction energy between the ions of TBAB and a 92% decrease in the number of hydrogen bonds within CPL after the formation of the DES. They also revealed that the formation of the DES is dominated by the hydrogen bonds formed between the nitrogen atom in CPL and the bromide ion. Similar behavior was observed for TBAC/CPL DES too. When H_2S and CH_4 are added to TBAB/CPL DES, H_2S exhibited stronger interactions with CPL and both the ions of TBAB when compared to the interactions between H_2S and CH_4. This demonstrates that this DES can favorably remove H_2S from CH_4. It was also shown that H_2S had the strongest interaction with the bromide ion, possibly by the formation of a hydrogen bond. Similar behavior was observed with TBAC/CPL DES, although the chloride ion had a much stronger interaction with H_2S. In addition, sensitivity analysis of process parameters suggested that low temperatures (25 °C vs 60 °C), high pressures (10 bar vs 1 bar), and low feed-to-solvent ratio (0.5 vs 2.5) are advantageous for H_2S absorption in these DESs. While all the four DESs exhibit similar absorption interactions, the authors suggest TBAC/CPL DES for H_2S removal from CH_4.

Salehi et al. [217] attempted to compute solubilities of various gases in ChCl/urea and ChCl/ethylene glycol DESs using MC simulations. Although they could accurately reproduce the densities and radial distribution functions of pure DESs, the calculated solubilities are much lower than experimental values and are highly sensitive to the force field used. However, their calculations qualitatively predicted that CO_2 and H_2S ($H_2S > CO_2$) are much more soluble than CH_4, CO, H_2, and N_2 in both DESs. However, MC simulations are only one of the methods that can be used to predict solubilities in DESs [218]. As is the case with ILs, a popular approach to theoretical property predictions in DES-based systems is the use of COSMO-RS [219]. Słupek et al. [220] screened for the best DES for biogas upgrading from among 23 low-cost DESs based on thermodynamic properties calculated using COSMO-RS. They found that ChCl/urea (1:2) and ChCl/oxalic acid (1.2) are the best DESs that can simultaneously remove H_2S, CO_2, and siloxanes to within regulatory limits. A subsequent technoeconomic analysis demonstrated that both the DESs are competitive with alkanolamines, water, membranes, and pressure swing adsorption. Haider et al. [221] evaluated the technoeconomic performance of ChCl/urea (1:2) with varying (0–70 wt%) water content towards simultaneous removal of H_2S and CO_2 from biogas at 36 bar. These solvents are then compared to 30 wt% aqueous MEA and [bmim][PF_6]. All the studied solvents are able to satisfy the quality objectives, but the DES-based solvents generally required less number of stages in both the absorption and desorption columns (except for the IL for desorption). The specific thermal load for regeneration is only slightly higher in the DESs due to their larger pump loads. Economic evaluation for integrated biogas upgrading and biomethane liquefaction showed that 50–70 wt% aqueous DES can provide lower capital, operating, and annualized costs compared to both the amine-based and IL solvents. The 70 wt% ChCl/urea DES provides the best performance with savings in total annualized cost of 14.26% and 8.71% compared to 30 wt% aqueous MEA and [bmim][PF_6], respectively.

DESs are garnering a high degree of interest due to their potential advantages in terms of economics and sustainability. However, their application to H_2S absorption is still in the budding stage. Low absorption capacities and/or high viscosities [205] need to be overcome before they can be considered serious alternatives to the commercial technologies based on alkanolamines and organic physical solvents. Similar to the progress in IL solvents, task specific or functionalized DESs have been shown to induce chemical absorption and result in high absorption capacities and moderately lower viscosities. Such functionalization has already been applied for the absorption of other acid gases [222–224] but is yet to gain a foothold in H_2S absorption. More work in this area could lead to interesting breakthroughs. Overall, TSDESs present a vast potential that is waiting to be tapped.

2.2.5. Hybrid blends

All the aforementioned classes of absorbents have both advantages and disadvantages. One way to find a compromise between their features is to mix two or more of them. A hybrid blend made of two or more different kinds of solvents may provide better absorption performance than each of the constituents. For example, the combination of a chemical solvent and a physical solvent can result in a higher acid gas absorption capacity and a shorter absorption column than the pure physical solvent while also offering lower regeneration energy requirement and better removal of organosulfur compounds than the pure chemical solvent. A few well-known examples of hybrid solvents are Sulfinol-M (sulfolane + MDEA + water) and Sulfinol-D (sulfolane + DIPA + water) from Shell, Flexsorb PS (sterically hindered amine + physical solvent + water) from ExxonMobil, and Amisol (alkanolamine + methanol) from Lurgi [80].

Ghanbarabadi et al. [225] performed a feasibility study on Aspen Plus for the removal of H_2S, CO_2, and organosulfur compounds from natural gas using Sulfinol-M, 26.5 wt% DGA, and a blend of 45 wt% MDEA + 15 wt% AMP as replacements for 45 wt% MDEA. The results showed that Sulfinol-M, unlike MDEA, was able to remove organosulfur compounds to trace amounts while meeting the gas quality requirements for H_2S and CO_2. In addition, different Sulfinol-M formulations could reduce the solvent circulation rate by 35–50% and the energy consumption by 10–25%. Nejat et al. [226] tackled the same problem for a different industrial case and found similar results. They reported that Sulfinol-M with varying compositions could reduce the solvent

circulation rate by 11% and the energy consumption by 31–43% while achieving an exergy efficiency of >98.85%. Abd and Naji [227] compared piperazine and sulfolane to be the activator in a blend of 40 wt % MDEA + 5 wt% activator to remove CO_2 and H_2S from natural gas. They found that replacing piperazine with sulfolane in the blend increases H_2S removal efficiency by 16% and decreases CO_2 removal efficiency by 6%. This behavior is as expected since PZ is known to enhance CO_2 absorption while sulfolane is known to be selective towards H_2S over CO_2 [228]. Moreover, the authors also observed that the sulfolane system saved more reboiler energy compared to the piperazine system. However, care must be taken when using sulfolane with a primary alkanolamine since sulfolane is found to be a universal phase-splitting solvent in a series of aqueous primary alkanolamines if the feed gas contains CO_2 [229]. This phase-splitting effect can dramatically reduce the absorption efficiency of the solvent.

Due to the high cost and viscosity of most ILs, it is more economical to blend ionic liquids with other low-cost solvents, such as alkanolamines or organic physical solvents, to reduce viscosity and enhance mass transport. Tian et al. [112,230,231] evaluated the performance of MEA, $[N_{1111}][Gly]$, and $[N_{1111}][Arg]$ as promoters added at amounts below 7.5 wt% to 30–50 wt% MDEA solutions to remove H_2S at low partial pressures. They found that all three compounds enhanced the H_2S absorption capacity of the aqueous MDEA solution due to the increased number of interaction sites available for H_2S absorption. MEA, $[N_{1111}][Gly]$, and $[N_{1111}][Arg]$ provide one (amino), two (one amino and one carboxyl), and four (three amino and one carboxyl) additional interaction sites per molecule [174]. As such, the order of absorption capacities and efficiencies are in the order of MEA < $[N_{1111}][Gly]$ < $[N_{1111}][Arg]$.

Afsharpour and Haghtalab [232] studied the removal of H_2S and CO_2 using an aqueous blend of DIPA and [bmim][Ac] at varying concentrations of the constituents. The solubility measurements show that increasing IL concentration increases H_2S absorption capacity since [bmim][Ac] absorbs H_2S via both chemical and physical interactions. On the other hand, increasing IL concentration initially decreases CO_2 absorption capacity before increasing it at high pressures. The initial reduction in CO_2 absorption is due to the decrease in the quantity of water, which in turn limits bicarbonate formation. However, the IL still acts as a physical solvent at high pressures, thereby increasing CO_2 solubility. Since DIPA and [bmim][Ac] are both selective towards H2S, increasing DIPA and IL concentrations in the blend leads to better H_2S solubilities. Lemus et al. (2021) reported that the blend of 25 wt% [bmim][Ac] + 75 wt% TEGDME provides 98% H_2S recovery at 1 bar, resulting in a column performance remarkably better than the pure solvents, the [bmim][Ac] + [emim][DCN] blends, and the best [emim][(MeO)PO_2H] + TEGDME blend. The superior performance of the blend of 25 wt% [bmim][Ac] + 75 wt% TEGDME is due to the synergistic effect of the high absorption capacity of [bmim][Ac] and the low viscosity of TEGDME.

2.3. Adsorption

Adsorption is a surface–based process that leads to the transfer of a molecule from a fluid bulk to the solid surface of the adsorbent. In the case of H_2S removal, we describe only removal from a gas stream, which under dry conditions is an exothermic process and, therefore, does not require elevated temperatures. This dry desulfurization technology has received great attention in the recent years, owing to its affordability, flexibility, energy efficiency, and ease of operation [233]. Depending on the strength of the adsorbent-adsorbate interactions, adsorption may be classified as physisorption or chemisorption (reactive adsorption). While physisorption is dominated by Van der Waals forces and/or electrostatic interactions, chemisorption is dominated by covalent and/or hydrogen bonding interactions. Often, the distinction between physisorption and chemisorption is instead based solely on the strength of the interaction, regardless of the type of underlying interaction, especially for experimental studies. In such cases, weak interactions are denoted physisorption and strong interactions are denoted chemisorption. However, physisorption can be quite strong, at least for slightly larger molecules (e.g. [234]).

In addition to these interactions, the shape and size of molecules could affect the selectivity in multicomponent mixtures. Generally, a desirable adsorbent material would exhibit high breakthrough capacity and selectivity towards target molecules (here, H_2S), chemical and thermal stability, and structural regeneration. Over the past few years, numerous studies have focused on developing such cost-effective and high-performing adsorbents for H_2S removal, particularly at low temperatures. In this respect, porous materials emerged as promising solutions due to a wide variety of possible chemical architectures with tunable pore size, high surface area, and large pore volume [235].

Natural and synthetic zeolites, activated carbons, and porous metal oxides are the conventionally used adsorbents for H_2S removal. The virgin materials can be crystalline or amorphous and porous or non-porous, but they can be modified to augment their affinity for H_2S. The application of an adsorbent for a specific process is highly dependent on its porosity, structural stability, and reusability [236]. The presence of other compounds in the feed mixtures also has an impact on the material used. Since fuel gas mixtures often require H_2S to be separated from non-polar molecules (e.g. CH_4), a polar adsorbent surface is chosen. However, separation based solely on polarity could be challenging in the presence of moisture since water has a higher dipolar moment than H_2S. As discussed later in this section, depending on the material and its modifications, the presence of a small amount of water may aid or hinder H_2S adsorption. The line between enhancement and hindrance of H_2S adsorption in the presence of water is likely based on the amount of water present and the strength of interactions between water and the sorbent. Since H_2S is a stronger acid than water, it would be beneficial to employ base functionalization to make adsorbents selective for H_2S. On the other hand, the presence of CO_2 poses further limitations since both components are acidic. More recently, a new class of adsorbents called metal–organic frameworks (MOFs) have grown in popularity due to their high adsorption capacity and selectivity towards H_2S [237–239].

The rapid growth in the development and characterization of H_2S adsorbents (~2000 published works in the past 15 years, >1500 in the past 10 years, and >1000 in the past 5 years) has resulted in a number of reviews published over the past few years: adsorption [233,235,236,240–243], zeolites [244], metal oxides [245], and MOFs [246–248]. In the interest of not repeating the same information that can be found in the aforementioned sources, this section will review the most recent developments in the field. As such, the different H_2S adsorbents are classified into five categories: metal oxides, zeolites, carbon-based sorbents, MOFs, and composite materials. In addition, Table 4 reports the H_2S removal performance of few of the best and representative examples from each category. However, it must be noted that the calculated breakthrough capacities are impacted by several factors, such as the operating temperature, gas flow rate, bed height, initial concentration of H_2S in the gas stream, and the chosen breakthrough point, which are not consistent across studies. For example, most of the adsorbents in Table 4 that provide high adsorption capacities also have high H_2S content in the feed and/or report equilibrium-based values. Such considerations must be taken into account while comparing

Table 4
Recent developments in hydrogen sulfide adsorption.

Material	BET Surface Area (m^2/g)	Feed	Amount or Partial Pressure of H_2S	H_2S Breakthrough Concentration	Breakthrough Capacity (mg/g)	Reference
Zeolites						
NaX (13X)	571[a]	N_2 and H_2S at 1 bar and 298.15 K	50 ppmv 100 ppmv	2.5–5.0 ppmv 5–10 ppmv	8.94E-5 – 1.84E-4 2.14E-4 – 6.12E-4	[261]
AgNaA	201.79	N_2 and H_2S at 1 bar and 298.15 K	15 ppmv	1 ppmv	33.24	[263]
NaA	263.35				13.95	
NaX	515	N_2 and H_2S at 1 bar and 298.15 K	110–126 ppmv	5.5–6.3 ppmv	277.86	[281]
Fe-X	350				10.01	
IMS	590	Ar and H_2S at 1 atm and 298.15 K	200–10,000 ppmv	saturated	200 ppmv: 32.0 10,000 ppmv: 193.9	[270]
Metal Oxides						
CaO-Fe_2O_3	1.50	CO_2, H_2, NH_3, and H_2S at 1123 K	230 ppmv	na	na	[275]
$ZnFe_2O_4$	16	N_2, O_2, H_2O and H_2S at ambient conditions	1000 ppm	100 ppm	1.6	[287]
Mn_2O_3/Fe_2O_3	6.19	H_2S at 1 bar and 298.15 K	500 ppm	400 ppm	11.97	[278]
CoO/TiO_2	45.92	N_2 and H_2S at 1 bar and 673.15–753.15 K	2000 ppm	saturated	100–410	[276]
NiO/TiO_2	52.77				100–580	
CuO/TiO_2	44.34				40–300	
ZnO	2–3	N_2, CO, H_2, CO_2, H_2O and H_2S at 673.15–873.15 K	100 ppmv	20 ppmv	673.15 K: 10	[277]
28% Ni-ZnO					673.15 K: 210 773.15 K: 178 873.15 K: 117	
28% Co-ZnO					673.15 K: 184 773.15 K: 177 873.15 K: 145	
28% Cr-ZnO					673.15 K: 48	
28% Fe-ZnO					673.15 K: 101	
DMO-5	27	N_2, CO, H_2, CO_2, and H_2S at 823.15 K	2000 ppmv	100 ppmv	250	[279]
AMDS	155.65	N_2 and H_2S at 1 bar and 298.15 K	110–126 ppmv 1000 ppmv	5.5–6.3 ppmv 50 ppmv	8361 235.55E3 – 312.73E3	[281]
NMO-D	1.77	N_2, H_2O, and H_2S at ambient conditions	500 ppm	400 ppm	439.2	[512]
NMO-T	2.56				818.7	
NCO-D ($NaCo_{0.7}O_{2.4}$)	1.15	N_2 and H_2S at 298.15 K	500 ppm	10 ppm	154.6	[513]
NCO-T ($NaCo_{1.1}O_{3.3}$)	1.90				168.2	
Carbon-based Sorbents						
GAC	na	CH_4, CO_2, O_2, and H_2S at 293.15–298.15 K	932–2350 ppm	100 ppm	615–1293	[291]
EUC ALM COF	na	CH_4, CO_2, O_2, H_2S, and other minor gases at ambient conditions	970 ppm	saturated	460 230 22	[293]
$ZnAc_2$–CAC	620.55	N_2 and H_2S at ambient temperature	5000 ppmv	5–10 ppmv	2.37	[289]
Zn/AC	na	N_2, O_2, H_2O and H_2S at 303.15 K	100 ppmv	saturated	30.9	[514]
Cu/AC	559				129.2	
$Cu_{0.5}Zn_{0.5}$/AC	570				118	
AC	1120	N_2, O_2, H_2O and H_2S at 303.15 K	850 mg/m^3	0.1 ppmv (0.15 mg/m^3)	3.4	[294]
Zn/AC	769				38.5	
$Mg_{0.2}Zn_{0.8}$/AC	653				113.4	
Mg/AC	366				32.7	
BAX (wood-based AC)	2158	N_2, O_2, H_2O and H_2S at ambient conditions	1000 ppm	100 ppm	5.6	[287]
10 wt% $ZnFe_2O_4$/BAX	1403				122.5	
RBC-500 (rice-based AC)	2.76	N_2, O_2, H_2O and H_2S at 298.15 K	300 ppm	270 ppm	12.11	[296]
50 wt% $ZnFe_2O_4$/rice (RZF-500–1:1)	1065				228.29	
$CaCO_3$/CH-600	22	N_2, O_2, and H_2S at 303.15 K	1000 ppmv	50 ppmv	< 100	[286]
CaO/CH-700	162				9100	
CaO/CH-800	203				4400	
CaO/CH-900	312				2380	
PC	1340	N_2, O_2, H_2O and H_2S at 303.15 K	1000 ppmv	50 ppmv	12.5	[301]
NC	187				19.5	
NPC-0.5	2459				119.1	
NPC-1	1839				426.2	
NPC-1.5	1274				334.5	
NPC-2	1048				267.2	
HNAC-802	1544	H_2S at 298.15 K and 1–10 bar	pure	saturated	1 bar: 284.05 10 bar: 669.7	[303]
HNAC-812	1477				1 bar: 316.45 10 bar: 613.8	
NMCS-0–5	1389	N_2, O_2, H_2O and H_2S at ambient conditions	1000 ppm	250 ppm	48	[307]
20 wt% Na_2CO_3/NMCS-0–5	na				65	
NMCS-50–8	1937				510	
20 wt% Na_2CO_3/NMCS-50–8	983				1370	

(*continued on next page*)

Table 4 (*continued*)

Material	BET Surface Area (m^2/g)	Feed	Amount or Partial Pressure of H_2S	H_2S Breakthrough Concentration	Breakthrough Capacity (mg/g)	Reference
A-N-OMC-700	1538	N_2, O_2, and H_2S at 1 bar and 298.15 K	5000 ppm	saturated	276.21	[515]
N-OMCS-700	1575	N_2, O_2, and H_2S at 1 bar and 273.15 K	5000 ppm	saturated	456.94 (ca. 270 at 298.15 K)	[300]
N-OMCS-800	1201				371.69	
N-OMCS-900	1202				303.49	
N-PCNF-1/2–800-40%	na	N_2, O_2, H_2O and H_2S at 1 atm and 298.15 K	1000 ppm	50 ppm (B), 980 ppm (S)	B: 3340 S: 3570	[312]
N-PCNF-1/2–800	1308				B: 1840 S: 2070	
N-PCNF-1/2–700	1279				B: 1490 S: 1740	
MCNs-PEI-25	193	N_2, O_2, and H_2S at 298.15 K N_2, O_2, CO_2 and H_2S at 298.15 K	1000 ppm	50 ppm	466.23 438.62	[313]
AGA	40	N_2, O_2, and H_2S at 303.15 K	1000 ppmv	50 ppm	3190	[516]
Metal Organic Frameworks and Porous Organic Polymers						
CuBDC	217.8	N_2, H_2O, and H_2S at 298.15 K	500 ppm	400 ppm	105.6	[326]
CuBDC-N	38.0				1.3	
CuBTC	317.0				27.1	
CuBTC	231.94	N_2 and H_2S at 298.15 K	500 ppm	saturated	77.1	[517]
CuBTC	434–1380	N_2 and H_2S at 1 bar and 298.15 K	99.6 ppm	5 ppmv	17.1–56.3	[518]
$Cu(BDC)_{0.5}(BDC\text{-}NH_2)_{0.5}$	19.4	N_2 and H_2S at 298.15 K	500 ppm	50 ppm	128.4	[327]
SU-101	412	N_2 and H_2S at 1 bar and 298.15 K	4.3 vol%	saturated	543.58	[330]
MFM-300(Sc)	1360	N_2 and H_2S at 1 bar and 298.15 K	10 vol%	saturated	564	[329]
MFM-300(In)	1060				310	
MIL-53(Al)-TDC	1150	N_2 and H_2S at 1 bar and 303.15 K	5 vol%	saturated	606–654	[328]
ED-ZIF-8 1st	1389	CH_4, CO_2, H_2S, and He at 2 bar and 298.15 K	3 vol%	1500 ppmv	3299	[337]
UiO-66	1351	N_2 and H_2S at 303.15–323.15 K	4000 ppm	saturated	50–80	[519]
			4500 ppm	2250 ppm	51.12–95.43	[520]
MOF-199 (CuBTC)	725	N_2 and H_2S at 1 bar and 298 K	10 ppmv	1 ppmv (B), saturated (S)	B: 40 S: 69	[239]
MOF-5	424				B: 1.2 S: 4.97	
UiO-66-NH_2	963				B: 0.04 S: 0.07	
CBAP-1-EDA	672				B: 0.033 S: 0.12	
CBAP-1-DETA	667				B: 0.026 S: 0.1	
N-HPP-*p*-phenylenediamine	1186	H_2S at 1 bar and 298.15 K	pure	saturated	177	[521]
N-HPP-bipyridine	1350				188	
N-HPP-HMTA	1397				198	
N-HPP-3-aminophenol	1229				153	
N-HPP-pyridine	792				170	
HPP	1605				94	
Composite Materials						
ZnBDC/ZnO	12.35	N_2 and H_2S at 298.15 K	500 ppm	400 ppm	Dry: 10.6 Moist: 13.6	[347]
ZnBDC-N/ZnO	14.99				Dry: 9.4 Moist: 7.9	
ZnBTC/ZnO	20.63				Dry: 14.3 Moist: 7.8	
SBA-15-PEI-25	495	N_2, O_2, and H_2S at 298.15 K	1000 ppm	50 ppm	26.58	[313]
HKUST-1/GO-PEI	56–489	N_2 and H_2S at 1 bar and 298.15 K	99.6 ppm	5 ppmv	30.67–55.55	[518]
CuO/SiO_2	13.44–175.75	N_2 and H_2S at 1 bar and 423.15 K	100 ppm	5 ppm	32–363	[349]
CuO/SiO_2	na	N_2 and H_2S at 303.15 K	850 mg/m^3	0.15 mg/m^3	145.6	[522]
ZnO/SiO_2	106.3–168.5				28.6–108.9	
Co_3O_4/SiO_2	na				114.3	
20 wt% ZnO/MCM-41	686	N_2, H_2O, and H_2S at 298.15 K	500 mg/m^3	1.5 mg/m^3	54.9	[523]
20 wt% ZnO/SBA-15	213				41.0	
30 wt% ZnO/MCM-48	323				53.2	
30 wt% ZnO/MCM-41	459	N_2, CO, H_2, CO_2, and H_2S at 773.15 K	2000 ppmv	100 ppmv	~84	[348]
30 wt% ZnO/MCM-48	308				~54	
5 % N-TiO_2/GO	145	N_2 and H_2S at 1 bar and 493.15 K	4400 ppm	2200 ppm	250	[524]
5% TiO_2/GO	154				200	
1% TiO_2/UiO-66	1171	N_2 and H_2S at 303.15–323.15 K	4000 ppm	saturated	180–210	[519]
3% TiO_2/UiO-66	986				140–180	
5% TiO_2/UiO-66	652				80–130	
UiO-66/GO	1002–1432	N_2 and H_2S at 303.15–323.15 K	4500 ppm	2250 ppm	115.9–296.5	[520]

[a] Langmuir surface area.

the results reported in the literature.

2.3.1. Zeolites

Zeolites, also commonly referred to as molecular sieves, are microporous crystalline materials that are widely used as ion exchangers (e.g. in water softening), catalysts, adsorbents, additives, etc. [249–252]. Structurally, they are principally comprised of a three-dimensional framework of TO_4 tetrahedra (T denotes tetrahedrally coordinated Si, Al, P, etc.) linked to each other by sharing their vertex O atoms [253,254]. The different ways in which these primary building blocks are linked to each other give rise to a many distinct types of frameworks. In general, these materials have a large surface area, unique and tunable pore structure, and high thermal stability. Natural zeolites and many commonly used synthetic zeolites are aluminosilicates whose frameworks are typically anionic and have alkali metals or alkali earth metals as charge-compensating cations to retain electrical neutrality. These mobile, non-framework cations take part in ion-exchange processes, making them suitable for selective H_2S adsorption. There is an abundance of literature on synthesis, structure, and properties of different types of synthetic zeolites, such as zeolite-A (LTA), zeolite-Y (FAU), zeolite-X (FAU), and ZSM-5 (MFI), and natural zeolites, such as mordenite, clinoptilolite, erionite, phillipsite, and ferrierite [255–259]. In addition to the framework type, extra framework species, and porous architecture, chemical composition (Si/Al ratio) plays a crucial role in determining the applicability of a zeolite material for adsorption. Zeolites containing lower Si/Al ratios are more hydrophilic with an affinity for polar substances such as H_2S via chemisorption. On the other hand, high-silica zeolites (including charge-neutral pure-silica frameworks such as silicalite-1) often possess fewer structural defects and are considerably hydrophobic, resulting in H_2S adsorption via physisorption [252,260].

Several previously published studies [244] on different types of synthetic zeolites have concluded that zeolite 13X (Na-X) and its derivatives are the best adsorbents for the removal of sulfur compounds. Bareschino et al. [261] studied the impact of 13X on H_2S (50–100 ppm) removal at typical biogas operating conditions. From the analysis of the concentration profiles, they observed that the system never reaches complete saturation due to the formation of sulfur and polysulfides. They also noted that the presence of a small amount of water aided the adsorption of H_2S. Temperature profiles from adiabatic tests showed that the adsorption mechanism was initially physisorption but shifts to chemisorption after saturation. Barelli et al. [262] prepared a Cu-exchanged 13X zeolite sorbent (13X Ex-Cu) for hydrogen sulfide capture from biogas (200–1000 ppm H_2S) to obtain a desulfurized fuel suitable for molten carbonate fuel cell systems (H_2S requirement of <1 ppm). The performance of the material is not only measured across a range of operating conditions but also compared to other sorbents, such as impregnated and virgin activated carbons (ACs), sepiolite, natural zeolite, etc. As discussed in section 2.3.3, carbon materials possess the highest surface areas (817–1599 m^2/g) followed by sepiolite (275 m^2/g) and 13X Ex-Cu (239 m^2/g). At 30 °C, 200 ppm H_2S, and a GHSV of 10000 h^{-1}, breakthrough times and adsorption capacities followed the order: AC Cu-Cr (4.4 hr, 27.15 mg/g) > AC KOH (3.6 hr, 20.43 mg/g) > 13X Ex-Cu (2.1 hr, 11.46 mg/g) > AC KOH-KI (1.0 hr, 6.60 mg/g) > virgin AC (0.27 hr, 1.71 mg/g) with the natural zeolite and sepiolite adsorbing virtually no H_2S. Compared to 13X studied by Bareschino et al. [261] in similar conditions, the enhanced desulfurization performance of 13X Ex-Cu is attributed to the presence of numerous Cu^{2+} ions, leading to an efficient physical–chemical adsorption. Decreasing GHSV and increasing temperature led to increasing capacities in 13X Ex-Cu. Moreover, an increase in inlet sulfide content expectedly resulted in a decrease in breakthrough time and capacity.

Bahraminia et al. [263] synthesized and modified the NaA nano-zeolite by silver ions using the ion-exchange process to evaluate the performance of the resulting AgNaA nano-zeolite in removing H_2S from biogas for fueling solid oxide fuel cells. Increasing the surface area of the adsorbent by decreasing its crystallite size and introducing Ag^+ ions into the zeolite structure have improved the H_2S removal performance of the sorbent, and AgNaA nano zeolite showed a longer breakthrough time of 310 min and a higher capacity of 33.24 mg/g to achieve 1 ppmv of H_2S in the outlet gas in comparison to the unmodified NaA nano-zeolite and commercial 4A. In addition, AgNaA also performed better than 13X Ex-Cu discussed above. FT-IR, TGA, and XRD analyses suggest the formation of water during adsorption, which is a product of the reaction between H_2S and the zeolite. The higher quantity of water formed in the AgNaA sample could indicate that the chemisorption of H_2S is more likely in this adsorbent, resulting in better performance. The change in adsorption capacity from regeneration of AgNaA is quite small (around 5% each cycle) and is attributed to the zeolitic water loss due to high regeneration temperatures.

Yan et al. [264] performed grand canonical ensemble Monte Carlo (GCMC) simulations to examine the capability of 95 kinds of all-silica zeolites in the removal of the six toxic gases: SO_2, NH_3, H_2S, NO_2, NO, and CO. The simulation results showed that H_2S, NO, NO_2, CO and NH_3 are well captured by zeolite structures with accessible surface area of 1600–1800 $m^2 \cdot g^{-1}$ and pore diameter of 0.6–0.7 nm, such as AFY and PAU. However, their results show that both the adsorbents (including most of the top 10 adsorbents for H_2S based on maximum loading) exhibit either the same or a larger capacity for NH_3 over H_2S. Specifically for H_2S adsorption, AFY, PAU, and MER are found to be the best adsorbents with loadings of 7.8, 5.5 and 5.4 $mmol \cdot g^{-1}$, respectively. Moreover, the authors suggested that zeolites with a surface area around 1700 $m^2 \cdot g^{-1}$ and a void fraction around 0.3 are good candidates to remove H_2S. On the other hand, zeolites RWY, IRR, JSR, TSC, and ITT are found to exhibit better abilities to capture all the gases at saturated adsorption. RWY exhibits the highest H_2S storage capacity with 17.74 $mmol \cdot g^{-1}$, and the other 9 zeolites have a capacity of 8–10 $mmol \cdot g^{-1}$ for H_2S adsorption.

A similar study by Song et al. [265] for various all-silica zeolites found that the best materials for H_2S adsorption have an accessible surface area of 800–1600 $m^2 \cdot g^{-1}$ and a pore diameter of 0.7–0.9 nm, which are approximately in the range of the values reported by Yan et al. [264]. They observed that the Van der Waals force is dominant at low pressures and that space or cavity size of zeolites assumes a critical role at high pressures. For a blast furnace gas as feed (H_2S, CO, CO_2, H_2O and N_2), CHA exhibited the highest adsorption capacity with good selectivity for H_2S, while FAU and LTA exhibited excellent selectivities for H_2S at low adsorption capacities. To enhance CHA's selectivity to H_2S, they studied the performance of metal-modified SSZ (CHA topology). The considered metals are Cu, Fe, Ni, and Co. The authors found that Co-SSZ exhibits the highest gap between adsorption energies of H_2S and other gases and, therefore, could be a promising material for this application. As shown by these studies and a few that came before them [266–268], the use of molecular modeling tools can provide a great deal of insight into the behavior and performance of zeolites in adsorption processes [269]. Similar studies aimed at understanding the interactions of various feed gas molecules with the secondary and composite building blocks of zeolites can help identify the most suitable frameworks for H_2S adsorption.

Georgiadis et al. [270] employed an industrial molecular sieve (IMS) with a Si/Al ratio of 0.97, non-framework cations of Na and Ca, and a structure closely resembling that of an LTA-type zeolite such as 3A or 4A. Analyses based on changing temperature, activation energy, and thermodynamic studies indicate physisorption that is exothermic and spontaneous. The material was successfully regenerated for 15 cycles with a loss in capacity that is within the bounds of experimental error. For a feed gas mixture of Ar and 200–10,000 ppmv H_2S at 1 atm and 25–100 °C, the highest equilibrium capacity of 193.9 mg/g was obtained at 10,000 ppmv H_2S and 25 °C. However, H_2S adsorption capacity decreases with increasing CO_2 content in the feed gas. For a 3000 ppmv H_2S in the feed gas, the equilibrium capacity decreased from 164.5 mg/g in a CO_2-free feed matrix to 57.7 mg/g in a feed matrix with 36% CO_2. In

this study, the desorption step was carried out at 200 °C, which is lower than many other studies that performed regeneration at temperatures above 350 °C. Nevertheless, this highlights one of the drawbacks of using zeolites: high regeneration temperature. This regeneration imposes a substantial energy requirement for hydrogen sulfide adsorption and remains as the main bottleneck for industrial applications. On the other hand, zeolites are usually the only class of commercial adsorbents (such as AxSorb series) that can be regenerated. In addition to the regeneration penalty, these materials suffer from insufficient selectivity in the presence of other compounds, such as H_2O, CO_2, NH_3, etc. One example of an application where this poses an issue is biogas upgrading. There are also two other key challenges that must be addressed to facilitate progress in this field: (a) quickly and effectively assessing the feasibility of new zeolite materials found by modeling methods and (b) targeted synthesis of zeolites with new pore structures and compositions. On the other hand, the interesting properties of zeolites may present opportunities for modified zeolites and zeolite-based composite materials that can likely counter some of the disadvantages of their unmodified counterparts.

2.3.2. Metal oxides

Due to their high chemical affinity for H_2S, metal oxides have long been the most widely used adsorbents for high-temperature desulfurization [245,271]. As such, a large variety of adsorbents based on the oxides of Zn, Cu, Fe, Mn, Co, Mo, Ca, etc., have been investigated. Among them, sorbents based on iron oxide, cobalt oxide, copper oxide, and zinc oxide are the most commonly used even at low temperatures for selective catalytic oxidation of H_2S [272]. In general, bulk metal oxides have low surface-to-volume ratios, poor dispersion, and insufficient porosity, which results in limited sulfidation rates. Thus, porous metal oxides emerged as better and viable alternatives [273]. They offer larger surface areas, higher porosity, additional H_2S adsorption sites, and better H_2S diffusion through the internal open pores. Over time, mixed metal oxides either as single-phase materials or as nanocomposites have gained increased attention due to the possibility of an improved performance compared to their constituent oxides [274]. The capture mechanism in metal oxides is predominantly chemisorption which results in the formation of sulfides, elemental sulfur, and/or sulfates. This generally leads to higher adsorption capacities at a lower material price when compared to zeolites, but the higher capacity comes at the cost of limited regeneration ability.

Dashtestani et al. [275] studied the performance of a CaO-Fe_2O_3 sorbent in the calcium looping process for CO_2 removal in the presence of ammonia (2300 ppmv) and H_2S (230 ppmv). They reported that the average H_2S removal efficiencies for the three cycles of the carbonation stage were 97.8%, 90.2% and 89.2%, while the corresponding outlet H_2S concentrations were 6.6, 30.4 and 32.3 ppmv. In addition, the sorbent was more effective for NH_3 decomposition than H_2S adsorption. Because of the presence of these contaminants, the removal efficiencies of CO_2 in each of the three cycles have slightly gone down. Furthermore, the concentration of S-based compounds in the outlet gas streams was below 0.4 ppmv, except for 60 min into the first cycle when there was a peak value of 2.7 ppmv. The authors attributed this peak to the high removal efficiencies in the first cycle of the carbonation stage, resulting in a higher concentration of S-compounds released during the subsequent calcination stage.

Orojlou et al. [276] studied the impact of various operating parameters on the performance of NiO/TiO_2, CuO/TiO_2, and CoO/TiO_2 nanocomposites for H_2S removal at relatively high temperatures. All three promoted TiO_2 nanocomposites have removed H_2S considerably better than the pure TiO_2 support or the pure metal oxides. They found that there is no distinct difference between the surface properties of the prepared samples. Therefore, the difference in adsorption capability of the nanocomposites should not be associated with the surface characteristics. XRD analysis showed that NiO, CuO, and CoO promote H_2S adsorption by actively reacting with it. At 480 °C, the CoO/TiO_2 sorbent showed the best performance. However, after decreasing the temperature to 400 °C, the performance of the sorbents changed considerably with the best results observed for the NiO/TiO_2 nanocomposite. This behavior between CoO-based and NiO-based mixed metal oxides was also observed by Pan et al. [277], who noted that the NiO-based sorbent performs better until around 500 °C after which CoO-based sorbent takes over as the better one. Regeneration experiments by Orojlou et al. clearly indicate that the drop in the sulfur adsorption capacities remained limited after one sulfidation-regeneration cycle. However, more experiments are needed to properly assess the cycle dependency of these TiO_2-based nanocomposites. On the other hand, regeneration experiments by Pan et al., who used ZnO instead of TiO_2 as the base metal oxide, found that the adsorption capacity of CoO-ZnO sorbent after regeneration was higher than the fresh sorbent for two cycles. Performance measurement over additional cycles would help in evaluating the regeneration ability of these materials too.

Kim et al. [278] reported the use of a coral-like Mn_2O_3/Fe_2O_3 nanocomposite at 298 K and 1 bar at different bed loadings and H_2S flow rates. This material, which was synthesized by surfactant-mediated co-precipitation, has a surface area of 6.18 $m^2\ g^{-1}$ with a pore volume and diameter of 0.117 $cm^3\ g^{-1}$ and 75.4 nm, respectively. The highest adsorption capacity of 11.97 mg g^{-1} was found for an adsorbent mass of 0.75 g and a flow rate of 0.2 L min^{-1}. The authors observed that a further increase in the bed length (adsorbent mass) at the same flow rate lowers the adsorption capacity, possibly due to the formation of large dead zones in the bed, which remain unutilized during the initial phase of the adsorption process. Similarly, a further increase in the gas flow rate for the same bed length also lowers the adsorption capacity, possibly due to insufficient residence time which limited gas diffusion into the pores. Analysis of the spent adsorbent showed that adsorbed sulfur species were mostly in the form of sulfate ions with minor contributions from elemental sulfur and sulfide ions. In addition, XPS and XRD analyses suggest that Mn_2O_3 played an important role in the oxidation of H_2S at room temperature while Fe_2O_3 did not.

Wu et al. [279] synthesized a series of mesoporous double metal oxides (DMOs) derived from Zn-Fe-based layered double hydroxides [280] with the Zn/Fe molar ratios ranging from 1:1 to 5:1. These DMOs contain both ZnO and $ZnFe_2O_4$. The authors reported a sheet-shaped morphology for most of the DMOs, which affords a high specific surface area for adsorption. Breakthrough time and capacity increased with increasing Zn/Fe ratio as expected since ZnO has a higher thermodynamic desulfurization potential than $ZnFe_2O_4$ and Fe_2O_3. Compared to DMO-2 (DMO with a Zn/Fe ratio of 2) which is composed of both particles and sheets, DMOs with higher Zn/Fe ratios have hierarchical microstructures composed of sheets. At 500 °C, these sheet-like DMOs have breakthrough times and capacities increased by 309–515% and 155–282%, respectively. The authors found that DMO-5 performed the best. Temperature analysis between 450 °C and 700 °C showed that the best operating temperature is 550 °C where DMO-5 has the highest breakthrough time (321 min), breakthrough capacity (250 mg/g), and saturation capacity (302 mg/g). Further increase in temperature led to the formation of denser surfaces at 600 °C and sintering at 700 °C, both of which are undesirable. In addition, DMO-5 showed the least change in pore volume from before and after sulfidation, indicating a better ability for regeneration. Regeneration tests showed complete regeneration at the optimal conditions of 600–650 °C and 2–4% oxygen levels. Addition of Fe allowed for a lower regeneration temperature and higher structural integrity than many Zn-based adsorbents. The regenerated DMO-5 exhibited higher surface area, pore volume, breakthrough time, and sulfur capacity than the fresh sorbent over four sulfidation-regeneration cycles. The combination of high capacity, low deactivation constant for sulfidation, complete regeneration, and relatively low regeneration temperature make DMO-5 an attractive choice for high-temperature desulfurization.

Ahn et al. [281] employed a waste material, acid mine drainage sludge (AMDS), for H_2S removal and compared it against zeolites and

sands. AMDS is a nontoxic, highly stable, low-cost material that contains various metal oxides and is rich in iron oxide (56.6%). The results showed that AMDS had the best adsorption efficiency. It also has a higher surface area, lower density, and smaller grain size when compared to the other adsorbents. This is largely attributed to the higher amounts of Fe_2O_3 and FeOOH, which result in better performance of H_2S removal. The breakthrough curve was directly proportional to the initial concentration of H_2S, so the curve reached capacity quickly when the initial concentration of H_2S was increased. H_2S adsorption capacity also decreased with increasing H_2S flow rate. In the case of AMDS, a H_2S flow rate of 0.5 L min^{-1} was associated with a 1.33-fold higher H_2S adsorption capacity than a flow rate of 2.0 L min^{-1}. With an initial H_2S concentration of 110–126 ppmv and a gas flow rate of 0.02 L min^{-1} at ambient conditions, AMDS exhibits a 5% breakthrough capacity of 8361 mg/g, which is one of the highest values reported in the literature and is 30 times higher than that of zeolite 13X.

Although metal oxides, such as AMDS, exhibit good adsorption capacities for H_2S, there are several disadvantages that arise with their use. Since the absorption mechanism is usually irreversible chemisorption, it leads to high costs from replacement and disposal of spent adsorbents. For example, the adsorption capacity of regenerated AMDS in the next two cycles dropped to 22% and 12% of that of the fresh sample, when the regeneration took place at room temperature. When regenerated at 200 °C, the adsorption capacity of AMDS reduced to 11%. In addition, the utilization of unsupported metal oxides may lead to the reduction of desulfurization performance with time because they would rapidly sinter and aggregate during sulfidation-regeneration cycles at high temperatures. They must also be carefully monitored for spalling and sublimation. Overall, their use is limited by poor chemical and mechanical stability at high temperatures and low surface areas at low temperatures.

2.3.3. Carbon-based sorbents

Activated carbons and other carbon-based materials are widely used as adsorbents for low temperature desulfurization due to their large specific surface area (>1000 m^2/g), high pore volume, high thermal stability, and controllable surface chemistry. Since AC is produced from different types of easily available carbon sources, such as coal, wood, coconut shell, rice husks, peat, etc., it is generally cheaper than other types of adsorbents. The adsorption chemistry of ACs and other porous carbon materials is highly controlled by their surface functionalization [282,283], which largely determines the strength of adsorbate-adsorbent interactions and, consequently, the extents of physical and chemical absorption. As such, a wide range of functionalized carbon-based sorbents synthesized via heteroatom doping, impregnation, or deposition–precipitation has been investigated so far [284–289]. Recently, a direct integration method has been proposed as a better alternative to impregnation [290].

Ou et al. [291] investigated the application of granular activated carbon (GAC) for H_2S removal from the biogas generated by small- to medium-sized cattle or pig farms. In this regard, they conducted a long-term investigation of the sorbent performance for biogas generated from treating wastewater collected from 200 dairy farms. The tests were performed at different gas volumes, adsorbent masses, and inlet H_2S concentrations without a systematic procedure to analyze the impact of different factors. Therefore, it is not possible to draw proper conclusions. However, for inlet H_2S concentrations of 932–1560 ppm and a breakthrough concentration of 100 ppm, GAC provides breakthrough capacities of 745–1293 mg/g at 20–25 °C. For higher inlet H_2S concentrations of 1920–2060 ppm, the breakthrough capacities were found to be 615–703 mg/g. These values are quite high when compared to other types of adsorbents. Low cost and high adsorption capacities make GAC an attractive choice for the application. Nevertheless, no attempt was made to regenerate the sorbent.

Using waste biomass sources to make carbon-based adsorbents lowers the cost of adsorption and increases resource efficiency. The lignin and cellulose content of the waste biomass positively impacts the yield and microporous surface area of the resulting biochar [292]. Sawalha et al. [293] synthesized activated carbons from spent coffee grains (COF), eucalyptus barks (EUC), and almond shells (ALM), which are all locally available biomass wastes in Palestine, to capture H_2S from biogas containing an average of 970 ppm H_2S. Following the order of the lignin content in the biomass sources, the obtained biochar yields (w/w) were 36%, 28.5%, and 23.9% for EUC, ALM, and COF, respectively. This order remains the same for breakthrough time, adsorption capacity, and removal efficiency. For a bed height of 2 cm and gas flow rate of 1.5 L/min at ambient conditions, EUC performed the best by a significant margin with an adsorption capacity of 490 mg/g and a time to saturation of 180 min, while COF was quite poor with an adsorption capacity of 22 mg/g and a time to saturation of 10 min. In comparison, GAC studied by Ou et al. [291] performed much better at similar conditions. Sawalha et al. observed that increasing bed height provides increasing adsorption capacity and removal efficiencies. For example, the saturation time of COF increased from 10 min to 170 min when the bed height was increased from 2 cm to 8 cm, likely due to the longer contact time between adsorbent and adsorbate. The authors then impregnated EUC with 20 wt% KOH or $ZnCl_2$ to create functionalized ACs and found that KOH/EUC provides a much better performance than $ZnCl_2$/EUC. The basic nature of KOH promotes dissociative adsorption of H_2S while the acidic nature of $ZnCl_2$ prevents it. This is the cause for the difference in capacities between the two functionalized EUCs. However, the authors did not calculate the adsorption capacities for these materials. Upon comparison between the breakthrough curves of EUC, KOH/EUC, and $ZnCl_2$/EUC, we conclude that the performance of EUC and KOH/EUC is practically identical, whereas the performance of $ZnCl_2$/EUC is worse than EUC but better than ALM. This wasn't addressed by the authors. Since the distribution of pore diameters and volumes before and after impregnation was not provided, we can only speculate that the effect of pore blocking or collapse balances out the effect of increased pH and additional active sites in the case of KOH/EUC. On the other hand, loss of pore structure and decreased pH compounded each other to decrease the adsorption capacity of $ZnCl_2$/EUC when compared to EUC.

Surface functionalization with metal oxides or hydroxides is one of the most common ways of imparting basicity to the surface of the carbon sorbent and provide additional active sites for H_2S capture. In simple terms, the favorable chemical properties of the metal oxides combined with the favorable textural and structural properties of the carbon materials offer a beneficial pathway to enhance H_2S adsorption [284]. Yang et al. [294] reported the use of ZnO-MgO/AC adsorbents with a total metal oxide content of 20 wt%. The authors expected that ZnO would lead to chemisorption of H_2S while MgO would facilitate the dissociation of H_2S, the latter of which is beneficial for both reactive adsorption and catalytic oxidation [295]. In moist conditions and for a breakthrough concentration of 0.1 ppmv, the sorbent with a molar ratio Mg/(Mg + Zn) of 0.2 provides uniform dispersion of the oxides, the longest breakthrough time (380 min), and the highest breakthrough capacity (113.4 mg/g). This sorbent also showed a high adsorption capacity of 96.5 mg/g in dry conditions. The results confirmed the key role played by MgO in enhancing the H_2S adsorption capacity of the ZnO-based AC. Addition of MgO promoted dissociative adsorption, but increasing the MgO content beyond a certain amount led to pore blocking. No regeneration experiments were performed to assess the cycle dependency.

Yang et al. [287] also prepared $ZnFe_2O_4$/AC adsorbents using commercial pelletized wood-based AC with various $ZnFe_2O_4$ loadings (5–30 wt%) via impregnation followed by calcination. They found that the optimum loading was 10 wt%, which results in a breakthrough capacity of 122.5 mg/g. The pure mixed metal oxide and the unmodified AC have breakthrough capacities of 1.6 mg/g and 5.6 mg/g, respectively. The authors explored the effect of the surface oxygen-containing groups on the performance of 10 wt% $ZnFe_2O_4$/AC and found that, as long as the pore structure remains intact, the surface functional groups have negligible impact on the adsorption capacity. Thermal treatment at 500

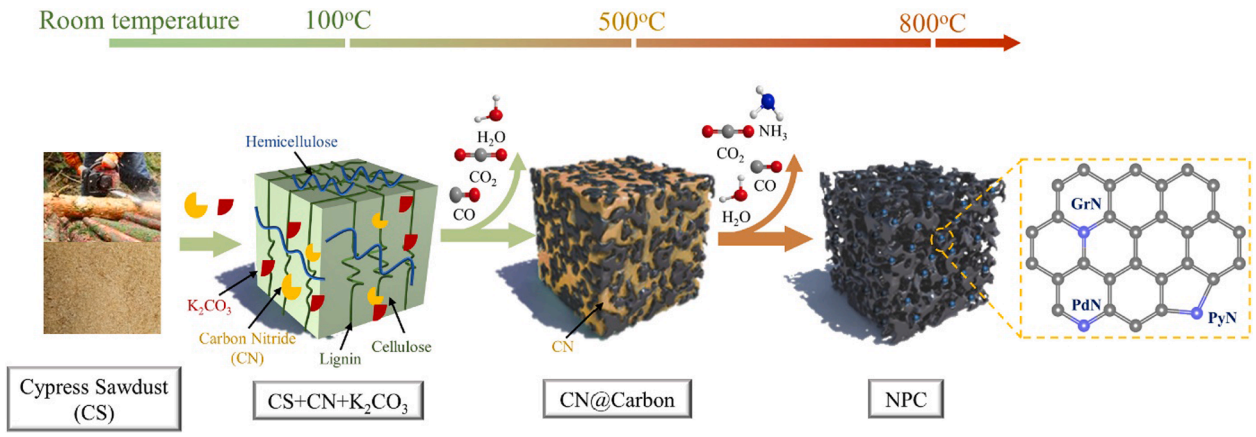

Fig. 4. Formation of N-rich hierarchical porous carbons via pyrolysis of cypress sawdust and carbon nitride. Reprinted with permission from [301]. © 2021 Elsevier.

°C under N_2 for 2 h led to the regeneration of the adsorbent with little loss (2.2%) in the adsorption capacity over three regeneration cycles. Yuan et al. [296] prepared the same sorbent in a one-step strategy. However, instead of using a commercial AC material, they used leftover kitchen rice. In addition, the loading of the mixed metal oxide was varied from 25 wt% to 75 wt% and the activation temperature from 400 °C to 600 °C. The rice-derived carbon without the addition of metal-based activators exhibited a low surface area of 2.76 m^2/g and a low breakthrough capacity of 12.11 mg/g. The results showed that the best metal oxide loading was 50 wt% and the best activation temperature was 500 °C. This is in stark contrast to the study by Yang et al., who found that increasing the oxide content over 20 wt% resulted in a drop in sorption capacity. The difference becomes greater considering yield of biochar that was not reported by Yuan et al. Since the actual AC content is much less than the amount of rice used, the resulting oxide loading in AC is higher than 50 wt%. The corresponding adsorbent, RZF-500–1:1 (500 °C activation temperature with a 1:1 mass ratio of rice to mixed metal oxide), exhibited the highest breakthrough capacity of 228.29 mg/g with a surface area of 1065 m^2/g. This material can also be regenerated by thermal treatment with a minimal loss of 4.5% and 8.6% after three and five regeneration cycles, respectively. Moreover, Yang et al. and Yuan et al. hypothesized that the FeOOH, a possible intermediate in the desulfurization process, promotes the dissociation of H_2S. The major difference between the $ZnFe_2O_4$/AC materials studied in these two works is the presence of N-groups in rice-based carbon matrix. These groups are known to increase the sorption capacity of porous carbon materials and will be discussed further below.

On a similar note, Pan et al. [286] synthesized 2D CaO/carbon heterostructures (CHs) from calcium gluconate in a facile, one-step carbonization method. The obtained catalysts were named as CaO/CH-x, where 'x' represented the carbonization temperature (≥700 °C). Morphological analyses confirmed the formation of ultrathin 2D carbon nanosheets with C, O, and Ca homogeneously distributed on the surface. The 2D nanosheet structure could not only provide faster reaction kinetics by shortening the H_2S diffusion pathway into the bulk but also enhance the sulfur capacity at room temperature by serving as the storage space to accommodate the produced elemental sulfur [297]. The authors also found the presence of numerous oxygen-containing functional groups in the carbon matrix. The surface area of these structures increased with increasing carbonation temperature. CaO/CH-700 exhibited the strongest alkalinity and a breakthrough capacity of 9100 mg/g, a high value for any class of adsorbents. CaO/CH-800 and CaO/CH-900 exhibit surface roughness, lower alkalinities, and increased particle sizes, thus hindering the dissociation of H_2S and the subsequent oxidation reaction. Despite its high sulfur capacity, CaO/CH-700 shows an extremely poor regeneration ability (<0.2 g/g) owing to the irreversible chemical reaction between CaO and H_2S.

Over the past decade, nitrogen-rich carbonaceous materials have emerged as metal-free adsorbents and catalysts for H_2S capture and oxidation [298]. They are touted as safer, more sustainable, and more efficient alternatives to carbons functionalized with metals, metal oxides, or caustic compounds [299,300]. Chen et al. [301] synthesized N-rich hierarchical porous carbons (NPCs) via one-step strategy from cypress sawdust (CS) with carbon nitride (CN) loading and K_2CO_3 activation (see Fig. 4). The prepared carbons were named NPC-*n*, where *n* represented the weight ratio of CN to CS. Porous carbon material without CN loading was named as PC while the porous carbon material without K_2CO_3 activation was named as NC (CN/CS = 1). The authors reported that the NPCs showed hierarchical porous structure with microporous and mesoporous volumes up to 0.434 and 0.597 cm^3/g, respectively. It must be noted that the one-step, in-situ synthesis allowed NPCs to maintain similar or higher surface areas than PC. Except NPC-0.5 which has an N content of 4.56 wt%, the other NPCs had >9.69 wt% of N content, higher than the 8.11 wt% in NC which has a CS/CN loading of 1 without chemical activation. In contrast to post-synthesis urea modification followed by K_2CO_3 activation [302], the one-step strategy used in this work resulted in the activator having no impact on the N content. The breakthrough capacities of NPCs increased rapidly when the ratio of CN/CS increased from 0.5 to 1 and then decreased slightly when the ratio of CN/CS increased from 1 to 2. While PC exhibited a relatively weak H_2S removal performance (19.5 mg/g), the NPCs achieved a maximum breakthrough capacity of 426.6 mg/g, demonstrating the enormous impact of N-doping. Although CN loading significantly enhances the H_2S removal by increasing N content and introducing active N-containing functional groups to the carbon, excessive CN may cause the partial micropores and mesopores to collapse into some macropores during carbon pyrolysis process. With S and SO_4^{2-} as the main desulfurization products, a two-step water scrubbing and heating treatment method efficiently regenerated the exhausted NPCs. The breakthrough capacities are reported to be 99.03% and 86.3% of the initial value after one and five regeneration runs, respectively.

Fakhraie et al. [303] prepared activated carbons with high nitrogen-doping (HNAC) derived from nitrogen-rich carbon quantum dots (N-CQDs) after high-temperature activation with KOH. The pore structures of HNACs differed for different activation temperatures, activation times, and KOH/N-CQD mass ratios. Just as in the work of Chen et al. [301], the N-rich carbon structures exhibited low surface area and porosity before the activation step. After KOH activation at high temperatures (ca. 800 °C), the amorphous and spherical of N-CQDs was transformed into micro-mesoporous, graphene-like structures with uniform nanosheet fragments. However, increasing the activation time beyond 1 h and KOH/N-CQD ratio beyond 2 would lead to a significant loss in porosity and structure. Although KOH activation imparted a

porous structure, it also lowered the N content from 16.49 at% in N-CQDs to 2.63 at% in HNAC-812 (activated at 800 °C for 1 h with a KOH/N-CQD ratio of 2). This behavior is in line with prior literature [304–306], which demonstrates that high-temperature KOH activation leads to decomposition or consumption of some N-species. Among the prepared HNACs at 1 bar and 25 °C, HNAC-812 and HNAC-802 possessed the highest H_2S adsorption capacities of 316.35 mg/g (H_2S/CO_2 selectivity of 2.17) and 284.05 mg/g (H_2S/CO_2 selectivity of 1.83), respectively. In addition, regeneration tests on HNAC-812 at 120 °C for 4 h under vacuum pressure via pressure swing adsorption showed that the adsorbent maintained 94% of its initial capacity at the end of 10 cycles.

Similarly, Yu et al. [307] reported high-performing N-doped mesoporous carbon nanosheets (NMCS) derived from microporous Zn-based zeolitic imidazole framework (ZIF), ZIF-8. Since the carbon source is also the nitrogen source, this method also comes under in situ N-incorporation methods. Unlike NC from the work of Chen et al. and N-CQDs from the work of Fakraie et al., NMCS itself has a high surface area of 1937 m^2/g and a high adsorption capacity of 510 mg/g. After impregnation with 20 wt% Na_2CO_3, the surface area and pore volume reduced nearly by 50%, but the adsorption capacity jumped to 1370 mg/g. However, no regeneration experiments were performed. With N-doping, the nitrogen functional groups could directly incorporate within the carbon matrix and provide stable Lewis basic sites on the surface of carbon catalysts. This promotes the surface polarity and electron donating ability of the material, thus dramatically improving the catalytic performance of the carbon-based metal-free catalyst [308,309]. However, in situ N-doping is not the only way to introduce such functional groups to different carbon-based sorbents [310–312].

Wang et al. [313] loaded polyethyleneimine (PEI) into mesoporous carbon nanosheets (MCNs) via impregnation to promote the selective oxidation of H_2S. Due to the interconnected pore network, PEI was uniformly dispersed into the carbon matrix at nanoscale, enabling a high H_2S/active site interfacial area. Although the pristine MCNs themselves have a high surface area of 872 m^2/g, a large pore volume of 2.97 cm^3/g, and an average pore size of 7.5 nm, they have negligible H_2S catalytic oxidation capacity. After PEI loading, the porosity of the support decreases dramatically due to abundant PEI molecules covering the pores. This is an inherent risk of post-treatment N-functionalization routes such as impregnation. With the increasing PEI amount from 0 wt% to 65 wt%, the surface area and pore volume decrease from 872 to 31 m^2/g and 2.97 to 0.15 $cm^3\ g^{-1}$, respectively. The breakthrough sulfur capacity gradually raises with the PEI loading content and reaches a maximum value of 13.68 mmol/g at the PEI loading of 25 wt%. Further increasing the loading amount of PEI to 50 wt% leads to loss of performance owing to the disappearance of the H_2S/PEI interfacial area caused by the pore blocking, making it difficult for H_2S diffusion into the deeper carbon layers. The authors also replaced MCNs with SBA-15 to demonstrate the role of the 2D carbon matrix. They found that the breakthrough capacity of SBA-15 loaded with 25 wt% PEI is over 17 times lower with almost no sulfur detected on its surface. This demonstrates that the carbon nanosheet matrix not only contributes to the catalytic oxidation of H_2S but also enhances the removal efficiency. MCNs-PEI-25 also displays a remarkable regeneration ability with no loss in performance over six regeneration cycles.

Thermal treatment with ammonia is another common way to introduce N-groups into porous carbon materials. For example, Xu et al. [314] obtained N-doped porous carbons from waste air-laid paper through KOH impregnation following by high-temperature ammonification. They observed that the fibrous-like morphology of the raw biomass turned into 3D honeycomb-like porous structure after KOH impregnation and remained the same after NH_3 post-treatment. This 3D structure possessed high surface area and a largely microporous structure with the additional presence of both mesopores and macropores. For feed gas containing 1 vol% H_2S, the N-doped carbons were able to obtain >85% H_2S conversion and >80% sulfur selectivity. They attributed this performance to the combination of defect degree, high surface area, and abundant pyridinic N. As discussed so far, the effect of the N-groups in enhancing the properties of the carbon material depends on the strategy used to incorporate those groups and the type of N-groups that are formed. Li et al. [315] and Leng et al. [316] provide a more targeted and detailed review of these strategies and their effects.

Although carbon-based materials have been studied for H_2S adsorption for a long time, the past decade has seen an increased focus on the development of cost-effective, high-capacity, regenerable, and sustainable adsorbents. As it stands, they are some of the best materials reported for H_2S capture at low temperatures. However, more emphasis must be placed on regeneration tests in experimental studies. The future research in this field is likely to heavily focus on materials with 1D or 2D hierarchical porous structures functionalized with N-groups or metal oxides that can be prepared using low-cost, sustainable precursors in easy one-step syntheses. Although the cost of material would go up with functionalization, the increases capacities and satisfactory regeneration exhibited by some of these sorbents could soon make hierarchical porous carbons functionalized by metals or N-groups an extremely competitive choice for H_2S removal in many applications.

2.3.4. Metal organic frameworks

Metal-organic frameworks (MOFs) are a special class of solid-state organic–inorganic hybrids that have recently emerged as modular and functional porous materials [317]. They are crystalline materials with ultrahigh porosity (up to 90% free volume), enormous internal surface areas (1000 to 10,000 m^2/g), high thermal and chemical stability, and an extraordinary degree of variability for both the organic and inorganic components of their structures [318,319]. This makes MOFs target candidates for potential applications as gas (hydrogen, methane, etc.) storage media in clean energy infrastructure and as high-capacity adsorbents (CO_2, SO_2, H_2S, NH_3, etc.) to meet various separation needs [320–325]. As such, MOFs are gradually gaining popularity as adsorbents for H_2S.

Gupta et al. [326] studied three copper-based MOFs (CuBDC, CuBTC, and CuBDC-N) for H_2S removal at room temperature. The surface area of CuBDC and CuBTC was significantly higher than CuBDC-N. CuBDC formed thin sheet-like structures with micropores and mesopores. CuBTC formed crystals with no well-defined morphology with micropores and mesopores. CuBDC-N, on the other hand, is largely in the form on prismatic-shaped microcrystallites with mesopores. The large particle size of CuBDC-N was responsible for its low surface area. The H_2S absorption capacities of CuBDC, CuBTC, and CuBDC-N are calculated to be 105.6, 27.1, and 1.3 mg/g, respectively. The Cu^+/Cu^{2+} ratio governed this trend since the strong interactions of HS^- or S^{2-} with Cu^{2+} sites dominated the adsorption process. For instance, CuBDC has the lowest Cu^+/Cu^{2+} ratio and the highest absorption capacity. Surprisingly, amine-functionalized CuBDC performed much worse than CuBDC. This could be due to several reasons, such as its much smaller surface area and lower Cu^{2+} content. Zhang et al. [238] previously reported that the presence of primary or secondary amine groups adversely affects the structure of MOF-199 (or HKUST-1 or CuBTC) while a tertiary amine group up to a certain amount enhances its H_2S removal performance. FTIR spectra showed that CuBDC-N has distinct bands for N–H bond vibrations, suggesting the presence of secondary amine groups. The strong interaction between these groups and the copper center likely caused the collapse of the porous structure, which in turn resulted in a low surface area and a low adsorption capacity. Gupta et al. also observed that the breakthrough capacities of CuBDC-N and CuBTC increased in moist conditions due to the easier dissociation of H_2S to HS^- in the water film. However, CuBDC experienced a decrease in its capacity in the presence of moisture. In addition, the XRD pattern of spent CuBTC showed a partial loss in the crystallinity due to the formation of sulfuric acid and Cu–S bonds.

Although the irreversible nature of the chemisorption process makes it difficult to regenerate H_2S-loaded Cu-MOFs, Gupta et al. [326]

adopted a two-step methanol and UV-assisted regeneration method in an attempt to remove physically adsorbed H_2S and generate new binding sites. However, this process could not regenerate CuBDC-N. CuBDC was partially regenerated with the breakthrough capacity of regenerated CuBDC only 32% of the fresh CuBDC, suggesting that most of the Cu-sites were bound to sulfide and could not be regenerated. On the other hand, regenerated CuBTC showed an exceptional adsorption capacity of 95.6 mg g^{-1} which is 3.5 times that of the fresh CuBTC. The authors attribute this significant rise in capacity to the increased surface area and availability of unoccupied Cu sites that were previously inaccessible. This shows that the regeneration process proposed here is a cost-effective method to recycle a few chemisorbed MOFs without compromising their structural and functional integrity.

Gupta et al. [327] also investigated a Cu-based mixed-ligand MOF, $Cu(BDC)_{0.5}(BDC\text{-}NH_2)_{0.5}$, at the same conditions. It has a similar thin sheet-like morphology as the CuBDC discussed above but with a much smaller surface area due to the aggregation of nanosheets into microsheets and pore blocking by the amine groups. Nonetheless, it showed an absorption capacity of 128.4 mg g^{-1} for 500 ppm of H_2S flowing at a rate of 0.1 L min^{-1}. The feed flow rate had a market effect on the adsorption capacity, which decreased drastically from 128.4 mg/g at 0.1 L/min to 64 mg/g at 0.2 L/min to 2.6 mg/g at 0.4 L/min. Presence of moisture was found to be detrimental to the performance of the MOF. The authors observed that the adsorption takes place by breaking Cu-carboxylate while forming covellite CuS nanoparticles and sulfates. The amine groups also took part in the adsorption process by strongly interacting with H_2S. The methanol and UV-assisted regeneration method could only partially regenerate the MOF with the absorption capacities successively dropping to 22.9, 17.4, and 9.9 mg/g after the first thre8e regeneration cycles. Moreover, various characterization tests indicate a structural collapse after UV-based regeneration due to the loss in the node-linker interactions.

Zárate et al. [328] employed a water-stable microporous MOF, MIL-53(Al)-TDC, for H_2S removal at 30 °C and 1 bar from a feed gas containing 5 vol% H_2S. They reported a breakthrough capacity of 18.13 mmol/g or 618 mg/g, which is the highest reported value among MOFs albeit at high inlet and breakthrough concentrations of H_2S. Their results showed the formation of hydrogen bonds between H_2S molecules themselves confined in the pores of MIL-53(Al)-TDC, a relatively weak hydrogen bonding interaction between H_2S and the μ-OH group that bridges two Al metal centers, interactions between H_2S and the thiophene linkers, and an overall weak H_2S adsorption within the pores of MIL-53(Al)-TDC. They demonstrated that MIL-53(Al)-TDC retains its crystal structure upon H_2S exposure. Moreover, cyclic absorption–desorption experiments at the same conditions showed that the H_2S absorption capacity remained constant at around 18.5 mmol/g over five cycles, indicating that H_2S is completely desorbed in the MOF regeneration step. The MOF was regenerated by simply flowing dry N_2 gas between 65 and 200 °C. Overall, this MOF stands out as one of the best adsorbents and arguably the best MOF in terms of fresh adsorption capacity, chemical stability towards H_2S adsorption, mild regeneration conditions, and cyclic regeneration capacity.

Flores et al. [329] studied the performance of another water-stable MOF, MFM-300(Sc), for H_2S adsorption and reported an adsorption capacity of 16.55 mmol/g or 564 mg/g at 25 °C with a feed gas containing 10 vol% H_2S. Although this MOF also retained its crystalline structure upon adsorption and desorption, its pore volume reduced by 34%, signifying the presence of irreversibly adsorbed species. The reactivation of this MOF is carried out by simply purging with dry N_2 for 15 min at 25 °C. Cyclic absorption–desorption experiments showed that the adsorption capacity fell by 39% to 10.08 mmol/g after the first regeneration cycle. However, the capacity remains almost constant from the second to the fifth cycle. Increasing the regeneration temperature to 250 °C does not influence the capacities, confirming that the reduction in capacity after the first cycle is due to irreversible chemisorption. They found that the irreversibly chemisorbed species are polysulfides resulting from the strong hydrogen bonding between H_2S molecules themselves confined in the pores. In addition, they postulated that only low-order polysulfides ($n = 2$) are formed and that it occurred only during the first adsorption cycle. Since such small polysulfides cannot completely block the pores, a majority of the pore volume was still available. Beyond this, no more polysulfides are formed in the consequent cycles, and H_2S is only physisorbed.

Grape et al. [330] synthesized the first bioinspired microporous MOF, $Bi_2O(H_2O)_2(C_{14}H_2O_8)\cdot H_2O$ (SU-101), using phytochemical ellagic acid under ambient aqueous conditions without any external energy input. They reported that it is thermally stable up to 250 °C in air and that the overall chemical stability of SU-101 appears to be better or similar to that of commonly used MOFs such as UiO-66 and ZIF-8. Applied towards H_2S removal at 25 °C from a feed gas containing 4.3 vol% H_2S, the adsorption capacity is found to be 15.95 mmol g^{-1} or 543.6 mg/g. Although the adsorption capacity of SU-101 is close to that of MFM-300(Sc), the surface area is much smaller (412 vs. 1360 m^2 g^{-1}). After the MOF was regenerated, they found that the absorption capacity and surface area decreased to 0.2 mmol g^{-1} and 15 m^2 g^{-1}, indicating that the capture mechanism in SU-101 is irreversible chemisorption. The chemisorbed species is found to be polysulfides, which completely block the pores of SU-101 and exhibit relatively strong interaction with the phenolate group of SU-101. Although SU-101 and MFM-300(Sc) cannot be regenerated, their high stability and polysulfide formation could pave the way towards MOF-based lithium/sulfur batteries [331].

As seen in Table 4, MOF-based studies tend to report the adsorption capacities at saturation and/or high H_2S concentrations in the feed. These conditions often inflate the performance of the material beyond what can be achieved in realistic conditions. Lee et al. [239] compared the performance of three MOFs (MOF-199, MOF-5, and $UiO\text{-}66\text{-}NH_2$), two amine-functionalized covalent organic polymers (CBAP-1-EDA and CBAP-1-DETA), and commercial carbonaceous sorbents (Carbopack-X and charcoal AC) at a low partial pressure (1 Pa = 10 ppmv) of H_2S at 1 bar and 25 °C. MOF-199 (CuBTC) significantly outperformed the rest with breakthrough (10%) and saturation capacities of 40 and 69 mg/g, respectively. The adsorption performance at the breakthrough point followed the order: MOF-199 > MOF-5 > AC > $UiO\text{-}66\text{-}NH_2$ > CBAP-1-EDA > CBAP-1-DETA > Carbopack-X. However, all the MOFs in this study were found to undergo structural deformation upon interaction with H_2S.

ZIFs are a subclass of MOFs with structures similar to conventional aluminosilicate zeolites. Simply put, ZIFs can be pictured as zeolites with the tetrahedral Si(Al) and the bridging O replaced with transition metal ion and imidazolate linkers, respectively [332,333]. As a result, ZIFs possess the combined advantages of both MOFs and zeolites. Generally, they have higher thermal and chemical stability than MOFs and higher porosity than zeolites [334]. This has led to explosive research activities employing ZIFs for various applications, including CO_2 capture and separation [335,336]. However, studies on their potential for H_2S capture have been rather limited. Over the past three years (as of December 2021 in the Web of Science Core Collection), there have only been two experimental studies applying ZIFs for H_2S removal. Jameh et al. [337] investigated the effect of ethylenediamine (ED) functionalization on the performance of ZIF-8 nanoparticles. As has been the trend with functionalization via impregnation, ED enhanced the adsorption capacity of ZIF-8 up to a certain amount of loading (here, ED: ZIF-8 = 5:100 by mass) after which its beneficial effect became inferior to the pore blocking it causes. For pure H_2S at 1 bar and 25 °C, ED-ZIF-8 1st (5:100 wt ratio of ED and ZIF-8) exhibited the highest saturation capacity of approximately 325 mg/g. For an industrially relevant feed gas stream containing 3 vol% H_2S at 2 bar and 25 °C, the same material had a breakthrough (1500 ppmv) capacity of about 3299 mg/g. Both physical and chemical adsorption took place with the former being the dominant capture mechanism. Although it was mentioned that the material maintained its structural stability after regeneration under vacuum at 120 °C, no information on the adsorption performance of the

regenerated sample was provided. Moreover, in the same mixed gas conditions, ED-ZIF-8 1st had 3 times higher breakthrough capacity for CO_2, making it a promising choice for acid gas removal but not for selective removal of H_2S. The only other experimental study [338] on ZIFs for H_2S capture used ZIF-67 modified by triethylamine. Although the prepared materials were reported to have high removal efficiencies, their adsorption capacities have not been reported. Besides, the material could not maintain structural integrity after H_2S adsorption.

The major theme in most of the studies on H_2S capture using MOFs is the lack of structural stability under external stimuli, especially in the presence of H_2S [339,340]. In general, this property should be possible to be tuned by varying the nature of the metal sites. MOFs based on Cu, Zn, and Fe are commonly used yet unstable for H_2S adsorption, whereas MOFs based on Al, Mg, Ni, V, Zr, and Ti demonstrate robustness to H_2S environments [340,341]. Furthermore, the organic linkers and their functionalization also has a major effect on the material's stability [342]. For example, fluorinated MOFs exhibited high stability against H_2S and H_2O [343–345]. Even though the exact mechanism or cause of structural deformation in MOFs is still unknown, a few studies [341,346] have theoretically evaluated the interactions between MOFs and acid gases (H_2S and SO_2) and proposed strategies to tune the topology and functionalization of MOFs towards stability. In addition to chemical stability, the high price of MOFs is a hurdle for their industrial adoption. Despite these disadvantages, MOFs hold high promise among the research community. Since the application of MOFs towards H_2S adsorption is a relatively young endeavor, there is still much to explore.

2.3.5. Composite materials

A composite sorbent is formed by combining two or more different adsorbents to benefit from their synergistic properties. These are analogous to hybrid blends in the case of absorbents. Many of these have been covered in the previous subsections as seen fit, attesting to the widespread adoption of composites over pure, virgin materials. Gupta et al. [347] studied three Zn-MOF/ZnO nanocomposites with different organic linkers for adsorptive removal of H_2S gas at room temperature. The authors found a large presence of ZnO in the MOFs with the Zn content of 5.25%, 5.47%, and 4.82% in ZnBDC/ZnO, ZnBDC-N/ZnO, and ZnBTC/ZnO, respectively. The surface area of Zn-MOF/ZnO nanocomposites was in the range of 12–21 $m^2\ g^{-1}$ with negligible microporosity. Owing to its surface area and porosity, ZnBTC/ZnO exhibited the highest adsorption capacity of 14.2 mg g^{-1}. The order of adsorption capacities is ZnBTC/ZnO > ZnBDC/ZnO > ZnBDC-N/ZnO. In addition, Zn-HKUST-1 performed poorly compared to the nanocomposites, demonstrating the importance of ZnO nanoparticles in the MOF for a higher H_2S uptake. In moist conditions, the adsorption capacity increased for ZnBDC/ZnO but decreased for ZnBTC/ZnO and ZnBDC-N/ZnO. As a result, the order changed to ZnBDC/ZnO > ZnBDC-N/ZnO > ZnBTC/ZnO. The spent ZnBDC/ZnO experienced a significant loss in the MOF crystallinity due to the chemical interaction of S^{2-} with Zn^{2+} ions. Combined methanol- and UV-assisted regeneration method could partially recover the capacities of the composites. Regenerated ZnBDC/ZnO, ZnBDC-N/ZnO, and ZnBTC/ZnO in the second cycle exhibited about 34%, 11%, and 54% of their original capacities.

A popular strategy to mitigate issues arising from the usage of metal oxides is to support the metal oxides on mesoporous silica-based structures or other porous carriers. Such carriers should ideally offer high specific surface areas and structural stabilities. They should also increase the efficiency of mass transfer by reducing the resistance to gas diffusion. Carbon-based carriers were discussed in Section 2.3.3. Wu et al. [348] compared the hot coal gas desulfurization performance of Zn-based sorbents supported on MCM-41 and MCM-48. Based on material characterization, the authors opined that the introduction of the active component is more likely to cause pore plugging in the 3D cubic channel arrangement of MCM-48 than the 2D hexagonal pore arrangement of MCM-41. Although MCM-41 and MCM-48 have similar pore sizes and specific surface areas, the breakthrough sulfur capacity of 30 wt% ZnO/MCM-41 is 24.4–56.3% greater than that of 30 wt% ZnO/MCM-48. At desulfurization temperatures of 400–700 °C, ZnO/MCM-41 has its best performance at 500 °C and ZnO/MCM-48 at 600 °C. The initial desulfurization reaction rate constants of ZnO/MCM-41 are 1–13 times greater than those of ZnO/MCM-48, suggesting that the former provides higher number of active sites for desulfurization. This is attributed to the disparity in the structure of these sorbents. Larger wall thicknesses of MCM-41 compared to MCM-48 makes the former more stable at higher temperatures. On top of this, the introduction of ZnO into MCM-41 increased the wall thickness of the material, which was in contrast to the decreased wall thickness in ZnO/MCM-48. ZnO/MCM-41 also exposes more active sites due to the smaller sizes of both the support particles and the ZnO grains, while its higher porosity is beneficial for gas diffusion into and out of sorbents. Furthermore, the authors observed that the simultaneous presence of CO and H_2 in the coal gas has a synergistic effect on the breakthrough capacities of both the sorbents, with a higher improvement in ZnO/MCM-41 (7.1–24.5%) than ZnO/MCM-48 (0.7–11.5%). However, supported metal oxides have a major drawback that must be addressed. The nature of desulfurization using metal oxides is such that oxides are converted to sulfides which, due to their larger size, cause an expansion of pore structure and may lead to breaking of the carrier.

Basina et al. [349] proposed the use of heterostructures made of CuO encapsulated in an ultra-thin mesoporous SiO_2 matrix that are prepared using a surfactant-based method with $Cu(OH)_2$ as the intermediate seeds of CuO. Depending on the synthesis conditions, composites with diverse morphologies (spheres, fibers, wires, and leaves) and sizes (ranging from <2 nm to 25 nm) were obtained. These composites possessed a combination of relatively large meso/macro cavities interconnected by mesoporous channels. This allowed for protection against sintering. H_2S adsorption studies revealed that the best composites had a high loading of CuO, a crystallite size of 14–25 nm, large macro-cavities providing ample space for the particles to expand and contract, and a high degree of interconnectivity for easy diffusion. The highest stable cyclic sulfur capacity of 10.224 ± 1.076 mmol/g_{CuO} (a fresh capacity of 11.10 ± 1.25 mmol/g_{CuO}) was observed in the composite of 16.7 nm CuO/SiO_2 with a loading of about 91 wt% CuO and a leaf-like morphology.

Okonkwo et al. [350–352] investigated the performance of sterically hindered and unhindered amines grafted onto SBA-15 under both dry and humid conditions. Over the course of the three studies, they studied 3-aminopropyltrimethoxysilane (APS), (*N*-methylaminopropyl)trimethoxysilane (MAPS), (*N*,*N*-dimethylaminopropyl)trimethoxysilane (DMAPS), (3-amino-3-methylbutyl)trimethoxysilane (AMBS), (N-cyclohexylaminopropyl)trimethoxysilane (CHAPS), and (*tert*-butylaminopropyl)trimethoxysilane (TBAPS). Among these, only TBAPS and DMAPS were used to evaluate the impact of humidity on sorption performance. The amine loading of the sorbents was set to 1.7–2.0 mmol N/g under dry conditions and 2.2–2.9 mmol N/g under humid conditions. Under dry conditions at 30 °C with a feed gas containing 1% H_2S in N_2, the adsorption capacities of the sorbents follow the trend of MAPS > APS > TBAPS > CHAPS ≈ AMBS > DMAPS. The cyclic stability of the unhindered primary amine, APS, is found to be relatively unsatisfactory (35% loss from the second to fourth cycle), while the rest of the amines showed good to excellent cyclic stability over at least three cycles. When the feed gas was changed to 1% H_2S and 10% CO_2 in CH_4, the H_2S adsorption capacity of MAPS/SBA-15 halved from about 6.8 mg/g to 3.4 mg/g. In contrast, the sorption capacity of TBAPS/SBA-15 increased by a little over 10%. The trend in sorbent capacities changed to TBAPS ≈ MAPS > CHAPS ≈ AMBS > DMAPS. These results show that steric hindrance plays a key role in the capacity stability and H_2S/CO_2 selectivity of the supported amines. Although unhindered MAPS (secondary) provides relatively high adsorption capacity, it exhibits poor selectivity for H_2S. Moderately hindered CHAPS (secondary) and AMBS (primary) exhibited relatively stable capacities with moderate increase in CO_2 concentrations (e.g. 0 to 10%), while severely hindered TBAPS (secondary) and DMAPS (tertiary) exhibited highly stable capacities even at

high CO_2 concentrations (0 to 30%). Moreover, as discussed in the case of absorption, hindered amines offer selective H_2S capture. The H_2S/CO_2 selectivity of TBAPS, CHAPS, and AMBS are found to be 40, 11, and 5, respectively. Most importantly, TBAPS/SBA-15 matches some of the most selective adsorbents for desulfurization with essentially no CO_2 or CH_4 uptake.

However, Okonkwo et al. [352] observed that the presence of humidity makes a significant impact on the performance of these silica-supported amines. Under humid conditions (49% relative humidity) at 30 °C with a feed gas containing 1% H_2S in N_2, the capacities of TBAPS/SBA-15 and DMAPS/SBA-15 markedly increased by a factor of 9.4 and 33.3, respectively. As a result, DMAPS/SBA-15 provides 50% higher capacity than TBAPS/SBA-15 in the presence of water. Through DFT calculations and spectroscopic analysis, the authors concluded that H_2O promotes proton transfer from H_2S to the amine group, resulting in chemisorbed HS^- species. This is in contrast to weak H-bonding interactions under dry conditions. In addition, the kinetics of H_2S adsorption were found to be significantly faster than that of CO_2, leading to high selectivities observed for both the sorbents. When the humid adsorption is followed by dry He desorption at 120 °C, the capacities decreased significantly each cycle because of incomplete desorption. As noted frequently in this section, chemisorption is usually partially or fully irreversible. However, when the authors tried humid He desorption at 80 °C, TBAPS/SBA-15 and DMAPS/SBA-15 exhibited a loss of 6% and 15% in amine efficiency from the first to second cycles but remained stable from the second to third cycle. The authors opined that the strong bonds of chemisorption formed under humid conditions can likely be reversed only under humid conditions during desorption. Although this provides a potentially valuable pathway towards improved structural reversibility for these and many other sorbents, it must be noted that this would require higher energy and water usage in the regeneration step.

In general, well-designed composite materials provide advantages in performance. However, considering the massive domain of adsorbent materials, it is often a difficult task to pick the right combination of materials and modifications that would ultimately lead to an improved performance. This underlines the major disadvantage of adsorption processes: the lack of accurate understanding of the underlying mechanisms. Another glaring drawback is the apparent choice between high performing sorbents and regenerative sorbents. Barring a few exceptions, all the adsorbents for H_2S capture can be largely divided into these two groups. Materials that provide high breakthrough capacities and selectivities for H_2S do it through partially or completely irreversible chemisorption with the spent sorbents facing some form of structural impairment within a few cycles. Such materials (especially, metal oxides and ACs) are relatively cheaper and generally used as a deep removal step after primary treatment. On the other hand, materials exhibiting complete or a high degree of regeneration capture H_2S through physisorption but do not provide sufficient capacities and/or selectivities for H_2S. Such materials (such as zeolites) are usually more expensive and therefore used in applications where regeneration of the spent sorbent is prioritized. MOFs, being the new materials, currently fall into the category of expensive materials that cannot be regenerated, thus making them unlikely candidates for industrial use.

2.4. Advanced oxidation processes

Advanced oxidation processes (AOPs) were first introduced by Glaze [353] as processes that generate and use reactive species, mainly hydroxyl radicals (·OH), for the acceleration of the decomposition of target compounds. ·OH is a well-known highly oxidant species with a redox potential of 2.8 V, which is higher than other known oxidants, such as sulfate radicals, hydroperoxyl, chlorine, permanganate, persulfate anion, hydrogen peroxide and ozone; it's lower than only fluorine (3.03 V) [354]. Over the years, AOPs have seen a rapid increase in their application for the removal of various compounds in different industrial matrices, such as air and aqueous polluted streams. AOPs come in various forms, including photo-irradiated processes, hydrogen peroxide (H_2O_2)- and/or ozone (O_3)-mediated systems, photo/H_2O_2, photo/O_3, photocatalysis, Fenton and electro-Fenton processes, and plasma-based processes, which all produce ·OH to decompose the target compounds [355,356]. The characteristics of AOPs stated in the literature show that this technology has some significant advantages over the others, including the high efficiencies in very short reaction times, long-term performance stability, the lack of mass transfer limitations, small footprint, high degree of mineralization and yields, the possibility to operate at ambient conditions, and little to no sludge production [357,358]. Some drawbacks have been also expressed by researchers, including requiring UV light to activate catalysts, cost of the photo-reactor, toxicity due to residual H_2O_2 in the effluent, and decreasing efficiency of the photo-mediated process with suspended solids or less soluble salts (more possible for H_2S oxidation process) [359]. However, applying combined AOPs, e.g. photocatalytic/H_2O_2 reactors, or more recently developed systems, e.g. UV–vis/catalyst, can diminish the drawbacks of the conventional AOPs by utilizing the synergy between the individual methods.

In recent years, a few investigations have employed AOPs for the oxidation of gaseous and aqueous H_2S [360–365]. A comprehensive review of the H_2S-degrading reactors is also provided in Table 5, and some of them are discussed here. Yu et al. [360] evaluated the photocatalytic degradation of H_2S using TiO_2 film and a microwave electrodeless discharge lamp (MEDL) as an irradiation source. They could achieve a significant amount of the reactive oxygen species, oxidizing H_2S to sulfate (SO_4^{2-}) as a main product in the purified air stream. At the optimal condition (TiO_2/660 W irradiation), the maximum and minimum removal efficiency of about 68% and 25% were obtained at H_2S concentrations of 5 and 130 mg m^{-3}, respectively. Wang et al. [362] examined a corona discharge plasma system to degrade H_2S along with carbonyl sulfide (COS) and dust (as a carrier for these gases under the electric field). In the plasma reactor, H_2S and COS were decomposed and converted into a higher oxidation state of sulfur compounds such as S, SO_2, and SO_4^{2-} as well as carbon-containing products after interaction with reactant radicals, ozone, and electrons. In this reactor, about 98% and 90% conversions were achieved for COS and H_2S, respectively. The feed to the system contained a concentration of each pollutants in the order of 2100 ppm, O_2 concentration of about 0.8%, and dust content of 5600 (± 5%) mg m^{-3}. Dang et al. [361] reported a non-thermal dielectric barrier discharge (DBD) plasma reactor containing metal oxide catalysts for simultaneous decomposition of H_2S and O_3 and found that adding the catalysts to the plasma process enhanced the H_2S removal efficiency by around 30%. The catalysts performed in the order of Mn > Ag > Cu > Fe. The highest removal of 100% was with Mn, while the lowest removal of almost 75% was with Fe, both recorded at a highest applied voltage of 22 kV. Wang et al. [363] employed a wet bubbling reactor irradiated with UV in the presence of persulfate for degradation of H_2S vapors. Under photolysis of persulfate, the leading active species for oxidation of the sulfide ions (HS^-) are sulfate radical anion ($SO_4{\cdot}^-$) and ·OH, leading to the formation of SO_4^{2-} and sulfur (S^0) as the main products in a liquid phase. A removal efficiency of over 90% was obtained in this reactor under UV irradiation of 72 W with an initial H_2S concentration of up to 1000 ppm.

As an example of the degradation reaction, an oxidation pathway of H_2S is listed in equations (12)-(18) for a UV/TiO_2 reactor. This is a commonly used AOP system because TiO_2 has a proper bandgap, high stability, reasonable cost, and low toxicity [366–368]. In this process, protons and electrons detached from the valence and conduction bands in an irradiated catalyst (TiO_2) can dissociate water and oxygen molecules to produce ·OH and H_2O_2, respectively, which attack H_2S adsorbed on the surface of the catalyst and oxidize it to SO_4^{2-}.

Table 5
AOP-based H_2S removal studies.

Process	Apparatus	Reaction Media	H_2S Amount	Mass of Chemical	Gas Residence Time	Conversion Efficiency (%)	Final Products	Reference
Gas-phase oxidation								
UVA/TiO_2	8 W UV-A lamp/TiO_2 supported by polyethylene terephthalate and cellulose acetate	An annular borosilicate glass	35 ppm	23–30 mg TiO_2	0.7 s with a space time of 1.2×10^6 mg S mol^{-1}	40%	SO_2, SO_4^{2-}	[369]
UVA/Vis/TiO_2	8 W UV-A lamp and 8 W vis light /20% TiO_2–M−MCM−41 (M = Cr or Ce)	Tubular gas flow cylinder	30 ppm	200 mg TiO_2	A residence time of 0.43 s and a space time of 8×10^{10} mg S mol^{-1}	Close to 80%	With Cr: SO_4^{2-} and with Ce: SO_2, SO_4^{2-}	[367]
UV/VUV	Irradiation from microwave (mercury and iodine) discharge electrodeless lamps	Gas flow pipe	0–25 mg m^{-3}	–	1–5 s	~65–93%	SO_4^{2-}	[525]
UV/ TiO_2–SiMgOx	TiO_2-coated glass plates irradiated by two 8 W UV-A lamps	Tubular gas flow cylinder	15 ppm	na	3.6 s	80%	SO_2, SO_4^{2-}	[358]
Plasma/ catalyst:	Plasma/catalyst: Non-thermal dielectric barrier discharge Plasma + catalysts (Mn > Ag > Cu > Fe)	A plasma quartz cylindrical tube having tungsten discharge wire	200 mg m^{-3}	Each catalyst 0.75 wt%	na	75–100%	S, H_2SO_3, H_2SO_4, and likely SO_2 and SO_3	[361]
TiO_2/UV/VUV	Irradiated by a microwave (mercury) electrodeless discharge lamp	Cylindrical TiO_2-coated gas reactor	0–140 mg m^{-3}	na	3.35 s	25–68%	SO_2, SO_4^{2-}	[360]
CdS-ZnS/Fe_2O_3	34 W Vis-light lamp	Packed bed reactor	25 ppm	1000 mg catalyst	na	92%	na	[526]
Corona discharge (plasma)	Reactor consists of a ground electrode, a negative discharge electrode	Gas cylinder	1200 ppm	–	na	98%	S, SO_2, SO_4^{2-}	[362]
Liquid-phase oxidation								
Catalytic oxidative absorption	Sodium carbonate solution, as an absorbent, doped with a commercial "‘888" catalyst	Gas-liquid contactor (rotating packed bed)	1400–1700 ppm	20 mg L^{-1} catalyst/ 0.11–0.17 mol L^{-1} Na_2CO_3	na	~99.5% (of 1400 ppm)	na	[370]
Fenton-like AOP	Adding Fe^{3+}/H_2O_2 and Cu^{2+}/H_2O_2 in a column equipped with a bubbler	Bubbler column	400–5000 ppm	0–1.5 (0.6 optimum) mol L^{-1} H_2O_2 and 25 mol L^{-1} Fe^{3+} and Cu^{2+}	1.32–19.98 min (based on reactor dimensions and air flow rate)	Fe^{3+}/H_2O_2: 98.3% (of 400 ppm) and 72.5% (of 5000 ppm) Cu^{2+}/H_2O_2: 91.8% (400 ppm) and 52.5% (5000 ppm)	SO_4^{2-}, S, FeS, CuS	[371]
Photo-Fenton wet oxidation process	Four UV-C lamps with powers of 18, 36, 54, and 72 W	Bubble column scrubber	600–3200 ppm	0–0.3 mol L^{-1} H_2O_2 and 0–0.12 mol L^{-1} Fe^{2+}	na	From ~100% (of 600 ppm) to ~20% (of 3200 ppm)	SO_4^{2-}, S	[364]
Fenton	Adding Fe^{2+}/H_2O_2 in a spraying column equipped with a bubbler	Scrubber	200–3000 ppm	0 to 1 (0.4 optimum) mol L^{-1} H_2O_2 and 0–0.16 mol L^{-1} Fe^{2+}	na	98.3% (of 200 ppm) to 70.5% (of 3000 ppm)	SO_4^{2-}, S	[372]
UV/ Persulfate	A bubbler occupied with UV-C lamp	Bubbler column	600–2400 ppm	0–0.03 mol L^{-1} Persulfate	na	Maximum 96.1% (at H_2S:1500 ppm)	S and SO_4^{2-}	[363]
UV/Oxone-induced oxidation	36 W UV-Cadding oxone ($KHSO_5 \cdot KHSO_4 \cdot K_2SO_4$)	Scrubber	500–2500 ppm	0–0.04 mol L^{-1} Oxone	na	98.3%	S and SO_4^{2-}	[527]

$$TiO_2 + hv \rightarrow h^+ + e^- \quad (12)$$

$$h^+ + H_2O_{ads} \rightarrow HO^* + H^+ \quad (13)$$

$$h^+ + OH^-_{superf} \rightarrow HO^* \quad (14)$$

$$O_2 + 2e^- + 2H^+ \rightarrow H_2O_2 \quad (15)$$

$$H_2S_{ads} + 4HO^* \rightarrow SO_{2ads} + 2H^+ \rightarrow 2H_2O_{ads} \quad (16)$$

$$H_2S_{ads} + 8HO^* \rightarrow SO^{2-}_{4ads} + 2H^+ \rightarrow 4H_2O_{ads} \quad (17)$$

$$H_2S_{ads} + 4H_2O_2 \rightarrow SO^{2-}_{4ads} + 2H^+ \rightarrow 4H_2O_{ads} \quad (18)$$

In the case of matrices containing organic compounds, the final goal of the purification system is the conversion of the compounds into CO_2, which is the main index for mineralization in the oxidation systems. In an advanced oxidation system targeted for treating the H_2S-containing effluent, the production of non-toxic sulfur compounds, such as bisulfite, sulfite, and sulfate, or even sulfur, is desired. As can be seen in the above equations and the results obtained by the reviewed studies, SO_4^{2-} is the main byproduct of H_2S oxidation reactors. Although SO_4^{2-} anion is not considered as a toxic mineral matter, it can produce insoluble salt

particles that can precipitate on the light source or the catalysts. These insoluble particles can also block the light-shining path in the photo-dependent reaction sink. Such impediments hinder the progress of the oxidation process. As equation (16) shows, the other potential limitation with the oxidation of H_2S is the emission of toxic and corrosive sulfur dioxide (SO_2), which has been reported in the literature. Portela et al. [369] detected SO_4^{2-} and SO_2 as byproducts of the H_2S oxidation in a UV/TiO_2 reactor and reported a decline in the photocatalytic activity due to the accumulation of SO_4^{2-} precipitate on the lamp surface. They found that simple washing with distilled water is successful in recovering most of the initial activity of the photocatalyst and that alkaline pH and higher temperatures accelerate SO_4^{2-} removal. These challenges will remain until we find a fundamental solution, such as developing an oxidation system to partially oxidize H_2S to S^0, to completely solve the production SO_4^{2-} while preventing the emission of SO_2 in the system. However, sulfur can also cause deposit formation or turbidity that may pose a problem.

Portela et al. [358] developed a photocatalyst composite to prevent SO_2 release. They synthesized porous TiO_2 using a sol–gel method to provide an immobilized thin film of the catalyst. By incorporating surfactants (Brij58 and F127), they observed the catalyst selectivity for SO_2 enhanced compared to reference dense sample. Afterward, they combined the catalyst with a metal oxide adsorbent to build an incorporated hybrid TiO_2–SiMgOx composite, aiming to enhance the adsorption of H_2S and SO_2 using SiMgOx and to have an SO_2-selective photocatalysis process using surfactant/TiO_2 interactions. Thus, by integrating adsorptive properties with the SO_2-selective photocatalysis process they claimed that the SO_2 production problem has been solved while improving the lifetime of the photocatalyst. In another study by Portela et al. [367], they used TiO_2/M−MCM−41 (M = Ce or Cr) for UV or Vis light-mediated H_2S oxidation and found that adding Cr into the composite not only led to an enhanced H_2S conversion efficiency with both light sources but also resulted in no generation of SO_2. However, they had a catalyst blockage issue due to the formation of precipitates arising from the reduction of Cr^{6+} to Cr^{3+} and SO_4^{2-} accumulation, leading to deactivation of the catalyst active sites.

An H_2S oxidation process can be performed in either the gas phase or the liquid phase media. Considering Table 5, it is worthwhile to mention that using liquid phase AOPs processes may limit the SO_2 release problem, whereas it can be seen that most of the gas phase oxidation reactors produced SO_2. The results revealed by some studies [363,364,370–372] indicate that a liquid phase reaction is also capable of processing higher amount of H_2S while providing high conversion efficiency. Gas absorption coupled with the oxidation in a liquid phase can be reasonably potent enough to explain this difference between the systems. For instance, a photo-Fenton wet oxidation process designed by Liu et al. [364] is one of the most powerful processes reported for the conversion of H_2S in a scrubber column. 600 ppm of inlet H_2S were completely removed, while >90% of 1800 ppm of inlet H_2S was removed, both without releasing SO_2 in the treated gas stream. Therefore, compared to the gas phase systems, aqueous free radical AOPs may be greener with stronger oxidation capacity, making them more appealing for industrial application. However, the discharge of sulfur-rich wastewater by these reactors can be a challenge that should be managed.

As mentioned above, the H_2S-oxidizing photocatalytic methods face the catalyst blockage issue due to the deposition of SO_4^{2-} in the active sites of catalysts. Therefore, the regeneration efficiency of the deactivated spent catalyst is a significant challenge particularly in field applications. Deactivation caused by SO_4^{2-} precipitates is an irreversible phenomenon as sulfate is a non-volatile product. Methods like air blower or high-temperature process can be used for reversible deactivation, but addressing sulfate-induced deactivation needs a specific chemical solution [358]. Portela et al. [358] reported that rising TiO_2–SiMgOx composites with a 1 M KOH solution increased the catalytic activity as a result of the creation of new basic active sites. In another study, Liu et al. [366] successfully regenerated the TiO_2/zeolite composite by washing with 0.01 M NaOH aqueous solution and using ultrasonic calcination, which was employed for the catalyst coating on the zeolite adsorbent. The activation effect of calcination was due to the improvement in TiO_2 dispersion on the adsorbent, thereby increasing the surface area and volume of the composite with a site-blocking effect. Similarly, Tellez et al. [373] showed that using a weakly basic washing with 0.01 M NaOH not only regenerated the photocatalytic activity but also increased the adsorption of H_2S molecules by TiO_2/zeolite composite. However, this highlights possibly the biggest drawback of AOPs: high cost. The energy and chemical reagents required to operate the system contribute significantly towards the high operating and maintenance costs. Moreover, the scalability of many AOPs is still unexplored. Currently, the best application for AOPs is likely as a secondary or tertiary treatment option, such as after biological treatment or in tail gas treatment.

2.5. Electrochemical processes

Electrochemical technologies for environmental remediation have been around for three decades. However, capture and/or oxidation of hydrogen sulfide from aqueous solutions using an electrochemical unit was reported about 50 years ago [374–376]. In an electrochemical unit, a series of oxidation and reduction reactions take place due to an electron flow produced by external power sources. This can be an advantage over the chemical-intensive processes to use chemical-less electrical oxidation instead of dosing, transport, and storage of potentially toxic material to conduct an oxidation process [377]. Furthermore, easy control of the cell performance by adjustable operational parameters, such as current and voltage, and no limit on electron flux are significant advantages over some technologies like photocatalytic reactors [378]. The energy expense of an electrochemical cell sometimes is the most dominant problem in field applications. But when renewable energy resources are utilized, this method can be a sustainable and versatile technology applicable to various concentrated waste streams with high operational and energy efficiencies as well as an easily compatibility with remote applications [379,380].

An electrochemical cell comprises of the following elements: i) two electrodes, anode and cathode, where oxidation and reduction reactions take place; ii) one or several electrolytes that are electronically conductive materials supporting less or non-electroactive ions, thereby increasing conductivity in the cell; iii) one or several separators, usually ion-exchange membranes (IEM), which can selectively allow ion transfer between the two sides of the cell (see Fig. 5).

H_2S-removing electrochemical systems can be implemented under two mechanisms: oxidation and precipitation. The oxidation process in an electrochemical cell can take place in two forms, direct and indirect

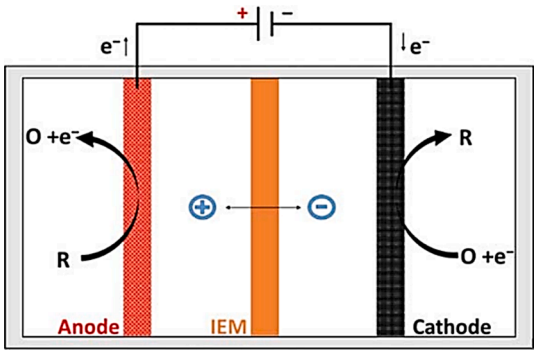

Fig. 5. A typical electrochemical cell. The anode is a positively charged electrode (allowing oxidation reactions) and cathode is negatively charged (allowing reduction reactions). IEM selectively transfers positively or negatively charged ions. Reprinted from [378]. Licensed under CC BY-NC-ND 4.0.

Table 6
Studies on electrochemical removal of H_2S.

Electrolyte	Potential/Current Density	Anode Material	H_2S Amount	Temperature (°C)/ Initial pH	Maximum Conversion Efficiency	Main Products	Reference
Electro-oxidation							
Hot fuel gas + $(Li_{0.62}, K_{0.38})_2CO_3$	76 mA cm^{-2}	$Gd_2Ti_{2-x}Mo_xO_7$	0.2–2 M%	650–750 °C/na	removal flux of 4.6×10^{-6} mol min^{-1} cm^{-2}	S	[389]
Synthetic	11.9 A m^{-2}	Carbon fibre brush	2–3.5 g S L^{-1}	21 °C/7	na	S	[397]
Synthetic (geothermal fluid) + 3.5% NaCl	0.197 V	Pyrolytic graphite	0.01 M	25–150 °C/na	Removal rate of 6.75 mmol h^{-1}	S, SO_4^{2-}	[384]
Synthetic sour brines	100 A m^{-2}	Ti_4O_7 (Ebonex®)	30 mM L^{-1}	na/13	na	SO_4^{2-}	[395]
Synthetic (3.5% NaCl + sulfide)	From –0.95 to + 0.80 V	Platinum	0.15 mM	25 °C/(9–12)	na	S, SO_4^{2-}	[528]
Oil (4.5 mg L^{-1}) wastewater containing NaCl (3549 mg L^{-1})	ORP –300 to –600 mV/16.67 mA cm^{-2}	Ti/IrO_2	4.21–50 mg L^{-1}	11–60 °C/(~2–12)	100% (25 min for 50 mg S L^{-1})	SO_4^{2-}	[387]
Petrochemical effluent	2.2 V/200 mA	Vitreous Carbon	0.055 M	na/13	~65%	$S_2O_3^{2-}$, SO_4^{2-}	[388]
10 mM NaCl	300–500 A m^{-2}	DSA covered with Iridium and tantalum	5.0 vol% of carrier gas (N_2)	25 °C/8	99%	na	[390]
Na_2SO_4 (0.5 mol L^{-1})	3, 6 V	Graphite	600–1600 ppm (with O_2 and carrier N_2)	na/na	100%	CdS, CuS, S, SO_4^{2-}	[393]
Electro-precipitation							
Pulp and paper mill	3.6–17.9 mA cm^{-2}	Iron	7.5–9.5 mg L^{-1}	na/6.5–7.1	88%	FeS	[398]
Swine manure	0.7 V	Low carbon steel	169 mg L^{-1}	4, 19, 31 °C/6.71	95%	FeS	[399]
Synthetic produced water	32.5 mA cm^{-2}	Iron and aluminum rods	100 mg S L^{-1}	Ambient/7.7	99%	FeS	[529]
Beet sugar wastewater	0.7, 1 V	Low carbon steel	na	4, 19, 30 °C/4.6–7	90% $H_2S_{(aq)}$ and 99% $H_2S_{(g)}$	FeS	[400]

reactions. Direct oxidation reaction occurs at the electrode and electrolyte interface, so-called electrode surface, when the target compound is electrochemically active. Indirect oxidation takes place in the electrolyte in the presence of oxidants, e.g. chlorine and oxygen, released from the electrode into the bulk liquid. Oxidation of H_2S can take place by both reaction routes as it is an electrochemically active compound [377].

Direct oxidation of H_2S can produce S^0, $S_2O_3^{2-}$, SO_3^{2-}, or SO_4^{2-}, depending on the anode material and its applied potential. It is shown that elemental sulfur is stable in acid solutions but dissociates to HS^-, SO_4^{2-} and polysulfides (S_n^{2-}) in alkaline regions. However, SO_4^{2-} is stable in aqueous solutions at all pH ranges [381]. Dutta et al. [382] found that direct oxidation of sulfide can take place at both low and high potential voltages. However, applying a low voltage results in selective oxidation process, which limits unnecessary side reactions. In other words, at low potentials, it is possible to only partially oxidize sulfide to S^0 as it needs only two electrons. The formation of S^0 is a preferred reaction from an economical viewpoint as it needs less electrical energy, and solid sulfur can be easily separated from the system. At high potentials, in the presence of at least 8 electrons or more, sulfate is supposed to be the most common product that can be further oxidized to form thiosulfate. Compared to direct oxidation, indirect oxidation of sulfide takes place at a higher potential. Therefore, all oxidation reactions can occur in the electrolyte, where the oxidants can non-selectively oxidize the sulfur compounds. This, consequently, reduces the current efficiency for target (sulfide) oxidation and requires high energy consumption. In this mechanism, there is no need to diffuse sulfide to the electrode surface. The type and level of formation of the oxidants in the electrolyte depend on the electrolyte content, sulfide-containing waste streams, and the anode material and potential. Considering the process taking place in an oxidative electrochemical environment, an in-situ recovery of valuable products in the industry, such as sulfur, sulfuric acid (H_2SO_4), H_2, or caustic soda (NaOH), can reduce the operational costs.

In electrochemical precipitation (also called electrocoagulation), H_2S is removed from the system by the precipitation process. In these systems, a metal (usually iron) acts as a sacrificial anode and releases metal ions ($Metal_{(s)} \rightarrow Metal^{2+} + 2e^-$) into the electrolyte. These ions react with dissolved sulfide to produce insoluble metal sulfide solids ($Metal^{2+} + HS^- \rightarrow Metal\text{-}S + H^+$), which can then be removed from the treated aqueous solution. At the cathode, H_2 gas bubbles can be produced as a result of the dissociation of water molecules ($H_2O + e^- \rightarrow H_2 + OH^-$). The hydrogen bubbles rise towards the surface of the cell and cause the suspended metal sulfide particles to float. This phenomenon is called electroflotation, which simplifies the cell operation by periodic removal of the precipitates [383].

The simple and efficient process of electro-precipitation makes it easily compatible with remote operation as it is not required to add salts and anions like chlorides, thus avoiding the accumulation of salts in the cell. It can also be a tunable process as the progress of the process is directly depends on the current. In addition, it could allow the separation of other compounds (e.g. oil) present in industrial waste streams alongside H_2S removal [383]. However, due to the low selectivity of the electrocoagulation process, a large amount of the precipitated sludge can be generated in these electrochemical cells, increasing the operational costs due to the sludge handling. The presence of heavy metal in the sludge can also be a limitation from an environmental point of view.

The studies that have recently been conducted for the electro-oxidation and electro-precipitation of H_2S from aqueous and gaseous matrixes are presented in Table 6. Electrochemical oxidation of hydrogen sulfide has been the subject of interest for the treatment of H_2S-containing liquid waste streams, such as geothermal brines [384–386] and wastewater streams in the petrochemical industry [387,388], and gaseous waste streams, such as fuel gas [389] and biogas [390].

Ateya et al. [384] evaluated the treatment of geothermal brine with oxidation mechanism by employing a graphite-made electrode and found that it is possible to oxidize sulfide to sulfate and sulfur at a low applied potential of 0.197 V for the anode. In this study, the anode passivation arising from the deposition of solid sulfur on the electrode was the main limitation of the system. The deposition of sulfur on the anode surface can be a significant limitation of any H_2S-oxidizing electrochemical system. To avoid this problem, Selvaraj et al. [391] proposed an electrochemical membrane process to generate elemental sulfur. They obtained sulfide oxidation using a titanium substrate

insoluble anode (TSIA) with low energy inputs (20 mA cm^{-2}). In this study, the current distribution of the TSIA allowed a sulfur recovery process. Feng et al. [379] countered the deposition problem using indirect oxidation. A partial cathodic recovery of produced sulfur (about 30%) is suggested by Sergienko et al. [392] as sufficient to limit electrode passivation and prolong electrode lifetime. In this work, electrochemical and chemical recovery processes did not remove the electrodeposited sulfur from the surface of the activated carbon electrode since sulfur incorporated into the carbon structure.

Li et al. [393] conducted a study on a catalytic (palladium and copper) oxidation-assisted electro-precipitation system. In the reactor, the catalyst oxidized a portion of H_2S to sulfur and sulfate by transition metals and electroactive substances, while the rest of the H_2S was removed from the system by electro-precipitation. The combination of the catalyst and the electrochemical process maximized the removal efficiency and demonstrated that the performance of this integrated system is better than either of those methods operated alone. Some studies evaluated the effect of the electrode material in the H_2S electro-oxidation process. Waterston et al. [385] obtained successful oxidation of sulfide to sulfate using BDD electrodes both in the presence and in the absence of chloride, but they found that the high price of the electrodes limits their application in industrial-scale goals. Haner et al. [386] showed that Titanium/IrO_2–Ta_2O_5 was poisoned by sulfide in long-term use. In another study, the carbon materials acted as sacrificial electrodes [394]. Ebonex electrodes studied by El-Sherif et al. [395] showed a sulfide conversion of 50% with the production of sulfate as the predominant oxidation product. Generally, carbon electrodes can be the most promising anodes since they are cheap and may cause selective oxidation towards elemental sulfur at low applied potentials [377,392]. Sergienko et al. [392] also successfully oxidized H_2S to elemental sulfur using low-cost carbon-based porous materials, activated carbon felt (ACF) and graphite felt (GF).

Although the versatile applicability of the electrochemical methods (e.g. the simultaneous removal of organic compounds along with sulfide) strengthens their case for some industrial streams, their high energy consumption for the removal of organic and inorganic compounds may limit their practical application for the treatment of the main streams containing sulfide ions. Szpyrkowicz et al. [396] reported removal efficiency of over 90% for Chemical Oxygen Demand (COD), Total Kjeldahl Nitrogen (TKN), and sulfide. However, it required a high energy consumption of up to 300 kWh m^{-3}. Kang et al. [390] achieved near complete removal of H_2S and NH_3 from biogas by employing an absorption column and an electrochemical oxidation reactor. In the electro-oxidation reactor, the generated reactive chlorine species oxidized almost all the transferred H_2S. In this system, the H_2S conversion efficiency was closely dependent on the mass ratio of the H_2S transferred and the reactive species generated. Although a high electrochemical conversion efficiency of gaseous sulfide to sulfur can be achieved, such systems have an anode passivation issue since a liquid absorber is used before the electrochemical cell to solubilize sulfide. This problem can be solved by switching the polarity of the electrodes alternatively [397].

H_2S has also been successfully removed using the electro-precipitation process [398–400]. Wang et al. [399] used carbon steel electrodes to precipitate H_2S from swine manure. An applied voltage of 0.7 V was sufficient to progress the precipitation process at the anode and to minimize H_2 formation at the cathode to limit floatation. They achieved an average sulfide removal rate of 0.97 mg S^{2-} cm^{-2}·d^{-1} and a maximum removal efficiency of 95%. In another study by Wang et al. [400] for H_2S removal from beet sugar wastewater, a low-cost sacrificial anode material was employed. Up to 90% aqueous sulfide removal and 99% hydrogen sulfide removal from the gas stream was achieved at 0.7–1 V without sulfate generation.

2.6. Membranes

Membrane technology is a relatively new method for gas separation with respect to the more classical technologies such as absorption and adsorption, as its industrial applications started only in the second half of the last century [401]. Indeed, even though the first studies on membranes date back to 19th century, the development of synthetic membranes for industrial-scale application can be traced to early 1962 with the fabrication of the first cellulose-acetate-based reverse osmosis membrane for water desalination by Loeb and Sourirajan [402]; membrane companies broke into the gas processing industry only in the 1980 s [403]. Since then, polymeric membrane technology has become one of the most important methods for gas separation because of its high performance and high efficiency in gas transport. Membranes can optimize the gas separation process by (a) reducing the equipment size and the capital costs, (b) by improving the process safety and operational simplicity, (c) the absence of complex control systems, and (d) low energy requirement, especially when pressurized gas is already available.

Applications in gas separation and/or natural gas sweetening are currently dominated by polymeric membranes since inorganic membranes, due to higher costs and difficulty of production, are generally limited to those systems where operating conditions, usually related to high temperatures, prevent the direct use of polymeric membranes [404]. Therefore, this review will not consider inorganic membranes, focusing mainly on polymeric membranes used and tested for H_2S separation in natural gas purification. Over the past decade or so, research in this field was devoted to attaining process stability and preparing more resistant and durable materials in the quest to obtain better performance in gas separation. When dealing with acid gas removal, membranes are usually tested for CO_2 capture and purification, while H_2S studies are far more limited because of the toxicity of the gas and the very high purification specification (down to ppm) that can be hardly reached with membranes alone. Nonetheless, owing to their high chemical stability, polymeric membranes are proven to work in harsh environments and can be a very effective pretreatment to increase the efficiency of other technologies when purification of streams with high H_2S content is desired [405–407]. In fact, most of the applications for membranes are focused on natural gas purification where hydrogen sulfide concentration is in the order of 10–20% or even higher [408]. In this regard, the two most important factors that drive this separation are selectivities of H_2S/CH_4 and H_2S/CO_2, which is also the case for biogas desulfurization [407]. However, it is interesting to note that, despite the similarity of the process and the widespread use of membranes, very limited information is reported about membrane performance in H_2S removal from biogas [409,410]. The amount of H_2S in indeed too low (in the order of 1% or less) to attain high separation with membranes alone

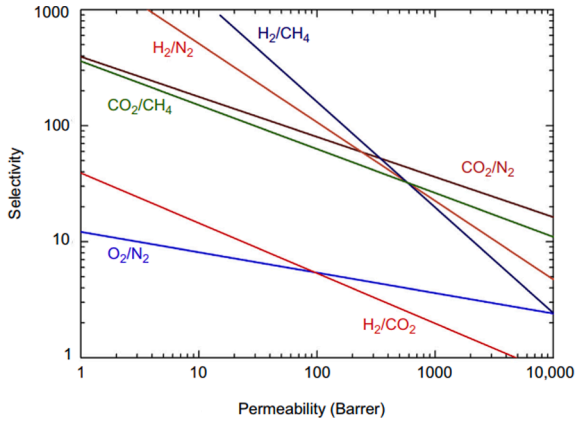

Fig. 6. Upper bound limit for different gas pairs. Permeability refers to the more permeable gas considered in the mixture. Modified from [487]. Licensed under CC BY.

even if, once again, membrane materials are reported to withstand the presence of the acid components in the feed stream [411].

2.6.1. Mass transport in membranes

Gas separation with membranes is a pressure-driven process, where a gas is flown on a thin selective layer that has the ability to separate different chemical species according to their different interactions with the material [412]. The driving force of the process is the pressure gradient across the membrane which allows the penetrants to move from the high- to the low-pressure side of the membrane according to their ability to solubilize and diffuse into the polymeric matrix. The permeation rate depends on thermodynamics factors (partitioning of species between feed phase and membrane phase), kinetics properties (diffusivity), thickness of the selective layer, and the interaction between the polymer and the penetrant [413]. In simple words, the more soluble the gas and the faster its diffusion across the membranes, the higher will be the final flow for a given pressure difference and a given membrane thickness.

The separation performance of polymeric membranes is described by two key parameters: permeability (P) and selectivity (α). Permeability (or permeance when it is reported per unit thickness) is the rate at which any compound permeates through a membrane, while selectivity is the ability of a membrane to accomplish a given separation and to achieve high product purity and high recovery [414]. They are generally defined as follows:

$$J_i = -\frac{P_i\left(p_i^{up} - p_i^{down}\right)A}{l} \quad \mathrm{i} = 1,2 \tag{19}$$

where J_i is the mola flow of the i^{th} component across the membrane, A is the membrane surface area, l is the membrane thickness, $(p_i^{up} - p_i^{down})$ is the partial pressure difference of the i^{th} component through the membrane (*up* for upstream and *down* for downstream).

$$\alpha_{i/j} = \frac{y_i^{down}/y_j^{down}}{y_i^{up}/y_j^{up}} = \left(\frac{P_i}{P_j}\right) \tag{20}$$

where the y refers to the molar fraction of the components of interest (i or j) at the two sides of the membrane and can be approximated to the ratio of components permeability when the downstream pressure is close to zero.

As reported by Robeson [415], for most of the polymeric membranes, there is a trade-off between permeability and selectivity. An increase in selectivity is accompanied by a decrease in permeability coefficient and vice versa (see Fig. 6). The challenge for an optimal gas separation process design is to try to overcome this limit by finding the best compromise between selectivity and permeability coefficients in order to obtain the highest performance of the membrane with the highest product purity and the highest recovery. Good membranes, in addition, must also have acceptable durability and high enough thermal and chemical stability under the operating conditions expected in the application environment.

2.6.2. Polymeric membranes

In the last few decades, new materials with higher permeability and selectivity towards the desired compounds have gained much attention [412]. Among the various materials, polymers have taken the spotlight because they present a compact configuration, a large-scale reproducibility, and low material and manufacturing cost. Moreover, polymeric materials possess advantageous properties, such as solution-processability and precise control over chemical functionality, especially in the case of chain flexibility and durability. Considerable efforts have also been directed towards fabricating longer-lasting, defect-free, and resilient polymeric membranes with increased mechanical resistance, thermal and chemical stability, and resistance to plasticization, making them much more suitable for acidic compound separation [416]. The high solubility of acid gases, such as CO_2 and H_2S, indeed allows to obtain high permeability in many polymeric materials that are, therefore, promising candidates for acid gas removal from less condensable gases such as methane, hydrogen, nitrogen, and oxygen.

The choice among the different materials, however, is not straightforward as it is well known that the high solubility of acid gases in polymers can induce swelling and plasticization [417] and can speed up aging in glassy polymers [418]. These phenomena lead to a modification of the polymeric structure and a reduction of the membrane separation performance [419,420]. Gas separation in polymeric membranes is also affected by the operating conditions where the interaction between the polymer and the gas can change according to the feed temperature and pressure. Furthermore, CO_2 and H_2S permeability in the same membrane can be different depending on whether the polymeric layer is exposed to a pure or to a mixed inlet stream. This phenomenon is called competitive sorption that is generally observed when both gases are present in the same current. Since H_2S can replace the CO_2 absorbed by the polymer, CO_2 permeability and CO_2/H_2S selectivity are consequently reduced. To avoid such a drop and to increase membrane lifetime, several studies have been carried out to identify the best polymeric materials for acid gas removal.

From this point of view, before analyzing the different options and reviewing different studies, it is worthwhile to recall that polymers can be divided into two main categories according to their glass transition temperature (T_g): they are defined glassy polymers when the T_g is higher than the room temperature, while when the T_g is lower than the room temperature, they are demarcated as rubbers. The glass transition temperature is specific for each type of polymer, it is influenced by their specific structure (saturated or unsaturated bonds and the presence of aromatic/aliphatic groups) and, moreover, it influences the mechanical properties of the material.

Rubbery polymers are softer and more flexible because they are free to rotate along their main axis implying high chain mobility. This condition is caused by their large amount of space, called free volume, existing among chains that leads with high permeability and a generally low selectivity of the membrane material for gas separation [421]. Selectivity is then mainly related to gas solubility as the high mobility of the polymeric matrix usually allows all the different gases to easily diffuse across the membrane. For this reason, considering the higher solubility of H_2S with respect to other gases, this compound can be separated with good efficiency by using rubbery polymers.

On the other hand, glassy polymers generally exhibit higher selectivity and lower permeability compared to rubbers since they have a limited chain mobility and a low free-volume fraction. Therefore, glassy polymers are generally hard and rigid materials with insufficient space and mobility for large-scale co-operative movements of the polymer backbone. Due to this physical status, glassy polymers offer size-selective separation that allows the possibility of diffusion-based selectivity based on the different kinetic diameters of the different compounds. For example, since the kinetic diameter of CH_4 is larger than that of CO_2 and H_2S (3.8 Å, 3.3 Å, and 3.6 Å for methane, CO_2, and H_2S respectively [403]), acid gases—CO_2 in particular—can also be separated through glassy polymers [240]. However, high partial pressure of carbon dioxide and other compounds (such as hydrocarbons, water, and aromatics) could affect the separation properties of the membranes by inducing plasticization effect. Moreover, glassy polymers can undergo to physical aging due to which the materials gradually lose their performance over time becoming much less permeable to H_2S and CO_2 with respect to methane.

The separation of acid gases and H_2S with membranes is therefore possible, as said above, even if problem like plasticization, aging and competitive sorption must be prevented to optimize membrane properties. Several techniques have been implemented to overcome these problems and more in general to improve the membrane performance and durability: these includes the use of facilitated transport membranes, which use a carrier-based approach to improve the acid gas permeability [422,423], as well as the modification of the base materials

Table 7
H_2S permeability and selectivity in polymeric membranes.

Polymer	H_2S Permeance [mol/(m^2s·Pa)]	H_2S Permeability [mol/(m·s·Pa)]	$S_{H2S/CH4}$	$S_{H2S/CO2}$	T [K]	*p* [bar]	Feed composition	Reference
PDMS	$2.9*10^{-10}$		6.5	1.8	308	1.1	pure	[530]
		$1.68*10^{-12}$	10	3.08	308		pure	[441]
PDMS + PEG + PSf	$2.6*10^{-8}$		140	5.7	298	4.4	pure	[240]
PDMS + PEG + PSf (glycerol)	$3.6*10^{-8}$		162	8.1	298	4.4	pure	
Pebax SA01 MV3000		$1.75*10^{-13}$	50.48	4.87	308	1.17	pure	[406]
		$2.1*10^{-13}$	60.43	5.83	308	2	pure	
		$2.25*10^{-13}$	67.32	5.83	308	2.76	pure	
		$2.42*10^{-13}$	64.94	6.49	308	3.45	pure	
Pebax 4033 SA00		$1.04*10^{-13}$	24	3.70	308	10	$yCH_4 = 70.8\%$ $yCO_2 = 27.9\%$ $yH_2S = 1.3\%$	[428]
Pebax 3533 SA00		$2.97*10^{-13}$	21	3.65	308	10	$yCH_4 = 70.8\%$ $yCO_2 = 27.9\%$ $yH_2S = 1.3\%$	
Pebax 6333 SA00		$1.26*10^{-14}$	20	5.11	308	10	$yCH_4 = 70.8\%$ $yCO_2 = 27.9\%$ $yH_2S = 1.3\%$	
Pebax 7233 SA00		$2.54*10^{-15}$	15	1.85	308	10	$yCH_4 = 70.8\%$ $yCO_2 = 27.9\%$ $yH_2S = 1.3\%$	
Pebax MX 1657		$8.3*10^{-14}$	50.6	3.59	308	10	$yCH_4 = 70.8\%$ $yCO_2 = 27.9\%$ $yH_2S = 1.3\%$	
Pebax MX 1074		$2.33*10^{-13}$	50.4	4.48	308	10	$yCH_4 = 69.4\%$ $yCO_2 = 18.1\%$ $yH_2S = 12.5\%$	
		$1.85*10^{-13}$	54	4.53	308	10	$yCH_4 = 70.8\%$ $yCO_2 = 27.9\%$ $yH_2S = 1.3\%$	
Pebax MX 1041		$5.85*10^{-14}$	49	4.41	308	10	$yCH_4 = 70.8\%$ $yCO_2 = 27.9\%$ $yH_2S = 1.3\%$	
PVDC	1.4*10–9				303	0.93	pure	[531]
PPG (poly ether urethane)_PU1		$7.99*10^{-14}$	21	3.0	308	10.8	$yCH_4 = 70.8\%$ $yCO_2 = 27.9\%$ $yH_2S = 1.3\%$	[428]
		$6.12*10^{-14}$	22.6	4.28	308	10.8	$yCH_4 = 69.4\%$ $yCO_2 = 18.1\%$ $yH_2S = 12.5\%$	
PEG (poly ether urethane)_PU3		$9.07*10^{-14}$	58	4.6	308	10.8	$yCH_4 = 70.8\%$ $yCO_2 = 27.9\%$ $yH_2S = 1.3\%$	
		$9.37*10^{-14}$	54.9	4.5	308	10.8	$yCH_4 = 69.4\%$ $yCO_2 = 18.1\%$ $yH_2S = 12.5\%$	
PPG (poly ether urethane urea)_PU2		$2.05*10^{-13}$	19	3.1	308	10.8	$yCH_4 = 70.8\%$ $yCO_2 = 27.9\%$ $yH_2S = 1.3\%$	
		$2.07*10^{-13}$	18	3.17	308	10.8	$yCH_4 = 69.4\%$ $yCO_2 = 18.1\%$ $yH_2S = 12.5\%$	
PEG (poly ether urethane urea)_PU4		$6.66*10^{-14}$	74	4.45	308	10.8	$yCH_4 = 70.8\%$ $yCO_2 = 27.9\%$ $yH_2S = 1.3\%$	
		$7.46*10^{-14}$	66	4.39	308	10.8	$yCH_4 = 69.4\%$ $yCO_2 = 18.1\%$ $yH_2S = 12.5\%$	
Cellulose Acetate (CA)		$2.91*10^{-15}$	30.5	1.01	308	34	$yCH_4 = 60\%$ $yCO_2 = 20\%$ $yH_2S = 20\%$	[445]
		$1.33*10^{-14}$	27.5	1.44	308	48	$yCH_4 = 60\%$ $yCO_2 = 20\%$ $yH_2S = 20\%$	
	9.4*10–12		19	0.88	308	10.8	$yCH_4 = 65\%$ $yCO_2 = 29\%$ $yH_2S = 6\%$	[428]
	3.8*10–11		30		308	35	$yCH_4 = 60\%$ $yCO_2 = 20\%$ $yH_2S = 20\%$	[445]
Modified Cellulose Acetate		$6.82*10^{-14}$	34.3	1.58	308	34	$yCH_4 = 60\%$ $yCO_2 = 20\%$ $yH_2S = 20\%$	
		$6.36*10^{-14}$	27.5	1.40	308	48		

(*continued on next page*)

Table 7 (*continued*)

Polymer	H_2S Permeance [mol/(m^2·s·Pa)]	H_2S Permeability [mol/(m·s·Pa)]	$S_{H2S/CH4}$	$S_{H2S/CO2}$	T [K]	*p* [bar]	Feed composition	Reference
							$yCH_4 = 60\%$ $yCO_2 = 20\%$ $yH_2S = 20\%$	
Poly(vinyl trifluoroacetate)	1.4*10–8				303	1	pure	[531]
PTBP		$5.35*10^{-15}$	9.4	0.94	303	2.1	pure	[532]
PDTBP		$6.69*10^{-15}$	4	0.74	303	2.1	pure	
PVBTAF	9.3*10–9		7000		303	1.2	$yCH_4 = 89.5\%$ $yCO_2 = 0\%$ $yH_2S = 10.5\%$	[533]
	4.3*10–9		950		303	5	$yCH_4 = 79.7\%$	
	5.4*10–9		3300	10.8	303	1.1	$yCO_2 = 10\%$	
	2.8*10–9		2100	8.7	303	8.5	$yH_2S = 10.3\%$	
PVTMS		$1.17*10^{-13}$	1.59		–	–	pure	[534]
6F-PAI-1		$2.07*10^{-15}$	8.1	0.19	308	4.48	pure	[535]
6F-PAI-2		$1.00*10^{-15}$	10.3	0.21				
6F-PAI-3		$1.67*10^{-15}$	10.9	0.23				
6FDA-DAM:DABA (3:2)		$1.00*10^{-14}$	10	0.29	308	2	pure	[454]
		$3.88*10^{-15}$	9.0	0.21	308	6.7	$yCH_4 = 70\%$ $yCO_2 = 20\%$ $yH_2S = 10\%$	
		$5.15*10^{-15}$	10.3		308	20.8	$yCH_4 = 70\%$ $yCO_2 = 20\%$ $yH_2S = 10\%$	
		$7.26*10^{-15}$	13.2		308	41.3	$yCH_4 = 70\%$ $yCO_2 = 20\%$ $yH_2S = 10\%$	
		$9.77*10^{-15}$	15.6		308	62	$yCH_4 = 70\%$ $yCO_2 = 20\%$ $yH_2S = 10\%$	
PPO	2.6*10–8		3.1		295	4.5	$yCH_4 = 99.96\%$ $yH_2S = 0.4\%$	[448]
PPOP		$4.01*10^{-15}$	10	2.5	303	2.1	pure	[532]
Poly(ester urethane urea) + teflon	4.4*10–8		43	3.79	308	10	$yCH_4 = 91.6\%$ $yCO_2 = 5.4\%$ $yH_2S = 3\%$	[429]
	3.0*10–8		27	2.72	308	30	$yCH_4 = 91.6\%$ $yCO_2 = 5.4\%$ $yH_2S = 3\%$	
	8.2*10–8		43	3.91	328	10	$yCH_4 = 91.6\%$ $yCO_2 = 5.4\%$ $yH_2S = 3\%$	
	2.9*10–8		12	1.90	328	30	$yCH_4 = 91.6\%$ $yCO_2 = 5.4\%$ $yH_2S = 3\%$	
Cytop	3.8*10–12				310	1	$yCO_2 = 10.5\%$ $yH_2S = 15\%$	[441]
Nafion NE111		$1.87*10^{-13}$			293	1	pure	[466]
Nafion NE117		$7.56*10^{-13}$						
Aquivion		$1.07*10^{-14}$ [RH 20%]	12	0.53	308	1	$yCH_4 = 90\%$ $yH_2S = 10\%$	[465]
		$1.26*10^{-13}$ [RH 85%]	28	0.93	308	2	$yCH_4 = 90\%$ $yH_2S = 10\%$	
PBI composite membranes		$2.72*10^{-13}$	140	7.5	323	1.15	$yCH_4 = 89.6\%$ $yCO_2 = 5.1\%$ $yH_2S = 5.3\%$	[477]
PVDF + [bmim][BF_4]		$5.35*10^{-14}$-$3.68*10^{-13}$	130–260		308–338	4	pure	[478–479]
PVDF + [bmim][BF_4]		$1.36*10^{-12}$	36.6	3.7	313	1	Pure——	[423]
PVDF + [bmim][PF_6]		$6.38*10^{-13}$	29.8	3.7				
PVDF + [bmim][Tf_2N]		$8.7*10^{-13}$	19.8	2.1				
PVDF + [bmim][CF_3SO_3]		$1.44*10^{-12}$	50.7	4.0				
PVDF + [bmim][AC]		$2.44*10^{-12}$	136	11.7				

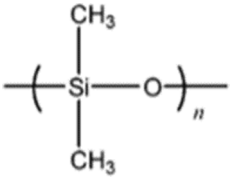

Fig. 7. PDMS chemical structure. Reprinted with permission from [432]. © 2006 American Chemical Society.

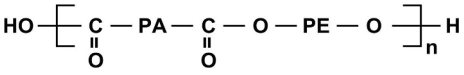

Fig. 8. PEBAX chemical structure. Reprinted from [443].

by cross-linking or/and coupling with different types of filler obtaining hybrid or mixed matrix membranes more resistant in the presence of swelling penetrants and possibly more selective towards the gas of interest [403,424,425].

Vaughn and Koros [406] analyzed the main differences in gas

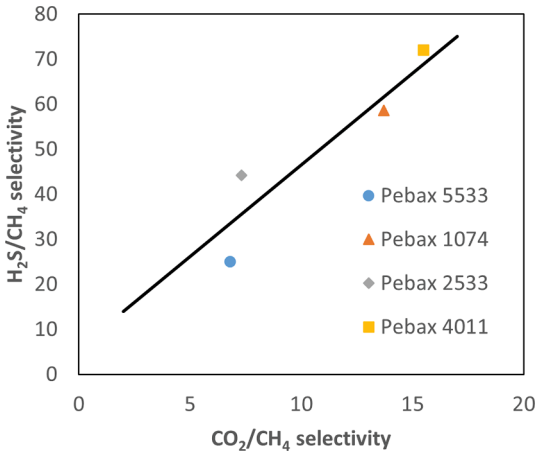

Fig. 9. Correlation between CO_2/CH_4 and H_2S/CH_4 selectivity. Adapted from [443].

separation properties between rubbery and glassy polymers, focusing on plasticization resistance and swelling sorption of condensable components. Several different polymers have been considered such as high free volume polymers, Polyimides, PDMS, PEBAX, PEG, polyurethanes and fluorinated polymers [406,426–437], which all proved to be very promising due to their high selectivity towards acid compounds such as CO_2 and more importantly to H_2S. Some of the most promising results obtained from different studies are reported in Table 7, which provides an overview of the most common polymeric materials for membrane-based H_2S separation.

2.6.3. Rubbery polymers

2.6.3.1. PDMS. Polydimethylsiloxane (PDMS) (see Fig. 7) is one of the most used rubbery polymers for membrane module separation. It has a glass transition temperature of around −123 °C [435] and elevated mobility chains at room temperature, which gives the material a high permeability but a poor ability to sieve molecules based on size [438]. On the other hand, its good selectivity is governed by the differences in penetrant solubilities that make this polymer very suitable for CO_2, CH_4, and hydrocarbon separation from natural gas [439].

PDMS polymeric membranes have been also tested for H_2S removal, although to a lesser extent. The presence of H_2S tends to increase the elasticity of the polymeric matrix, resulting in a very high permeability value of 10,000 Barrer for H_2S compared to 3250 Barrer for CO_2 and 950 Barrer for CH_4 as reported by Robb [440]. As is the case for many rubbery polymers, permeability with respect to acidic compounds is very high, while the H_2S/CH_4 and H_2S/CO_2 selectivities are in the order of 10 and 3, respectively. However, the author stated that no plasticization took place during the test since the permeability coefficients remained the same even when the feed pressure was increased. Other authors found that the permeability of H_2S in PDMS membrane is much higher than that of CO_2. In particular, Merkel et al. [441] reported a permeability of 5100 Barrer at 23 °C, while Bhide et al. [442] calculated a permeability of 10,000 Barrer at 25 °C. Therefore, hydrogen sulfide proves to be very soluble in the matrix, as reported by Merket and Toy [432], much more than CO_2. This behavior increases by increasing the feed pressure and concentration, likely due to the competitive sorption of acid gases for the gas transport across the membrane [433,435].

2.6.3.2. PEBAX. PEBAX® is a commercial copolymer characterized by material coexistence of rigid blocks of polyamide chains (PA) and flexible blocks consisting of polyether chains (PE), whose chemical structure is reported in Fig. 8. The properties of this material strictly depend on the chemical nature and on the relative content of the two types of PA and PE segments. Polyether is known for its high affinity to acid gases, CO_2 in particular [443], while polyamide confers stability to the structure, avoiding the PE crystallization. The ratio between AP and PE can change in the polymeric structure, producing different types of PEBAX.

In this regard, Amo et al. [443] found a correlation between the polymer structure and the selectivity of acidic gases over methane. In fact, the different types of PEBAX used showed different transport and separation properties following the changes in chemical formula both in terms of composition and monomers used. They used four different membranes for their experiments: PEBAX 2533 and 5533 (which contain polyamide PA12 and polytetramethylene glycol PTMG) and PEBAX 4011 and 1074 (which contain Polyamide PA6 and Polyethylene glycol PEG). Separation performance of different materials is shown in Fig. 9, which shows that CO_2/CH_4 selectivity increases together with the H_2S/CH_4 selectivity. They are also reported in Table 7.

Amo et al. [443] also noticed that, among the various materials, PEBAX 4011 has the highest selectivity for H_2S/CH_4 and H_2S/CO_2 of greater than 70 and 15, respectively. They underlined that the presence of CO_2 causes the swelling of the polymeric matrix, leading to an increase of H_2S and CH_4 flux across the membrane. This has been explained, once again, through the absorption competition's effect in the polymer between CO_2 and H_2S, which leads to a decrease in their solubility but, at the same time, to an increase in the diffusivity of all components caused by the matrix swelling [435].

Other authors studied the effect of H_2S permeability on PEBAX membrane for gas separation. In particular, Vaughn and Koros [406] tested PEBAX membranes for CO_2 and H_2S removal from natural gas at 35 °C and different feed pressure. They noticed that as the pressure increases from 15 to 100 psia, the permeabilities of CO_2 and H_2S increase by 10% and 70% (to 600–900 Barrer) respectively, while CH_4 permeability remains the same. This behavior could be attributed to a higher diffusivity coefficient of the two acidic compounds in the polymeric matrix due to an increase of the mobility chains. Moreover, solubility of H_2S also increases since the material contains amide groups which have a high affinity for hydrogen sulfide.

2.6.3.3. Polyurethanes. Polyurethanes are thermoplastic elastomers made by rigid and flexible domains. The first one gives strength and mechanical properties to the matrix, resulting in a good selectivity of the polymer, while the second one confers the material high permeability. Due to their structure conformation (see Figs. 10 and 11), they are largely investigated as a suitable membrane for natural gas purification since they exhibit high selectivity to H_2S/CH_4. Chatterjee et al. [428] synthetized two types of polyurethanes in the form of dense homogeneous membrane: the poly(ether urethanes) and the poly(ether urethane ureas) using PEG or poly(propylene glycol) for the ether block. They noticed that all these modules present higher H_2S permeability than CO_2 and CH_4, both at low and high pressures (10 atm) and both for pure and mixed gas feed. These results demonstrate that the permeation of the three gases is controlled by the gas solubility and that, in polyurethanes

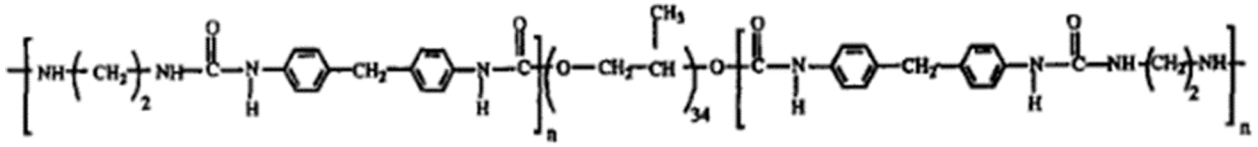

Fig. 10. Poly(ether urethanes) chemical structure. Reprinted from [428]. Licensed under CC BY-NC-ND 4.0.

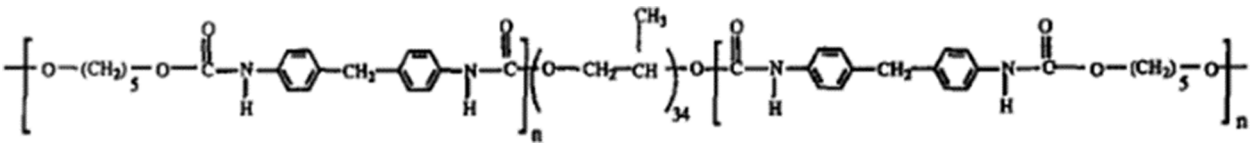

Fig. 11. Poly(ether urethanes ureas) chemical structure. Reprinted from [428]. Licensed under CC BY-NC-ND 4.0.

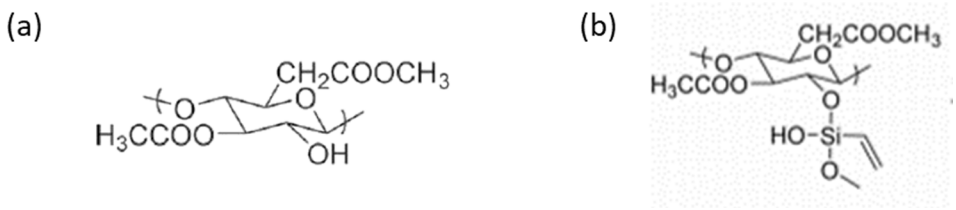

Fig. 12. Chemical structures of (a) cellulose acetate and (b) silane-modified cellulose acetate. Adapted with permission from [445]. © 2013 American Chemical Society.

membranes, the permeability increases with increasing the feed pressure. For these polymers, H_2S permeability goes from around 95–130 Barrer at 4–15 atm and 20 °C to 600 Barrer at 10 atm and 35 °C indicating that polyurethanes are highly plasticized by H_2S, much more than CO_2. However, even if permeability increases in PU4, selectivity is not negatively affected by plasticization phenomena with values that remain close to 102 for α_{H_2S/CH_4} and 4.59 for α_{H_2S/CO_2} at 10 atm and 20 °C when the feed composition ($CH_4/CO_2/H_2S$) is 70.8/27.9/1.3.

Another explanation is given by Mohammadi et al. [429] who attributed the higher selectivity coefficient to an increase in the available free volume of polar hydroxyl groups in PEG compared to PPG. They also noticed that the separation performance of the membrane can be improved by increasing the feed temperature and pressure.

2.6.4. Glassy polymers

2.6.4.1. Cellulose acetate. Cellulose acetate (CA) is a glassy polymer derived from cellulose where parts of the hydroxyl group are replaced with acetates (see Fig. 12a). It was the first material used as membrane for acidic compounds removal from natural gas [403,413] since it is durable and easy to process with fairly good separation performance. This type of membranes generally possess a H_2S/CH_4 selectivity of around 15–30 [428,444,445]. Nevertheless, it has been reported that the presence of H_2S on cellulose acetate membrane, together with CO_2, induces membrane plasticization even at low concentration, thus decreasing separation performance [446].

Furthermore, as reported by Baker et al. [447], the H_2S flux shows an irreversible decline as the relative humidity increases: in fact, the cellulose acetate membranes are hydrophilic and they tend to lose their structural rigidity when they are in contact with liquid water [448]. For these reasons, their use in industrial scale is limited to optimal operating conditions so that the water vapor content in the flue gas must be knocked down in order to ensure high selectivity and permeability. US 4,589,896 patent by Chen et al. [449] describes a possible process for CO_2 and H_2S removal from natural gas with cellulose acetate membranes. The process consists of a multistage membrane module separation and, although the ratio of CO_2 and H_2S content is high (about 400:1), the gas must pass through a minimum of four modules to achieve good hydrogen sulfide separation. Even though CA is not a good separation membrane for Natural gas sweetening, in different studies it has been modified with different agents and solvents to improve its mechanical resistance and separation performances. Cellulose acetate has

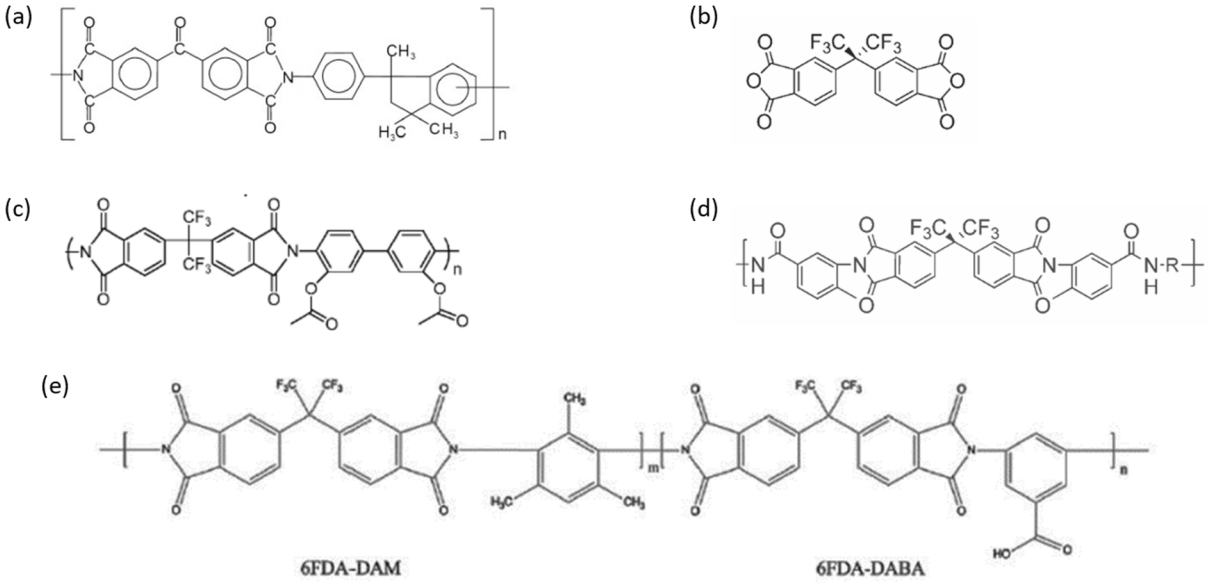

Fig. 13. Chemical structures of (a) Matrimid [488], (b) 6FDA [489] (© 2020 American Chemical Society), (c) 6FDA-HAB [453] (© 2002 Elsevier), (d) 6F-PAI [406] (© 2014 Elsevier), and (e) 6FDA-DAM:DABA [454] (© 2013 Elsevier). Reprinted with permission.

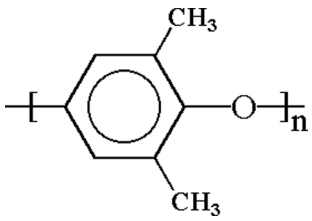

Fig. 14. PPO chemical structure. Reprinted with permission from [448]. © 2011 Elsevier.

been modified by grafting the vinyl methoxysilane onto the polymer–OH groups (see Fig. 12b). The modified material shows similar selectivity to pure cellulose acetate (in the order of 25–30 for H_2S/CH_4 and around 1.4 for H_2S/CO_2), but permeability is almost one order of magnitude higher (from 8.7 Barrer previously to 200 Barrer after modification) [445].

Liu et al. [450] studied the effect of plasticization on the removal of H_2S and CO_2 from mixed gas feed stream by using cellulose triacetate hollow fibers (CTA). Even in this case, hollow fiber demonstrates higher H_2S and CO_2 permeance which tends to increase with the feed pressure. In fact, when the gas composition is 20/5/3/3/300 ppm of $H_2S/CO_2/C_2H_6/C_3H_8$/toluene balanced with CH_4 and the pressure is increased from 5 to 30 bar at 35 °C, the permeance of H_2S goes from 80 to 140 GPU, while that of CO_2 goes from 80 to 120 GPU. This behavior in CTA hollow fiber confirmed the plasticization effect of the material at high pressure and the presence of a competitive sorption with higher hydrocarbon present in the feed mixture. Contrary to what one would expect, CO_2/CH_4 selectivity decreases with pressure, but that of H_2S/CH_4 increases from 26 at 7 bar to 28 at 31.8 bar. The higher H_2S separation efficiency allows the membrane to remove more H_2S than CO_2 and the plasticization effect given by the acid gases provides a benefit for the H_2S/CH_4 separation in the glassy polymer [451].

2.6.4.2. Polyimide. Polyimide polymers (PI) (see Fig. 13) are thermoplastic materials that are extremely resistant to high temperatures and corrosion while possessing good chemical stability. They are widely used as membrane materials for gas separation because they exhibit strong separation performance (in terms of both selectivity and permeability), excellent mechanical properties, and high resistance to plasticization caused by acid compounds. The most known polyimide is Matrimid®, a commercial polymer used as membrane's material even though it is not the best one for mixture gas separation. In fact, as reported by Scholes et al. [452], when Matrimid is tested with a mixture of CO_2 and H_2S, its permeability result to be rather low due to competitive sorption between the two gases even at low concentration.

Other polyimide materials that better fit the need for H_2S separation are partially fluorinated modified polyimides such as 6FDA (4,4′-hexafluoroisopropylidene diphthalic anhydride), 6FDA-HAB (4,4′-hexafluoroisopropylidene diphthalic anhydride hydroxybenzoic acid), 6F-PAI-1 (4,4′-hexafluoroisopropylidene dianiline) and 6FDA-DAM:DABA membranes [406,453,454]. All these types of polymers proved to be highly selective to CO_2 and H_2S respect to CH_4, with a selectivity ranging from 30 to 60 for CO_2/CH_4 and from 10 to 16 for H_2S/CH_4. Moreover, Kraftschik et al. [454], demonstrated that in dense film membranes of the copolyimide 6FDA-DAM:DABA (3:2), tested with H_2S/CH_4 mixture, the plasticization effect can be reduced by thermal treatment resulting in hydrogen sulfide permeability in the order of 100 Barrer. Similar results were obtained also with $CO_2/H_2S/CH_4$ ternary mixtures proving that the penetrant-polymer interaction increases the membrane selectivity. In their work, Vaughn and Koros [406] studied the H_2S separation performances in different types of modified polyimide, in particular 6FDA and 6F-PAI-1. They obtained results similar to the existing literature data [453] with $\alpha_{CO2/CH4}$ over 30 and $\alpha_{H2S/CH4}$ over 10. In general, the presence of fluorinated groups in the matrix gives more strength and stability to the polymeric membrane ensuring higher resistance and increased selectivity and permeability of the material with respect to the acidic compounds.

2.6.4.3. Polyphenylene oxide. Polyphenylene oxide (PPO) materials are amorphous thermoplastic glassy polymers that generally exhibit optimal separation properties, especially for CO_2/CH_4 and H_2S/CH_4, making them very suitable for membrane process separation. As shown in Fig. 14, PPO exhibits a phenyl ring inside its polymer chains that gives the structure a hydrophobic character and makes it resistant to alcohols, acids and bases [455,456].

In their work, Chenar et al. [448] studied the permeability of H_2S in PPO hollow fiber module at different feed pressure and acid concentration. They found out that the permeance of H_2S increases by increasing the feed pressure and concentration, while the permeance of CH_4 remains almost the same. On the other hand, both CH_4 and H_2S permeability increases by increasing the temperature of the system. In the first case, they justified this behavior by the higher driving force of hydrogen sulfide partial pressure in the feed; meanwhile, in the latter case, those rise in permeability with temperature can be imputed to the higher and faster molecular flux of gases across the membrane. However, the selectivity of H_2S/CH_4 in PPO membranes still stays quite low, in the order of 4. This parameter could slightly increase with the H_2S concentration in the feed, but it remains unchanged with the temperature.

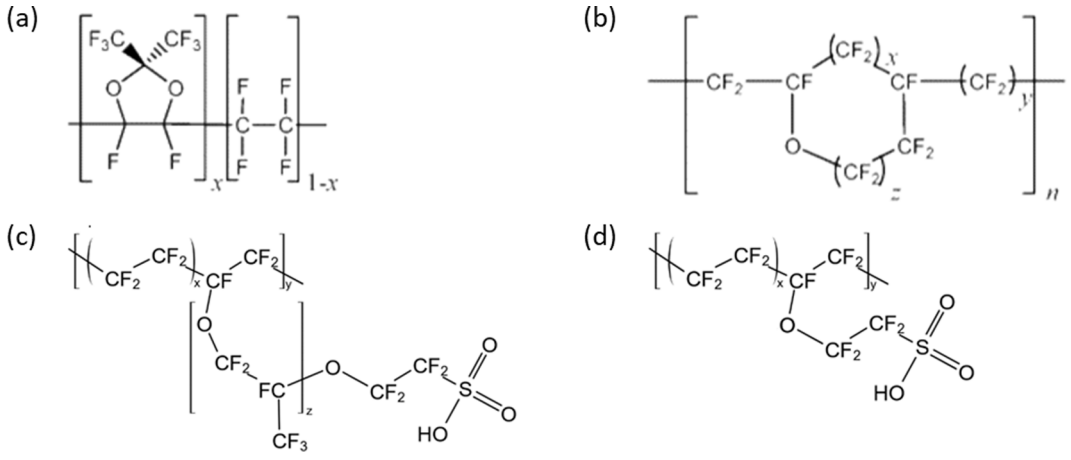

Fig. 15. Chemical structures of (a) Teflon [432] (© 2006 American Chemical Society), (b) Cytop [432] (© 2006 American Chemical Society), (c) Nafion [465] (© 2021 Elsevier), and (d) Aquivion [465] (© 2021 Elsevier). Reprinted with permission.

2.6.4.4. Fluorinated polymers. Fluoropolymers are fluorocarbon-based polymers with multiple covalent bonds between carbon and fluorine atoms. They have been found as materials with elevated thermal and chemical stability, even though they are generally costly and difficult to process. For these reasons and due to their low gas permeability related to their high semi-crystalline and crystalline structure, fluorinated polymers were initially not used as a membrane material [432]. However, they have unusual transport properties, especially for H_2S, so they have been modified in order to synthetize a new class of amorphous and glassy perfluoropolymers suitable for membrane separation. The most used fluoropolymers are polytetrafluoroethylene (PTFE or Teflon), polyvinylidene fluoride (PVDF) and Perfluoro sulfonic acid (PFSA) [344]. All the chemical structures of those materials are reported in Fig. 15.

Merkel and Toy [432] compared different type of fluoropolymers and nonfluorinated polymers for H_2S and CO_2 separation from natural stream. They noticed that Teflon and Cytop sorb more CO_2 than H_2S, demonstrating the existence of unfavourable interactions between H_2S and fluoridated polymers that lead to lower solubility and permeability when compared to nonfluorinated polymers. However, these results suggest that fluorinated polymers are more resistant to plasticization from acidic compounds than other types of polymer and, as a consequence, should not suffer from performance losses in the presence of such acidic compounds.

Different considerations can be made for perfluorosulfonic acid (PFSA) membranes, such as Nafion and Aquivion, which present a similar chemical structure to fluoropolymers, but also possess side chain ending with highly acidic -SO_3H groups. These ionomers have a heterogeneous matrix since they have a hydrophobic phase consisting of perfluorinated chains and a hydrophilic phase consisting of polar sulfonic acid groups (-SO_3H) [457–460].

As reported by many authors [459,461,462], in dry conditions they have a typical glassy behaviour where the gas transport is governed by solution-diffusion and the separation performance depends on the kinetic diameter of the penetrant. Permeability, however, is very low and far from that of interest for membrane separations. On the other hand, when used in humid conditions, PFSAs show a very interesting affinity to polar compounds and also good separation performance in view of their use in natural gas sweetening [459,463].

Although these materials do not have particularly interesting properties in dry conditions due to their low permeability [458], their behavior changes when exposed to water vapor. They become much more permeable to gases without changing substantially their permeability. This behavior is due to the polymer hydrophilic phase that absorb large quantities of water creating interconnected channels of water swollen polymer in which CO_2 and H_2S can easily diffuse because of the high solubility of these gases in water [461,463,464]. The H_2S permeability indeed at 35 °C increases from 32 to 370 Barrer when increasing the relative humidity, which is similar to the change of CO_2 permeability (from around 40 to 250 Barrer) also considering the differences between the two gases [465].

Despite their poor separation performances in dry condition, perfluorosulfonated iononomers can be considered as promising materials for acidic compounds removal due to their high resistance and low H_2S-plasticization ability and consequent performance losses. Moreover, the H_2S solubility can be largely increased by increasing the water content which allow membranes to reach higher permeability coefficient, H_2S/CH_4 selectivity that goes from 19 to 32, and H_2S/CO_2 selectivity around 0.8–1.2 due to the different temperature and water content in the matrix. Literature data in this concern refers to permeability for H_2S as 100 and 160 Barrer for NE 111 and N117, Na substituted Nafion® membranes, respectively, at 20 °C [466] and as up to 450 Barrer at 27 °C and 95% relative humidity for Aquivion® E87-12S material [465]. The latter membrane also showed a selectivity of 36 for H_2S with respect to methane in the same conditions.

2.6.5. Other materials

Several research groups have been investigating polymeric membranes for H_2S removal and the data from some of those works are presented in Table 7. As mentioned above, polymeric membranes can be modified to increase their separation performance to try to overcome the permeability and selectivity trade-off. They can be produced by altering the matrix through the addition of selective nanofiller, obtaining the so-called Mixed Matrix Membrane (MMM), or through the use of reactive carrier, creating the facilitated transport membranes (FTM) [467].

MMMs are considered a new generation membrane for gas purification, and they are processed by including molecular sieving material into the polymer matrix. These innovative materials put together the best properties of polymeric and inorganic membranes. In this concern, membranes meet the economical demand (due to the polymeric part) with the transport properties and high performance of gas separation (due to the inorganic part) [407]. MMMs generally exhibit high temperature and chemical resistances, high mechanical strength, and durability [468], even if their preparation maybe difficult due to the poor adherence between inorganic filler and the polymer, which can create defects that alter the membrane permeability and selectivity. Even in this case, the major data available consider CO_2 permeability condition in different type of membranes, since the separation condition depends on gas dimension and the H_2S kinetic diameter is smaller than CO_2 [344,469–471]. Nonetheless, some work exists mainly related to the use of metal organic frameworks in the contemporary separation of H_2S and CO_2 from natural gas both from the simulation [472] and experimental point of view [344,473].

The facilitated transport approach is used to selectively increase the affinity of one penetrant over the others is based on the incorporation of active agents into the polymer. Those chemical carriers react with the target component during the permeation, increasing its physical flux in view of a chemical reaction, whereas all the other penetrants permeate through the membrane only by physical mechanism [412]. The addition of those chemical carriers allows increase the flux for the component of interest (so its permeability) without alter the one of other components thus simultaneously increasing also the selectivity of the membrane for the target molecule.

FTMs can be divided in three categories according to the type of carrier is used: fixed membrane, solvent-swollen membrane, and immobilized liquid membrane. Fixed carrier membranes are generally prepared by introducing reactive functional groups into the polymer chain, while solvent-swollen membranes are prepared by swelling the polymer in a suitable solvent followed by the introduction of carrier species. At last, the immobilized liquid membranes (ILM) are obtained by saturating an inorganic porous membrane with a liquid contained carriers [407].

A typical example of facilitated transport mechanism in polymeric membranes is given by the carrier's amine-based solvent or other type of basic solvents since they react with acidic compounds and the complex can freely move into the swollen matrix, allowing the transport through the membrane's layer. However, there are not a lot of permeability and selectivity data in literature that explore H_2S facilitated transport because this system is largely characterized and effective for CO_2 transport, which results in very high CO_2 permeability. But this parameter is not as satisfactory as expected when it comes to H_2S. Way and Noble [474] studied the sorption of CO_2 and H_2S in perfluorosulfonic acid membrane functionalized with an amine carrier (HEDA, EDA) which should increase the flux of both compounds. They found out that the permeability of both CO_2 and H_2S increased due to the presence of amine-carrier gas. Nevertheless, they also noticed, as confirmed by other authors [423,475], that a competitive sorption occurs between the two gases because carbon dioxide exhibits a higher reaction rate than hydrogen sulfide. Thus, the higher the CO_2 flux, the lower that of H_2S.

Instead of amine-based carriers, Ilconich [476], Quinn [477] and Park [478] proved the possibility of increasing H_2S/CH_4 selectivity by

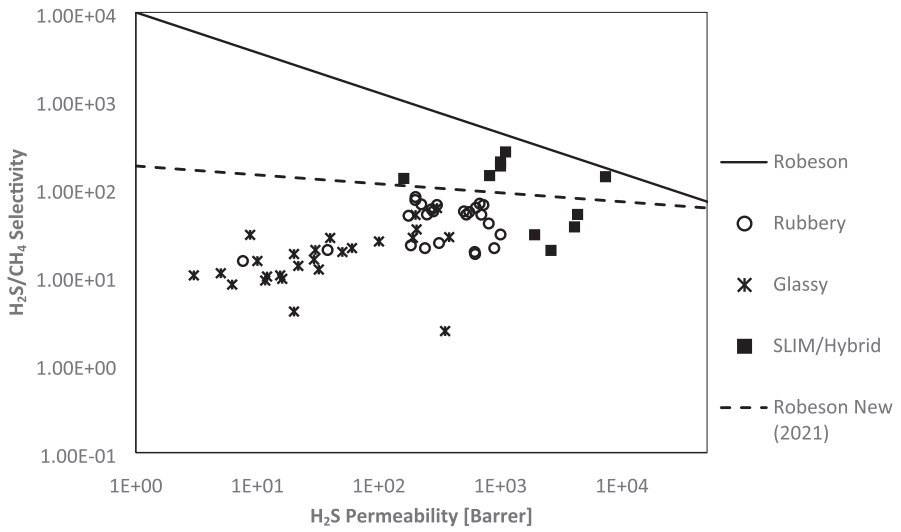

Fig. 16. H_2S/CH_4 Robeson plot. Adapted with permission from [490]. © 2021 Royal Society of Chemistry.

Table 8
Suggestions for current cost-effective primary treatment strategies.

	Gas Flow Rate	
Inlet H_2S Content	Low–Moderate	High
Low–Moderate	Scavenger or Redox or Biological Treatment	Redox or Biological Treatment or (Membrane + Adsorption)
High	Membrane + (Adsorption or Absorption)	Membrane + Absorption

using ionic liquid-facilitated solvent. Each of them characterized different type of liquid, based on various organic/inorganic salts (ammonium, phosphonium, bromide, tetrafluoroborate), that are able to react with H_2S and increase its solubility in the matrix. Higher solubility means higher selectivity, which is now in the range 500–800 for H_2S/CH_4 [476,479].

From the data and the results reported in this work, it is possible to understand that, nowadays, the available polymeric materials usable for H_2S separation from natural gas are limited, even though they can be increasingly modified to improve their resistance and separation performances. The separation performances of polymeric membranes are determined by their permeability and selectivity coefficient which can be compared one to another and synthetized in the Robeson's plot, namely the physical limit for membrane separation. As can be noticed from Fig. 16, the best exploitation of the permeability-selectivity trade-off is given by FTMs that in terms of separation performances probably represent the most promising material for acid gas separation and purification through membranes. However, they still suffer from other limitations related to stability and loss of performances at high pressure (carrier saturation phenomena) [480] which currently prevent their deployment in many industrial applications.

Other polymeric materials are therefore generally used for this purpose even if with lower intrinsic performances. Interestingly, while glassy polymers are usually preferred for CO_2 capture, when it comes to H_2S, rubbery polymers exhibit higher permeability and, in the case of block copolymers like Pebax, also a good stability and a sufficient mechanical resistance for application in industrial separation. In this regard, it is worthwhile to recall that the most promising application for this technology is in the field of natural gas sweetening, where the feed has a high pressure to provide a high driving force to the process and where high initial contents of H_2S can be found which makes membranes attractive in comparison to other separation technologies. It holds the advantages of reduced cost of construction and operation and simplified operation which still leads to a high degree of purification of the feed stream.

3. Status, opportunities, and challenges

The wide breadth of techniques and materials developed to capture H_2S from various (mainly gaseous) streams is a testament to the immense need to address this problem. Suitability of a technique to a specific application depends on numerous factors, such as operating conditions, cost, space and weight restrictions, gas volume, inlet H_2S content, outlet specification, technological maturity, etc. Although this choice usually requires a detailed analysis, Table 8 provides general suggestions for current cost-effective strategies divided into four broad application envelopes, and Table 9 provides a general comparison between various techniques of wide interest to serve as an initial guide. It must be noted that this general comparison does not directly apply to every material used in every technique. For example, technology readiness level (TRL) of a particular material may not be the same as that of the technique it is employed for. If we consider the case of chemical absorption, Table 9 presents a TRL of 9 due to its widespread industrial implementation using some of the most common alkanolamines as absorbents. However, chemical absorption using functionalized ionic liquids would only have a TRL of 2–4. On the other hand, it is more likely for an absorbent material at TRL 4 to be more readily integrated into the current industrial environment than a membrane material at the same TRL since absorption as a technique has a higher TRL than membrane technology for selective H_2S removal. As such, TRL is an important metric that depicts the progress of a material's (and technique's) development and the ease of its industrial implementation.

However, the metrics that drive this innovation are economics and sustainability. The most commonly used materials now are aqueous amines, zeolites, activated carbon, metal oxides, chelated iron solution (LO-CAT or Sulferox), and triazine-based liquid scavengers. Despite their disadvantages in one or both of the metrics, most of these materials have been used for decades. Cost-effective and sustainable alternatives are yet to be found. ILs were long believed to be sustainable solvents, but this was refuted for most traditional ILs. Protic ILs and DESs have since shown promise as cheaper, simpler, and more sustainable than normal ILs, but they are still more expensive than amines. In the recent years, MOFs have taken the world of materials science by storm, especially for adsorption applications. Although they exhibit performance on par with or exceeding that of zeolites, MOFs tend to be more expensive than zeolites and amines. Carbonaceous materials functionalized with active basic sites display an exciting enhancement in their H_2S removal ability,

Table 9
General comparison between common techniques for H_2S capture.

		Liquid Scavenger	Membrane	Biological Treatment	Chemical Solvent	Physical Solvent	Hybrid Solvent	Adsorption
Major Benefits		Small footprint, no intervention operation required	Small footprint, linear scaling up, no moving parts, no phase change	No toxic or hazardous chemicals, simple operation, mild operating conditions	Selective removal of H_2S with a regenerative solvent			Compact and scalable design, deep contaminant removal
Major Limitations		Too expensive at high inlet H_2S content, disposal of toxic waste, plugging and corrosion of equipment	Low H_2S/CO_2 selectivity, multistage setup with inter-stage compressors required, uncertainty	Uneven oxygen profile, may require multistage setup, clogging	High space and weight requirement, expensive regeneration step for chemical solvents, operational inflexibility			Complex control, uncertainty over regeneration, spent sorbent treatment
Inlet H_2S Content		< 0.02 vol% (200 ppmv)	Up to 90 vol%	< 10 vol%	Up to 70 vol%	> 10–15 vol%	> 10–15 vol%	< 2.0 vol%
Outlet H_2S Content		1–50 ppmv	Bulk removal (>50 ppmv)	< 50 ppmv	< 4 ppmv	< 1 vol%	< 0.5 vol%	0.05–50 ppmv
Hydrocarbon (HC) Loss		None	High (up to 25%)	Low–Medium	Negligible–Low	Low–Medium	Low–Medium	Low–Medium
Common Side/Waste Stream(s)		Spent scavenger	–	Sulfur or sulfuric acid, sludge	–	Heavy HC	Heavy HC	Heavy HC + water, spent adsorbent
Typical Operating Conditions	**Temperature**	As is	< 60 °C	Ambient	15 to 60 °C	−70 °C to ambient	5 to 60 °C	25 to 850 °C
	Pressure	As is	25 to 100 bar	Ambient to 15 bar	Ambient to 30 bar	> 50 bar	> 20 bar	Ambient to 70 bar
Cost	**CAPEX**	Low–Medium	Medium–High	Medium–High	Medium–High	Medium–High	Medium–High	Medium–High
	OPEX	Medium–High	Medium	Low–Medium	Medium–High	Medium	Medium	Medium
Technology Readiness Level (1–9)		9	6	9	9	9	9	9

but more studies are required to assess the various functionalization strategies and the effect of other commonly encountered compounds on the material performance. In general, many adsorbents suffer from a high regeneration penalty caused by irreversible chemical reactions on the surface. Biological techniques, such as biotrickling filtration and microaerobic oxidation, are interesting solutions with lower operational costs and high removal efficiencies, but their high capital costs largely confine their application to relatively small-scale applications. Membrane systems offer many advantages and have high potential. Their lightweight and compact nature make them ideal for use in remote locations and in small-scale applications. Their ease of adaptability to changes in flowrates and H_2S concentrations also give them attractive technical and operational advantages over amine plants. However, they are usually not economical as a standalone solution. Currently, their most effective application is in conjunction with either adsorption or absorption where a membrane's bulk separation capabilities could reduce the feed flowrate to adsorption or absorption columns, which in turn leads to a reduction in column size and energy usage.

Considering all this information, rough technology mapping can provide a guide for the selection of an appropriate process for H_2S capture. Building on Tables 8 and 9, a more specific discussion is provided here. As mentioned already, the choice of a suitable technology depends on various process conditions and operational requirements. For small and modular applications (offshore, associated gas, sometimes biogas, etc.), processes with smaller footprint are required. When the amount of sulfur to be treated is <1 ton per day (TPD) and on offshore platforms where sulfur recovery is not a priority, triazine-based liquid scavengers may be the best option. It must be noted that this would result in a spent waste stream that could contain toxic unspent scavenger. When the sulfur load is between 0.5 and 20 TPD, liquid redox processes (such as LO-CAT) or biological processes (such as THIOPAQ) may be appropriate. Biological removal would be the most suitable for biogas applications where the H_2S removal operation is in symbiosis with another step in the process, such as when a suitable liquid stream from another unit is used either in a bioscrubber or a biotrickling filter. As the total gas flowrate gets higher, a bulk separation step using a membrane or a biological solution followed by a deep removal step using a catalytic adsorbent (such as metal oxides or impregnated AC) can be considered. As the partial pressure of hydrogen sulfide increases and the sulfur load is higher than 20 TPD, absorption becomes the economical option, possibly in combination with a membrane as a bulk removal step prior to absorption. When the operating pressure is between atmospheric pressure and around 25 bar, chemical solvents should be considered. When the operating pressure is around 15–40 bar, hybrid solvents become an option. When the operating pressure is higher than 30 bar (especially 50 bar and above), physical solvents may be the better option. If liquefaction of methane (or other light gases) is desired, cryogenic distillation could be economically competitive or better than other processes. On the other hand, if the acid gases are to be re-injected into the geological reservoir at high pressure without liquefying methane, cryogenic distillation followed by either an absorption or adsorption process can be used. In general, adsorption is most economical when used as a deep removal step with low inflow of H_2S (<10–20 ppm) since most spent adsorbents currently cannot be regenerated and may even require landfilling.

Cost of a material plays an important role in determining the applicability of the material. A material's cost typically goes down as its TRL goes up and its production is scaled up. The current state of laboratory-scale development of the new materials discussed in this work is far from what's required to transition to higher TRLs. Most of the experimental studies are yet to consider the effect of realistic feed gas compositions on the material performance. The presence of carbon dioxide, other impurities, and water is known to affect H_2S removal efficiency. This also highlights a clear gap between science and engineering. For example, nearly all the studies on absorbents and adsorbents report the material performance in terms of equilibrium loading or breakthrough capacity

and aim to maximize them in single gas experiments. However, relying solely on these parameters often does not result in the best (or even a feasible) process performance. Purity, selectivity, recovery, kinetics, regeneration energy requirement, material-to-feed ratio, working capacity, etc., are crucial process parameters that dictate the overall capture cost of H_2S. As such, a more holistic assessment of material properties and performance must be adopted. Moreover, the particular issues that must be overcome by each class of materials are discussed in their respective sections. Addressing these issues is paramount to advancing the development of these materials.

Recent years have seen an increasing number of studies on hybrid and/or composite materials. N-functionalized mesoporous silica or carbon adsorbents, amine-functionalized MOFs, supported amine membranes, supported IL membranes, mixed matrix membranes based on zeolites or MOFs are some of the promising examples. Much of the work on the use of these materials for acid gas removal has so far focused on the capture of carbon dioxide, and their use for H_2S capture could be exciting. It is likely that these next-generation adsorbents and membranes, along with functionalized ionic liquids and deep eutectic solvents, will occupy most of the research attention in this field over the next few years. Advancement in the TRLs of AOPs and electrochemical systems is also expected, making these technologies potentially cost-effective for low–moderate sulfur loads either with or without a prior liquid-phase absorption step. In addition, the early use of computational tools for molecular design and process modeling is expected to rise and provide a strong impetus towards the realization of 'designer materials' with respect to technical, economic, and sustainability criteria.

Elemental sulfur is the end-product of all the H_2S removal processes today. While a large amount of this sulfur is converted to sulfuric acid, there is still a significant quantity of surplus sulfur that has no use. With increasing exploitation of sour gas reserves around the world and adoption of biomass-based processes, the amount of recovered sulfur from these processes is only bound to increase. This presents a significant challenge to the growing public momentum to achieve a circular economy. Therefore, there is a need for new and innovative solutions in this area. A large set of opportunities exist in the field of sulfur-based products. Development of different sulfur-derived products, such as batteries [481], will be a massive step towards resource efficiency and circular economy. Conversion of captured H_2S directly to value-added chemicals is another pathway to circular economy. For example, a multiphase reactor using phase transfer catalysis could potentially replace the expensive regeneration column in the alkanolamine-based absorption process and convert dissolved H_2S to dibenzyl sulfide bypassing the need for a sulfur recovery unit [482]. This could have a huge impact on the overall economics and sustainability of H_2S removal processes [483]. In this regard, process intensification could lead to multifunctional unit operations and innovative flowsheets in gas sweetening applications, providing promising alternatives to the conventional H_2S removal strategies [484].

Declaration of Competing Interest

The authors declare that they have no known competing financial interests or personal relationships that could have appeared to influence the work reported in this paper.

Acknowledgements

Funding: This work was supported by the Danish Offshore Technology Centre and the Sino-Danish Center for Education and Research.

References

[1] Hydrogen Sulfide - Hazards | Occupational Safety and Health Administration, (n.d.). https://www.osha.gov/hydrogen-sulfide/hazards (accessed May 7, 2021).
[2] R.O. Beauchamp, J.S. Bus, J.A. Popp, C.J. Boreiko, D.A. Andjelkovich, P. Leber, A critical review of the literature on hydrogen sulfide toxicity, Crit. Rev. Toxicol. 13 (1984) 25–97, https://doi.org/10.3109/10408448409029321.
[3] R.J. Reiffenstein, W.C. Hulbert, S.H. Roth, Toxicology of hydrogen sulfide, Annu. Rev. Pharmacol. Toxicol. 32 (1992) 109–134, https://doi.org/10.1146/annurev.pa.32.040192.000545.
[4] S. Mokhatab, W.A. Poe, J.Y. Mak, Basic Concepts of Natural Gas Processing, in: Handb. Nat. Gas Transm. Process, 4th ed.,, Gulf Professional Publishing, 2019, pp. 177–189, https://doi.org/10.1016/B978-0-12-815817-3.00004-6.
[5] R. Mohtadi, W.K. Lee, S. Cowan, J.W. Van Zee, M. Murthy, Effects of Hydrogen Sulfide on the Performance of a PEMFC, Electrochem. Solid-State Lett. 6 (2003) A272, https://doi.org/10.1149/1.1621831/XML.
[6] Z. Du, C. Liu, J. Zhai, X. Guo, Y. Xiong, W. Su, G. He, A Review of Hydrogen Purification Technologies for Fuel Cell Vehicles, Catalysts. 11 (2021) 393, https://doi.org/10.3390/CATAL11030393.
[7] T.N.A.T. Hassan, A.M. Shariff, M.M.M. Pauzi, M.S. Khidzir, A. Surmi, Insights on Cryogenic Distillation Technology for Simultaneous CO2 and H2S Removal for Sour Gas Fields, Molecules 27 (2022) 1424, https://doi.org/10.3390/MOLECULES27041424.
[8] P.S. Northrop, J.A. Valencia, The CFZ^{TM} process: A cryogenic method for handling high- CO2 and H2S gas reserves and facilitating geosequestration of CO2 and acid gases, Energy Procedia 1 (2009) 171–177, https://doi.org/10.1016/J.EGYPRO.2009.01.025.
[9] S.E. Hashemi, S. Sarker, K.M. Lien, S.K. Schnell, B. Austbø, Cryogenic vs. absorption biogas upgrading in liquefied biomethane production – An energy efficiency analysis, Fuel 245 (2019) 294–304, https://doi.org/10.1016/J.FUEL.2019.01.172.
[10] K. Rana, N. Rana, B. Singh, Applications of sulfur oxidizing bacteria, INC (2020), https://doi.org/10.1016/b978-0-12-818322-9.00010-1.
[11] B.C. Behera, R.R. Mishra, S.K. Dutta, H.N. Thatoi, Sulphur oxidising bacteria in mangrove ecosystem: A review, African, J. Biotechnol. 13 (2014) 2897–2907, https://doi.org/10.5897/AJB2013.13327.
[12] M. Syed, G. Soreanu, P. Falletta, M. Béland, Removal of hydrogen sulfide from gas streams using biological processes - A review, Can. Biosyst. Eng. 48 (2006), 2.1–2.14.
[13] C.B. van Niel, On the morphology and physiology of the purple and green sulphur bacteria, Arch. Mikrobiol. 3 (1932) 1–112, https://doi.org/10.1007/BF00454965.
[14] H. Larsen, On the culture and general physiology of the green sulfur bacteria, J. Bacteriol. 64 (1952) 187–196, https://doi.org/10.1128/jb.64.2.187-196.1952.
[15] L.M. Prescott, J.P. Harley, D.A. Klein, Microbiology, 5th ed., McGraw-Hill, New York, NY, 2002.
[16] B. Takano, M. Koshida, Y. Fujiwara, K. Sugimori, S. Takayanagi, Influence of sulfur-oxidizing bacteria on the budget of sulfate in Yugama crater lake, Kusatsu-Shirane volcano, Japan, Biogeochemistry 38 (1997) 227–253, https://doi.org/10.1023/A:1005805100834.
[17] J. Myung Cha, W. Suk Cha, J.H. Lee, Removal of organo-sulphur odour compounds by Thiobacillus novellus SRM, sulphur-oxidizing microorganisms, Process Biochem. 34 (1999) 659–665, https://doi.org/10.1016/S0032-9592(98)00139-3.
[18] E.V. Odintsova, H.W. Jannasch, J.A. Mamone, T.A. Langworthy, Thermothrix azorensis sp. nov., an Obligately Chemolithoautotrophic, Sulfur-Oxidizing, Thermophilic Bacterium, Int. J. Syst. Evol. Microbiol. 46 (1996) 422–428, https://doi.org/10.1099/00207713-46-2-422.
[19] D. Pokorna, J. Zabranska, Sulfur-oxidizing bacteria in environmental technology, Biotechnol. Adv. 33 (2015) 1246–1259, https://doi.org/10.1016/j.biotechadv.2015.02.007.
[20] G. Tóth, N. Nemestóthy, K. Bélafi-Bakó, D. Vozik, P. Bakonyi, Degradation of hydrogen sulfide by immobilized Thiobacillus thioparus in continuous biotrickling reactor fed with synthetic gas mixture, Int. Biodeterior. Biodegrad. 105 (2015) 185–191, https://doi.org/10.1016/j.ibiod.2015.09.006.
[21] W. Doungprasopsuk, P. Suwanvitaya, Effect of oxygen on sulfur products from H2S removal by thiobacillus in a biotrickling filter column, Eng. Appl. Sci. Res. 44 (2017) 214–221, https://doi.org/10.14456/easr.2017.33.
[22] Y. Liu, N. Chen, Y. Liu, H. Liu, C. Feng, M. Li, Simultaneous removal of nitrate and hydrogen sulfide by autotrophic denitrification in nitrate-contaminated water treatment, Environ. Technol. (United Kingdom) 40 (2019) 2325–2336, https://doi.org/10.1080/09593330.2018.1441333.
[23] P. Oyarzún, F. Arancibia, C. Canales, G.E. Aroca, Biofiltration of high concentration of hydrogen sulphide using Thiobacillus thioparus, Process Biochem. 39 (2003) 165–170, https://doi.org/10.1016/S0032-9592(03)00050-5.
[24] J.S. Devinny, M.A. Deshusses, T.S. Webster, Biofiltration for Air Pollution Control, 1st ed., CRC Press, Boca Raton, 1998 https://doi.org/10.1201/9781315138275.
[25] D.Y. Sorokin, T.P. Tourova, T.V. Kolganova, K.A. Sjollema, J.G. Kuenen, Thioalkalispira microaerophila gen. nov., sp. nov., a novel lithoautotrophic, sulfur-oxidizing bacterium from a soda lake, Int. J. Syst. Evol. Microbiol. 52 (2002) 2175–2182, https://doi.org/10.1099/00207713-52-6-2175.
[26] K. Vikrant, S.K. Kailasa, D.C.W. Tsang, S.S. Lee, P. Kumar, B.S. Giri, R.S. Singh, K. H. Kim, Biofiltration of hydrogen sulfide: Trends and challenges, J. Clean. Prod. 187 (2018) 131–147, https://doi.org/10.1016/j.jclepro.2018.03.188.
[27] M. Kumar, M.T. Zeyad, P. Choudhary, S. Paul, H. Chakdar, M.V. Singh Rajawat, Thiobacillus, Benef. Microbes Agro-Ecology. (2020) 545–557, https://doi.org/10.1016/b978-0-12-823414-3.00026-5.
[28] Y.C. Chung, C. Huang, C.P. Tseng, Biological elimination of H2S and NH3 from wastegases by biofilter packed with immobilized heterotrophic bacteria,

Chemosphere 43 (2001) 1043–1050, https://doi.org/10.1016/S0045-6535(00)00211-3.
[29] R. Howarth, R.F. Unz, E.M. Seviour, R.J. Seviour, L.L. Blackall, R.W. Pickup, J. G. Jones, J. Yaguchi, I.M. Head, Phylogenetic relationships of filamentous sulfur bacteria (Thiothrix spp. and Eikelboom type 021N bacteria) isolated from wastewater-treatment plants and description of Thiothrix eikelboomii sp. nov., Thiothrix unzii sp. nov., Thiothrix fructosivorans sp, Int. J. Syst. Bacteriol. 49 (1999) 1817–1827, https://doi.org/10.1099/00207713-49-4-1817.
[30] C. Pagella, D.M. De Faveri, H2S gas treatment by iron bioprocess, Chem. Eng. Sci. 55 (2000) 2185–2194, https://doi.org/10.1016/S0009-2509(99)00482-0.
[31] D.V. Meier, P. Pjevac, W. Bach, S. Hourdez, P.R. Girguis, C. Vidoudez, R. Amann, A. Meyerdierks, Niche partitioning of diverse sulfur-oxidizing bacteria at hydrothermal vents, ISME J. 11 (2017) 1545–1558, https://doi.org/10.1038/ismej.2017.37.
[32] M. Rezaei, M. Fazlzadehdavil, Y. Hajizadeh, Formaldehyde removal from airstreams using a biofilter with a mixture of compost and woodchips medium, Water. Air. Soil Pollut. 226 (2014), https://doi.org/10.1007/s11270-014-2242-0.
[33] R. Natarajan, J. Al-Sinani, S. Viswanathan, R. Manivasagan, Biodegradation of ethyl benzene and xylene contaminated air in an up flow mixed culture biofilter, Int. Biodeterior. Biodegrad. 119 (2017) 309–315, https://doi.org/10.1016/j.ibiod.2016.10.041.
[34] R.A.S. Lestari, W.B. Sediawan, S. Syamsiah, J.A.T. Sarto, Hydrogen sulfide removal from biogas using a salak fruit seeds packed bed reactor with sulfur oxidizing bacteria as biofilm, J. Environ Chem. Eng. 4 (2016) 2370–2377, https://doi.org/10.1016/j.jece.2016.04.014.
[35] M. Ben Jaber, B. Anet, A. Amrane, C. Couriol, T. Lendormi, P. Le Cloirec, G. Cogny, R. Fillières, Impact of nutrients supply and pH changes on the elimination of hydrogen sulfide, dimethyl disulfide and ethanethiol by biofiltration, Chem. Eng. J. 258 (2014) 420–426, https://doi.org/10.1016/j.cej.2014.07.085.
[36] A. Courtois, Y. Andrès, É. Dumont, H2S biofiltration using expanded schist as packing material: Influence of packed bed configurations at constant EBRT, J. Chem. Technol. Biotechnol. 90 (2015) 50–56, https://doi.org/10.1002/jctb.4456.
[37] Y. Zhang, H. Zhu, U. Szewzyk, S. Lübbecke, S., Uwe Geissen, Removal of emerging organic contaminants with a pilot-scale biofilter packed with natural manganese oxides, Chem. Eng. J. 317 (2017) 454–460, https://doi.org/10.1016/j.cej.2017.02.095.
[38] G.K. Kafle, L. Chen, H. Neibling, B. Brian He, Field evaluation of wood bark-based down-flow biofilters for mitigation of odor, ammonia, and hydrogen sulfide emissions from confined swine nursery barns, J. Environ. Manage. 147 (2015) 164–174, https://doi.org/10.1016/j.jenvman.2014.09.004.
[39] B.C. Aita, F.D. Mayer, D.T. Muratt, M. Brondani, S.B. Pujol, L.B. Denardi, R. Hoffmann, D.D. Da Silveira, Biofiltration of H2S-rich biogas using Acidithiobacillus thiooxidans, Clean Technol. Environ, Policy. 18 (2016) 689–703, https://doi.org/10.1007/s10098-015-1043-5.
[40] Y. Cheng, H. He, C. Yang, G. Zeng, X. Li, H. Chen, G. Yu, Challenges and solutions for biofiltration of hydrophobic volatile organic compounds, Biotechnol. Adv. 34 (2016) 1091–1102, https://doi.org/10.1016/j.biotechadv.2016.06.007.
[41] R.W. Melse, J.M.G. Hol, Biofiltration of exhaust air from animal houses: Evaluation of removal efficiencies and practical experiences with biobeds at three field sites, Biosyst. Eng. 159 (2017) 59–69, https://doi.org/10.1016/j.biosystemseng.2017.04.007.
[42] J. Das, E.R. Rene, C. Dupont, A. Dufourny, J. Blin, E.D. van Hullebusch, Performance of a compost and biochar packed biofilter for gas-phase hydrogen sulfide removal, Bioresour. Technol. 273 (2019) 581–591, https://doi.org/10.1016/j.biortech.2018.11.052.
[43] R. Zhu, S. Li, X. Bao, É. Dumont, Comparison of biological H2S removal characteristics between a composite packing material with and without functional microorganisms, Sci. Rep. 7 (2017) 1–8, https://doi.org/10.1038/srep42241.
[44] M.A. Lever, O. Rouxel, J.C. Alt, N. Shimizu, S. Ono, R.M. Coggon, W.C. Shanks III, L. Lapham, M. Elvert, X. Prieto-Mollar, K. Henrichs, F. Inagaki, A. Teske, Evidence for Microbial Carbon, Science. 339 (6125) (2013) 1305–1309. https://doi.org/10.1126/science.1229240.
[45] J.S. Berg, A. Schwedt, A.C. Kreutzmann, M.M.M. Kuypers, J. Milucka, Polysulfides as intermediates in the oxidation of sulfide to sulfate by Beggiatoa spp, Appl. Environ. Microbiol. 80 (2014) 629–636, https://doi.org/10.1128/AEM.02852-13.
[46] K.A. Rabbani, W. Charles, A. Kayaalp, R. Cord-Ruwisch, G. Ho, Biofilter for generation of concentrated sulphuric acid from H2S, Environ. Sci. Pollut. Res. 23 (2016) 16781–16789, https://doi.org/10.1007/s11356-016-6858-z.
[47] R. Lebrero, A. Toledo-Cervantes, R. Muñoz, V. del Nery, E. Foresti, Biogas upgrading from vinasse digesters: a comparison between an anoxic biotrickling filter and an algal-bacterial photobioreactor, J. Chem. Technol. Biotechnol. 91 (2016) 2488–2495, https://doi.org/10.1002/jctb.4843.
[48] M. Ben Jaber, A. Couvert, A. Amrane, P. Le Cloirec, E. Dumont, Removal of hydrogen sulfide in air using cellular concrete waste: Biotic and abiotic filtrations, Chem. Eng. J. 319 (2017) 268–278, https://doi.org/10.1016/j.cej.2017.03.014.
[49] G. Jiang, J. Keller, P.L. Bond, Z. Yuan, Predicting concrete corrosion of sewers using artificial neural network, Water Res. 92 (2016) 52–60, https://doi.org/10.1016/j.watres.2016.01.029.
[50] E. Kuliczkowska, Risk of structural failure in concrete sewers due to internal corrosion, Eng. Fail. Anal. 66 (2016) 110–119, https://doi.org/10.1016/j.engfailanal.2016.04.026.
[51] S. Gerrity, C. Kennelly, E. Clifford, G. Collins, Hydrogen sulfide oxidation in novel Horizontal-Flow Biofilm Reactors dominated by an Acidithiobacillus and a Thiobacillus species, Environ. Technol. (United Kingdom) 37 (2016) 2252–2264, https://doi.org/10.1080/09593330.2016.1147609.
[52] R.B. Solcia, M. Ramírez, M. Fernández, D. Cantero, D. Bevilaqua, Hydrogen sulphide removal from air by biotrickling filter using open-pore polyurethane foam as a carrier, Biochem. Eng. J. 84 (2014) 1–8, https://doi.org/10.1016/j.bej.2013.12.019.
[53] M. Ben Jaber, A. Couvert, A. Amrane, F. Rouxel, P. Le Cloirec, E. Dumont, Biofiltration of high concentration of H2S in waste air under extreme acidic conditions, N, Biotechnol. 33 (2016) 136–143, https://doi.org/10.1016/j.nbt.2015.09.008.
[54] K. Ziemiński, W.J. Kopycki, Impact of Different Packing Materials on Hydrogen Sulfide Biooxidation in Biofilters Installed in the Industrial Environment, Energy Fuels 30 (2016) 9386–9395, https://doi.org/10.1021/ACs.energyfuels.6b01374.
[55] M. Rezaei, G. Moussavi, K. Naddafi, M.S. Johnson, Enhanced biodegradation of styrene vapors in the biotrickling filter inoculated with biosurfactant-generating bacteria under H2O2 stimulation, Sci. Total Environ. 704 (2020), 135325, https://doi.org/10.1016/j.scitotenv.2019.135325.
[56] A.P. Lopez, A.R. Franco, Cloning and expression of cDNA encoding translationally controlled tumor protein from strawberry fruits, Biol. Plant. 50 (2006) 447–449, https://doi.org/10.1007/s10535-006-0067-4.
[57] J. Wu, X. Jiang, Z. Jin, S. Yang, J. Zhang, The performance and microbial community in a slightly alkaline biotrickling filter for the removal of high concentration H2S from biogas, Chemosphere 249 (2020), 126127, https://doi.org/10.1016/j.chemosphere.2020.126127.
[58] A. Turpin, A. Couvert, A. Laplanche, A. Paillier, Experimental study of mass transfer and H2S removal efficiency in a spray tower, Chem. Eng. Process. Process Intensif. 47 (2008) 886–892, https://doi.org/10.1016/j.cep.2007.02.002.
[59] S.P. Tayar, R.de B.S. Guerrero, L.F. Hidalgo, D. Bevilaqua, Evaluation of biogas biodesulfurization using different packing materials, ChemEngineering. 3 (2019) 1–12, https://doi.org/10.3390/chemengineering3010027.
[60] G. Soreanu, M. Béland, P. Falletta, B. Ventresca, P. Seto, Evaluation of different packing media for anoxic H2S control in biogas, Environ. Technol. 30 (2009) 1249–1259, https://doi.org/10.1080/09593330902998314.
[61] M. Fortuny, J.A. Baeza, X. Gamisans, C. Casas, J. Lafuente, M.A. Deshusses, D. Gabriel, Biological sweetening of energy gases mimics in biotrickling filters, Chemosphere 71 (2008) 10–17, https://doi.org/10.1016/j.chemosphere.2007.10.072.
[62] M. Fernández, M. Ramírez, R.M. Pérez, J.M. Gómez, D. Cantero, Hydrogen sulphide removal from biogas by an anoxic biotrickling filter packed with Pall rings, Chem. Eng. J. 225 (2013) 456–463, https://doi.org/10.1016/j.cej.2013.04.020.
[63] N. Vikromvarasiri, N. Pisutpaisal, Hydrogen sulfide removal in biotrickling filter system by Halothiobacillus neapolitanus, Int. J. Hydrogen Energy. 41 (2016) 15682–15687, https://doi.org/10.1016/j.ijhydene.2016.04.180.
[64] X. Tu, J. Guo, Y. Yang, R. Feng, G. Sun, J. Li, Biofilms formed within the acidic and the neutral biotrickling filters for treating H2S-containing waste gases, RSC Adv. 7 (2017) 25475–25482, https://doi.org/10.1039/c7ra04053a.
[65] Y. Cheng, T. Yuan, Y. Deng, C. Lin, J. Zhou, Z. Lei, K. Shimizu, Z. Zhang, Use of sulfur-oxidizing bacteria enriched from sewage sludge to biologically remove H2S from biogas at an industrial-scale biogas plant, Bioresour. Technol. Reports. 3 (2018) 43–50, https://doi.org/10.1016/j.biteb.2018.01.006.
[66] D. Gabriel, M.A. Deshusses, Performance of a full-scale biotrickling filter treating H2S at a gas contact time of 1.6 to 2.2 seconds, Environ. Prog. 22 (2003) 111–118, https://doi.org/10.1002/ep.670220213.
[67] S. Kim, M.A. Deshusses, Understanding the limits of H2S degrading biotrickling filters using a differential biotrickling filter, Chem. Eng. J. 113 (2005) 119–126, https://doi.org/10.1016/J.CEJ.2005.05.001.
[68] G. Rodriguez, A.D. Dorado, M. Fortuny, D. Gabriel, X. Gamisans, Biotrickling filters for biogas sweetening: Oxygen transfer improvement for a reliable operation, Process Saf. Environ. Prot. 92 (2014) 261–268, https://doi.org/10.1016/j.psep.2013.02.002.
[69] A.M. Montebello, M. Baeza, J. Lafuente, D. Gabriel, Monitoring and performance of a desulphurizing biotrickling filter with an integrated continuous gas/liquid flow analyser, Chem. Eng. J. 165 (2010) 500–507, https://doi.org/10.1016/j.cej.2010.09.053.
[70] X. Tu, M. Xu, J. Li, E. Li, R. Feng, G. Zhao, S. Huang, J. Guo, Enhancement of using combined packing materials on the removal of mixed sulfur compounds in a biotrickling filter and analysis of microbial communities, BMC Biotechnol. 19 (2019) 1–13, https://doi.org/10.1186/s12896-019-0540-8.
[71] X. Qiu, M.A. Deshusses, Performance of a monolith biotrickling filter treating high concentrations of H2S from mimic biogas and elemental sulfur plugging control using pigging, Chemosphere 186 (2017) 790–797, https://doi.org/10.1016/j.chemosphere.2017.08.032.
[72] A.M. Montebello, T. Bezerra, R. Rovira, L. Rago, J. Lafuente, X. Gamisans, S. Campoy, M. Baeza, D. Gabriel, Operational aspects, pH transition and microbial shifts of a H2S desulfurizing biotrickling filter with random packing material, Chemosphere 93 (2013) 2675–2682, https://doi.org/10.1016/j.chemosphere.2013.08.052.
[73] B. Khoshnevisan, P. Tsapekos, N. Alfaro, I. Díaz, M. Fdz-Polanco, S. Rafiee, I. Angelidaki, A review on prospects and challenges of biological H2S removal from biogas with focus on biotrickling filtration and microaerobic desulfurization, Biofuel Res. J. 4 (2017) 741–750. 10.18331/BRJ2017.4.4.6.
[74] M. Fortuny, X. Gamisans, M.A. Deshusses, J. Lafuente, C. Casas, D. Gabriel, Operational aspects of the desulfurization process of energy gases mimics in

biotrickling filters, Water Res. 45 (2011) 5665–5674, https://doi.org/10.1016/j.watres.2011.08.029.
[75] A. Singh, Z. Shareefdeen, O.P. Ward, Bio scrubber technology, Biotechnol. Odor Air Pollut, Control. (2005) 169–193, https://doi.org/10.1007/3-540-27007-8_8.
[76] A. Benschop, A. Janssen, A. Hoksberg, M. Seriwala, R. Abry, C. Ngai, The Shell-Paques/THIOPAQ Gas Desulphurisation Process, Successful Start Up First Commercial Unit (2002).
[77] P. San-Valero, J.M. Penya-roja, F. Javier Álvarez-Hornos, G. Buitrón, C. Gabaldón, G. Quijano, Fully aerobic bioscrubber for the desulfurization of H2S-rich biogas, Fuel 241 (2019) 884–891, https://doi.org/10.1016/j.fuel.2018.12.098.
[78] S. Potivichayanon, P. Pokethitiyook, M. Kruatrachue, Hydrogen sulfide removal by a novel fixed-film bioscrubber system, Process Biochem. 41 (2006) 708–715, https://doi.org/10.1016/j.procbio.2005.09.006.
[79] J. Kanjanarong, B.S. Giri, D.P. Jaisi, F.R. Oliveira, P. Boonsawang, S. Chaiprapat, R.S. Singh, A. Balakrishna, S.K. Khanal, Removal of hydrogen sulfide generated during anaerobic treatment of sulfate-laden wastewater using biochar: Evaluation of efficiency and mechanisms, Bioresour. Technol. 234 (2017) 115–121, https://doi.org/10.1016/j.biortech.2017.03.009.
[80] A.L. Kohl, R.B. Nielsen, Physical solvents for acid gas removal, in: Gas Purif., Elsevier, 1997, pp. 1187–1237. https://doi.org/10.1016/b978-088415220-0/50014-8.
[81] B. Burr, L. Lyddon, A comparison of physical solvents for acid gas removal, in: Gas Process. Assoc. Conv. Grapevine, TX, 2008.
[82] G.T. Rochelle, Amine scrubbing for CO2 capture, Science (80-) 325 (2009) 1652–1654, https://doi.org/10.1126/science.1176731.
[83] G. Puxty, R. Rowland, A. Allport, Q. Yang, M. Bown, R. Burns, M. Maeder, M. Attalla, Carbon dioxide postcombustion capture: A novel screening study of the carbon dioxide absorption performance of 76 amines, Environ. Sci. Technol. 43 (2009) 6427–6433, https://doi.org/10.1021/es901376a.
[84] J.C. Abanades, B. Arias, A. Lyngfelt, T. Mattisson, D.E. Wiley, H. Li, M.T. Ho, E. Mangano, S. Brandani, Emerging CO2 capture systems, Int. J. Greenh. Gas Control. 40 (2015) 126–166, https://doi.org/10.1016/j.ijggc.2015.04.018.
[85] M. Wang, A.S. Joel, C. Ramshaw, D. Eimer, N.M. Musa, Process intensification for post-combustion CO2 capture with chemical absorption: A critical review, Appl. Energy. 158 (2015) 275–291, https://doi.org/10.1016/j.apenergy.2015.08.083.
[86] M. Caplow, Kinetics of Carbamate Formation and Breakdown, J. Am. Chem. Soc. 90 (1968) 6795–6803, https://doi.org/10.4028/www.scientific.net/AMM.443.629.
[87] A. Haghtalab, M.D. Tafti, Electrolyte UNIQUAC-NRF model to study the solubility of acid gases in alkanolamines, Ind. Eng. Chem. Res. 46 (2007) 6053–6060, https://doi.org/10.1021/ie070259r.
[88] N. Haimour, O.C. Sand All, Selective Removal of Hydrogen Sulfide from Gases Containing Hydrogen Sulfide and Carbon Dioxide Using Diethanolamine, Sep. Sci. Technol. 18 (1983) 1221–1249, https://doi.org/10.1080/01496398308059925.
[89] R.K. Abdulrahman, I.M. Sebastine, Natural gas sweetening process simulation and optimization: A case study of Khurmala field in Iraqi Kurdistan region, J. Nat. Gas Sci. Eng. 14 (2013) 116–120, https://doi.org/10.1016/j.jngse.2013.06.005.
[90] N. Haimour, O.C. Sandall, Absorption of H2S into aqueous methyldiethanolamine, Chem. Eng. Commun. 59 (1987) 85–93, https://doi.org/10.1080/00986448708911987.
[91] N. Haimour, A. Bidarian, O.C. Sandall, Simultaneous Absorption of H2s and C02 Into Aqueous Methyldiethanotamine, Sep. Sci. Technol. 22 (1987) 921–947, https://doi.org/10.1080/01496398708068990.
[92] M. Bolhàr-Nordenkampf, A. Friedl, U. Koss, T. Tork, Modelling selective H2S absorption and desorption in an aqueous MDEA-solution using a rate-based non-equilibrium approach, Chem. Eng. Process. Process Intensif. 43 (2004) 701–715, https://doi.org/10.1016/S0255-2701(03)00011-4.
[93] A. Vrachnos, G. Kontogeorgis, E. Voutsas, Thermodynamic modeling of acidic gas solubility in aqueous solutions of MEA, MDEA and MEA-MDEA blends, Ind. Eng. Chem. Res. 45 (2006) 5148–5154, https://doi.org/10.1021/ie0600792.
[94] G. Sartori, D.W. Savage, Sterically Hindered Amines for CO2 Removal from Gases, Ind. Eng. Chem. Fundam. 22 (1983) 239–249, https://doi.org/10.1021/i100010a016.
[95] B.P. Mandal, A.K. Biswas, S.S. Bandyopadhyay, Selective absorption of H2S from gas streams containing H2S and CO2 into aqueous solutions of N-methyldiethanolamine and 2-amino-2-methyl-1-propanol, Sep. Purif. Technol. 35 (2004) 191–202, https://doi.org/10.1016/S1383-5866(03)00139-4.
[96] J.G. Lu, Y.F. Zheng, D.L. He, Selective absorption of H2S from gas mixtures into aqueous solutions of blended amines of methyldiethanolamine and 2-tertiarybutylamino-2-ethoxyethanol in a packed column, Sep. Purif. Technol. 52 (2006) 209–217, https://doi.org/10.1016/j.seppur.2006.04.003.
[97] L. Du, H. Li, L. Li, J. Xu, Y. Li, Investigation of selective desulfurization performance of sterically hindered amines, Pet. Sci. Technol. 37 (2019) 56–60, https://doi.org/10.1080/10916466.2018.1490758.
[98] H. Li, L. Li, J. Xu, Y. Li, Selective absorption of H 2 S from CO 2 using sterically hindered amines at high pressure, Pet. Sci. Technol. 37 (2019) 1825–1829, https://doi.org/10.1080/10916466.2019.1608239.
[99] U. Shoukat, D. Pinto, H. Knuutila, Study of Various Aqueous and Non-Aqueous Amine Blends for Hydrogen Sulfide Removal from Natural Gas, Processes. 7 (2019) 160, https://doi.org/10.3390/pr7030160.
[100] S.A. Freeman, R. Dugas, D.H. Van Wagener, T. Nguyen, G.T. Rochelle, Carbon dioxide capture with concentrated, aqueous piperazine, Int. J. Greenh. Gas Control. 4 (2010) 119–124, https://doi.org/10.1016/j.ijggc.2009.10.008.
[101] C.C. Lin, Y.H. Lin, C.S. Tan, Evaluation of alkanolamine solutions for carbon dioxide removal in cross-flow rotating packed beds, J. Hazard. Mater. 175 (2010) 344–351, https://doi.org/10.1016/j.jhazmat.2009.10.009.
[102] M. Sheng, C. Xie, X. Zeng, B. Sun, L. Zhang, G. Chu, Y. Luo, J.F. Chen, H. Zou, Intensification of CO2 capture using aqueous diethylenetriamine (DETA) solution from simulated flue gas in a rotating packed bed, Fuel 234 (2018) 1518–1527, https://doi.org/10.1016/j.fuel.2018.07.136.
[103] C.H. Yu, C.S. Tan, Mixed alkanolamines with low regeneration energy for CO2 capture in a rotating packed bed, in, Energy Procedia, Elsevier Ltd (2013) 455–460, https://doi.org/10.1016/j.egypro.2013.05.131.
[104] T. Nguyen, M. Hilliard, G.T. Rochelle, Amine volatility in CO2 capture, Int. J. Greenh. Gas Control. 4 (2010) 707–715, https://doi.org/10.1016/j.ijggc.2010.06.003.
[105] S.K. Dash, A.N. Samanta, S.S. Bandyopadhyay, Solubility of carbon dioxide in aqueous solution of 2-amino-2-methyl-1-propanol and piperazine, Fluid Phase Equilib. 307 (2011) 166–174, https://doi.org/10.1016/j.fluid.2011.05.009.
[106] S. Yunhai, L. Shan, L. Wei, L. Dong, G. Remy, D. JianPeng, Influence of MEA and piperazine additives on the desulfurization ability of MDEA aqueous for natural gas purification, Int. J. Ind. Chem. 7 (2016) 297–307, https://doi.org/10.1007/s40090-016-0072-1.
[107] J. Zhan, B. Wang, L. Zhang, B.C. Sun, J. Fu, G.W. Chu, H. Zou, Simultaneous Absorption of H2S and CO2 into the MDEA + PZ Aqueous Solution in a Rotating Packed Bed, Ind. Eng. Chem. Res. 59 (2020) 8295–8303, https://doi.org/10.1021/ACs.iecr.9b06437.
[108] A. Haghtalab, A. Izadi, Simultaneous measurement solubility of carbon dioxide+ hydrogen sulfide into aqueous blends of alkanolamines at high pressure, Fluid Phase Equilib. 375 (2014) 181–190, https://doi.org/10.1016/j.fluid.2014.05.017.
[109] W.Y. Lee, S.Y. Park, K.B. Lee, S.C. Nam, Simultaneous Removal of CO2 and H2S from Biogas by Blending Amine Absorbents: A Performance Comparison Study, Energy Fuels 34 (2020) 1992–2000, https://doi.org/10.1021/ACs.energyfuels.9b03342.
[110] C.K. Foo, C.Y. Leo, R. Aramesh, M.K. Aroua, N. Aghamohammadi, M. S. Shafeeyan, A. Shamiri, Density and viscosity of aqueous mixtures of N-methyldiethanolamines (MDEA), piperazine (PZ) and ionic liquids, J. Mol. Liq. 209 (2015) 596–602, https://doi.org/10.1016/j.molliq.2015.05.041.
[111] D. Fu, P. Zhang, C.L. Mi, Effects of concentration and viscosity on the absorption of CO2 in [N1111][Gly] promoted MDEA (methyldiethanolamine) aqueous solution, Energy. 101 (2016) 288–295, https://doi.org/10.1016/j.energy.2016.02.052.
[112] X.F. Tian, L.M. Wang, D. Fu, C. Li, Absorption and Removal Efficiency of Low-Partial-Pressure H 2 S in a Monoethanolamine-Activated N-Methyldiethanolamine Aqueous Solution, Energy Fuels 33 (2019) 629–635, https://doi.org/10.1021/ACs.energyfuels.8b03550.
[113] Z. Qian, L. Bin Xu, Z.H. Li, H. Li, K. Guo, Selective absorption of H2S from a gas mixture with CO2 by aqueous N-methyldiethanolamine in a rotating packed bed, Ind. Eng. Chem. Res. 49 (2010) 6196–6203, https://doi.org/10.1021/ie100678c.
[114] H. Zhao, L. Shao, J.F. Chen, High-gravity process intensification technology and application, Chem. Eng. J. 156 (2010) 588–593, https://doi.org/10.1016/j.cej.2009.04.053.
[115] S. Wu, L. Zhang, B. Sun, H. Zou, X. Zeng, Y. Luo, Q. Li, J. Chen, Mass-Transfer Performance for CO2 Absorption by 2-(2-Aminoethylamino)ethanol Solution in a Rotating Packed Bed, Energy Fuels 31 (2017) 14053–14059, https://doi.org/10.1021/ACs.energyfuels.7b03002.
[116] L. Sang, Y. Luo, G.W. Chu, J.P. Zhang, Y. Xiang, J.F. Chen, Liquid flow pattern transition, droplet diameter and size distribution in the cavity zone of a rotating packed bed: A visual study, Chem. Eng. Sci. 158 (2017) 429–438, https://doi.org/10.1016/j.ces.2016.10.044.
[117] K. Guo, J. Wen, Y. Zhao, Y. Wang, Z. Zhang, Z. Li, Z. Qian, Optimal packing of a rotating packed bed for H2S removal, Environ. Sci. Technol. 48 (2014) 6844–6849, https://doi.org/10.1021/es404913e.
[118] W. Jiao, P. Yang, G. Qi, Y. Liu, Selective absorption of H2S with High CO2 concentration in mixture in a rotating packed bed, Chem. Eng. Process. - Process Intensif. 129 (2018) 142–147, https://doi.org/10.1016/j.cep.2018.05.009.
[119] I. Iliuta, F. Larachi, CO2 and H2S absorption by MEA solution in packed-bed columns under inclined and heaving motion conditions - Hydrodynamics and reactions performance for marine applications, Int. J. Greenh. Gas Control. 79 (2018) 1–13, https://doi.org/10.1016/j.ijggc.2018.09.016.
[120] H. Cho, M. Binns, K.J. Min, J.K. Kim, Automated process design of acid gas removal units in natural gas processing, Comput. Chem. Eng. 83 (2015) 97–109, https://doi.org/10.1016/j.compchemeng.2015.05.030.
[121] T.N.G. Borhani, M. Afkhamipour, A. Azarpour, V. Akbari, S.H. Emadi, Z. A. Manan, Modeling study on CO2 and H2S simultaneous removal using MDEA solution, J. Ind. Eng. Chem. 34 (2016) 344–355, https://doi.org/10.1016/j.jiec.2015.12.003.
[122] M.S. Jassim, Sensitivity analyses and optimization of a gas sweetening plant for hydrogen sulfide and carbon dioxide capture using methyldiethanolamine solutions, J. Nat. Gas Sci. Eng. 36 (2016) 175–183, https://doi.org/10.1016/j.jngse.2016.10.012.
[123] C. Song, Q. Liu, N. Ji, S. Deng, J. Zhao, Y. Kitamura, Natural gas purification by heat pump assisted MEA absorption process, Appl. Energy. 204 (2017) 353–361, https://doi.org/10.1016/j.apenergy.2017.07.052.
[124] X. Gu, K. Qiu, J. Kuai, J. Weng, Z. Fan, K. Zhang, Energy-Efficiency Evaluation of Gas Sweetening Based on Yield-Energy-Selectivity Indicators, Chem. Eng. Technol. 41 (2018) 2034–2042, https://doi.org/10.1002/ceat.201700474.

[125] W. Li, Y. Zhuang, L. Liu, L. Zhang, J. Du, Economic Evaluation and Environmental Assessment of the Shale Gas Sweetening Process, Chem. Eng. Technol. 42 (2019) 753–760, https://doi.org/10.1002/ceat.201800554.
[126] S.Z. Naji, A.A. Abd, Sensitivity analysis of using diethanolamine instead of methyldiethanolamine solution for GASCO'S Habshan acid gases removal plant, Front, Energy. 13 (2019) 317–324, https://doi.org/10.1007/s11708-019-0622-2.
[127] U. Zahid, A. Sakheta, C.J. Lee, Techno-economic analysis of acid gas removal from associated and non-associated sour gas using amine blend, Int. J. Greenh. Gas Control. 98 (2020), 103078, https://doi.org/10.1016/j.ijggc.2020.103078.
[128] J. Park, S.Y. Lee, J. Kim, W. Um, I.B. Lee, C. Yoo, Energy, safety, and absorption efficiency evaluation of a pilot-scale H2S abatement process using MDEA solution in a coke-oven gas, J. Environ. Chem. Eng. 9 (2021), 105037, https://doi.org/10.1016/j.jece.2021.105037.
[129] H. Suleman, A.S. Maulud, Z. Man, Review and selection criteria of classical thermodynamic models for acid gas absorption in aqueous alkanolamines, Rev. Chem. Eng. 31 (2015) 599–639, https://doi.org/10.1515/revce-2015-0030.
[130] N. Sadegh, E.H. Stenby, K. Thomsen, Thermodynamic modeling of hydrogen sulfide absorption by aqueous N-methyldiethanolamine using the Extended UNIQUAC model, Fluid Phase Equilib. 392 (2015) 24–32, https://doi.org/10.1016/j.fluid.2015.01.024.
[131] N. Sadegh, E.H. Stenby, K. Thomsen, Thermodynamic modelling of acid gas removal from natural gas using the Extended UNIQUAC model, Fluid Phase Equilib. 442 (2017) 38–43, https://doi.org/10.1016/j.fluid.2017.02.020.
[132] C. Cleeton, O. Kvam, R. Rea, L. Sarkisov, M.G. De Angelis, Competitive H2S – CO2 absorption in reactive aqueous methyldiethanolamine solution: Prediction with ePC-SAFT, Fluid Phase Equilib. 511 (2020), 112453, https://doi.org/10.1016/j.fluid.2019.112453.
[133] A. Idrissi, P. Jedlovszky, Thermodynamics of Mixing Primary Alkanolamines with Water, J. Phys. Chem. B. 122 (2018) 6251–6259, https://doi.org/10.1021/ACs.jpcb.8b01052.
[134] F.A. Perdomo, S.H. Khalit, C.S. Adjiman, A. Galindo, G. Jackson, Description of the thermodynamic properties and fluid-phase behavior of aqueous solutions of linear, branched, and cyclic amines, AIChE J. 67 (2021), e17194, https://doi.org/10.1002/aic.17194.
[135] A. Muhammad, Y. GadelHak, Simulation based improvement techniques for acid gases sweetening by chemical absorption: A review, Int. J. Greenh. Gas Control. 37 (2015) 481–491, https://doi.org/10.1016/j.ijggc.2015.03.014.
[136] G.S. Hwang, H.M. Stowe, E. Paek, D. Manogaran, Reaction mechanisms of aqueous monoethanolamine with carbon dioxide: A combined quantum chemical and molecular dynamics study, Phys. Chem. Chem. Phys. 17 (2015) 831–839, https://doi.org/10.1039/c4cp04518a.
[137] T. Davran-Candan, DFT modeling of CO2 interaction with various aqueous amine structures, J. Phys. Chem. A. 118 (2014) 4582–4590, https://doi.org/10.1021/jp503929g.
[138] M. Narimani, S. Amjad-Iranagh, H. Modarress, Performance of tertiary amines as the absorbents for CO2 capture: Quantum mechanics and molecular dynamics studies, J. Nat. Gas Sci. Eng. 47 (2017) 154–166, https://doi.org/10.1016/j.jngse.2017.09.009.
[139] C. Chiappe, C.S. Pomelli, Hydrogen Sulfide and Ionic Liquids: Absorption, Separation, and Oxidation, Top. Curr. Chem. 375 (2017) 1–25, https://doi.org/10.1007/s41061-017-0140-9.
[140] J.F. Brennecke, E.J. Maginn, Ionic liquids: Innovative fluids for chemical processing, AIChE J. 47 (2001) 2384–2389, https://doi.org/10.1002/aic.690471102.
[141] T. Welton, Ionic liquids: a brief history, Biophys. Rev. 10 (2018) 691–706, https://doi.org/10.1007/s12551-018-0419-2.
[142] L.A. Blanchard, D. Hancu, E.J. Beckman, J.F. Brennecke, Green processing using ionic liquids and CO2, Nature 398 (1999) 28–29, https://doi.org/10.1038/19887.
[143] T. Welton, Room-Temperature Ionic Liquids. Solvents for Synthesis and Catalysis, Chem. Rev. 99 (1999) 2071–2083, https://doi.org/10.1021/cr980032t.
[144] S. Babamohammadi, A. Shamiri, M.K. Aroua, A review of CO2 capture by absorption in ionic liquid-based solvents, Rev. Chem. Eng. 31 (2015) 383–412, https://doi.org/10.1515/revce-2014-0032.
[145] G. Cui, J. Wang, S. Zhang, Active chemisorption sites in functionalized ionic liquids for carbon capture, Chem. Soc. Rev. 45 (2016) 4307–4339, https://doi.org/10.1039/c5cs00462d.
[146] S. Sarmad, J.-P. Mikkola, X. Ji, Carbon Dioxide Capture with Ionic Liquids and Deep Eutectic Solvents: A New Generation of Sorbents, ChemSusChem 10 (2017) 324–352, https://doi.org/10.1002/cssc.201600987.
[147] S. Zeng, X. Zhang, L. Bai, X. Zhang, H. Wang, J. Wang, D. Bao, M. Li, X. Liu, S. Zhang, Ionic-Liquid-Based CO2 Capture Systems: Structure, Interaction and Process, Chem. Rev. 117 (2017) 9625–9673, https://doi.org/10.1021/ACs.chemrev.7b00072.
[148] J. Haider, S. Saeed, M.A. Qyyum, B. Kazmi, R. Ahmad, A. Muhammad, M. Lee, Simultaneous capture of acid gases from natural gas adopting ionic liquids: Challenges, recent developments, and prospects, Renew. Sustain. Energy Rev. 123 (2020), 109771, https://doi.org/10.1016/j.rser.2020.109771.
[149] F.Y. Jou, A.E. Mather, Solubility of hydrogen sulfide in [bmim][PF6], Int. J. Thermophys. 28 (2007), 490, https://doi.org/10.1007/s10765-007-0185-z.
[150] C.S. Pomelli, C. Chiappe, A. Vidis, G. Laurenczy, P.J. Dyson, Influence of the interaction between hydrogen sulfide and ionic liquids on solubility: Experimental and theoretical investigation, J. Phys. Chem. B. 111 (2007) 13014–13019, https://doi.org/10.1021/jp076129d.
[151] S. Aparicio, M. Atilhan, Computational study of hexamethylguanidinium lactate ionic liquid: A candidate for natural gas sweetening, Energy Fuels 24 (9) (2010) 4989–5001, https://doi.org/10.1021/ef1005258.
[152] H. Sakhaeinia, V. Taghikhani, A.H. Jalili, A. Mehdizadeh, A.A. Safekordi, Solubility of H_2S in 1-(2-hydroxyethyl)-3-methylimidazolium ionic liquids with different anions, Fluid Phase Equilib. 298 (2010) 303–309, https://doi.org/10.1016/j.fluid.2010.08.027.
[153] X. Zhou, B. Cao, S. Liu, X. Sun, X. Zhu, H. Fu, Theoretical and experimental investigation on the capture of H2S in a series of ionic liquids, J. Mol. Graph. Model. 68 (2016) 87–94, https://doi.org/10.1016/j.jmgm.2016.06.013.
[154] X. Wang, S. Zeng, J. Wang, D. Shang, X. Zhang, J. Liu, Y. Zhang, Selective Separation of Hydrogen Sulfide with Pyridinium-Based Ionic Liquids, Ind. Eng. Chem. Res. 57 (2018) 1284–1293, https://doi.org/10.1021/ACs.iecr.7b04477.
[155] A.H. Jalili, M. Shokouhi, G. Maurer, A.T. Zoghi, J. Sadeghzah Ahari, K. Forsat, Measuring and modelling the absorption and volumetric properties of CO2 and H2S in the ionic liquid 1-ethyl-3-methylimidazolium tetrafluoroborate, J. Chem. Thermodyn. 131 (2019) 544–556, https://doi.org/10.1016/j.jct.2018.12.005.
[156] A.H. Jalili, M. Shokouhi, G. Maurer, M. Hosseini-Jenab, Solubility of CO2 and H2S in the ionic liquid 1-ethyl-3-methylimidazolium tris(pentafluoroethyl) trifluorophosphate, J. Chem. Thermodyn. 67 (2013) 55–62, https://doi.org/10.1016/j.jct.2013.07.022.
[157] A.H. Jalili, M. Safavi, C. Ghotbi, A. Mehdizadeh, M. Hosseini-Jenab, V. Taghikhani, Solubility of CO2, H2S, and their mixture in the ionic liquid 1-octyl-3-methylimidazolium bis(trifluoromethyl)sulfonylimide, J. Phys. Chem. B. 116 (2012) 2758–2774, https://doi.org/10.1021/jp2075572.
[158] M.B. Shiflett, A. Yokozeki, Separation of CO2 and H2S using room-temperature ionic liquid [bmim][PF6], Fluid Phase Equilib. 294 (2010) 105–113, https://doi.org/10.1016/j.fluid.2010.01.013.
[159] M. Safavi, C. Ghotbi, V. Taghikhani, A.H. Jalili, A. Mehdizadeh, Study of the solubility of CO2, H2S and their mixture in the ionic liquid 1-octyl-3-methylimidazolium hexafluorophosphate: Experimental and modelling, J. Chem. Thermodyn. 65 (2013) 220–232, https://doi.org/10.1016/j.jct.2013.05.038.
[160] A.E. Visser, R.P. Swatloski, W.M. Reichert, R. Mayton, S. Sheff, A. Wierzbicki, J. Davis, R.D. Rogers, Task-specific ionic liquids for the extraction of metal ions from aqueous solutions, Chem. Commun. (2001) 135–136, https://doi.org/10.1039/b008041l.
[161] J.H. Davis Jr., Task-Specific Ionic Liquids, Chem. Lett. 33 (2004) 1072–1077, https://doi.org/10.1246/cl.2004.1072.
[162] K. Huang, D.-N. Cai, Y.-L. Chen, Y.-T. Wu, X.-B. Hu, Z.-B. Zhang, Thermodynamic validation of 1-alkyl-3-methylimidazolium carboxylates as task-specific ionic liquids for H_2S absorption, AIChE J. 59 (2013) 2227–2235, https://doi.org/10.1002/aic.13976.
[163] K. Huang, D.-N. Cai, Y.-L. Chen, Y.-T. Wu, X.-B. Hu, Z.-B. Zhang, Dual Lewis Base Functionalization of Ionic Liquids for Highly Efficient and Selective Capture of H_2S, Chempluschem. 79 (2014) 241–249, https://doi.org/10.1002/cplu.201300365.
[164] K. Huang, X.-M. Zhang, Y. Xu, Y.-T. Wu, X.-B. Hu, Y. Xu, Protic ionic liquids for the selective absorption of H_2S from CO_2: Thermodynamic analysis, AIChE J. 60 (2014) 4232–4240, https://doi.org/10.1002/aic.14634.
[165] M. Volland, V. Seitz, M. Maase, M. Flores, R. Papp, K. Massonne, V. Stegmann, K. Halbritter, R. Noe, M. Bartsch, W. Siegel, M. Becker, O. Huttenloch, Method for the separation of acids from chemical reaction mixtures by means of ionic fluids, WO/2003/062251 (2003).
[166] T.L. Greaves, C.J. Drummond, Protic ionic liquids: Properties and applications, Chem. Rev. 108 (2008) 206–237, https://doi.org/10.1021/cr068040u.
[167] T.L. Greaves, C.J. Drummond, Protic Ionic Liquids: Evolving Structure-Property Relationships and Expanding Applications, Chem. Rev. 115 (2015) 11379–11448, https://doi.org/10.1021/ACs.chemrev.5b00158.
[168] T. Zhao, P. Li, X. Feng, X. Hu, Y. Wu, Study on absorption and spectral properties of H2S in carboxylate protic ionic liquids with low viscosity, J. Mol. Liq. 266 (2018) 806–813, https://doi.org/10.1016/j.molliq.2018.07.011.
[169] K. Huang, X.-M. Zhang, X.-B. Hu, Y.-T. Wu, Hydrophobic protic ionic liquids tethered with tertiary amine group for highly efficient and selective absorption of H_2S from CO_2, AIChE J. 62 (2016) 4480–4490, https://doi.org/10.1002/aic.15363.
[170] K. Huang, J.Y. Zhang, X.B. Hu, Y.T. Wu, Absorption of H2S and CO2 in Aqueous Solutions of Tertiary-Amine Functionalized Protic Ionic Liquids, Energy Fuels 31 (2017) 14060–14069, https://doi.org/10.1021/ACs.energyfuels.7b03049.
[171] C.F. Patzschke, J. Zhang, P.S. Fennell, J.P.M. Trusler, Density and Viscosity of Partially Carbonated Aqueous Solutions Containing a Tertiary Alkanolamine and Piperazine at Temperatures between 298.15 and 353.15 K, J. Chem. Eng. Data. 62 (2017) 2075–2083, https://doi.org/10.1021/ACs.jced.7b00144.
[172] K. Huang, X.M. Zhang, L. Sen Zhou, D.J. Tao, J.P. Fan, Highly efficient and selective absorption of H2S in phenolic ionic liquids: A cooperative result of anionic strong basicity and cationic hydrogen-bond donation, Chem. Eng. Sci. 173 (2017) 253–263, https://doi.org/10.1016/j.ces.2017.07.048.
[173] L.Y. Wang, Y.L. Xu, Z.D. Li, Y.N. Wei, J.P. Wei, CO2/CH4 and H2S/CO2 Selectivity by Ionic Liquids in Natural Gas Sweetening, Energy Fuels 32 (2018) 10–23, https://doi.org/10.1021/ACs.energyfuels.7b02852.
[174] B. Seyedhosseini, M. Izadyar, M.R. Housaindokht, A Computational Exploration of H2S and CO2 Capture by Ionic Liquids Based on α-Amino Acid Anion and N7, N9-Dimethyladeninium Cation, J. Phys. Chem. A. 121 (2017) 4352–4362, https://doi.org/10.1021/ACs.jpca.7b01280.
[175] X. Zhang, W. Xiong, L. Peng, Y. Wu, X. Hu, Highly selective absorption separation of H_2S and CO_2 from CH_4 by novel azole-based protic ionic liquids, AIChE J. 66 (2020), e16936, https://doi.org/10.1002/aic.16936.

[176] X. Zhang, W. Xiong, M. Shi, Y. Wu, X. Hu, Task-specific ionic liquids as absorbents and catalysts for efficient capture and conversion of H2S into value-added mercaptan acids, Chem. Eng. J. 408 (2021), 127866, https://doi.org/10.1016/j.cej.2020.127866.
[177] W. Xiong, M. Shi, L. Peng, X. Zhang, X. Hu, Y. Wu, Low viscosity superbase protic ionic liquids for the highly efficient simultaneous removal of H2S and CO2 from CH4, Sep. Purif. Technol. 263 (2021), 118417, https://doi.org/10.1016/j.seppur.2021.118417.
[178] C. Wang, H. Luo, D. Jiang, H. Li, S. Dai, Carbon Dioxide Capture by Superbase-Derived Protic Ionic Liquids, Angew. Chemie Int. Ed. 49 (2010) 5978–5981, https://doi.org/10.1002/anie.201002641.
[179] Z. Lei, C. Dai, B. Chen, Gas solubility in ionic liquids, Chem. Rev. 114 (2014) 1289–1326, https://doi.org/10.1021/cr300497a.
[180] S. Mortazavi-Manesh, M.A. Satyro, R.A. Marriott, Screening ionic liquids as candidates for separation of acid gases: Solubility of hydrogen sulfide, methane, and ethane, AIChE J. 59 (2013) 2993–3005, https://doi.org/10.1002/aic.14081.
[181] R. Farahipour, A. Mehrkesh, A.T. Karunanithi, A systematic screening methodology towards exploration of ionic liquids for CO2 capture processes, Chem. Eng. Sci. 145 (2016) 126–132, https://doi.org/10.1016/j.ces.2015.12.015.
[182] Y. Zhao, R. Gani, R.M. Afzal, X. Zhang, S. Zhang, Ionic liquids for absorption and separation of gases: An extensive database and a systematic screening method, AIChE J. 63 (2017) 1353–1367, https://doi.org/10.1002/aic.15618.
[183] J. Wang, Z. Song, H. Cheng, L. Chen, L. Deng, Z. Qi, Computer-Aided Design of Ionic Liquids as Absorbent for Gas Separation Exemplified by CO2 Capture Cases, ACS Sustain. Chem. Eng. 6 (2018) 12025–12035, https://doi.org/10.1021/ACssuschemeng.8b02321.
[184] A. Klamt, Conductor-like screening model for real solvents: A new approach to the quantitative calculation of solvation phenomena, J. Phys. Chem. 99 (1995) 2224–2235, https://doi.org/10.1021/j100007a062.
[185] A. Klamt, V. Jonas, T. Bürger, J.C.W. Lohrenz, Refinement and parametrization of COSMO-RS, J. Phys. Chem. A. 102 (1998) 5074–5085, https://doi.org/10.1021/jp980017s.
[186] D.Y. Peng, D.B. Robinson, A New Two-Constant Equation of State, Ind. Eng. Chem. Fundam. 15 (1976) 59–64, https://doi.org/10.1021/i160057a011.
[187] R. Santiago, J. Lemus, A.X. Outomuro, J. Bedia, J. Palomar, Assessment of ionic liquids as H2S physical absorbents by thermodynamic and kinetic analysis based on process simulation, Sep. Purif. Technol. 233 (2020), 116050, https://doi.org/10.1016/j.seppur.2019.116050.
[188] J. Lemus, R. Santiago, D. Hospital-Benito, T. Welton, J.P. Hallett, J. Palomar, Process Analysis of Ionic Liquid-Based Blends as H2S Absorbents: Search for Thermodynamic/Kinetic Synergies, ACS Sustain. Chem. Eng. 9 (2021) 2080–2088, https://doi.org/10.1021/ACssuschemeng.0c07229.
[189] J. Wang, Z. Song, H. Cheng, L. Chen, L. Deng, Z. Qi, Multilevel screening of ionic liquid absorbents for simultaneous removal of CO2 and H2S from natural gas, Sep. Purif. Technol. 248 (2020), 117053, https://doi.org/10.1016/j.seppur.2020.117053.
[190] B. Kazmi, J. Haider, M.A. Qyyum, S. Saeed, M.R. Kazmi, M. Lee, Heating load depreciation in the solvent-regeneration step of absorption-based acid gas removal using an ionic liquid with an imidazolium-based cation, Int. J. Greenh. Gas Control. 87 (2019) 89–99, https://doi.org/10.1016/j.ijggc.2019.05.007.
[191] Y. Wang, X. Liu, A. Kraslawski, J. Gao, P. Cui, A novel process design for CO2 capture and H2S removal from the syngas using ionic liquid, J. Clean. Prod. 213 (2019) 480–490, https://doi.org/10.1016/j.jclepro.2018.12.180.
[192] S. Yang, Y. Qian, S. Yang, Development of a Full CO2 Capture Process Based on the Rectisol Wash Technology, Ind. Eng. Chem. Res. 55 (2016) 6186–6193, https://doi.org/10.1021/ACs.iecr.6b00747.
[193] J. Haider, M. Abdul Qyyum, A. Riaz, A. Naquash, B. Kazmi, M. Yasin, A.S. Nizami, M. Byun, M. Lee, H. Lim, State-of-the-art process simulations and techno-economic assessments of ionic liquid-based biogas upgrading techniques: Challenges and prospects, Fuel 314 (2022), 123064, https://doi.org/10.1016/J.FUEL.2021.123064.
[194] M.J. Earle, K.R. Seddon, Ionic liquids. Green solvents for the future, in: Pure Appl. Chem., Walter de Gruyter GmbH, 2000: pp. 1391–1398. 10.1351/pac200072071391.
[195] M.J. Earle, J.M.S.S. Esperança, M.A. Gilea, J.N.C. Lopes, L.P.N. Rebelo, J. W. Magee, K.R. Seddon, J.A. Widegren, The distillation and volatility of ionic liquids, Nature 439 (2006) 831–834, https://doi.org/10.1038/nature04451.
[196] P. Wasserscheid, Chemistry: Volatile times for ionic liquids, Nature 439 (2006) 797, https://doi.org/10.1038/439797a.
[197] J.H. Clark, S.J. Tavener, Alternative solvents: Shades of green, Org. Process Res. Dev. 11 (2007) 149–155, https://doi.org/10.1021/op060160g.
[198] P.G. Jessop, Searching for green solvents, Green Chem. 13 (2011) 1391–1398, https://doi.org/10.1039/c0gc00797h.
[199] G. Cevasco, C. Chiappe, Are ionic liquids a proper solution to current environmental challenges? Green Chem. 16 (2014) 2375–2385, https://doi.org/10.1039/c3gc42096e.
[200] C.J. Clarke, W.C. Tu, O. Levers, A. Bröhl, J.P. Hallett, Green and Sustainable Solvents in Chemical Processes, Chem. Rev. 118 (2018) 747–800, https://doi.org/10.1021/ACs.chemrev.7b00571.
[201] H. Luo, G.A. Baker, J.S. Lee, R.M. Pagni, S. Dai, Ultrastable superbase-derived protic ionic liquids, J. Phys. Chem. B. 113 (2009) 4181–4183, https://doi.org/10.1021/jp901312d.
[202] Y. Cao, T. Mu, Comprehensive investigation on the thermal stability of 66 ionic liquids by thermogravimetric analysis, Ind. Eng. Chem. Res. 53 (2014) 8651–8664, https://doi.org/10.1021/ie5009597.
[203] A.P. Abbott, G. Capper, D.L. Davies, H.L. Munro, R.K. Rasheed, V. Tambyrajah, Preparation of novel, moisture-stable, lewis-acidic ionic liquids containing quaternary ammonium salts with functional side chains, Chem. Commun. 1 (2001) 2010–2011, https://doi.org/10.1039/b106357j.
[204] A.P. Abbott, G. Capper, D.L. Davies, R.K. Rasheed, V. Tambyrajah, Novel solvent properties of choline chloride/urea mixtures, Chem. Commun. (2003) 70–71, https://doi.org/10.1039/b210714g.
[205] G. García, S. Aparicio, R. Ullah, M. Atilhan, Deep eutectic solvents: Physicochemical properties and gas separation applications, Energy Fuels 29 (2015) 2616–2644, https://doi.org/10.1021/ef5028873.
[206] B.B. Hansen, S. Spittle, B. Chen, D. Poe, Y. Zhang, J.M. Klein, A. Horton, L. Adhikari, T. Zelovich, B.W. Doherty, B. Gurkan, E.J. Maginn, A. Ragauskas, M. Dadmun, T.A. Zawodzinski, G.A. Baker, M.E. Tuckerman, R.F. Savinell, J. R. Sangoro, Deep Eutectic Solvents: A Review of Fundamentals and Applications, Chem. Rev. 121 (2021) 1232–1285, https://doi.org/10.1021/ACs.chemrev.0c00385.
[207] A. Paiva, R. Craveiro, I. Aroso, M. Martins, R.L. Reis, A.R.C. Duarte, Natural deep eutectic solvents - Solvents for the 21st century, ACS Sustain. Chem. Eng. 2 (2014) 1063–1071, https://doi.org/10.1021/sc500096j.
[208] Y. Liu, J.B. Friesen, J.B. McAlpine, D.C. Lankin, S.N. Chen, G.F. Pauli, Natural Deep Eutectic Solvents: Properties, Applications, and Perspectives, J. Nat. Prod. 81 (2018) 679–690, https://doi.org/10.1021/ACs.jnatprod.7b00945.
[209] T. Aissaoui, I.M. Alnashef, U.A. Qureshi, Y. Benguerba, Potential applications of deep eutectic solvents in natural gas sweetening for CO2 capture, Rev. Chem. Eng. 33 (2017) 523–550, https://doi.org/10.1515/revce-2016-0013.
[210] Y. Zhang, X. Ji, X. Lu, Choline-based deep eutectic solvents for CO2 separation: Review and thermodynamic analysis, Renew. Sustain. Energy Rev. 97 (2018) 436–455, https://doi.org/10.1016/j.rser.2018.08.007.
[211] Y. Chen, X. Han, Z. Liu, D. Yu, W. Guo, T. Mu, Capture of Toxic Gases by Deep Eutectic Solvents, ACS Sustain. Chem. Eng. 8 (2020) 5410–5430, https://doi.org/10.1021/ACssuschemeng.0c01493.
[212] F. Liu, W. Chen, J. Mi, J. Zhang, X. Kan, F. Zhong, K. Huang, A. Zheng, L. Jiang, Thermodynamic and molecular insights into the absorption of H 2 S, CO 2, and CH 4 in choline chloride plus urea mixtures, AIChE J. 65 (2019), e16574, https://doi.org/10.1002/aic.16574.
[213] H. Wu, M. Shen, X. Chen, G. Yu, A.A. Abdeltawab, S.M. Yakout, New absorbents for hydrogen sulfide: Deep eutectic solvents of tetrabutylammonium bromide/carboxylic acids and choline chloride/carboxylic acids, Sep. Purif. Technol. 224 (2019) 281–289, https://doi.org/10.1016/j.seppur.2019.04.082.
[214] M. Shi, W. Xiong, Z. Tu, X. Zhang, X. Hu, Y. Wu, Task-specific deep eutectic solvents for the highly efficient and selective separation of H2S, Sep. Purif. Technol. 276 (2021), 119357, https://doi.org/10.1016/J.SEPPUR.2021.119357.
[215] M. Shi, W. Xiong, X. Zhang, J. Ji, X. Hu, Z. Tu, Y. Wu, Highly efficient and selective H2S capture by task-specific deep eutectic solvents through chemical dual-site absorption, Sep. Purif. Technol. 283 (2022), 120167, https://doi.org/10.1016/J.SEPPUR.2021.120167.
[216] M. Karibayev, D. Shah, Comprehensive Computational Analysis Exploring the Formation of Caprolactam-Based Deep Eutectic Solvents and Their Applications in Natural Gas Desulfurization, Energy Fuels 34 (2020) 9894–9902, https://doi.org/10.1021/ACs.energyfuels.0c01721.
[217] H.S. Salehi, R. Hens, O.A. Moultos, T.J.H. Vlugt, Computation of gas solubilities in choline chloride urea and choline chloride ethylene glycol deep eutectic solvents using Monte Carlo simulations, J. Mol. Liq. 316 (2020), 113729, https://doi.org/10.1016/j.molliq.2020.113729.
[218] A. González De Castilla, J.P. Bittner, S. Müller, S. Jakobtorweihen, I. Smirnova, Thermodynamic and Transport Properties Modeling of Deep Eutectic Solvents: A Review on gE-Models, Equations of State, and Molecular Dynamics, J. Chem. Eng. Data. 65 (2020) 943–967, https://doi.org/10.1021/ACs.jced.9b00548.
[219] H. Palmelund, M.P. Andersson, C.J. Asgreen, B.J. Boyd, J. Rantanen, K. Löbmann, Tailor-made solvents for pharmaceutical use? Experimental and computational approach for determining solubility in deep eutectic solvents (DES), Int. J. Pharm. X. 1 (2019), 100034, https://doi.org/10.1016/j.ijpx.2019.100034.
[220] E. Słupek, P. Makoś, J. Gębicki, Theoretical and Economic Evaluation of Low-Cost Deep Eutectic Solvents for Effective Biogas Upgrading to Bio-Methane, Energies. 13 (2020) 3379, https://doi.org/10.3390/en13133379.
[221] J. Haider, M.A. Qyyum, B. Kazmi, I. Ali, A.S. Nizami, M. Lee, Simulation study of deep eutectic solvent-based biogas upgrading process integrated with single mixed refrigerant biomethane liquefaction, Biofuel Res. J. 7 (2020) 1245–1255, https://doi.org/10.18331/BRJ2020.7.4.3.
[222] D. Deng, X. Liu, B. Gao, Physicochemical Properties and Investigation of Azole-Based Deep Eutectic Solvents as Efficient and Reversible SO2 Absorbents, Ind. Eng. Chem. Res. 56 (2017) 13850–13856, https://doi.org/10.1021/ACs.iecr.7b02478.
[223] Y. Chen, B. Jiang, H. Dou, L. Zhang, X. Tantai, Y. Sun, H. Zhang, Highly Efficient and Reversible Capture of Low Partial Pressure SO2 by Functional Deep Eutectic Solvents, Energy Fuels 32 (2018) 10737–10744, https://doi.org/10.1021/ACs.energyfuels.8b01794.
[224] Y. Gu, Y. Hou, S. Ren, Y. Sun, W. Wu, Hydrophobic Functional Deep Eutectic Solvents Used for Efficient and Reversible Capture of CO2, ACS Omega 5 (2020) 6809–6816, https://doi.org/10.1021/ACsomega.0c00150.
[225] H. Ghanbarabadi, B. Khoshandam, Simulation and comparison of Sulfinol solvent performance with Amine solvents in removing sulfur compounds and acid gases from natural sour gas, J. Nat. Gas Sci. Eng. 22 (2015) 415–420, https://doi.org/10.1016/j.jngse.2014.12.024.
[226] T. Nejat, A. Movasati, D.A. Wood, H. Ghanbarabadi, Simulated exergy and energy performance comparison of physical–chemical and chemical solvents in a sour gas

treatment plant, Chem. Eng. Res. Des. 133 (2018) 40–54, https://doi.org/10.1016/j.cherd.2018.02.040.
[227] A.A. Abd, S.Z. Naji, Comparison study of activators performance for MDEA solution of acid gases capturing from natural gas: Simulation-based on a real plant, Environ. Technol. Innov. 17 (2020), 100562, https://doi.org/10.1016/j.eti.2019.100562.
[228] A.H. Jalili, M. Shokouhi, F. Samani, M. Hosseini-Jenab, Measuring the solubility of CO2 and H2S in sulfolane and the density and viscosity of saturated liquid binary mixtures of (sulfolane + CO2) and (sulfolane + H2S), J. Chem. Thermodyn. 85 (2015) 13–25, https://doi.org/10.1016/j.jct.2015.01.001.
[229] S. Liu, H. Ling, J. Lv, H. Gao, Y. Na, Z. Liang, New Insights and Assessment of Primary Alkanolamine/Sulfolane Biphasic Solutions for Post-combustion CO2 Capture: Absorption, Desorption, Phase Separation, and Technological Process, Ind. Eng. Chem. Res. 58 (2019) 20461–20471, https://doi.org/10.1021/ACs.iecr.9b03670.
[230] X. Tian, L. Wang, D. Fu, Absorption and Removal Efficiency of Low-Partial-Pressure H2S in a Tetramethylammonium Glycinate Activated N-Methyldiethanolamine Aqueous Solution, Energy Fuels 33 (2019) 8413–8422, https://doi.org/10.1021/ACs.energyfuels.9b01983.
[231] X.F. Tian, L.M. Wang, P. Zhang, D. Fu, Z.Y. Wang, A high efficient absorbent for the separation of H2S from low partial pressure coke oven gas, Environ. Sci. Pollut. Res. 28 (2021) 5822–5832, https://doi.org/10.1007/s11356-020-10968-w.
[232] A. Afsharpour, A. Haghtalab, Simultaneous measurement absorption of CO2 and H2S mixture into aqueous solutions containing Diisopropanolamine blended with 1-butyl-3-methylimidazolium acetate ionic liquid, Int. J. Greenh. Gas Control. 58 (2017) 71–80, https://doi.org/10.1016/j.ijggc.2017.01.004.
[233] D. Liu, B. Li, J. Wu, Y. Liu, Sorbents for hydrogen sulfide capture from biogas at low temperature: a review, Environ. Chem. Lett. 18 (2020) 113–128, https://doi.org/10.1007/s10311-019-00925-6.
[234] M.P. Andersson, Density functional theory with modified dispersion correction for metals applied to molecular adsorption on Pt(111), Phys. Chem. Chem. Phys. 18 (2016) 19118–19122, https://doi.org/10.1039/C6CP03289C.
[235] M. Khabazipour, M. Anbia, Removal of Hydrogen Sulfide from Gas Streams Using Porous Materials: A Review, Ind. Eng. Chem. Res. 58 (2019) 22133–22164, https://doi.org/10.1021/ACs.iecr.9b03800.
[236] A. Peluso, N. Gargiulo, P. Aprea, F. Pepe, D. Caputo, Nanoporous Materials as H2S Adsorbents for Biogas Purification: a Review, Sep. Purif. Rev. 48 (2019) 78–89, https://doi.org/10.1080/15422119.2018.1476978.
[237] J.N. Joshi, G. Zhu, J.J. Lee, E.A. Carter, C.W. Jones, R.P. Lively, K.S. Walton, Probing Metal-Organic Framework Design for Adsorptive Natural Gas Purification, Langmuir 34 (2018) 8443–8450, https://doi.org/10.1021/ACs.langmuir.8b00889.
[238] H.Y. Zhang, C. Yang, Q. Geng, H.L. Fan, B.J. Wang, M.M. Wu, Z. Tian, Adsorption of hydrogen sulfide by amine-functionalized metal organic framework (MOF-199): An experimental and simulation study, Appl. Surf. Sci. 497 (2019), 143815, https://doi.org/10.1016/j.apsusc.2019.143815.
[239] M.H. Lee, K. Vikrant, S.A. Younis, J.E. Szulejko, K.H. Kim, Chemisorption of hydrogen sulfide by metal-organic frameworks and covalent-organic polymers based on experimental/theoretical evaluation, J. Clean. Prod. 250 (2020), 119486, https://doi.org/10.1016/j.jclepro.2019.119486.
[240] M.S. Shah, M. Tsapatsis, J.I. Siepmann, Hydrogen Sulfide Capture: From Absorption in Polar Liquids to Oxide, Zeolite, and Metal-Organic Framework Adsorbents and Membranes, Chem. Rev. 117 (2017) 9755–9803, https://doi.org/10.1021/ACs.chemrev.7b00095.
[241] H. Bamdad, K. Hawboldt, S. MacQuarrie, A review on common adsorbents for acid gases removal: Focus on biochar, Renew. Sustain. Energy Rev. 81 (2018) 1705–1720, https://doi.org/10.1016/j.rser.2017.05.261.
[242] A.G. Georgiadis, N.D. Charisiou, M.A. Goula, Removal of hydrogen sulfide from various industrial gases: A review of the most promising adsorbing materials, Catalysts. 10 (2020) 521, https://doi.org/10.3390/catal10050521.
[243] D. Mao, J.M. Griffin, R. Dawson, A. Fairhurst, G. Gupta, N. Bimbo, Porous materials for low-temperature H2S-removal in fuel cell applications, Sep. Purif. Technol. 277 (2021), 119426, https://doi.org/10.1016/J.SEPPUR.2021.119426.
[244] M. Ozekmekci, G. Salkic, M.F. Fellah, Use of zeolites for the removal of H2S: A mini-review, Fuel Process. Technol. 139 (2015) 49–60, https://doi.org/10.1016/j.fuproc.2015.08.015.
[245] Y. Feng, J. Lu, J. Wang, J. Mi, M. Zhang, M. Ge, Y. Li, Z. Zhang, W. Wang, Desulfurization sorbents for green and clean coal utilization and downstream toxics reduction: A review and perspectives, J. Clean. Prod. 273 (2020), 123080, https://doi.org/10.1016/j.jclepro.2020.123080.
[246] E. Martínez-Ahumada, A. López-Olvera, V. Jancik, J.E. Sánchez-Bautista, E. González-Zamora, V. Martis, D.R. Williams, I.A. Ibarra, MOF Materials for the Capture of Highly Toxic H2S and SO2, Organometallics 39 (2020) 883–915, https://doi.org/10.1021/ACs.organomet.9b00735.
[247] T. Islamoglu, Z. Chen, M.C. Wasson, C.T. Buru, K.O. Kirlikovali, U. Afrin, M. R. Mian, O.K. Farha, Metal-Organic Frameworks against Toxic Chemicals, Chem. Rev. 120 (2020) 8130–8160, https://doi.org/10.1021/ACs.chemrev.9b00828.
[248] A.G. Georgiadis, N. Charisiou, I.V. Yentekakis, M.A. Goula, Hydrogen Sulfide (H2S) Removal via MOFs, Materials (Basel). 13 (2020) 3640, https://doi.org/10.3390/MA13163640.
[249] A. Corma, From Microporous to Mesoporous Molecular Sieve Materials and Their Use in Catalysis, Chem. Rev. 97 (1997) 2420, https://doi.org/10.1021/CR960406N.
[250] M.E. Davis, Ordered porous materials for emerging applications, Nature 417 (2002) 813–821, https://doi.org/10.1038/NATURE00785.
[251] Y. Li, L. Li, J. Yu, Applications of Zeolites in Sustainable Chemistry, Chem. 3 (2017) 928–949, https://doi.org/10.1016/J.CHEMPR.2017.10.009.
[252] Y. Li, J. Yu, Emerging applications of zeolites in catalysis, separation and host–guest assembly, Nat. Rev. Mater. 6 (2021) 1156–1174, https://doi.org/10.1038/S41578-021-00347-3.
[253] J. Yu, R. Xu, Rich Structure Chemistry in the Aluminophosphate Family, Acc. Chem. Res. 36 (2003) 481–490, https://doi.org/10.1021/AR0201557.
[254] Y. Li, J. Yu, New Stories of Zeolite Structures: Their Descriptions, Determinations, Predictions, and Evaluations, Chem. Rev. 114 (2014) 7268–7316, https://doi.org/10.1021/CR500010R.
[255] L.H. Chen, X.Y. Li, J.C. Rooke, Y.H. Zhang, X.Y. Yang, Y. Tang, F.S. Xiao, B.L. Su, Hierarchically structured zeolites: synthesis, mass transport properties and applications, J. Mater. Chem. 22 (2012) 17381–17403, https://doi.org/10.1039/C2JM31957H.
[256] M. Moliner, C. Martínez, A. Corma, Synthesis Strategies for Preparing Useful Small Pore Zeolites and Zeotypes for Gas Separations and Catalysis, Chem. Mater. 26 (2013) 246–258, https://doi.org/10.1021/CM4015095.
[257] M.E. Davis, Zeolites from a materials chemistry perspective, Chem. Mater. 26 (2014) 239–245, https://doi.org/10.1021/CM401914U.
[258] M. Moliner, C. Martínez, A. Corma, Multipore Zeolites: Synthesis and Catalytic Applications, Angew. Chemie Int. Ed. 54 (2015) 3560–3579, https://doi.org/10.1002/ANIE.201406344.
[259] E. Koohsaryan, M. Anbia, Nanosized and hierarchical zeolites: A short review, Cuihua Xuebao/Chinese, J. Catal. 37 (2016) 447–467, https://doi.org/10.1016/S1872-2067(15)61038-5.
[260] E.M. Flanigen, J.M. Bennett, R.W. Grose, J.P. Cohen, R.L. Patton, R.M. Kirchner, J.V. Smith, Silicalite, a new hydrophobic crystalline silica molecular sieve, Nature 271 (1978) 512–516, https://doi.org/10.1038/271512A0.
[261] P. Bareschino, E. Mancusi, A. Forgione, F. Pepe, Biogas purification on Na-X Zeolite: Experimental and numerical results, Chem. Eng. Sci. 223 (2020), 115744, https://doi.org/10.1016/j.ces.2020.115744.
[262] L. Barelli, G. Bidini, L. Micoli, E. Sisani, M. Turco, 13X Ex-Cu zeolite performance characterization towards H2S removal for biogas use in molten carbonate fuel cells, Energy. 160 (2018) 44–53, https://doi.org/10.1016/j.energy.2018.05.057.
[263] S. Bahraminia, M. Anbia, E. Koohsaryan, Hydrogen sulfide removal from biogas using ion-exchanged nanostructured NaA zeolite for fueling solid oxide fuel cells, Int. J. Hydrogen Energy. 45 (2020) 31027–31040, https://doi.org/10.1016/j.ijhydene.2020.08.091.
[264] Z. Yan, S. Tang, X. Zhou, L. Yang, X. Xiao, H. Chen, Y. Qin, W. Sun, All-silica zeolites screening for capture of toxic gases from molecular simulation, Chinese, J Chem. Eng. 27 (2019) 174–181, https://doi.org/10.1016/j.cjche.2018.02.025.
[265] L. Song, X. Du, Y. Chen, Z. Yang, J. Ran, G. Yang, Q. Shi, Z. Xue, Screening of zeolites for H2S adsorption in mixed gases: GCMC and DFT simulations, Microporous Mesoporous Mater. 328 (2021), 111495, https://doi.org/10.1016/J.MICROMESO.2021.111495.
[266] P. Cosoli, M. Ferrone, S. Pricl, M. Fermeglia, Hydrogen sulphide removal from biogas by zeolite adsorption: Part I. GCMC molecular simulations, Chem. Eng. J. 145 (2008) 86–92, https://doi.org/10.1016/J.CEJ.2008.07.034.
[267] M.S. Shah, M. Tsapatsis, J.I. Siepmann, Identifying Optimal Zeolitic Sorbents for Sweetening of Highly Sour Natural Gas, Angew, Chemie. 128 (2016) 6042–6046, https://doi.org/10.1002/ANGE.201600612.
[268] T. Liu, E.L. First, M.M. Faruque Hasan, C.A. Floudas, A multi-scale approach for the discovery of zeolites for hydrogen sulfide removal, Comput. Chem. Eng. 91 (2016) 206–218, https://doi.org/10.1016/J.COMPCHEMENG.2016.03.015.
[269] V. Van Speybroeck, K. Hemelsoet, L. Joos, M. Waroquier, R.G. Bell, C.R.A. Catlow, Advances in theory and their application within the field of zeolite chemistry, Chem. Soc. Rev. 44 (2015) 7044–7111, https://doi.org/10.1039/C5CS00029G.
[270] A.G. Georgiadis, N.D. Charisiou, S. Gaber, K. Polychronopoulou, I.V. Yentekakis, M.A. Goula, Adsorption of Hydrogen Sulfide at Low Temperatures Using an Industrial Molecular Sieve: An Experimental and Theoretical Study, ACS Omega 6 (2021) 14774–14787, https://doi.org/10.1021/ACSOMEGA.0C06157.
[271] P.R. Westmoreland, D.P. Harrison, Evaluation of Candidate Solids for High-Temperature Desulfurization of Low-Btu Gases, Environ. Sci. Technol. 10 (1976) 659–661, https://doi.org/10.1021/es60118a010.
[272] X. Zhang, Y. Tang, S. Qu, J. Da, Z. Hao, H2S-Selective Catalytic Oxidation: Catalysts and Processes, ACS Catal. 5 (2015) 1053–1067, https://doi.org/10.1021/CS501476P.
[273] L.R. Pahalagedara, A.S. Poyraz, W. Song, C.H. Kuo, M.N. Pahalagedara, Y. T. Meng, S.L. Suib, Low temperature desulfurization of H2S: High sorption capacities by mesoporous cobalt oxide via increased H2S diffusion, Chem. Mater. 26 (2014) 6613–6621, https://doi.org/10.1021/CM503405A.
[274] S. Cheah, D.L. Carpenter, K.A. Magrini-Bair, Review of Mid- to High-Temperature Sulfur Sorbents for Desulfurization of Biomass- and Coal-derived Syngas, Energy Fuels 23 (2009) 5291–5307, https://doi.org/10.1021/EF900714Q.
[275] F. Dashtestani, M. Nusheh, V. Siriwongrungson, J. Hongrapipat, V. Materic, S. Pang, Effect of H2S and NH3 in biomass gasification producer gas on CO2 capture performance of an innovative CaO and Fe2O3 based sorbent, Fuel 295 (2021), 120586, https://doi.org/10.1016/j.fuel.2021.120586.
[276] S.H. Orojlou, B. Zargar, S. Rastegarzadeh, Metal oxide/TiO2 nanocomposites as efficient adsorbents for relatively high temperature H2S removal, J. Nat. Gas Sci. Eng. 59 (2018) 363–373, https://doi.org/10.1016/j.jngse.2018.09.016.
[277] Z. Pan, W.P. Chan, W. Da Oh, A. Veksha, A. Giannis, K.S.O. TamILselvam, J. Lei, D.K. Binte Mohamed, H. Wang, G. Lisak, T.T. Lim, Regenerable Co-ZnO-based nanocomposites for high-temperature syngas desulfurization, Fuel Process. Technol. 201 (2020), 106344, https://doi.org/10.1016/J.FUPROC.2020.106344.

[278] S. Kim, N.K. Gupta, J. Bae, K.S. Kim, Fabrication of coral-like Mn2O3/Fe2O3nanocomposite for room temperature removal of hydrogen sulfide, J. Environ. Chem. Eng. 9 (2021), 105216, https://doi.org/10.1016/j.jece.2021.105216.
[279] M. Wu, E. Guo, Q. Li, J. Mi, H. Fan, Mesoporous Zn-Fe-based binary metal oxide sorbent with sheet-shaped morphology: Synthesis and application for highly efficient desulfurization of hot coal gas, Chem. Eng. J. 389 (2020), 123750, https://doi.org/10.1016/J.CEJ.2019.123750.
[280] G. Mishra, B. Dash, S. Pandey, Layered double hydroxides: A brief review from fundamentals to application as evolving biomaterials, Appl. Clay Sci. 153 (2018) 172–186, https://doi.org/10.1016/J.CLAY.2017.12.021.
[281] Y. Ahn, K. Pandi, M. Lee, J. Choi, Removing hydrogen sulfide from a feed stream using suitable adsorbent materials, J. Clean. Prod. 272 (2020), 122849, https://doi.org/10.1016/j.jclepro.2020.122849.
[282] T.J. Bandosz, On the Adsorption/Oxidation of Hydrogen Sulfide on Activated Carbons at Ambient Temperatures, J. Colloid Interface Sci. 246 (2002) 1–20, https://doi.org/10.1006/JCIS.2001.7952.
[283] W. Shen, Z. Li, Y. Liu, Surface Chemical Functional Groups Modification of Porous Carbon, Recent Patents, Chem. Eng. 1 (2008) 27–40, https://doi.org/10.2174/2211334710801010027.
[284] B. Bajaj, H.I. Joh, S.M. Jo, J.H. Park, K.B. Yi, S. Lee, Enhanced reactive H_2S adsorption using carbon nanofibers supporte with Cu/Cu_xO nanoparticles, Appl. Surf. Sci. 429 (2018) 253–257, https://doi.org/10.1016/j.apsusc.2017.06.280.
[285] E. Ghasemy, H.B.M. Emrooz, A. Rashidi, T. Hamzehlouyan, Highly uniform molybdenum oxide loaded N-CNT as a remarkably active and selective nanocatalyst for H2S selective oxidation, Sci. Total Environ. 711 (2020), 134819, https://doi.org/10.1016/j.scitotenv.2019.134819.
[286] Y. Pan, M. Chen, Z. Su, K. Wu, Y. Zhang, D. Long, Two-dimensional CaO/carbon heterostructures with unprecedented catalytic performance in room-temperature H2S oxidization, Appl. Catal. B Environ. 280 (2021), 119444, https://doi.org/10.1016/j.apcatb.2020.119444.
[287] C. Yang, M. Florent, G. de Falco, H. Fan, T.J. Bandosz, ZnFe2O4/activated carbon as a regenerable adsorbent for catalytic removal of H2S from air at room temperature, Chem. Eng. J. 394 (2020), 124906, https://doi.org/10.1016/j.cej.2020.124906.
[288] V. Adavan Kiliyankil, B. Fugetsu, I. Sakata, Z. Wang, M. Endo, Aerogels from copper (II)-cellulose nanofibers and carbon nanotubes as absorbents for the elimination of toxic gases from air, J. Colloid Interface Sci. 582 (2021) 950–960, https://doi.org/10.1016/j.jcis.2020.08.100.
[289] N.N. Zulkefli, M.S. Masdar, W.N.R. Wan Isahak, S.N.H. Abu Bakar, H. Abu Hasan, N. Mohd Sofian, Application of Response Surface Methodology for Preparation of ZnAC2/CAC Adsorbents for Hydrogen Sulfide (H2S), Capture, Catalysts. 11 (2021) 545, https://doi.org/10.3390/catal11050545.
[290] B. Liu, S. Zuo, Catalytic performance improved by catalyst-integration technology and boosting H2S catalytic adsorption, Environ. Prog. Sustain. Energy. (2021), e13781, https://doi.org/10.1002/EP.13781.
[291] H.W. Ou, M.L. Fang, M.S. Chou, H.Y. Chang, T.F. Shiao, Long-term evaluation of activated carbon as an adsorbent for biogas desulfurization, J. Air Waste Manage. Assoc. 70 (2020) 641–648, https://doi.org/10.1080/10962247.2020.1754305.
[292] N. Mohamad Nor, L.C. Lau, K.T. Lee, A.R. Mohamed, Synthesis of activated carbon from lignocellulosic biomass and its applications in air pollution control—a review, J. Environ Chem. Eng. 1 (2013) 658–666, https://doi.org/10.1016/J.JECE.2013.09.017.
[293] H. Sawalha, M. Maghalseh, J. Qutaina, K. Junaidi, E.R. Rene, Removal of hydrogen sulfide from biogas using activated carbon synthesized from different locally available biomass wastes - a case study from Palestine, Bioengineered. 11 (2020) 607–618, https://doi.org/10.1080/21655979.2020.1768736.
[294] C. Yang, Y. Wang, H. Fan, G. de Falco, S. Yang, J. Shangguan, T.J. Bandosz, Bifunctional ZnO-MgO/activated carbon adsorbents boost H2S room temperature adsorption and catalytic oxidation, Appl. Catal. B Environ. 266 (2020), 118674, https://doi.org/10.1016/j.apcatb.2020.118674.
[295] L. Ling, R. Zhang, P. Han, B. Wang, DFT study on the sulfurization mechanism during the desulfurization of H2S on the ZnO desulfurizer, Fuel Process. Technol. 106 (2013) 222–230, https://doi.org/10.1016/J.FUPROC.2012.08.001.
[296] Y. Yuan, L. Huang, T.C. Zhang, L. Ouyang, S. Yuan, One-step synthesis of ZnFe2O4-loaded biochar derived from leftover rice for high-performance H2S removal, Sep. Purif. Technol. 279 (2021), 119686, https://doi.org/10.1016/J.SEPPUR.2021.119686.
[297] Q. Chen, J. Wang, X. Liu, X. Zhao, W. Qiao, D. Long, L. Ling, Alkaline carbon nanotubes as effective catalysts for H2S oxidation, Carbon N. Y. 49 (2011) 3773–3780, https://doi.org/10.1016/j.carbon.2011.05.011.
[298] K. Chizari, A. Deneuve, O. Ersen, I. Florea, Y. Liu, D. Edouard, I. Janowska, D. Begin, C. Pham-Huu, Nitrogen-Doped Carbon Nanotubes as a Highly Active Metal-Free Catalyst for Selective Oxidation, ChemSusChem 5 (2012) 102–108, https://doi.org/10.1002/CSSC.201100276.
[299] F. Sun, J. Liu, H. Chen, Z. Zhang, W. Qiao, D. Long, L. Ling, Nitrogen-rich mesoporous carbons: Highly efficient, regenerable metal-free catalysts for low-temperature oxidation of H2S, ACS Catal. 3 (2013) 862–870, https://doi.org/10.1021/CS300791J.
[300] X. Kan, X. Chen, W. Chen, J. Mi, J.Y. Zhang, F. Liu, A. Zheng, K. Huang, L. Shen, C. Au, L. Jiang, Nitrogen-Decorated, Ordered Mesoporous Carbon Spheres as High-Efficient Catalysts for Selective Capture and Oxidation of H2S, ACS Sustain. Chem. Eng. 7 (2019) 7609–7618, https://doi.org/10.1021/ACSSUSCHEMENG.8B05852.
[301] L. Chen, J. Yuan, T. Li, X. Jiang, S. Ma, W. Cen, W. Jiang, A regenerable N-rich hierarchical porous carbon synthesized from waste biomass for H2S removal at room temperature, Sci. Total Environ. 768 (2021), 144452, https://doi.org/10.1016/j.scitotenv.2020.144452.
[302] L. Yue, Q. Xia, L. Wang, L. Wang, H. DaCosta, J. Yang, X. Hu, CO2 adsorption at nitrogen-doped carbons prepared by K2CO3 activation of urea-modified coconut shell, J. Colloid Interface Sci. 511 (2018) 259–267, https://doi.org/10.1016/J.JCIS.2017.09.040.
[303] S. Fakhraie, H.R. Rajabi, A. Rashidi, Y. Orooji, E. Ghasemy, A. Shayesteh Zeraati, R. Rahighi, A. Mirhashemi, In situ simultaneous chemical activation and exfoliation of carbon quantum dots for atmospheric adsorption of H2S and CO2 at room temperature, Appl. Surf. Sci. 559 (2021), 149892, https://doi.org/10.1016/J.APSUSC.2021.149892.
[304] M. Yang, L. Guo, G. Hu, X. Hu, L. Xu, J. Chen, W. Dai, M. Fan, Highly cost-effective nitrogen-doped porous coconut shell-based CO2 sorbent synthesized by combining ammoxidation with KOH activation, Environ. Sci. Technol. 49 (2015) 7063–7070, https://doi.org/10.1021/ACS.EST.5B01311.
[305] J. Chen, J. Yang, G. Hu, X. Hu, Z. Li, S. Shen, M. Radosz, M. Fan, Enhanced CO2 Capture Capacity of Nitrogen-Doped Biomass-Derived Porous Carbons, ACS Sustain. Chem. Eng. 4 (2016) 1439–1445, https://doi.org/10.1021/ACSSUSCHEMENG.5B01425.
[306] L. Rao, R. Ma, S. Liu, L. Wang, Z. Wu, J. Yang, X. Hu, Nitrogen enriched porous carbons from d-glucose with excellent CO2 capture performance, Chem. Eng. J. 362 (2019) 794–801, https://doi.org/10.1016/J.CEJ.2019.01.093.
[307] Z. Yu, X. Wang, Y.N. Hou, X. Pan, Z. Zhao, J. Qiu, Nitrogen-doped mesoporous carbon nanosheets derived from metal-organic frameworks in a molten salt medium for efficient desulfurization, Carbon N. Y. 117 (2017) 376–382, https://doi.org/10.1016/J.CARBON.2017.02.100.
[308] D.V. Cuong, L. Truong-Phuoc, T. Tran-Thanh, J.M. Nhut, L. Nguyen-Dinh, I. Janowska, D. Begin, C. Pham-Huu, Nitrogen-doped carbon nanotubes decorated silicon carbide as a metal-free catalyst for partial oxidation of H2S, Appl. Catal. A Gen. 482 (2014) 397–406, https://doi.org/10.1016/j.apcata.2014.06.010.
[309] Z. Yu, X. Wang, X. Song, Y. Liu, J. Qiu, Molten salt synthesis of nitrogen-doped porous carbons for hydrogen sulfide adsorptive removal, Carbon N. Y. 95 (2015) 852–860, https://doi.org/10.1016/j.carbon.2015.08.105.
[310] C. Yang, S. Yang, H. Fan, Y. Wang, J. Shangguan, Tuning the ZnO-activated carbon interaction through nitrogen modification for enhancing the H2S removal capacity, J. Colloid Interface Sci. 555 (2019) 548–557, https://doi.org/10.1016/j.jcis.2019.08.014.
[311] G. Lei, Z. Dai, Z. Fan, X. Zheng, Y. Cao, L. Shen, Y. Xiao, C. Au, L. Jiang, Porous nanosheets of carbon-conjugated graphitic carbon nitride for the oxidation of H2S to elemental sulfur, Carbon N. Y. 155 (2019) 204–214, https://doi.org/10.1016/j.carbon.2019.08.052.
[312] M. Sun, X. Wang, X. Pan, L. Liu, Y. Li, Z. Zhao, J. Qiu, Nitrogen-rich hierarchical porous carbon nanofibers for selective oxidation of hydrogen sulfide, Fuel Process. Technol. 191 (2019) 121–128, https://doi.org/10.1016/j.fuproc.2019.03.020.
[313] J. Wang, C. Ke, X. Jia, C. Ma, X. Liu, W. Qiao, L. Ling, Polyethyleneimine-functionalized mesoporous carbon nanosheets as metal-free catalysts for the selective oxidation of H2S at room temperature, Appl. Catal. B Environ. 283 (2021), 119650, https://doi.org/10.1016/j.apcatb.2020.119650.
[314] Chi Xu, Jian Chen, Shiyan Li, Qingqing Gu, Dajun Wang, Chengfa Jiang, Yuefeng Liu, N-doped honeycomb-like porous carbon derived from biomass as an efficient carbocatalyst for H_2S selective oxidation, J. Hazard. Mater. 403 (2021), https://doi.org/10.1016/j.jhazmat.2020.123806.
[315] D. Li, W. Chen, J. Wu, C.Q. Jia, X. Jiang, The preparation of waste biomass-derived N-doped carbons and their application in acid gas removal: focus on N functional groups, J. Mater. Chem. A. 8 (2020) 24977–24995, https://doi.org/10.1039/D0TA07977D.
[316] L. Leng, S. Xu, R. Liu, T. Yu, X. Zhuo, S. Leng, Q. Xiong, H. Huang, Nitrogen containing functional groups of biochar: An overview, Bioresour. Technol. 298 (2020), 122286, https://doi.org/10.1016/J.BIORTECH.2019.122286.
[317] D. Alezi, Y. Belmabkhout, M. Suyetin, P.M. Bhatt, L.J. Weseliński, V. Solovyeva, K. Adil, I. Spanopoulos, P.N. Trikalitis, A.H. Emwas, M. Eddaoudi, MOF Crystal Chemistry Paving the Way to Gas Storage Needs: Aluminum-Based soc -MOF for CH4, O2, and CO2 Storage, J. Am. Chem. Soc. 137 (2015) 13308–13318, https://doi.org/10.1021/jACs.5b07053.
[318] H.C. Zhou, J.R. Long, O.M. Yaghi, Introduction to metal-organic frameworks, Chem. Rev. 112 (2012) 673–674, https://doi.org/10.1021/cr300014x.
[319] T.R. Cook, Y.R. Zheng, P.J. Stang, Metal-organic frameworks and self-assembled supramolecular coordination complexes: Comparing and contrasting the design, synthesis, and functionality of metal-organic materials, Chem. Rev. 113 (2013) 734–777, https://doi.org/10.1021/cr3002824.
[320] K. Sumida, D.L. Rogow, J.A. Mason, T.M. McDonald, E.D. Bloch, Z.R. Herm, T. H. Bae, J.R. Long, Carbon dioxide capture in metal-organic frameworks, Chem. Rev. 112 (2012) 724–781, https://doi.org/10.1021/cr2003272.
[321] P. Nugent, E.G. Giannopoulou, S.D. Burd, O. Elemento, E.G. Giannopoulou, K. Forrest, T. Pham, S. Ma, B. Space, L. Wojtas, M. Eddaoudi, M.J. Zaworotko, Porous materials with optimal adsorption thermodynamics and kinetics for co2 separation, Nature 495 (2013) 80–84, https://doi.org/10.1038/nature11893.
[322] H. Furukawa, K.E. Cordova, M. O'Keeffe, O.M. Yaghi, The chemistry and applications of metal-organic frameworks, Science 341 (6149) (2013) 341, https://doi.org/10.1126/science.1230444.
[323] O. Shekhah, Y. Belmabkhout, Z. Chen, V. Guillerm, A. Cairns, K. Adil, M. Eddaoudi, Made-to-order metal-organic frameworks for trace carbon dioxide removal and air capture, Nat. Commun. 5 (2014) 1–7, https://doi.org/10.1038/ncomms5228.

[324] K. Tan, S. Zuluaga, E. Fuentes, E.C. Mattson, J.F. Veyan, H. Wang, J. Li, T. Thonhauser, Y.J. Chabal, Trapping gases in metal-organic frameworks with a selective surface molecular barrier layer, Nat. Commun. 7 (2016) 1–8, https://doi.org/10.1038/ncomms13871.
[325] E.J. Kim, R.L. Siegelman, H.Z.H. Jiang, A.C. Forse, J.H. Lee, J.D. Martell, P.J. Milner, J.M. Falkowski, J.B. Neaton, J.A. Reimer, S.C. Weston, J.R. Long, Cooperative carbon capture and steam regeneration with tetraamine-appended metal-organic frameworks, Science (80-.). 369 (2020) 392–396. 10.1126/science.abb3976.
[326] N.K. Gupta, S. Kim, J. Bae, K.S. Kim, Chemisorption of hydrogen sulfide over copper-based metal-organic frameworks: Methanol and UV-assisted regeneration, RSC Adv. 11 (2021) 4890–4900, https://doi.org/10.1039/d0ra09017d.
[327] N.K. Gupta, S. Kim, J. Bae, K.S. Kim, Fabrication of Cu(BDC)0.5(BDC-NH2)0.5 metal-organic framework for superior H2S removal at room temperature, Chem. Eng. J. 411 (2021), 128536, https://doi.org/10.1016/j.cej.2021.128536.
[328] J.A. Zárate, E. Sánchez-González, T. Jurado-Vázquez, A. Gutiérrez-Alejandre, E. González-Zamora, I. Castillo, G. Maurin, I.A. Ibarra, Outstanding reversible H2S capture by an Al(iii)-based MOF, Chem. Commun. 55 (2019) 3049–3052, https://doi.org/10.1039/c8cc09379b.
[329] J.G. Flores, J.A. Zárate-Colín, E. Sánchez-González, J.R. Valenzuela, A. Gutiérrez-Alejandre, J. Ramírez, V. Jancik, J. Aguilar-Pliego, M.C. Zorrilla, H.A. Lara-García, E. González-Zamora, G. Guzmán-González, I. González, G. Maurin, I. A. Ibarra, Partially Reversible H2S Adsorption by MFM-300(Sc): Formation of Polysulfides, ACS Appl. Mater. Interfaces. 12 (2020) 18885–18892, https://doi.org/10.1021/ACsami.0c02340.
[330] E.S. Grape, J. Gabriel Flores, T. Hidalgo, E. Martínez-Ahumada, A. Gutierrez-Alejandre, A. Hautier, D.R. Williams, M. O'Keeffe, L. Ohrström, T. Willhammar, P. Horcajada, I.A. Ibarra, A. Ken Inge, A robust and biocompatible bismuth ellagate MOF synthesized under green ambient conditions, J. Am. Chem. Soc. 142 (2020) 16795–16804, https://doi.org/10.1021/jACs.0c07525.
[331] A. López-Olvera, J.G. Flores, J. Aguilar-Pliego, C.K. Brozek, A. Gutiérrez-Alejandre, I.A. Ibarra, Chemical Transformation of H2S within the Pores of Metal-Organic Frameworks: Formation of Polysulfides †, Chem. Mater. 33 (2021) 6269–6276, https://doi.org/10.1021/ACS.CHEMMATER.1C01918.
[332] K.S. Park, Z. Ni, A.P. Côté, J.Y. Choi, R. Huang, F.J. Uribe-Romo, H.K. Chae, M. O'Keeffe, O.M. Yaghi, Exceptional chemical and thermal stability of zeolitic imidazolate frameworks, Proc. Natl. Acad. Sci. 103 (2006) 10186–10191, https://doi.org/10.1073/PNAS.0602439103.
[333] H. Hayashi, A.P. Côté, H. Furukawa, M. O'Keeffe, O.M. Yaghi, Zeolite A imidazolate frameworks, Nat. Mater. 6 (2007) 501–506, https://doi.org/10.1038/NMAT1927.
[334] R. Banerjee, A. Phan, B. Wang, C. Knobler, H. Furukawa, M. O'Keeffe, O.M. Yaghi, High-throughput synthesis of zeolitic imidazolate frameworks and application to CO2 capture, Science 319 (5865) (2008) 939–943, https://doi.org/10.1126/science.1152516.
[335] A. Phan, C.J. Doonan, F.J. Uribe-Romo, C.B. Knobler, M. Okeeffe, O.M. Yaghi, Synthesis, structure, and carbon dioxide capture properties of zeolitic imidazolate frameworks, Acc. Chem. Res. 43 (2010) 58–67, https://doi.org/10.1021/AR900116G.
[336] B. Chen, Z. Yang, Y. Zhu, Y. Xia, Zeolitic imidazolate framework materials: recent progress in synthesis and applications, J. Mater. Chem. A. 2 (2014) 16811–16831, https://doi.org/10.1039/C4TA02984D.
[337] A.A. Jameh, T. Mohammadi, O. Bakhtiari, M. Mahdyarfar, Synthesis and modification of Zeolitic Imidazolate Framework (ZIF-8) nanoparticles as highly efficient adsorbent for H2S and CO2 removal from natural gas, J. Environ. Chem. Eng. 7 (2019), 103058, https://doi.org/10.1016/J.JECE.2019.103058.
[338] X. Liu, B. Wang, J. Cheng, Q. Meng, Y. Song, M. Li, Investigation on the capture performance and influencing factors of ZIF-67 for hydrogen sulfide, Sep. Purif. Technol. 250 (2020), 117300, https://doi.org/10.1016/J.SEPPUR.2020.117300.
[339] S. Reljic, A. Broto-Ribas, C. Cuadrado-Collados, E.O. Jardim, D. Maspoch, I. Imaz, J. Silvestre-Albero, Structural Deterioration of Well-Faceted MOFs upon H2S Exposure and Its Effect in the Adsorption Performance, Chem. – A Eur. J. 26 (2020) 17110–17119, https://doi.org/10.1002/CHEM.202002473.
[340] L. Feng, K.Y. Wang, G.S. Day, M.R. Ryder, H.C. Zhou, Destruction of Metal-Organic Frameworks: Positive and Negative Aspects of Stability and Lability, Chem. Rev. 120 (2020) 13087–13133, https://doi.org/10.1021/ACS.CHEMREV.0C00722.
[341] P. Lyu, G. Maurin, H2S Stability of Metal-Organic Frameworks: A Computational Assessment, ACS Appl. Mater. Interfaces. 13 (3) (2021) 4813–4822, https://doi.org/10.1021/acsami.0c21285.
[342] A.J. Rieth, A.M. Wright, M. Dincă, Kinetic stability of metal–organic frameworks for corrosive and coordinating gas capture, Nat. Rev. Mater. 4 (2019) 708–725, https://doi.org/10.1038/S41578-019-0140-1.
[343] A. Cadiau, Y. Belmabkhout, K. Adil, P.M. Bhatt, R.S. Pillai, A. Shkurenko, C. Martineau-Corcos, G. Maurin, M. Eddaoudi, Hydrolytically stable fluorinated metal-organic frameworks for energy-efficient dehydration, Science 356 (6339) (2017) 731–735, https://doi.org/10.1126/science.aam8310.
[344] G. Liu, A. Cadiau, Y. Liu, K. Adil, V. Chernikova, I.D. Carja, Y. Belmabkhout, M. Karunakaran, O. Shekhah, C. Zhang, A.K. Itta, S. Yi, M. Eddaoudi, W.J. Koros, Enabling Fluorinated MOF-Based Membranes for Simultaneous Removal of H2S and CO2 from Natural Gas, Angew. Chemie - Int. Ed. 57 (2018) 14811–14816, https://doi.org/10.1002/anie.201808991.
[345] Y. Belmabkhout, P.M. Bhatt, K. Adil, R.S. Pillai, A. Cadiau, A. Shkurenko, G. Maurin, G. Liu, W.J. Koros, M. Eddaoudi, Natural gas upgrading using a fluorinated MOF with tuned H2S and CO2 adsorption selectivity, Nat. Energy. 3 (2018) 1059–1066, https://doi.org/10.1038/S41560-018-0267-0.
[346] K. Cui, S. Bhattacharyya, S. Nair, J.R. Schmidt, Origins of Acid-Gas Stability Behavior in Zeolitic Imidazolate Frameworks: The Unique High Stability of ZIF-71, J. Am. Chem. Soc. 143 (2021) 18061–18072, https://doi.org/10.1021/JACS.1C06321.
[347] N.K. Gupta, J. Bae, S. Kim, K.S. Kim, Fabrication of Zn-MOF/ZnO nanocomposites for room temperature H2S removal: Adsorption, regeneration, and mechanism, Chemosphere 274 (2021), 129789, https://doi.org/10.1016/j.chemosphere.2021.129789.
[348] M. Wu, Q. Li, X. Wang, J. Mi, Structure Characteristics and Hot-Coal-Gas Desulfurization Properties of Zn-Based Sorbents Supported on Mesoporous Silica with Different Pore-Arrangement Patterns: A Comparison Study, Energy Fuels 35 (2021) 2456–2467, https://doi.org/10.1021/ACs.energyfuels.0c03794.
[349] G. Basina, D.A. Gaber, S. Al Yafei, V. Tzitzios, S.A. Gaber, I. Ismail, B. V. Vaithilingam, K. Polychronopoulou, S. Al Hashimi, Y., Al Wahedi, Mesoporous silica "plated" copper hydroxides/oxides heterostructures as superior regenerable sorbents for low temperature H2S removal, Chem. Eng. J. 398 (2020), 125585, https://doi.org/10.1016/j.cej.2020.125585.
[350] C.N. Okonkwo, C. Okolie, A. Sujan, G. Zhu, C.W. Jones, Role of Amine Structure on Hydrogen Sulfide Capture from Dilute Gas Streams Using Solid Adsorbents, Energy Fuels 32 (6) (2018) 6926–6933, https://doi.org/10.1021/acs.energyfuels.8b00936.
[351] C.N. Okonkwo, J.J. Lee, A. De Vylder, Y. Chiang, J.W. Thybaut, C.W. Jones, Selective removal of hydrogen sulfide from simulated biogas streams using sterically hindered amine adsorbents, Chem. Eng. J. 379 (2020), 122349, https://doi.org/10.1016/J.CEJ.2019.122349.
[352] C.N. Okonkwo, H. Fang, D.S. Sholl, J.E. Leisen, C.W. Jones, Effect of Humidity on the Sorption of H2S from Multicomponent Acid Gas Streams on Silica-Supported Sterically Hindered and Unhindered Amines, ACS Sustain. Chem. Eng. 8 (27) (2020) 10102–10114, https://doi.org/10.1021/acssuschemeng.0c02012.
[353] W.H. Glaze, J. wun Kang, Advanced Oxidation Processes: Test of a Kinetic Model for the Oxidation of Organic Compounds with Ozone and Hydrogen Peroxide in a Semibatch Reactor, Ind. Eng. Chem. Res. 28 (1989) 1580–1587, https://doi.org/10.1021/ie00095a002.
[354] G. Boczkaj, A. Fernandes, Wastewater treatment by means of advanced oxidation processes at basic pH conditions: A review, Chem. Eng. J. 320 (2017) 608–633, https://doi.org/10.1016/j.cej.2017.03.084.
[355] G. Moussavi, M. Rezaei, Exploring the advanced oxidation/reduction processes in the VUV photoreactor for dechlorination and mineralization of trichloroacetic acid: Parametric experiments, degradation pathway and bioassessment, Chem. Eng. J. 328 (2017) 331–342, https://doi.org/10.1016/j.cej.2017.07.006.
[356] G. Moussavi, M. Rezaei, M. Pourakbar, Comparing VUV and VUV/Fe2+ processes for decomposition of cloxacillin antibiotic: Degradation rate and pathways, mineralization and by-product analysis, Chem. Eng. J. 332 (2018) 140–149, https://doi.org/10.1016/j.cej.2017.09.057.
[357] A.S. Stasinakis, Use of selected advanced oxidation processes (AOPs) for wastewater treatment - A mini review, Glob. Nest J. 10 (3) (2008) 376–385, https://doi.org/10.30955/gnj.000598.
[358] R. Portela, S. Suárez, S.B. Rasmussen, N. Arconada, Y. Castro, A. Durán, P. Ávila, J.M. Coronado, B. Sánchez, Photocatalytic-based strategies for H2S elimination, Catal. Today. 151 (2010) 64–70, https://doi.org/10.1016/j.cattod.2010.03.056.
[359] M.A. Oturan, J.J. Aaron, Advanced oxidation processes in water/wastewater treatment: Principles and applications. A review, Crit. Rev. Environ. Sci. Technol. 44 (2014) 2577–2641, https://doi.org/10.1080/10643389.2013.829765.
[360] Y. Yu, T. Zhang, L. Zheng, J. Yu, Photocatalytic degradation of hydrogen sulfide using TiO2 film under microwave electrodeless discharge lamp irradiation, Chem. Eng. J. 225 (2013) 9–15, https://doi.org/10.1016/j.cej.2013.03.032.
[361] X. Dang, J. Huang, L. Kang, T. Wu, Q. Zhang, Research on decomposition of hydrogen sulfide using nonthermal plasma with metal oxide catalysis, Energy Procedia 16 (2012) 856–862, https://doi.org/10.1016/j.egypro.2012.01.137.
[362] L. Wang, X. Wang, P. Ning, C. Cheng, Y. Ma, R. Zhang, Simultaneous Removal of COS, H2S, and Dust in Industrial Exhaust Gas by DC Corona Discharge Plasma, Ind. Eng. Chem. Res. 57 (2018) 6568–6575, https://doi.org/10.1021/ACs.iecr.8b00028.
[363] Y. Wang, Y. Wang, Y. Liu, Absorption of H2S from Gas Streams by the Wet Ultraviolet/Persulfate Oxidation Process: Mechanism and Kinetics, Energy Fuels 34 (2020) 8037–8045, https://doi.org/10.1021/ACs.energyfuels.0c00755.
[364] Y. Liu, Y. Wang, Removal of Gaseous Hydrogen Sulfide by a Photo-Fenton Wet Oxidation Scrubbing System, Energy Fuels 33 (2019) 10812–10819, https://doi.org/10.1021/ACs.energyfuels.9b02720.
[365] C. Zhao, Y.X. Cai, Y. Yang, X.B. Zhu, C.H. Zheng, X. Gao, Energy efficiency optimization for H2S removal by dielectric barrier discharge plasma, Mod, Chem. Ind. 37 (10) (2017) 152–157, https://doi.org/10.16606/j.cnki.issn0253-4320.2017.10.036.
[366] C. Liu, R. Zhang, S. Wei, J. Wang, Y. Liu, M. Li, R. Liu, Selective removal of H2S from biogas using a regenerable hybrid TiO2/zeolite composite, Fuel 157 (2015) 183–190, https://doi.org/10.1016/j.fuel.2015.05.003.
[367] R. Portela, M.C. Canela, B. Sánchez, F.C. Marques, A.M. Stumbo, R.F. Tessinari, J. M. Coronado, S. Suárez, H2S photodegradation by TiO2/M-MCM-41 (M = Cr or Ce): Deactivation and by-product generation under UV-A and visible light, Appl. Catal. B Environ. 84 (2008) 643–650, https://doi.org/10.1016/j.apcatb.2008.05.020.
[368] S. Kato, Y. Hirano, M. Iwata, T. Sano, K. Takeuchi, S. Matsuzawa, Photocatalytic degradation of gaseous sulfur compounds by silver-deposited titanium dioxide, Appl. Catal. B Environ. 57 (2005) 109–115, https://doi.org/10.1016/j.apcatb.2004.10.015.

[369] R. Portela, B. Sánchez, J.M. Coronado, R. Candal, S. Suárez, Selection of TiO2-support: UV-transparent alternatives and long-term use limitations for H2S removal, Catal. Today. 129 (2007) 223–230, https://doi.org/10.1016/j.cattod.2007.08.005.

[370] H. Zou, M. Sheng, X. Sun, Z. Ding, M. Arowo, Y. Luo, L. Zhang, G. Chu, J.F. Chen, B. Sun, Removal of hydrogen sulfide from coke oven gas by catalytic oxidative absorption in a rotating packed bed, Fuel 204 (2017) 47–53, https://doi.org/10.1016/j.fuel.2017.05.017.

[371] Y. Wang, Z. Wang, Y. Liu, Oxidation Absorption of Gaseous H2S Using Fenton-Like Advanced Oxidation Systems, Energy Fuels 32 (2018) 11289–11295, https://doi.org/10.1021/ACs.energyfuels.8b02657.

[372] Y. Wang, Z. Wang, J. Pan, Y. Liu, Removal of gaseous hydrogen sulfide using Fenton reagent in a spraying reactor, Fuel 239 (2019) 70–75, https://doi.org/10.1016/j.fuel.2018.10.143.

[373] A. Alonso-Tellez, D. Robert, N. Keller, V. Keller, A parametric study of the UV-A photocatalytic oxidation of H 2S over TiO 2, Appl. Catal. B Environ. 115–116 (2012) 209–218, https://doi.org/10.1016/j.apcatb.2011.12.014.

[374] A.B. Ijzermans, Poisoning effects of hydrogen sulfide on noble metal electrodes. Part I. Rest potentials and stationary current density - potential measurements on Pt and Au electrodes in H2SO4 solutions containing H2S, Recl. Des Trav. Chim. Des Pays-Bas. 88 (1969) 334–343, https://doi.org/10.1002/RECL.19690880312.

[375] T. Loučka, Adsorption and oxidation of sulphur and of sulphur dioxide at the platinum electrode, J. Electroanal. Chem. Interfacial Electrochem. 31 (1971) 319–332, https://doi.org/10.1016/S0022-0728(71)80162-6.

[376] N. Ramasubramanian, Anodic behavior of platinum electrodes in sulfide solutions and the formation of platinum sulfide, J. Electroanal. Chem. 64 (1975) 21–37, https://doi.org/10.1016/S0022-0728(75)80276-2.

[377] I. Pikaar, E.M. Likosova, S. Freguia, J. Keller, K. Rabaey, Z. Yuan, Electrochemical abatement of hydrogen sulfide from waste streams, Crit. Rev. Environ. Sci. Technol. 45 (2015) 1555–1578, https://doi.org/10.1080/10643389.2014.966419.

[378] E. Ntagia, A. Prévoteau, K. Rabaey, Electrochemical removal of sulfur pollution, in: P.N.L. Lens (Ed.), Environ. Technol. to Treat Sulphur Pollut. Princ. Eng, 2nd ed., IWA Publishing, 2020, pp. 247–276. https://doi.org/10.2166/9781789060966_0247.

[379] Y. Feng, L. Yang, J. Liu, B.E. Logan, Electrochemical technologies for wastewater treatment and resource reclamation, Environ. Sci. Water Res. Technol. 2 (2016) 800–831, https://doi.org/10.1039/c5ew00289c.

[380] J. Radjenovic, D.L. Sedlak, Challenges and Opportunities for Electrochemical Processes as Next-Generation Technologies for the Treatment of Contaminated Water, Environ. Sci. Technol. 49 (2015) 11292–11302, https://doi.org/10.1021/ACs.est.5b02414.

[381] Marcel Pourbaix, Atlas of Electrochemical Equilibria in Aqueous Solutions, 1st, Pergamon Press, Oxford, 1966.

[382] P.K. Dutta, K. Rabaey, Z. Yuan, J. Keller, Spontaneous electrochemical removal of aqueous sulfide, Water Res. 42 (2008) 4965–4975, https://doi.org/10.1016/j.watres.2008.09.007.

[383] M.M. Emamjomeh, M. Sivakumar, Review of pollutants removed by electrocoagulation and electrocoagulation/flotation processes, J. Environ. Manage. 90 (2009) 1663–1679, https://doi.org/10.1016/j.jenvman.2008.12.011.

[384] B.G. Ateya, F.M. Al Kharafi, A.M. El-Shamy, A.Y. Saad, R.M. Abdalla, Electrochemical desulfurization of geothermal fluids under high temperature and pressure, J. Appl. Electrochem. 39 (2009) 383–389, https://doi.org/10.1007/s10800-008-9683-3.

[385] K. Waterston, D. Bejan, N.J. Bunce, Electrochemical oxidation of sulfide ion at a boron-doped diamond anode, J. Appl. Electrochem. 37 (2007) 367–373, https://doi.org/10.1007/s10800-006-9267-z.

[386] J. Haner, D. Bejan, N.J. Bunce, Electrochemical oxidation of sulfide ion at a Ti/IrO2-Ta 2O5 anode in the presence and absence of naphthenic acids, J. Appl. Electrochem. 39 (2009) 1733–1738, https://doi.org/10.1007/s10800-009-9873-7.

[387] Yuting Wang, Miao Li, Chuanping Feng, Zhenya Zhang, Electrochemical oxidation of sulfide in oil wastewater using Ti/IrO_2 anode, Environ. Progr. Sustain. Energy 31 (4) (2012) 500–506, https://doi.org/10.1002/ep.10565.

[388] E.M. Mattiusi, N.M.S. Kaminari, M.J.J.S. Ponte, H.A. Ponte, Behavior analysis of a porous bed electrochemical reactor the treatment of petrochemical industry wastewater contaminated by hydrogen sulfide (H2S), Chem. Eng. J. 275 (2015) 305–314, https://doi.org/10.1016/j.cej.2015.03.138.

[389] A. Burke, S. Li, J. Winnick, M. Liu, Sulfur-Tolerant Cathode Materials in Electrochemical Membrane System for H2 S Removal from Hot Fuel Gas, J. Electrochem. Soc. 151 (2004) D55, https://doi.org/10.1149/1.1758815.

[390] J.H. Kang, Y. Yoon, J.H. Song, Simultaneous removal of hydrogen sulfide and ammonia using a combined system with absorption and electrochemical oxidation, J. Environ. Sci. Heal. - Part A Toxic/Hazardous Subst, Environ. Eng. 54 (2019) 1430–1440, https://doi.org/10.1080/10934529.2019.1653108.

[391] H. Selvaraj, K. Chandrasekaran, R. Gopalkrishnan, Recovery of solid sulfur from hydrogen sulfide gas by an electrochemical membrane cell, RSC Adv. 6 (2016) 3735–3741, https://doi.org/10.1039/c5ra19116e.

[392] N. Sergienko, E. Irtem, O. Gutierrez, J. Radjenovic, Electrochemical removal of sulfide on porous carbon-based flow-through electrodes, J. Hazard. Mater. 375 (2019) 19–25, https://doi.org/10.1016/j.jhazmat.2019.04.033.

[393] J. Li, X. Ma, G. Qu, K. He, P. Lv, R. Xie, C. Zhao, Y. Cai, Efficient purification of hydrogen sulfide by synergistic effects of electrochemical and liquid phase catalysis, Sep. Purif. Technol. 218 (2019) 43–50, https://doi.org/10.1016/j.seppur.2019.01.055.

[394] J. Hastie, D. Bejan, N.J. Bunce, Oxidation of sulfide ion in synthetic geothermal brines at carbon-based anodes, Can. J. Chem. Eng. 89 (2011) 948–957, https://doi.org/10.1002/cjce.20454.

[395] S. El-Sherif, D. Bejan, N.J. Bunce, Electrochemical oxidation of sulfide ion in synthetic sour brines using periodic polarity reversal at Ebonex® electrodes, Can. J. Chem. 88 (9) (2010) 928–936, https://doi.org/10.1139/V10-081.

[396] L. Szpyrkowicz, S.N. Kaul, R.N. Neti, S. Satyanarayan, Influence of anode material on electrochemical oxidation for the treatment of tannery wastewater, Water Res. 39 (2005) 1601–1613, https://doi.org/10.1016/j.watres.2005.01.016.

[397] P.K. Dutta, R.A. Rozendal, Z. Yuan, K. Rabaey, J. Keller, Electrochemical regeneration of sulfur loaded electrodes, Electrochem. Commun. 11 (2009) 1437–1440, https://doi.org/10.1016/j.elecom.2009.05.024.

[398] M. Vepsalainen, J. Selin, P. Rantala, M. Pulliainen, H. Sarkka, K. Kuhmonen, A. Bhatnagar, M. Sillanpaa, Precipitation of dissolved sulphide in pulp and paper mill wastewater by electrocoagulation, Environ. Technol. 32 (2011) 1393–1400, https://doi.org/10.1080/09593330.2010.536790.

[399] Y. Wang, H. Lin, B. Hu, Electrochemical removal of hydrogen sulfide from swine manure, Chem. Eng. J. 356 (2019) 210–218, https://doi.org/10.1016/j.cej.2018.08.171.

[400] Y. Wang, H. Lin, L. Ding, B. Hu, Low-voltage electrochemical treatment to precipitate sulfide during anaerobic digestion of beet sugar wastewater, Sci. Total Environ. 747 (2020), https://doi.org/10.1016/j.scitotenv.2020.141243.

[401] P. Bernardo, G. Clarizia, 30 years of membrane technology for gas separation, in, Chem. Eng. Trans. (2013) 1999–2004, https://doi.org/10.3303/CET1332334.

[402] S. Loeb, S. Sourirajan, Sea Water Demineralization by Means of an Osmotic Membrane, Advances in Chemistry 38 (1963) 117–132, https://doi.org/10.1021/ba-1963-0038.ch009.

[403] R.W. Baker, K. Lokhandwala, Natural gas processing with membranes: An overview, Ind. Eng. Chem. Res. (2008), https://doi.org/10.1021/ie071083w.

[404] P. Pandey, R.S. Chauhan, Membranes for gas separation, Prog. Polym. Sci. (2001), https://doi.org/10.1016/S0079-6700(01)00009-0.

[405] Y. Alqaheem, A. Alomair, M. Vinoba, A. Pérez, Polymeric Gas-Separation Membranes for Petroleum Refining, Int. J. Polym. Sci. 2017 (2017), https://doi.org/10.1155/2017/4250927.

[406] J.T. Vaughn, W.J. Koros, Analysis of feed stream acid gas concentration effects on the transport properties and separation performance of polymeric membranes for natural gas sweetening: A comparison between a glassy and rubbery polymer, J. Memb. Sci. (2014), https://doi.org/10.1016/j.memsci.2014.03.029.

[407] G. George, N. Bhoria, S. Alhallaq, A. Abdala, V. Mittal, Polymer membranes for acid gas removal from natural gas, Sep. Purif. Technol. (2016), https://doi.org/10.1016/j.seppur.2015.12.033.

[408] D. Gong, S. Huang, W. Wu, C. Yu, C. Fang, D. Liu, Characteristics of gas compositions in giant gas fields of China, Energy Explor. Exploit. 32 (2014) 635–656, https://doi.org/10.1260/0144-5987.32.4.635.

[409] M. Harasimowicz, P. Orluk, G. Zakrzewska-Trznadel, A.G. Chmielewski, Application of polyimide membranes for biogas purification and enrichment, J. Hazard. Mater. 144 (2007) 698–702, https://doi.org/10.1016/j.jhazmat.2007.01.098.

[410] S.A. Stern, B. Krishnakumar, S.G. Charati, W.S. Amato, A.A. Friedman, D.J. Fuess, Performance of a bench-scale membrane pilot plant for the upgrading of biogas in a wastewater treatment plant, J. Memb. Sci. 151 (1998) 63–74, https://doi.org/10.1016/S0376-7388(98)00238-5.

[411] X.Y. Chen, H. Vinh-Thang, A.A. Ramirez, D. Rodrigue, S. Kaliaguine, Membrane gas separation technologies for biogas upgrading, RSC Adv. 5 (2015) 24399–24448, https://doi.org/10.1039/c5ra00666j.

[412] L. Ansaloni, L. Deng, Advances in polymer-inorganic hybrids as membrane materials, in: Recent Dev. Polym. Macro, Micro Nano Blends Prep. Characterisation, 2017. 10.1016/B978-0-08-100408-1.00007-8.

[413] P. Bernardo, E. Drioli, G. Golemme, Membrane gas separation: A review/state of the art, Ind. Eng. Chem. Res. (2009), https://doi.org/10.1021/ie8019032.

[414] L.M. Robeson, Polymeric membranes for gas separation, in: K.H.J. Buschow, R. W. Cahn, M.C. Flemings, B. Ilschner, E.J. Kramer, S. Mahajan, P. Veyssière (Eds.), Encyclopedia of Materials: Science and Technology, 2nd ed., Elsevier, Oxford, 2001, pp. 7629–7632, https://doi.org/10.1016/B0-08-043152-6/01364-4.

[415] L.M. Robeson, The upper bound revisited, J. Memb. Sci. 320 (1-2) (2008) 390–400, https://doi.org/10.1016/j.memsci.2008.04.030.

[416] K.A. Lokhandwala, R.W. Baker, K.D. Amo, Sour gas treatment process, US-5407467-A, 1995.

[417] M. Wessling, S. Schoeman, T. van der Boomgaard, C.A. Smolders, Plasticization of gas separation membranes, Gas Sep. Purif. (1991), https://doi.org/10.1016/0950-4214(91)80028-4.

[418] Y. Huang, X. Wang, D.R. Paul, Physical aging of thin glassy polymer films: Free volume interpretation, J. Memb. Sci. (2006), https://doi.org/10.1016/j.memsci.2005.10.032.

[419] A. Bos, I.G.M. Pünt, M. Wessling, H. Strathmann, CO2-induced plasticization phenomena in glassy polymers, J. Memb. Sci. (1999), https://doi.org/10.1016/S0376-7388(98)00299-3.

[420] A.F. Ismail, W. Lorna, Penetrant-induced plasticization phenomenon in glassy polymers for gas separation membrane, Sep. Purif. Technol. (2002), https://doi.org/10.1016/S1383-5866(01)00211-8.

[421] Marcel Mulder, Basic Principles of Membrane Technology, 1st ed., Springer, Dordrecht, 1991. https://doi.org/10.1007/978-94-017-0835-7.

[422] A.I. Akhmetshina, N.R. Yanbikov, A.A. Atlaskin, M.M. Trubyanov, A. Mechergui, K.V. Otvagina, E.N. Razov, A.E. Mochalova, I.V. Vorotyntsev, Acidic Gases Separation from Gas Mixtures on the Supported Ionic Liquid Membranes

Providing the Facilitated and Solution-Diffusion Transport Mechanisms, Membranes (Basel). 9 (2019) 9, https://doi.org/10.3390/membranes9010009.
[423] X. Zhang, Z. Tu, H. Li, K. Huang, X. Hu, Y. Wu, D.R. MacFarlane, Selective separation of H2S and CO2 from CH4 by supported ionic liquid membranes, J. Memb. Sci. 543 (2017) 282–287, https://doi.org/10.1016/j.memsci.2017.08.033.
[424] J.D. Wind, C. Staudt-Bickel, D.R. Paul, W.J. Koros, The effects of crosslinking chemistry on CO2 plasticization of polyimide gas separation membranes, Ind. Eng. Chem. Res. (2002), https://doi.org/10.1021/ie0204639.
[425] P.S. Tin, T.S. Chung, Y. Liu, R. Wang, S.L. Liu, K.P. Pramoda, Effects of cross-linking modification on gas separation performance of Matrimid membranes, J. Memb. Sci. (2003), https://doi.org/10.1016/j.memsci.2003.08.005.
[426] B. Comesaña-Gándara, J. Chen, C.G. Bezzu, M. Carta, I. Rose, M.C. Ferrari, E. Esposito, A. Fuoco, J.C. Jansen, N.B. McKeown, Redefining the Robeson upper bounds for CO2/CH4 and CO2/N2 separations using a series of ultrapermeable benzotriptycene-based polymers of intrinsic microporosity, Energy Environ. Sci. 12 (2019) 2733–2740, https://doi.org/10.1039/c9ee01384a.
[427] J. Deng, Z. Dai, J. Yan, M. Sandru, E. Sandru, R.J. Spontak, L. Deng, Facile and solvent-free fabrication of PEG-based membranes with interpenetrating networks for CO2 separation, J. Memb. Sci. (2019), https://doi.org/10.1016/j.memsci.2018.10.031.
[428] G. Chatterjee, A.A. Houde, S.A. Stern, Poly(ether urethane) and poly(ether urethane urea) membranes with high H2S/CH4 selectivity, J. Memb. Sci. (1997), https://doi.org/10.1016/S0376-7388(97)00134-8.
[429] T. Mohammadi, M.T. Moghadam, M. Saeidi, M. Mahdyarfar, Acid gas permeation behavior through poly(ester urethane urea) membrane, Ind. Eng. Chem. Res. (2008), https://doi.org/10.1021/ie071493k.
[430] C. Tsvigu, E. Pavesi, M.G. De Angelis, M.G. Baschetti, Effect of relative humidity and temperature on the gas transport properties of 6FDA-6FpDA polyimide: Experimental study and modelling, J. Memb. Sci. (2015), https://doi.org/10.1016/j.memsci.2015.02.032.
[431] G. Dong, H. Li, V. Chen, Plasticization mechanisms and effects of thermal annealing of Matrimid hollow fiber membranes for CO2 removal, J. Memb. Sci. (2011), https://doi.org/10.1016/j.memsci.2010.11.064.
[432] T.C. Merkel, L.G. Toy, Comparison of hydrogen sulfide transport properties in fluorinated and nonfluorinated polymers, Macromolecules (2006), https://doi.org/10.1021/ma061072z.
[433] C.A. Scholes, G.W. Stevens, S.E. Kentish, The effect of hydrogen sulfide, carbon monoxide and water on the performance of a PDMS membrane in carbon dioxide/nitrogen separation, J. Memb. Sci. 350 (2010) 189–199, https://doi.org/10.1016/j.memsci.2009.12.027.
[434] T.C. Merkel, V.I. Bondar, K. Nagai, B.D. Freeman, I. Pinnau, Gas Sorption, Diffusion, and Permeation in Poly(dimethylsiloxane), Membr. Technol. Res. 38 (3) (2000) 415–434, https://doi.org/10.1002/(SICI)1099-0488(20000201)38:3<415::AID-POLB8>3.0.CO;2-Z.
[435] B. Wilks, M.E. Rezac, Properties of rubbery polymers for the recovery of hydrogen sulfide from gasification gases, J. Appl. Polym. Sci. (2002), https://doi.org/10.1002/app.10881.
[436] R. Casadei, M.G. Baschetti, M.J. Yoo, H.B. Park, L. Giorgini, Pebax® 2533/Graphene Oxide Nanocomposite Membranes for Carbon Capture, Membranes (Basel). 10 (2020) 188, https://doi.org/10.3390/MEMBRANES10080188.
[437] M. Isanejad, N. Azizi, T. Mohammadi, Pebax membrane for CO 2 /CH 4 separation: Effects of various solvents on morphology and performance, J. Appl. Polym. Sci. 134 (2016) 44531, https://doi.org/10.1002/app.44531.
[438] K. Ghosal, B.D. Freeman, Gas separation using polymer membranes: an overview, Polym. Adv. Technol. (1994), https://doi.org/10.1002/pat.1994.220051102.
[439] C.A. Scholes, G.W. Stevens, S.E. Kentish, The effect of hydrogen sulfide, carbon monoxide and water on the performance of a PDMS membrane in carbon dioxide/nitrogen separation, J. Memb. Sci. (2010), https://doi.org/10.1016/j.memsci.2009.12.027.
[440] W.L. Robb, THIN SILICONE MEMBRANES-THEIR PERMEATION PROPERTIES AND SOME APPLICATIONS, Ann. N. Y. Acad. Sci. (1968), https://doi.org/10.1111/j.1749-6632.1968.tb20277.x.
[441] T.C. Merkel, R.P. Gupta, B.S. Turk, B.D. Freeman, Mixed-gas permeation of syngas components in poly(dimethylsiloxane) and poly(1-trimethylsilyl-1-propyne) at elevated temperatures, J. Memb. Sci. (2001), https://doi.org/10.1016/S0376-7388(01)00452-5.
[442] B.D. Bhide, S.A. Stern, Membrane processes for the removal of acid gases from natural gas. I. Process configurations and optimization of operating conditions, J. Memb. Sci. (1993), https://doi.org/10.1016/0376-7388(93)85175-V.
[443] K. Amo, R.W. Baker, V.D. Helm, T. Hofmann, K.A. Lokhandwala, I. Pinnau, M.B. Ringer, T.T. Su, L. Toy, J.G. Wijmans, Low-quality natural gas sulfur removal/recovery, Morgantown, WV, 1998. https://doi.org/10.2172/775213.
[444] W.J. Schell, C.G. Wensley, M.S.K. Chen, K.G. Venugopal, B.D. Miller, J.A. Stuart, Recent advances in cellulosic membranes for gas separation and pervaporation, Gas Sep. Purif. 3 (1989) 162–169, https://doi.org/10.1016/0950-4214(89)80001-5.
[445] C.S.K. Achoundong, N. Bhuwania, S.K. Burgess, O. Karvan, J.R. Johnson, W. J. Koros, Silane modification of cellulose acetate dense films as materials for acid gas removal, Macromolecules 46 (14) (2013) 5584–5594, https://doi.org/10.1021/ma4010583.
[446] A.Y. Houde, B. Krishnakumar, S.G. Charati, S.A. Stern, Permeability of dense (homogeneous) cellulose acetate membranes to methane, carbon dioxide, and their mixtures at elevated pressures, J. Appl. Polym. Sci. (1996), https://doi.org/10.1002/(SICI)1097-4628(19961226)62:13<2181::AID-APP1>3.0.CO;2-F.
[447] R.W. Baker, Membrane Technology and Applications (2012), https://doi.org/10.1002/9781118359686.
[448] M.P. Chenar, H. Savoji, M. Soltanieh, T. Matsuura, S. Tabe, Removal of hydrogen sulfide from methane using commercial polyphenylene oxide and Cardo-type polyimide hollow fiber membranes, Korean J. Chem. Eng. (2011), https://doi.org/10.1007/s11814-010-0437-7.
[449] M.S.K. Chen, S.P. Goff, J. Vanommeren, Process for separating CO2 and H2S from hydrocarbons, US-4589896-A, 1986.
[450] Y. Liu, Z. Liu, A. Morisato, N. Bhuwania, D. Chinn, W.J. Koros, Natural gas sweetening using a cellulose triacetate hollow fiber membrane illustrating controlled plasticization benefits, J. Memb. Sci. 601 (2020), 117910, https://doi.org/10.1016/j.memsci.2020.117910.
[451] Y. Liu, Z. Liu, G. Liu, W. Qiu, N. Bhuwania, D. Chinn, W.J. Koros, Surprising plasticization benefits in natural gas upgrading using polyimide membranes, J. Memb. Sci. 593 (2020), 117430, https://doi.org/10.1016/J.MEMSCI.2019.117430.
[452] C.A. Scholes, G.Q. Chen, W.X. Tao, J. Bacus, C. Anderson, G.W. Stevens, S. E. Kentish, The effects of minor components on the gas separation performance of membranes for carbon capture, Energy Procedia, Elsevier Ltd (2011) 681–687, https://doi.org/10.1016/j.egypro.2011.01.105.
[453] J. Hao, P.A. Rice, S.A. Stern, Upgrading low-quality natural gas with H2S- and CO2-selective polymer membranes: Part I. Process design and economics of membrane stages without recycle streams, J. Memb. Sci. 209 (2002) 177–206, https://doi.org/10.1016/S0376-7388(02)00318-6.
[454] B. Kraftschik, W.J. Koros, J.R. Johnson, O. Karvan, Dense film polyimide membranes for aggressive sour gas feed separations, J. Memb. Sci. 428 (2013) 608–619, https://doi.org/10.1016/j.memsci.2012.10.025.
[455] M.P. Chenar, M. Soltanieh, T. Matsuura, A. Tabe-Mohammadi, C. Feng, Gas permeation properties of commercial polyphenylene oxide and Cardo-type polyimide hollow fiber membranes, Sep. Purif. Technol. 51 (2006) 359–366, https://doi.org/10.1016/j.seppur.2006.02.018.
[456] M. Aguilar-Vega, D.R. Paul, Gas transport properties of polyphenylene ethers, J. Polym. Sci. Part B Polym. Phys. 31 (1993) 1577–1589, https://doi.org/10.1002/polb.1993.090311114.
[457] E.Y. Safronova, A.K. Osipov, A.B. Yaroslavtsev, Short Side Chain Aquivion Perfluorinated Sulfonated Proton-Conductive Membranes: Transport and Mechanical Properties, Pet. Chem. (2018), https://doi.org/10.1134/S0965544118020044.
[458] J.S. Chiou, D.R. Paul, Gas Permeation in a Dry Nafion Membrane, Ind. Eng. Chem. Res. (1988), https://doi.org/10.1021/ie00083a034.
[459] A. Kusoglu, A.Z. Weber, New Insights into Perfluorinated Sulfonic-Acid Ionomers, Chem. Rev. (2017), https://doi.org/10.1021/ACs.chemrev.6b00159.
[460] G. Gebel, Structural evolution of water swollen perfluorosulfonated ionomers from dry membrane to solution, Polymer (Guildf). (2000), https://doi.org/10.1016/S0032-3861(99)00770-3.
[461] L. Olivieri, H. Aboukeila, M.G. Baschetti, D. Pizzi, L. Merlo, G.C. Sarti, Humid permeation of CO2 and hydrocarbons in Aquivion® perfluorosulfonic acid ionomer membranes, experimental and modeling, J. Memb. Sci. (2017), https://doi.org/10.1016/j.memsci.2017.08.030.
[462] M.G. De Angelis, S. Lodge, M.G. Baschetti, G.C. Sarti, F. Doghieri, A. Sanguineti, P. Fossati, Water sorption and diffusion in a short-side-chain perfluorosulfonic acid ionomer membrane for PEMFCS: effect of temperature and pre-treatment, Desalination (2006), https://doi.org/10.1016/j.desal.2005.06.070.
[463] M.G. Baschetti, M. Minelli, J. Catalano, G.C. Sarti, Gas permeation in perflurosulfonated membranes: Influence of temperature and relative humidity, Int. J. Hydrogen Energy. (2013), https://doi.org/10.1016/j.ijhydene.2013.06.104.
[464] J. Catalano, T. Myezwa, M.G. De Angelis, M.G. Baschetti, G.C. Sarti, The effect of relative humidity on the gas permeability and swelling in PFSI membranes, Int. J. Hydrogen Energy (2012), https://doi.org/10.1016/j.ijhydene.2011.07.047.
[465] V. Signorini, M.G. Baschetti, D. Pizzi, L. Merlo, Hydrogen sulfide mix gas permeation in Aquivion® perfluorosulfonic acid (PFSA) ionomer membranes for natural gas sweetening, J. Memb. Sci. 640 (2021), 119809, https://doi.org/10.1016/J.MEMSCI.2021.119809.
[466] J.J. Pellegrino, P.J. Giarratano, Gas separation using ion exchange membranes for producing hydrogen from synthesis gas. Quarterly report 22 covering the period October 1, 1991–December 31, 1991, Pittsburgh, PA, and Morgantown, WV, 1992. https://doi.org/10.2172/10163992.
[467] A. Brunetti, F. Scura, G. Barbieri, E. Drioli, Membrane technologies for CO2 separation, J. Memb. Sci. 359 (1–2) (2010) 115–125, https://doi.org/10.1016/j.memsci.2009.11.040.
[468] T.S. Chung, L.Y. Jiang, Y. Li, S. Kulprathipanja, Mixed matrix membranes (MMMs) comprising organic polymers with dispersed inorganic fillers for gas separation, Prog. Polym. Sci. 32 (2007) 483–507, https://doi.org/10.1016/j.progpolymsci.2007.01.008.
[469] S. Hassanajili, E. Masoudi, G. Karimi, M. Khademi, Mixed matrix membranes based on polyetherurethane and polyesterurethane containing silica nanoparticles for separation of CO2/CH4 gases, Sep. Purif. Technol. 116 (2013) 1–12, https://doi.org/10.1016/j.seppur.2013.05.017.
[470] O.G. Nik, X.Y. Chen, S. Kaliaguine, Amine-functionalized zeolite FAU/EMT-polyimide mixed matrix membranes for CO2/CH4 separation, J. Memb. Sci. 379 (2011) 468–478, https://doi.org/10.1016/j.memsci.2011.06.019.
[471] J. Ahn, W.J. Chung, I. Pinnau, M.D. Guiver, Polysulfone/silica nanoparticle mixed-matrix membranes for gas separation, J. Memb. Sci. 314 (2008) 123–133, https://doi.org/10.1016/j.memsci.2008.01.031.

[472] S. Wang, D. Wu, H. Huang, Q. Yang, M. Tong, D. Liu, C. Zhong, Computational exploration of H2S/CH4 mixture separation using acid-functionalized UiO-66(Zr) membrane and composites, Chinese, J Chem. Eng. 23 (2015) 1291–1299, https://doi.org/10.1016/j.cjche.2015.04.017.
[473] S. Kanehashi, A. Aguiar, H.T. Lu, G.Q. Chen, S.E. Kentish, Effects of industrial gas impurities on the performance of mixed matrix membranes, J. Memb. Sci. 549 (2018) 686–692, https://doi.org/10.1016/j.memsci.2017.10.056.
[474] J.D. Way, R.D. Noble, Hydrogen Sulfide Facilitated Transport in Perfluorosulfonic Acid, Membranes (1987) 123–137, https://doi.org/10.1021/bk-1987-0347.ch009.
[475] J.J. Pellegrino, R. Nassimbene, R.D. Noble, Facilitated transport of CO2 through highly swollen ion-exchange membranes: The effect of hot glycerine pretreatment, Gas Sep. Purif. 2 (1988) 126–130, https://doi.org/10.1016/0950-4214(88)80028-8.
[476] J. Ilconich, C. Myers, H. Pennline, D. Luebke, Experimental investigation of the permeability and selectivity of supported ionic liquid membranes for CO2/He separation at temperatures up to 125 °C, J. Memb. Sci. 298 (2007) 41–47, https://doi.org/10.1016/j.memsci.2007.03.056.
[477] R. Quinn, J.B. Appleby, G.P. Pez, Hydrogen sulfide separation from gas streams using salt hydrate chemical absorbents and immobilized liquid membranes, Sep. Sci. Technol. 37 (2002) 627–638, https://doi.org/10.1081/SS-120001451.
[478] Y.I. Park, B.S. Kim, Y.H. Byun, S.H. Lee, E.W. Lee, J.M. Lee, Preparation of supported ionic liquid membranes (SILMs) for the removal of acidic gases from crude natural gas, Desalination (2009), https://doi.org/10.1016/j.desal.2007.10.085.
[479] P.J. Carvalho, J.A.P. Coutinho, The polarity effect upon the methane solubility in ionic liquids: A contribution for the design of ionic liquids for enhanced CO 2/CH 4 and H 2S/CH 4 selectivities, Energy Environ. Sci. 4 (2011) 4614–4619, https://doi.org/10.1039/c1ee01599k.
[480] Y. Han, D. Wu, W.S.W. Ho, Simultaneous effects of temperature and vacuum and feed pressures on facilitated transport membrane for CO2/N2 separation, J. Memb. Sci. 573 (2019) 476–484, https://doi.org/10.1016/j.memsci.2018.12.028.
[481] W.J. Chung, J.J. Griebel, E.T. Kim, H. Yoon, A.G. Simmonds, H.J. Ji, P.T. Dirlam, R.S. Glass, J.J. Wie, N.A. Nguyen, B.W. Guralnick, J. Park, Á. Somogyi, P. Theato, M.E. Mackay, Y.E. Sung, K. Char, J. Pyun, The use of elemental sulfur as an alternative feedstock for polymeric materials, Nat. Chem. 5 (2013) 518–524, https://doi.org/10.1038/NCHEM.1624.
[482] G. Singh, P.G. Nakade, D. Chetia, P. Jha, U. Mondal, S. Kumari, S. Sen, Kinetics and mechanism of phase transfer catalyzed synthesis of aromatic thioethers by H2S-rich methyldiethanolamine, J. Ind. Eng. Chem. 37 (2016) 190–197, https://doi.org/10.1016/j.jiec.2016.03.022.
[483] A. Pudi, A.P. Karcz, S. Keshavarz, V. Shadravan, M.P. Andersson, S.S. Mansouri, Modular and intensified — Reimagining manufacturing at the energy-chemistry nexus and beyond, Chem. Eng. Process. - Process Intensif. 174 (2022), 108883, https://doi.org/10.1016/J.CEP.2022.108883.
[484] W. Zhang, N. Garg, M.P. Andersson, Q. Chen, B. Zhang, R. Gani, S.S. Mansouri, Intensified separation alternatives for offshore natural gas sweetening, Sep. Purif. Technol. 286 (2022), 120436, https://doi.org/10.1016/J.SEPPUR.2021.120436.
[485] M.C. Delhoménie, M. Heitz, Biofiltration of air: A review, Crit. Rev. Biotechnol. 25 (2005) 53–72, https://doi.org/10.1080/07388550590935814.
[486] B.A.D. Neto, A.A.M. Lapis, R.Y. Souza, Task-Specific Ionic Liquids: Design, Properties and Applications, in: S. Zhang (Ed.), Encycl. Ion. Liq, Springer Singapore, 2019, pp. 1–11. https://doi.org/10.1007/978-981-10-6739-6_33-1.
[487] Saravanan Janakiram, Mahdi Ahmadi, Zhongde Dai, Luca Ansaloni, Liyuan Deng, Performance of nanocomposite membranes containing 0D to 2D nanofillers for CO_2 separation: A review, Membranes 8 (2) (2018) 24, https://doi.org/10.3390/membranes8020024.
[488] Mohammadreza Rahmani, Abbass Kazemi, Farid Talebnia, Matrimid mixed matrix membranes for enhanced CO_2/CH_4 separation, J. Polym. Eng. 36 (5) (2016) 499–511, https://doi.org/10.1515/polyeng-2015-0176.
[489] Mahmoud A. Abdulhamid, Giuseppe Genduso, Yingge Wang, Xiaohua Ma, Ingo Pinnau, Plasticization-resistant carboxyl-functionalized 6FDA-Polyimide of Intrinsic Microporosity (PIM–PI) for membrane-based gas separation, Indust. Eng. Chem. Res. 59 (12) (2020) 5247–5256, https://doi.org/10.1021/acs.iecr.9b04994.
[490] Y. Ma, H. Guo, R. Selyanchyn, B. Wang, L. Deng, Z. Dai, X. Jiang, Hydrogen sulfide removal from natural gas using membrane technology: a review, J. Mater. Chem. A. 9 (2021) 20211–20240, https://doi.org/10.1039/D1TA04693D.
[491] A.H. Wani, A.K. Lau, R.M.R. Branion, Biofiltration control of pulping odors - hydrogen sulfide: Performance, macrokinetics and coexistence effects of organo-sulfur species, J. Chem. Technol. Biotechnol. 74 (1999) 9–16, https://doi.org/10.1002/(SICI)1097-4660(199901)74:1<9::AID-JCTB981>3.0.CO;2-B.
[492] A. Elias, A. Barona, A. Arreguy, J. Rios, I. Aranguiz, J. Peñas, Evaluation of a packing material for the biodegradation of H2S and product analysis, Process Biochem. 37 (2002) 813–820, https://doi.org/10.1016/S0032-9592(01)00287-4.
[493] H. Kim, Y.J. Kim, J.S. Chung, Q. Xie, Long-term operation of a biofilter for simultaneous removal of H2S and NH3, J. Air Waste Manag. Assoc. 52 (2002) 1389–1398, https://doi.org/10.1080/10473289.2002.10470871.
[494] Z. Shareefdeen, B. Herner, S. WILson, Biofiltration of nuisance sulfur gaseous odors from a meat rendering plant, J. Chem. Technol. Biotechnol. 77 (2002) 1296–1299, https://doi.org/10.1002/jctb.709.
[495] L. Malhautier, C. Gracian, J.C. Roux, J.L. Fanlo, P. Le Cloirec, Biological treatment process of air loaded with an ammonia and hydrogen sulfide mixture, Chemosphere 50 (2003) 145–153, https://doi.org/10.1016/S0045-6535(02)00395-8.
[496] Y. Zhang, C. Li, B. Jiang, Full-scale study to treat hydrogen sulfide with biofilter, Appl. Mech. Mater. 443 (2014) 629–633.
[497] Z. Shareefdeen, Hydrogen sulfide (H2S) removal using schist packings in industrial biofilter applications, Korean J. Chem. Eng. 32 (2014) 15–19, https://doi.org/10.1007/s11814-014-0349-z.
[498] K. Rujisangvittaya, S. Phoolphundh, Sulfur Oxidizing Bacterial Biofilter for Removal of Hydrogen Sulfide (H2S) from Biogas, J. Sustain. Energy Environ. 6 (2015) 71–74.
[499] M. Ben Jaber, A. Couvert, A. Amrane, F. Rouxel, P. Le Cloirec, E. Dumont, Biofiltration of H2S in air-Experimental comparisons of original packing materials and modeling, Biochem. Eng. J. 112 (2016) 153–160, https://doi.org/10.1016/j.bej.2016.04.020.
[500] H.H.J. Cox, M.A. Deshusses, Co-treatment of H2S and toluene in a biotrickling filter, Chem. Eng. J. 87 (2002) 101–110, https://doi.org/10.1016/S1385-8947(01)00222-4.
[501] H.H.J. Cox, M.A. Deshusses, Biotrickling filters for air pollution control, in: Encycl. Environ. Microbiol., 2nd ed., Wiley & Sons., New York, NY, 2002: pp. 782–795.
[502] M. Fasihi, M.H. Fazaelipoor, M. Rezakazemi, H2S removal from sour water in a combination system of trickling biofilter and biofilter, Environ. Res. 184 (2020), https://doi.org/10.1016/j.envres.2020.109380.
[503] L.C.C. Koe, F. Yang, A bioscrubber for hydrogen sulphide removal, Water Sci. Technol. 41 (2000) 141–145, https://doi.org/10.2166/wst.2000.0103.
[504] E. Tilahun, E. Sahinkaya, B. Çalli, A Comparative Assessment of Membrane Bioscrubber and Classical Bioscrubber for Biogas Purification, ICBST 2018: 20th International Conference on Biomass Science and Technology. Berlin, 2018. https://www.researchgate.net/publication/328530558_A_Comparative_Assessment_of_Membrane_Bioscrubber_and_Classical_Bioscrubber_for_Biogas_Purification_ICBST_2018_20th_International_Conference_on_Biomass_Science_and_Technology_Berlin_Germany.
[505] F.Y. Jou, R.D. Deshmukh, F.D. Otto, A.E. Mather, Solubility of H2S, CO2, CH4 and C2H6 in sulfolane at elevated pressures, Fluid Phase Equilib. 56 (1990) 313–324, https://doi.org/10.1016/0378-3812(90)85111-M.
[506] H. Renon, J.Y. Lenoir, P. Renault, Gas Chromatographic Determination of Henry's Constants of 12 Gases in 19 Solvents, J. Chem. Eng. Data. 16 (1971) 340–342, https://doi.org/10.1021/je60050a014.
[507] F. Murrieta-Guevara, A.T. Rodríguez, Solubility of Carbon Dioxide, Hydrogen Sulfide, and Methane in Pure and Mixed Solvents, J. Chem. Eng. Data. 29 (1984) 456–460, https://doi.org/10.1021/je00038a027.
[508] F.Y. Jou, A.E. Mather, F.D. Otto, Solubility of H2S and CO2 in Aqueous Methyldiethanolamine Solutions, Ind. Eng. Chem. Process Des. Dev. 21 (1982) 539–544, https://doi.org/10.1021/i200019a001.
[509] E. Skylogianni, I. Mundal, D.D.D. Pinto, C. Coquelet, H.K. Knuutila, Hydrogen sulfide solubility in 50 wt% and 70 wt% aqueous methyldiethanolamine at temperatures from 283 to 393 K and total pressures from 500 to 10000 kPa, Fluid Phase Equilib. 511 (2020), 112498, https://doi.org/10.1016/j.fluid.2020.112498.
[510] K. Fischer, J. Chen, M. Petri, J. Gmehling, Solubility of H2S and CO2 in N-octyl-2-pyrrolidone and of H2S in methanol and benzene, AIChE J. 48 (2002) 887–893, https://doi.org/10.1002/aic.690480422.
[511] S.F. Sciamanna, S. Lynn, Solubility of Hydrogen Sulfide, Sulfur Dioxide, Carbon Dioxide, Propane, and n-Butane in Poly(glycol ethers), Ind. Eng. Chem. Res. 27 (1988) 492–499, https://doi.org/10.1021/ie00075a020.
[512] N.K. Gupta, J. Bae, K.S. Kim, Metal-organic framework-derived NaMnxOy hexagonal microsheets for superior adsorptive-oxidative removal of hydrogen sulfide in ambient conditions, Chem. Eng. J. 427 (2022), 130909, https://doi.org/10.1016/J.CEJ.2021.130909.
[513] N.K. Gupta, J. Bae, K.S. Kim, Metal organic framework derived NaCoxOy for room temperature hydrogen sulfide removal, Sci. Rep. 11 (2021), https://doi.org/10.1038/S41598-021-94265-7.
[514] S. Cimino, L. Lisi, A. Erto, F.A. Deorsola, G. de Falco, F. Montagnaro, M. Balsamo, Role of H2O and O2 during the reactive adsorption of H2S on CuO-ZnO/activated carbon at low temperature, Microporous Mesoporous Mater. 295 (2020), 109949, https://doi.org/10.1016/J.MICROMESO.2019.109949.
[515] S. Liang, J. Mi, F. Liu, Y. Zheng, Y. Xiao, Y. Cao, L. Jiang, Efficient catalytic elimination of COS and H2S by developing ordered mesoporous carbons with versatile base N sites via a calcination induced self-assembly route, Chem. Eng. Sci. 221 (2020), 115714, https://doi.org/10.1016/J.CES.2020.115714.
[516] Y. Pan, M. Chen, M. Hu, M. Tian, Y. Zhang, D. Long, Probing the room-temperature oxidative desulfurization activity of three-dimensional alkaline graphene aerogel, Appl. Catal. B Environ. 262 (2020), 118266, https://doi.org/10.1016/j.apcatb.2019.118266.
[517] N.K. Gupta, J. Bae, K.S. Kim, From MOF-199 Microrods to CuO Nanoparticles for Room-Temperature Desulfurization: Regeneration and Repurposing Spent Adsorbents as Sustainable Approaches, ACS Omega 6 (39) (2021) 25631–25641, https://doi.org/10.1021/acsomega.1c03712.
[518] N. Bhoria, G. Basina, J. Pokhrel, K.S. Kumar Reddy, S. Anastasiou, V. V. Balasubramanian, Y.F. AlWahedi, G.N. Karanikolos, Functionalization effects on HKUST-1 and HKUST-1/graphene oxide hybrid adsorbents for hydrogen sulfide removal, J. Hazard. Mater. 394 (2020), 122565, https://doi.org/10.1016/j.jhazmat.2020.122565.
[519] M. Daraee, R. Saeedirad, A. Rashidi, Adsorption of hydrogen sulfide over a novel metal organic framework –metal oxide nanocomposite: TOUO-x (TiO2/UiO-66), J. Solid State Chem. 278 (2019), 120866, https://doi.org/10.1016/j.jssc.2019.07.027.

[520] M. Daraee, E. Ghasemy, A. Rashidi, Synthesis of novel and engineered UiO-66/graphene oxide nanocomposite with enhanced H2S adsorption capacity, J. Environ. Chem. Eng. 8 (2020), 104351, https://doi.org/10.1016/j.jece.2020.104351.

[521] J. Mi, F. Liu, W. Chen, X. Chen, L. Shen, Y. Cao, C. Au, K. Huang, A. Zheng, L. Jiang, Design of Efficient, Hierarchical Porous Polymers Endowed with Tunable Structural Base Sites for Direct Catalytic Elimination of COS and H2S, ACS Appl. Mater. Interfaces. 11 (2019) 29950–29959, https://doi.org/10.1021/ACSAMI.9B09149/SUPPL_FILE/AM9B09149_SI_001.PDF.

[522] C. Yang, J. Kou, H. Fan, Z. Tian, W. Kong, J. Shangguan, Facile and Versatile Sol-Gel Strategy for the Preparation of a High-Loaded ZnO/SiO2 Adsorbent for Roomerature H2S Removal, Langmuir 35 (2019) 7759–7768, https://doi.org/10.1021/ACs.langmuir.9b00853.

[523] Q. Geng, L.J. Wang, C. Yang, H.Y. Zhang, Y.R. Zhao, H.L. Fan, C. Huo, Room-temperature hydrogen sulfide removal with zinc oxide nanoparticle/molecular sieve prepared by melt infiltration, Fuel Process. Technol. 185 (2019) 26–37, https://doi.org/10.1016/J.FUPROC.2018.11.013.

[524] M. Daraee, E. Ghasemy, A. Rashidi, Effective adsorption of hydrogen sulfide by intercalation of TiO2and N-doped TiO2in graphene oxide, J. Environ. Chem. Eng. 8 (2020), 103836, https://doi.org/10.1016/j.jece.2020.103836.

[525] L.Y. Xia, D.H. Gu, J. Tan, W.B. Dong, H.Q. Hou, Photolysis of low concentration H2S under UV/VUV irradiation emitted from microwave discharge electrodeless lamps, Chemosphere 71 (2008) 1774–1780, https://doi.org/10.1016/j.chemosphere.2008.01.050.

[526] V. Preethi, S. Kanmani, Optimization of operating parameters for gas-phase photocatalytic splitting of H_2S by novel vermiculate packed tubular reactor, J. Environ. Manage. 181 (2016) 674–680, https://doi.org/10.1016/j.jenvman.2016.08.039.

[527] Y. Wang, Y. Wang, Y. Liu, Removal of gaseous hydrogen sulfide using ultraviolet/Oxone-induced oxidation scrubbing system, Chem. Eng. J. 393 (2020), 124740, https://doi.org/10.1016/j.cej.2020.124740.

[528] I.M. Ghayad, F.M. Al Kharafi, A.Y. Saad, B.G. Ateya, Electrochemical Oxidation of Sulfide Ions on Platinum Electrodes, Mod. Appl. Sci. 4 (3) (2010) 2–11, https://doi.org/10.5539/mas.v4n3p2.

[529] H. Chow, A.L.T. Pham, Effective removal of silica and sulfide from oil sands thermal in-situ produced water by electrocoagulation, J. Hazard. Mater. 380 (2019), 120880, https://doi.org/10.1016/j.jhazmat.2019.120880.

[530] B.D. Bhide, A. Voskericyan, S.A. Stern, Hybrid processes for the removal of acid gases from natural gas, J. Memb. Sci. (1998), https://doi.org/10.1016/S0376-7388(97)00257-3.

[531] W. Heilman, V. Tammela, J.A. Meyer, V. Stannet, M. Szwarc, Permeability of polymer films to hydrogen sulfide gas, Ind. Eng. Chem. 48 (4) (1956) 821–824, https://doi.org/10.1021/ie50556a046.

[532] C.J. Orme, J.R. Klaehn, F.F. Stewart, Gas permeability and ideal selectivity of poly [bis-(phenoxy)phosphazene], poly[bis-(4-tert-butylphenoxy)phosphazene], and poly[bis-(3,5-di-tert- butylphenoxy)1.2(chloro)0.8phosphazene], J. Memb. Sci. 238 (2004) 47–55, https://doi.org/10.1016/j.memsci.2004.02.032.

[533] R. Quinn, D.V. Laciak, Polyelectrolyte membranes for acid gas separations, J. Memb. Sci. 131 (1997) 49–60, https://doi.org/10.1016/S0376-7388(97)00024-0.

[534] O.V. Malykh, A.Y. Golub, V.V. Teplyakov, Polymeric membrane materials: New aspects of empirical approaches to prediction of gas permeability parameters in relation to permanent gases, linear lower hydrocarbons and some toxic gases, Adv. Colloid Interface Sci. 164 (2011) 89–99, https://doi.org/10.1016/j.cis.2010.10.004.

[535] J. Vaughn, W.J. Koros, Effect of the amide bond diamine structure on the CO_2, H_2S, and CH_4 transport properties of a series of novel 6FDA-based polyamide-imides for natural gas purification, Macromolecules 45 (2012) 7036–7049, https://doi.org/10.1021/ma301249x.